Université Paris Ouest Nanterre La Defense
Ecole doctorale Connaissance, langage, modélisation
Laboratoire Energétique, Méchanique, Electromagnétisme

Thèse

présentée et soutenue publiquement le 22 Janvier 2015 par

Alexander Nikitin

pour obtenir le grade de
Docteur de l'Université Paris OUEST Nanterre La Defense
Discipline : Méchanique et Matériaux

La Fatigue Gigacyclique d'un alliage de Titane

Jury :

Rapporteurs
Prof. J. BERGSTROM (Karlstadt Univ, Sweeden)
Prof. G. HENAFF (ENSMA, Poitiers, France)
Examinateurs
Prof. G. GLINKA (Waterloo Univ, Canada)
Prof. N. BEKLEMISHEV (Université des technologies aeronautiques, Moscou, Russie)
Prof. A. SHANYAVSKIY (Université de l'aéronautique civile, Moscou, Russie)
Prof. C. BATHIAS (Université Paris X, Paris, France)
Prof. T. PALIN-LUC (Arts et Métiers ParisTech, campus de Bordeaux, France)

Contents

1 Literature Review **14**

1.1 History of Fatigue 14
1.2 General concepts of Fatigue 22
1.3 Regimes of Fatigue 26
1.4 Full SN-curve 28
1.5 Stages of Fatigue 32
1.5.1 Fatigue crack initiation 33
1.5.2 Fatigue crack growth 38
1.6 Very High Cycle Fatigue 41
1.6.1 Crack initiation in VHCF 42
1.6.2 Crack growth in VHCF 44
1.7 Fatigue in Titanium and Titanium alloys 46
1.7.1 Introduction 46
1.7.2 Titanium and Titanium alloys 46
1.8 Thermomechanical treatment of titanium alloys 50
1.9 Typical micro-structures of $(\alpha + \beta)$ titanium alloys 51
1.10 Slip in α (h.c.p.) and β (b.c.c) titanium 54
1.11 Fatigue in $(\alpha + \beta)$ Titanium alloys 56
1.12 Influence of micro-structural defects on fatigue 59
1.13 The Very-High-Cycle Fatigue in titanium alloy 61

2 Materials and Experimental method **65**

2.1 Forged VT3-1 titanium alloy 65
2.1.1 Chemical composition of forged VT3-1 66
2.1.2 Micro-structure of forged VT3-1 titanium alloy 67
2.1.3 Micro-hardness measurements 72
2.1.4 Quasi-static monotonic mechanical properties of forged titanium alloy 75
2.2 Extruded VT3-1 77

2.2.1 Chemical composition of extruded VT3-1 . . . 77
2.2.2 Microstructure of extruded VT3-1 titanium alloy . . . 78
2.2.3 Micro-hardness of extruded VT3-1 alloy . . . 81
2.2.4 Mechanical properties of extruded VT3-1 titanium alloy . . . 83
2.3 Specimens from forged VT3-1 titanium alloy . . . 85
2.3.1 Specimens for R=-1 tests . . . 86
2.3.2 Specimens for R > 0 tests . . . 89
2.4 Specimens from extruded VT3-1 titanium alloy . . . 89
2.5 Ultrasonic fatigue testing systems . . . 92
2.5.1 Tension-compression testing system . . . 92
2.5.2 Calibration of the system for R=-1 tensile tests . . . 94
2.5.3 Tension-tension testing system . . . 99
2.5.4 Calibration of system for R>0 tests . . . 100

3 Experimental results and discussions 102
3.1 Results of fatigue tests on forged VT3-1 titanium alloy at R=-1 . . . 103
3.1.1 Fatigue life between 10^6 - 10^7 cycles . . . 104
3.1.2 Fatigue life of 10^7 - 10^8 cycles . . . 107
3.1.3 Fatigue life between 10^8 - 10^{10} . . . 115
3.2 Results of fatigue tests on forged VT3-1 titanium alloy under tension (R=0.1) 125
3.2.1 Fatigue life in the range of 10^7 - 10^8 cycles . . . 126
3.3 Results of fatigue tests on forged VT3-1 from the plateau part under tension (R=-1) . . . 134
3.4 Results of fatigue tests on extruded VT3-1 titanium alloy under tension (R=-1) 140
3.5 Results of fatigue tests on extruded VT3-1 titanium alloy under tension (R=0.1) 143
3.6 Results of fatigue tests on extruded VT3-1 under tension (R=0.5) . . . 145
3.7 Influence of the fabrication process on the gigacycle fatigue behaviour of VT3-1 147

4 Ultrasonic Fatigue Torsion Testing System 151
4.1 Introduction . . . 151
4.2 Gigacycle Torsion Fatigue concept . . . 154
4.3 Design of torsion loading components . . . 157
4.4 Calibration of the torsion system . . . 162
4.5 Specimens for torsion tests made from VT3-1 titanium alloy . . . 166
4.6 Results of torsion tests on VT3-1 titanium alloy . . . 167
4.6.1 SN-diagram for extruded and forged VT3-1 . . . 167
4.6.2 Macroscopic view of torsion crack in VT3-1 titanium . . . 167

4.6.3 Procedure of torsion specimen 'opening' 169
4.6.4 Microscopic view of crack initiation area: SEM observations on fracture surfaces 170
4.7 Discussions and conclusion 174

5 Conclusion and perspectives **179**

6 Abstract in English **183**

7 Resumé étendu en français **187**
7.1 Matériaux 188
7.2 Microstructure 189
7.3 Microdureté 193
7.4 Les échantillons et les équipements expérimentaux 195
7.5 Les résultats des essais 199
7.6 L'Anisotropie de la propriété mécanique 204
7.7 L'effet de la contrainte moyenne 207
7.8 La fatigue gigacyclique dans l'alliage de titane VT3-1 extrudé 209
7.9 La Torsion 211
7.10 Conclusion 214

References **229**

ANNEXES **230**

I would like to dedicate this work to my Supervisor Professor Claude Bathias. The importance of Claude Bathias in my life is very difficult to overestimate. During these four years he helped me to pass the way from a child to young man. Thanks to M.Bathias I got the perfect education and it is not just knowledge in languages, material science or mechanics. M.Bathias is Gentleman, Professor, Scientist, Friend where each word is from the capital letter. In all the life situations you learn from him the best human behavior, the very high professionalism, respect to people, decision making and the best humor. If you will do a mistake he will never say to you that your are incompetent. He will softly make an accent on the wrong part of your sentences/phrase/work or behavior. After that you will rethink this situation. Of course you will become 'red' (because you will be ashamed for such mistake) and you will get this knowledge very effective. You are trying to match M.Bathias when you are next to him and year by year you form your personality. I am very grateful to M.Bathias for his care, help, the time spending for me and finally for the young man that he helped to grow up from me.

I would wish a good health, long life (gigacyclic plus) and all the best to my Supervisor. I will try to carry out all knowledge that I learn from You through the whole my life.

Acknowledgements

First, I would acknowledge all my supervisors: Prof. Claude Bathias, Prof. Andrey Shanyavskiy and Prof. Thierry Palin-Luc. It was the first project of cooperation between Paris University 10, Moscow State Technological University and Arts et Metiers. I would thank you for your continuous work, useful and productive contribution to this project, your patience and professionalism.

Personally I would like to thanks M. Bathias for the World which he opened for me. Many of my dreams were realized in connection to this PhD project. I was dreaming for the flight on the aircraft and the very first flight in my life was to Paris. I was dreaming to visit Europe one day and this day arrived the 6 october 2010. I saw many Paris monuments in an encyclopedia of my grandmother when I was child and I saw these monuments in reality during the PhD project. It is just one side of my dream. The second part of the dream is to become a more educated person. I learn many things from you and I want to say you 'Thank You'! I am grateful for getting to know You and to be your PhD student.

I would like to thank Andrey Shanyavskiy for his supervision. For long walks and discussing very different questions. I thank You for my education in literature, culture, arts, poesy, history and science. You are very originative, kind, interesting person. I would like to thank you for all your lectures that you did for me. I would like to thank you for the work that you did before this PhD project, because without this work, we never have this cooperation. I would like to thanks you for all the day-off that you spent with me in the laboratory in front of microscope. For the personal support and all the dinners with soup that you cooked. Thank You very much for that and many-many things that you did for me and for this project.

I would like to thanks Thierry Palin-Luc for the work with me. It is very interesting for me, I think that you broke one of the most strong barrier in my personality that was my own problem for a long time. With you I studied to be honest with himself and to be able to say: 'Yes, it is a problem and I don't know how to solve it, let's discuss!'. Might be my problem came from the USSR education because at the time we never had 'unsolved' problems. Thanks to our open discussions I becomes more open and I like this tendency. I would thank

you for your kind care about me. Each time when I had some difficulties (health, accident on the bicycle and many others) you were always very kind with me. Thank you for that very much. You give me many useful informations and skills during his PhD study. And moreover I remember the joint trip to Arcachon with You and Prof. Oleg Neimark. I thank you for discovering the south-west of France. You worked hard on organisation of my PhD for defence and with your work it become possible. I thank you for your supervising

I would like to thank France because it (or she) changed me a lots. I very love the spirit of France and culture. The life in this beautiful country opened for me a very new understanding of the life. I become more tolerant to different religions and nations. Right now for me there are no borders between countries and confessions. The human is his personality and just after nation and religions. The Science and Friendship have not borders. At the same time I love that we have many different nations, but it is very important to feel that all cultures are unique and therefore there is no the best one and worst one. I'm totally against any wars and dreaming to reach the peace in the World. France is very open country for exchange of culture and at the same time France keep its own culture. This is fantastic!
I would like to thank my very good friends from the laboratory LEME and I2M. Most of them are doctors now. First of all I would thank Prof. Eric Kuhn and Prof. Chang Wang (Alex). They became my very close friends and I thankful them for all moments of our PhD study. In fact all the people from the both laboratories were very friendly with me and grateful them for their attitude. Unfortunately I cannot say thank you personally to each of these people, but you have to know that I miss you and want to say thank you.

I want say thank you to M.Morel, president of LASUR company. He is very kind and nice man and it is pleasure to work and to discuss with him. You are very sensitive people and I want to say you thank you very much for some discussions and conversation in difficult moments of the life. It was very in time and very useful. Thank You M.Morel.

I want to say thank you to personal of State Centre for flight safety for your professional work and friendly atmosphere.

The last but not the least, I would like to say THANK YOU VERY MUCH to my family, my mama Nina Nikitina, my father Dmitriy Nikitin and my brother Alexey Nikitin. You were alway with me and support in all situation whatever happens. I think that just when you are far from the home you understand how it is important to have you family and your own home.

Introduction

This PhD thesis was prepared in the framework of a cooperation between the University of Paris Ouest Nanterre La Defense, Arts et Métiers ParisTech (Bordeaux campus) and Moscow State Aeronautic Technological University. This thesis was co-directed by Prof. Claude Bathias from LEME (Laboratoire Energetique Mechanique Electromagnetisme) in Ville d'Avray and Prof. Thierry Palin-Luc from I2M (Institute of Mechanics and Mechanical Engineering) in Bordeaux with the participation of Prof. Andrey Shanyavskiy from The State Centre for Flight Safety of Civil Aviation (Moscow). The main part of the financial support was provided by LASUR company through a CIFRE grant. Furthermore the material studied in this project was given by the State Centre for Flight Safety of Civil Aviation.

This PhD project concerns the problem of fatigue failure in bi-modal ($\alpha + \beta$) titanium alloy after very long fatigue life (10^6 - 10^{10} cycles). Such titanium alloys are commonly used for producing compressor disks and blades of aircraft engines. During their service life these components are subjected to repeated cycling loading due to the combination of "take off and landing" (or flight cycles), rotation of the engine and air flow through the compressor. Many works have been done in the world to study the fatigue strength of titanium alloys in low cycle fatigue (LCF) regime (less than $\sim 10^5$ cycles corresponding to "flight" cycles) and in the conventional high cycle fatigue (HCF) regime (about 10^6 - 10^7 cycles, corresponding to cyclic loading due to the rotation of the engine shaft). In spite of many investigations on the fatigue properties of two-phase titanium alloys in LCF and HCF some recent papers [1, 2] about in-service fatigue failures in aircraft engines have reported so-called 'unexpected' or premature failures. Detailed analysis of the reasons of such fatigue failures have shown that high frequency vibrations could play an important role on the fatigue life of the compressor blades. Indeed, it has been shown, that frequency of such vibrations are lying in the range: 1 kHz to several kHz, that lead to the accumulation of very high number of loading cycles during service life of an aircraft engine (about 3,000 hours). This range is called Gigacycle or Very High Cycle fatigue (VHCF). The VHCF regime is a relatively "young" domain of fatigue, that is why there are not so many available experimental results in literature for titanium alloys. Consequently, the first objective of this PhD thesis is to investigate the fatigue behaviour of two-phase ($\alpha + \beta$) titanium alloy in VHCF regime (10^6 - 10^{10} cycles).

The material which was chosen for this study is Russian aeronautic ($\alpha + \beta$) titanium alloy VT3-1 (Ti-6Al-4Mo). The material was obtained in two different ways: (1) forged compressor disk from aircraft Tu-154 and (2) extruded bars produced by 'VILS' (All Russian institution of Light Alloys). The main purpose of this investigation was to study the fatigue resistance of forged titanium alloy under high frequency vibrations in VHCF range. High frequency vibrations simulates an influence of in-service loading due to air flow. Typically,

such vibrations are imposed on the static mean stress due to the centrifugal force. Moreover, geometry of compressor blades and perturbations in both air flow and pressure can lead to some additional loading modes, such as torsion. So, the program of VHCF investigation on aeronautical two-phase titanium alloy contain the following ultrasonic fatigue tests: (1) fully reversed tension, (2) tension under positive load ratios and (3) fully reversed torsion fatigue tests. To do that the two ultrasonic fatigue testing machines in tension (for $R = -1$ and $R > 0$) were already developed and installed before this PhD project, while the torsion ultrasonic fatigue testing machine has been designed and made during this PhD work (second objective). This objective was successfully achieved, the new machine is presented in the last chapter of this document together with first results on $(\alpha + \beta)$ titanium alloy under pure ultrasonic torsion.

Since the first systematic investigations on fatigue behaviour of metallic materials in VHCF range [3] it become evident that fatigue resistance is closely related to micro-structure of material. Particularly in case of VHCF where the crack initiation stage is the major part (more than 99 %) of the total fatigue life (up to fracture) [3]. In this regime fatigue resistance is associated to the resistance to fatigue crack initiation. For most of structural materials, such as cast iron, high strength steels, aluminium alloys the critical features of micro-structure leading to crack initiations are: (1) non-metallic inclusions; (2) porosities; (3) pores; (4) micro-structure anomalies (perlite nodules in railway steels, graphite nodules in cast iron, and so on). Aeronautic two-phase titanium alloys are high quality materials without non-metallic inclusions, porosities and pores; fatigue crack initiation is related to the organisation of alpha-phase platelets [3]. In case of forged VT3-1 for real compressor disk it was assumed, that the organisation of α-platelets and micro-structure can be depending on the orientation in disk (because of material flow during the forging process). Thus, the next objective of this PhD project was to investigate a possible anisotropy of the VHCF properties of VT3-1 titanium alloy. To do that several sets of specimens were machined from different positions in the disk and subjected to the same testing procedure. The first procedure was tensile fully reversed (R=-1) fatigue tests on specimens machined from the rim and plateau parts of the compressor disk. Specimens from the plateau part were machined along the radius of the disk, specimens from the rim part were machined in axial direction (see Chapter 2). The second testing procedure is loading with positive stress ratio (R>0). The two sets of tensile specimens from the plateau part of the disk were machined in radial and circumferential directions. These specimens were tested under pull-pull fatigue loading with R=0.1. Based on these four sets of fatigue test data it was possible to characterise the influence of position and orientation of specimens on the fatigue behaviour of the alloy and therefore to characterise a possible fatigue anisotropy of forged VT3-1 titanium alloy due to the thermo-mechanical process (forging). Moreover, the comparison of the results in

push-pull and pull-pull tests on the specimens machined from the plateau part in the same direction (radial) allows to outline some conclusions about effect of mean stress on the fatigue behaviour of forged VT3-1.

The investigation on specimens from the real compressor disk is quite expensive and not numerous due to limitation of material. There is no government programs for investigation of VHCF properties of real compressor disks that makes extremely difficult to get material. That is why, the next question which was discussed in this PhD thesis is replacement forged VT3-1 titanium alloy by the same VT3-1 produced by less expensive technological procedure (extrusion). In order to compare the fatigue properties and crack initiation mechanisms in forged and extruded VT3-1 titanium alloy four sets of specimens were machined from extruded bars. The first set of specimens was designed for fully-reversed tension (R=-1); the second set of specimen was tested under pull-pull tension (R=0.1), both with an axial ultrasonic fatigue testing machine. The third set of specimen was for torsion ultrasonic fatigue tests with R=-1. Analysis of results for forged and extruded VT3-1 titanium alloy allows to outline a conclusion about the role of the technological process on the fatigue properties and crack initiation mechanisms in the two materials under different loading conditions (including torsion). The last set of specimens was used for pull-pull tension (R=0.5) ultrasonic fatigue tests in order to investigate the influence of different positive stress ratios on the fatigue behaviour of two-phase titanium alloy in VHCF regime.
Summarizing the objectives of this PhD project, the next key purposes can be outlined:

1. The investigation of the fatigue behaviour of forged VT3-1 (Ti-6Al-4Mo) titanium alloy in VHCF range (Fully-reversed tensile ultrasonic fatigue tests).

2. The investigation of anisotropy influence on fatigue properties and crack initiation mechanisms in forged VT3-1 titanium alloy (fully-reversed and pull-pull ultrasonic fatigue tests on specimens machined from different position in the compressor disk in different directions).

3. The investigation of mean stress effect on the crack initiation mechanisms in VT3-1 titanium alloy under VHCF loading.

4. Development a new ultrasonic fatigue testing system for pure torsion tests in VHCF range.

5. The investigation of different loading modes: tension (normal stress) and torsion (shear stress) on the crack initiation mechanisms in two-phase VT3-1 titanium alloy under VHCF loading.

6. Comparison of fatigue properties and crack initiation mechanisms under different loading conditions in the same VT3-1 titanium alloy produced by forging and extrusion technologies (fully-reversed, pull-pull tension and fully-reversed torsion ultrasonic fatigue tests).

This PhD report consists of four Chapters: (1) 'Literature review'; (2) 'Material and Experimental procedure'; (3) Results and Discussions (4) Torsion ultrasonic fatigue testing system. The first Chapter consists of two main parts: 'Fatigue in metals' and 'Fatigue in Titanium alloys'. Its first part 'Fatigue in metals' introduces a historical review on the problem of fatigue in metals since 1829 up to nowadays. Naturally, it has been shown the importance of accelerated fatigue testing methods for modern applications, which are typically subjected to very high number of loading cycles. The methodology and equipments for ultrasonic fatigue testing are discussed. The first part of Chapter 1 ending by a review on the problem of fatigue crack initiation and growth under VHCF loading. The second part 'Fatigue in titanium alloys' of Chapter 1 concerns a brief introduction of titanium and titanium alloys with typical classification and properties. The review is focused on two-phase titanium alloys. Common types of termo-mechanical treatments, realizing micro-structures, analysis of slip system and resistance of different types of micro-structure to fatigue loading are discussed. The second part of Chapter 1 ending by an overview of recent investigations on the VHCF strength of two-phase titanium alloys with typical crack initiation mechanisms.

In Chapter 2 the micro-structure, micro-hardness, chemical, mechanical properties for each investigated titanium alloys are discussed. The type, position and geometries of all the specimens used for the fatigue tests are listed and described. The two ultrasonic fatigue testing machines that was used for push-pull and pull-pull fatigue tests are presented with their associated calibration methods and results of calibration.

Chapter 3 is introducing the results of tensile fatigue tests on forged and extruded titanium alloy under push-pull and pull-pull loadings. The fracture surfaces of all the specimens are analysed by SEM in order to establish the crack initiation mechanism. Some additional techniques, such as EBSD and EDX are also employed for analysing the fracture surfaces.

The last Chapter is devoted to the design of a new ultrasonic fatigue testing system for gigacycle test under pure torsion. This machine was developed during this PhD project and was one of the objectives of the work. In this chapter the very first results on the fatigue resistance in torsion after very high number of cycles are presented for forged and extruded VT3-1 titanium alloy. The analysis of fracture surface was also carried out in order to explain the internal crack initiation which were found as for forged, as well for extruded titanium alloys.

All the results of fatigue tests and fracture surfaces with crack initiation sites are presented

in the Annexes to this document.

Chapter 1

Literature Review

This chapter is separated in two main parts: 'Fatigue in Metals' and 'Fatigue of Titanium and Titanium alloys'. The first part briefly introduces the history of fatigue science, its main terms, regimes, stages, key models and assumptions. The second part is devoted for the state of arts in the field of fatigue of titanium and titanium alloys. The present study is focused on the problem of fatigue failure in two-phase titanium alloy VT3-1 after a very high number of cycles (10^6 - 10^{10}). This range of fatigue life is known as Very High Cycle Fatigue (VHCF). Thus, a particular attention will be paid to the problem of VHCF as in the first part 'Fatigue in Metals' of this chapter, as well in the second-one 'Fatigue in Titanium and Titanium alloys'.

Fatigue in Metals

1.1 History of Fatigue

The XIX-century. 'Fatigue' in materials science is the weakening of a material caused by repeatedly applied loads. It is the progressive and localized structural damage that occurs when a material is subjected to cyclic loading. The first publication about repeated loads effect on material strength was published by Wilhelm Albert in 1837 [4, 5]. In 1829 Wilhelm Albert observed the failure of iron mine-hoist chains arising from repeated small amplitude loadings. He built a testing machine which repeatedly loaded a chain and studied a new phenomena. His finding was that such fracture was not associated with an accidental overload, but was dependent on load and the number of repetitions of load cycles [4].

The term 'Fatigue' was introduced by French engineer and mathematician Jean-Victor Poncelet in 1839 [6, 7]. He describes metals as being tired under repetitive loading and since that time the term 'Fatigue' has become commonly used. According to other scientists, the

term 'Fatigue' has been introduced by Englishman Braithwaite in 1854 [8, 5]. By the middle of XIX-century Fatigue became an important engineering problem for numerous industries (railways, bridges and vehicle). In that time, design of machines did not take into account any influence of repetitive loading that led to numerous fatigue failures in different engineering applications: water pomps, propeller shafts, crankshafts, railway axles, levers, cranes, etc [8]. In this period many disastrous rail-road accidents were occurred. One of the most dramatic and well known catastrophe in railway industry due to fatigue was the crash of a passenger train on the Versailles railway track in 1842 [9, 10]. Thus, few years after the first report about in-service failure under cyclic loading, fatigue became a very important engineering problem. Many engineers in Europe (England, France, Germany) were working on the problem of fatigue [11, 8, 12]. Special meetings on the problem of fatigue in railway industry were organized in the 'Institute of Mechanical Engineers', London [5, 7].

By the middle of the XIX-century it has been shown, that fatigue fracture surface shows some evidences of brittle cracking. The common hypothesis to explain that was an idea about changing in iron structure under repeated loads [13, 7]. It was erroneously assumed, that under repetitive loading a fibrous structure of iron turns to crystalline. This question was discussed for a long time in meetings in 'Institution of Mechanical Engineers' [7, 5] and was one of the first discussions about fatigue in material science sense. An important idea was proposed by Paul Raspey Hodge in 1850 [14]. He suggested to use microscopic analysis for studying changes in iron structure. Soon afterwards, Stephenson has presented results of his observations on iron 'known as fibrous' and 'known as crystalline'. He concluded that there is no noticeable difference in these two materials [15]. Similar result was found in tensile tests on axis subjected to high number of cyclic loads before tensile test [7]. Fracture surface of axis under monotonic tensile did not show any evidence of brittle cracking in spite of cyclic preloading.

An important work on fatigue in railway axis was published in 1842 by Scottish civil engineer William J.M. Rankine. He reported that fatigue rupture of railway axis under repeated loads starts from a small surface crack [12, 7]. He found, that such crack mainly occurs at the section changes of axis [5]. This is the first publication about the role of stress concentration in fatigue. The same results were found for axis of horse-drawn mail coaches. French physicist Arthur Morin in his book [16], discusses reports of two engineers working for horse-drawn mail. They suggested to thoroughly inspect axles of mail coaches after 70 000 km, because as usual small cracks were observed in section changes after such in-service [7]. The replacement of the axles of the coaches was prescribed after 60 000 km, it is an early example of 'safe life' design approach [5]. Moreover, an early approach of 'fatigue limit' can be found in experiments of Henry James and Galton [7]. They investigated bars, subjecting to reiterated strain corresponding to loads equal to some fractional part of the breaking weight

[17]. Henry James and Galton shown that iron bars can withstand cyclic loads amplitude of one-third of statical breaking-weight without having fatigue rupture after 10 000 cycles. Fairbairn discuss a question about maximal load amplitude, which can be applied to material without fatigue failure [17, 7].

Thus, by the beginning of 1860th a notable empirical knowledge about fatigue has been accumulated in different industries. Only in 'Institution of Mechanical Engineers' was a collection of hundreds, if not thousands of failed railway axles [5]. Nonetheless these investigations were not systematic.

Work of August Wohler 1858-1870. The first systematic investigation on the fatigue behaviour of materials is related to the name of German engineer August Wohler. August Wohler (22 June 1819 - 21 March 1914) Fig.1.1 was born in Soltau, graduated in the Technische Hochschule in Hannover and since 1840 was engaged in railway industry.

His first works were aimed at reducing of accidents on railway. In 1858 A.Wohler presented a self-developed deflection gage for measuring in-service loads of railway axles [18]. The first results has shown that spectrum of load consists of small amplitude loading mixed with a significant amplitude loads due to imperfection of railway track. In the following, he built the machine for fatigue tests and investigated railway axles under maximal loads which were measured during in-service. Based on his investigations he assumed that critical destructive influence on axis is related to significant amplitude loads. Wohler draws the following conclusion: 'The number of high amplitude cycle per trip is considerably smaller than the number of miles the axle travels during its life. Therefore, the safety requirements are met if the axles can withstand the maximum stresses measured as many times as its expected life in miles' [5]. Thus, Wohler implicitly suggested to design for finite fatigue life taking into consideration even the scatter of fatigue life. At early 1860, Wohler published the results of fatigue tests with railway axles [19, 5].

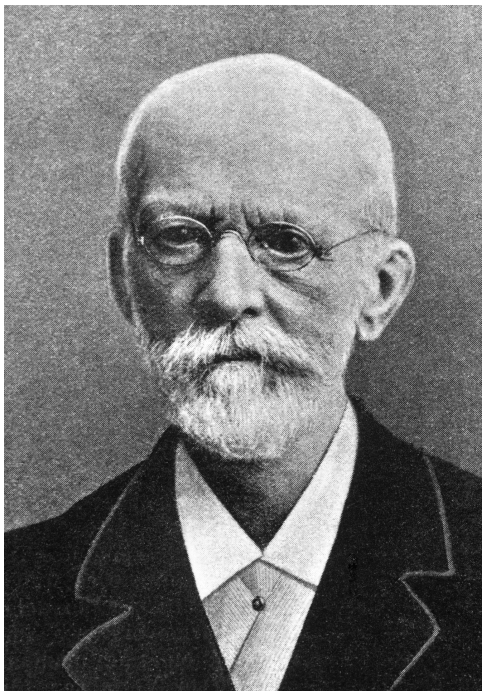

Figure 1.1: August Wohler

Fatigue tests on full-scale elements (railway axles) were expensive and time-consuming, that's why Wohler designed specimens for fatigue tests, which were smaller than railway axles [7]. He helped to establish a network of laboratories in Germany for investigation on material

properties and help to develop standards for fatigue tests. Wohler carried out torsion tests between zero and a maximum stress, torsion fully-reversed tests, tension between various limits of minimum and maximum (different stress ratios) and rotating bending where the stress were fully reversed [20]. In 1870 Wohler presented a final report on his fatigue investigations from 1858 to 1869 years [21, 5]. Wohler incidentally represented his test results in the form of tables. Only in 1874 Spangenberg [22] plotted them as curves, although in the unusual form of linear abscissa and ordinate. The SN curves were called "Wohler curves" since 1936 [5]. Wohler drew the following conclusions: 'Material can be induced to fail by many repetitions of stresses, all of which are lower than the static strength. The stress amplitudes are decisive for the destruction of the cohesion of the material. The maximum stress is of influence only in so far as the higher it is, the lower are the stress amplitudes which lead to failure.' are now known as 'Wohler laws' [5].

The 1870th - 1900th years. The important study on the problem of material behaviour under repeated loads in the last third of XIX-century was work of Johann Bauschinger. He studied the influence of stress beyond elastic limit and repeated cyclic loading on mechanical characteristics of metal (elastic limit, yield point) [20]. Bauschinger stated that a tensile stress above yield point increases the yield point, decreases elastic limit and lowers modulus of elasticity (idea about cyclic hardening). Tensile stress above elastic limit but below yield point, increases elastic limit in tension and reduces elastic limit in compression. Gradually increasing alternating stress in tension and compression will not decrease an opposite elastic limit unless one of the original elastic limits is exceeded (idea about mechanical hysteresis). Repeated stress between zero and upper limit which coincides with or close to elastic limit will not cause rupture (idea about 'fatigue limit'). Repeated loading beyond elastic limit will lead to failure after a limited number of repetitions. Many Bauschinger's ideas were used for models of fatigue behaviour developed in the XX-century.

Summarizing the results of investigation on fatigue in the XIX-century it should be pointed out, that problem of fatigue was mainly an engineering problem. Most of the fatigue tests were carried out on full-scale elements and were aimed to decrease accident numbers in different industries (mainly in railways). The first systematic investigations were carried out by August Wohler. Wohler introduced tests on specimens instead of 'full-scale' tests and carried out fatigue tests under different loading conditions (torsion, bending and axial tests with various stress ratio). Wohler introduced very important concept for engineering of finite fatigue life, safety factors, 'fatigue limit'. The first discussions on 'Fatigue' as about metallurgical problem are also dated by XIX century (fibrous and crystalline structure). Though this first hypothesis was erroneous, it contributed to the development of microscopic analysis in fatigue.

The 20th-century. Interest to the problem of fatigue has continued to increase in th

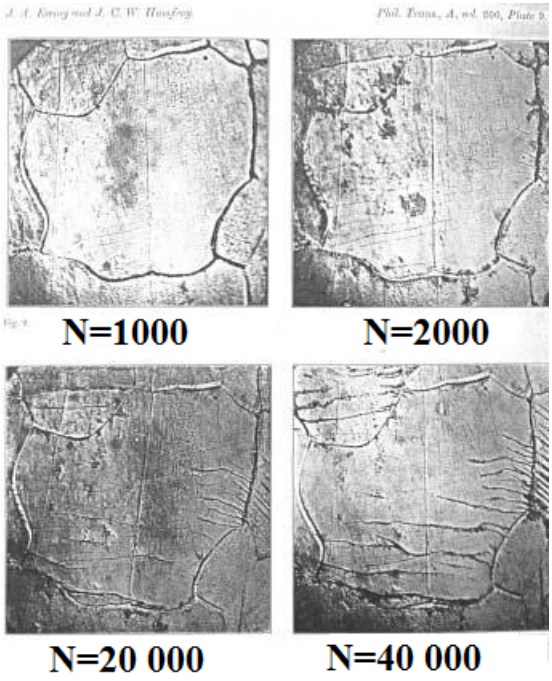

Figure 1.2: Slip Bands under cyclic loading [25]

XX-century, as shown by the number of publications. In the review paper [23], Schijve referenced to the book of John Mann [24] and said that more than 100,000 publications were presented in the XX-century on the problem of fatigue (compare with about 100 publications in the XIX-century). Thus, detailed discussion of all published in XX-century works is not possible within present section, that's why key publications and ideas will be covered only.

In the XX-century fatigue began to bee seen as a metal problem. A fundamental step in this development was made in 1903 by Ewing and Humfrey [25]. They carried out fatigue tests on Swedish iron with periodic observations of specimen's surface by microscopy. Results have shown that repeated loading initiates so-call 'slip-lines' [26] or 'slip-bands' in individual crystals, Fig.1.2.

Thus, Ewing and Humfrey stated the importance of plastic deformation in process of fatigue damage accumulation and associated it with crystalline structure of metals. Probably it was the first metallurgical description of the fatigue process. Since that time a huge number of metallurgical papers on fatigue has been published [5]. One of the following important work was investigations of Gough and Hanson by using X-ray technique [27]. They recognized the fundamental role played by plastic inhomogeneities in fatigue as well as in elastic after-working and hysteresis. Development of the dislocations theory allowed to explain the plasticity of crystals [28, 29]. In 1939 Orowan applied the theory of dislocations to fatigue [30]. Numerous models of fatigue has been developed and still developing based

on dislocation theory [23]. Dislocation theory was also employed for explaining as crack initiation [31, 32], as well a crack propagation [33]. Nonetheless, the fundamental nature of fatigue is not clear up to now.

In parallel, the knowledge about fatigue has been developed as engineering science. In 1910 Basquin [34] represented the finite life region of the 'Wohler curve' in the form '$log(\sigma_a)$' (stress amplitude) on the ordinate, '$log(N)$' (number of cycles) on the abscissa and described it by the simple equation $\sigma_a = C(2N_f)^n$ which is still used today [5]. The constants 'C' and 'n' can be determined from fatigue tests. By plotting the results of fatigue tests on such diagram a characteristic fact is revealed. In general, a curve consists of two straight parts: one inclined and one *practically* horizontal [30] Fig.1.3.

The horizontal asymptote of the S-N curve is called the fatigue limit (in some publications the name 'endurance limit' is used too) [23]. Nonetheless, it was shown, that not all structural materials shows a clear horizontal asymptote, like illustrated in Fig.1.3. Some materials, like aluminium and copper, may fail even under small stress amplitudes after sufficiently high number of cycles. Moreover, in 1980s it has been shown by Japanese researchers [35, 36], that even materials known as material with clear asymptote may be failed by alternating stress below 'fatigue limit'. Recently, in 1990s Prof. Claude Bathias have stated for the first time that there is no 'fatigue limit' in metallic materials [37, 38].

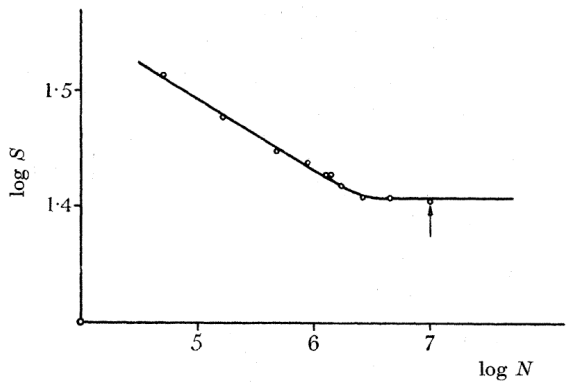

Figure 1.3: SN-curve in log-log scales

The curve presented in Fig.1.3 represents 'stress-controlled' model. However, under stress amplitudes close to yield point, almost all material is involved in plastic deformation. In this case plastic strain seems to be more sensitive measurement of life than the nominal stress [39]. This idea was developed by Coffin and Manson and introduced as 'strain-controlled' model of SN-curve [40, 41]. In this model a plastic strain is the key driven parameter instead of the nominal stress. Thus, fatigue data are plotted on $log(\Delta\varepsilon_p)$ ($\Delta\varepsilon_p/2$ is amplitude of plastic strain) versus $log(N)$ diagram. The obtained curve was described by equation 1.1, known nowadays as Coffin-Manson law.

$$\frac{\Delta\varepsilon_p}{2} = \epsilon_f(2N_f)^c \tag{1.1}$$

where $\Delta\varepsilon_p/2$ is the plastic strain amplitude, N_f - the number of cycles to failure, ϵ_f and c

are material constants

High amplitude loading leads to large plastic deformation and earlier fatigue crack nucleation. Thus, a significant fraction of total fatigue life is related to fatigue crack growth. In 1937 Langer in his work about fatigue damage accumulation [42] has separated fatigue life into crack initiation and propagation phases. In his damage accumulation hypothesis, Langer suggested a damage sum of 1.0 for each phase, however for application of this hypothesis crack-propagation curves were necessary. Fatigue crack growth models, which were developed before the 1960s are based on dislocation theory [33] and cyclic strain hardening [23]. After detection of striation in 1950s [43] these models become not credible. Fatigue striation has shown, that crack growth is cycle-by-cycle process [44], that contradicted discrete models based on cyclic strain hardening. Almost at the same time with detection of striations, Irwin has introduce the stress intensity factor (SIF) for analysing stress field around the crack tip [45]. It was a milestone in developing fracture mechanics.

In 1961 Paul C. Paris and co-workers [46] have introduced stress intensity factor for correlating the crack growth rate, da/dN, and the stress intensity factor range ΔK, equation 1.2. Soon afterward this equation was called as 'Paris law'.

$$\frac{da}{dN} = C(\Delta K)^m \tag{1.2}$$

where da/dN is increment of crack length per cycle, ΔK is range of SIF, C and m are experimentally obtained for each material and loading ratio. This relation can be plotted on $log(da/dN)$ - $log(\Delta K)$ graph, which is known as crack growth diagram (see Fig. 1.17). Experimental results have systematic deviations from the Paris equation at relatively high and low ΔK. It has led to the definition of three regions in da/dN - ΔK graph: threshold region; stable crack growth (Paris regime) and fast crack propagation. Thus, Paris' law allows to calculate the propagation of crack of arbitrary shape under arbitrary stress types (bending, axial, etc.) via ΔK in 'stable crack growth' region that is already an enormous step in fatigue science. The fundamental contribution to an improved calculation of crack propagation under service-like amplitudes was supplied by W. Elber. In 1968 he found out that after a high tensile load the crack close before the load is reduced to zero [47, 5].

In 1970 W.Elber stated that the tip of a growing fatigue crack could be closed at a positive tensile stress ('crack closure effect') [48]. The more detailed mechanism of fatigue crack closure can be found in the work of Ritchie [49]. Further, W. Elber argued that a load cycle is only effective in driving the growth of a fatigue crack if the crack tip is fully open and defined the 'effective' range of stress and SIF, equation 1.3

$$\sigma_{eff} = \sigma_{max} - \sigma_{open} \qquad and \qquad \Delta K_{eff} = \beta(\Delta\sigma_{eff})\sqrt{\pi a} \tag{1.3}$$

where β is the geometry factor, σ_{open} is the stress corresponding to crack opening. Thus, the crack growth equation 1.2 can be modified by replacing ΔK by ΔK_{eff}, but it will be still credible just in the 'Paris regime' of the crack growth diagram.

In the 1970s a particular attention has been paid to the 'threshold range' of fatigue crack growth. The main question was 'for which physical reason should there be a threshold ΔK_{th} below which the crack should not grow any more?' [23]. Experimental studies on the crack growth under low ΔK-values has shown, that micro-cracks or short cracks can develops even under $\Delta K < \Delta K_{th}$ [50]. The first relevant paper about such micro-cracks growth was published by Pearson in 1975 [51]. He has shown that these cracks occur as micro-cracks in the beginning of the fatigue life starting at the material surface or just subsurface. Moreover, micro-cracks are growing much faster than large macro-cracks under nominal similar ΔK-values. The development of short crack problem is related to the name of K.J.Miller [52].

Almost at the same time, in the 1980s, the new problem of fatigue failures after very long fatigue life appeared [35, 36]. The first systematic investigations on different materials (cast iron, bearing steels, aluminium and titanium alloys) has been carried out by Bathias [3]. He used self-developed ultrasonic fatigue testing machines [53] with piezoelectric transducer (see ANNEX B and [3]). Similar investigations were carried out in several laboratories over the World. C.Bathias introduced the term 'gigacycle fatigue' for this new range of fatigue life (beyond 10^7) and stated, that there is no infinite fatigue life ('fatigue limit') in metal materials [37]. The typical features of gigacycle regime was a changing (not for all metals) in crack initiation mechanisms from surface to subsurface location after a long fatigue life (beyond 10^7 cycles). The model of subsurface crack growth was developed by P.C.Paris and C.Bathias based on principles of fracture mechanics. This model deals with so-called 'fish-eye' crack. Such name of crack was proposed because of typical geometry of internal cracks which remains eye of fish. It has been found that internal crack initiates from material flaws like non-metallic inclusions, 'super-grain' (micro-structural inhomogeneity) or porosity [54] (see Section 1.6.1). For many materials, especially steels and nickel base alloys, inclusion can be significant crack initiation sites, especially under high stress ratios. The outstanding work about influence of non-metallic inclusions on fatigue behaviour was carried out by Yukitaka Murakami (Japan) [55]. Y.Murakami introduced formula (Eq.1.4) to estimate the fatigue strength of material at 10^6 cycles based on both its Vickers hardness Hv and the projected defect (inclusion) surface $\sqrt{area}$.

This equation has been adapted by C.Bathias and P.C.Paris for different fatigue life. They introduced a correlation factor depending on N_f. [3].

$$\sigma_{end} = \frac{C\,(Hv + 120)}{(\sqrt{area})^{1/6}} \left[\frac{(1-R)^3}{2}\right]^{\alpha} \tag{1.4}$$

where R is the stress ratio, C and α are constants

The investigations on fatigue in the XX century were stimulated as by the needs of industries for designing against fatigue, as well by scientific interest to understand the fatigue phenomenon. During the 20th century, and predominantly in the second half of this century, numerous research programmes on fatigue problems were carried out. Development of experimental and observations techniques allows to deeper understanding the nature of fatigue, however the character of the understanding is primarily qualitative. It was conclude that quantitative prediction of fatigue properties of a structure cannot be given because of the qualitative understanding of the complexity of fatigue damage accumulation [23] is still an open problem. Nonetheless, different quantitative models of fatigue has been developed: Coffin-Manson law [41], Miner law, Paris law [46], 'Fish-eye' crack, Murakami formula [55] and others. The fundamental nature of fatigue: irreversible deformation under cyclic loading, has been discovered [25], but specific mechanisms for certain materials with complex micro-structure are still under discussion. The new fatigue regime (fatigue after very high number of cycles [56]) has been discovered. The new problem of near threshold fatigue crack was introduced [51, 52] and the absence of fatigue limit in physical sense for metals has been stated [37, 38].

The recent development of experimental techniques, like in-situ tests under simultaneous Scanning Electron Microscopy (SEM) observations [57] and observation methods like a micro computed tomography [58] suggests further understanding of fundamental fatigue nature at micro and nano scale levels.

1.2 General concepts of Fatigue

Many different testing methods have been developed since the first fatigue tests: from uniaxial loading to multiaxial, from constant amplitude loading to variable and random loading, from extremely low loading frequencies (thousandths of a Hz) up to tens of kHz, from tests in aggressive environments to tests in vacuum, from fatigue tests at cryogenic temperature to elevated temperatures and so on. However, the general concepts of fatigue tests was kept almost the same over the whole history of Fatigue. This section introduces the basic terms and concepts of fatigue test procedure.

Since the 19th century a procedure of fatigue tests is based on cyclic loading applied to full-scale element or specimens. The shape of loading cycle can be different from sinusoidal to triangular, trapezoidal. Two types of loading controls are used nowadays: load-controlled and stain-controlled loading. The driving parameters for these loading are nominal stress

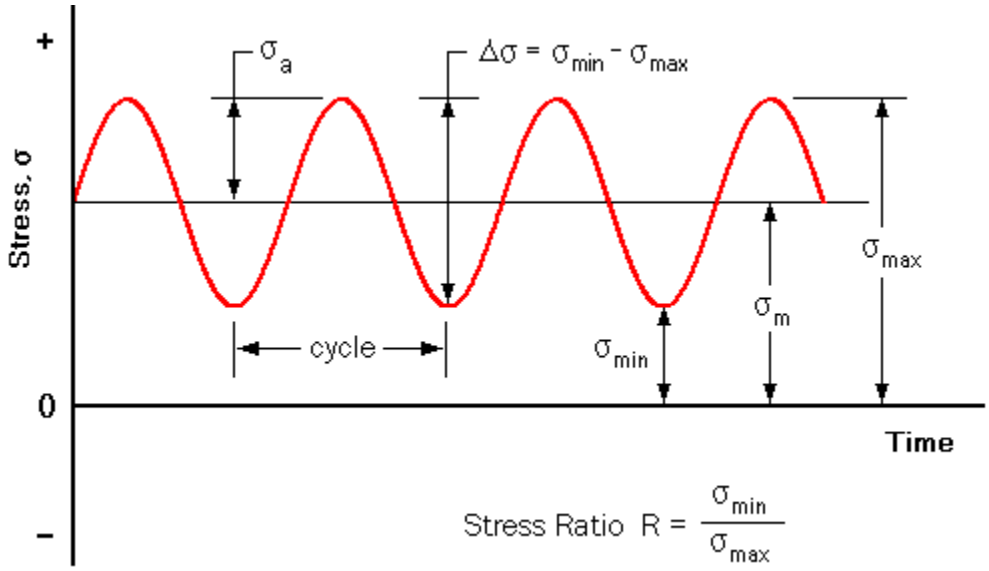

Figure 1.4: The typical cyclic loading parameters

amplitude σ_a and strain amplitude ε_a respectively. For low loading amplitudes compared to the yield point, the stress-controlled technique is commonly used. Without loss of generality only a stress-controlled procedure will be discussed below. Typical history of sinusoidal loading is shown on Fig. 1.4. The loading consists of two parts: static stress or mean stress σ_m and alternating stress with amplitude σ_a. Thus, the maximal stress can be expressed as $\sigma_{max} = \sigma_m + \sigma_a$ and minimum stress is $\sigma_{min} = \sigma_m - \sigma_a$. The static stress has a significant influence on the fatigue behaviour of material as shown for the first time by A.Wohler. The relation between minimum and maximum stress is called as 'stress ratio' $R = \sigma_{min}/\sigma_{max}$ or in terms of mean stress and amplitude, equation 1.5.

$$R = \frac{\sigma_m - \sigma_a}{\sigma_m + \sigma_a} \tag{1.5}$$

The tests with non zero-value of mean stress called asymmetric loading. When the mean stress is equal to zero, the cycle becomes symmetrical and called fully-reversed loading with *R=-1*. The range of stress is introduced by difference between maximum and minimum stresses $\Delta\sigma = \sigma_{max} - \sigma_{min}$. This value is often used for the calculation of crack growth rate according to the 'Paris's law', Eq. 1.2. As usual fatigue tests are carrying out up to reach one of the following conditions: fatigue failure or a certain fatigue life which is called 'run-out limit'. The conventional interpretation of fatigue data is so-called 'S-N curve' or Wohler curve Fig.1.5. The axis of abscissa is the number of cycles to failure N_f in logarithmic scale; the axis of ordinate is stress amplitude σ_a. Some metals shows a distinct knee in SN-curve (these materials are called as having 'a physical fatigue limit'), other does not show such

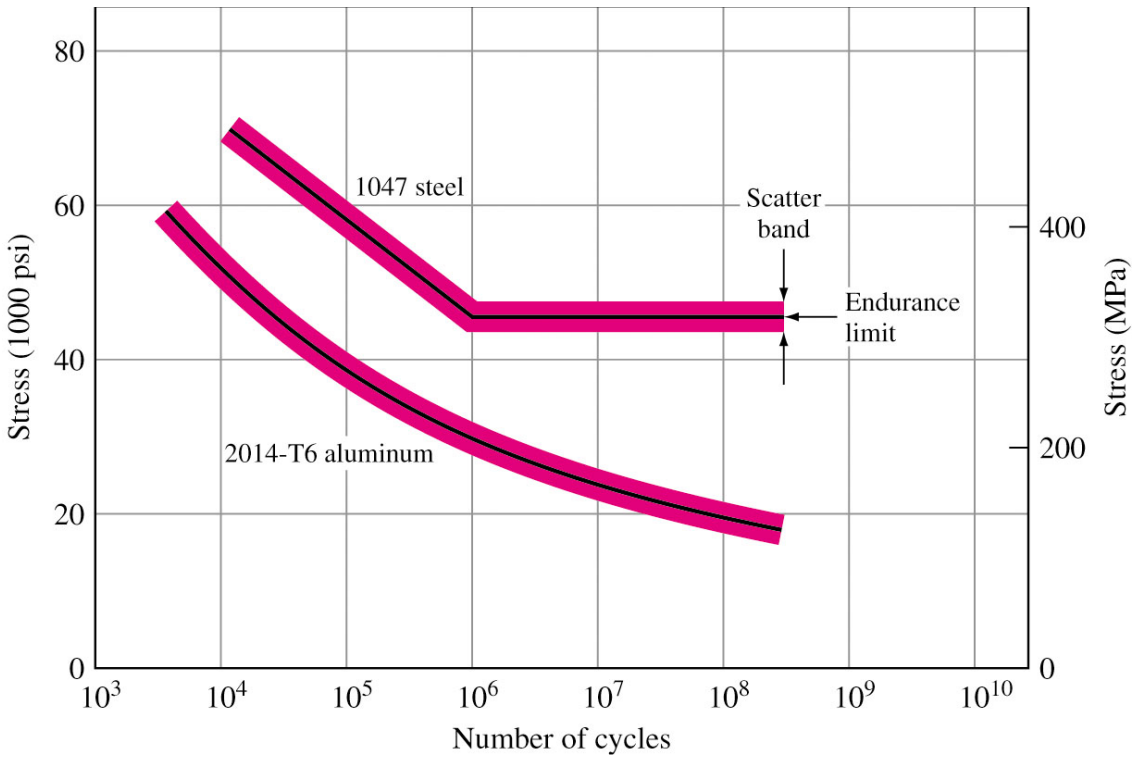

Figure 1.5: Typical SN-curve for metals

knee (materials without 'physical fatigue limit'). Recent investigations on material fatigue strength slightly below the 'fatigue limit' have shown, that there is no 'safe' stress amplitude and failures may occur after a high number of loading cycles. Thus, it is more correct to use the term 'fatigue endurance' σ_{end} or 'fatigue strength' at a given number of cycles. In case of asymmetric loading the maximum stress σ_{max} is usually used for ordinate.

Another common representation of fatigue data for asymmetric fatigue tests data are so-called 'Smith diagram', 'Haigh diagram', 'Goodman diagram' [59] and so on. The tendency to associate personal names with particular concepts sometimes led to numerous different names for the same concept [60]. The main idea of these diagrams is plotting alternating stress σ_a versus mean stress σ_m Fig.1.6 (a). The diagram is separated by linear Eq.1.7 - 1.9 or parabolic curves Eq.1.6 into 'finite fatigue life region' and 'infinite fatigue life region'. It is assumed, that below these line the fatigue failure will not occurs under a certain combination of σ_a and σ_m. Names of diagrams are associated with authors of these equations. Since 1874 several models explaining an effect of mean stress were developed. The outstanding equations are following: Gerber model, Eq.1.6 (1874), Goodman model, Eq.1.7 (1899), Soderberg model, Eq.1.8 (1930) and Morrow model, Eq.1.9 (1960s).

$$\frac{\sigma_a}{\sigma_{end}} + \left(\frac{\sigma_m}{\sigma_{UTS}}\right)^2 = 1 \tag{1.6}$$

$$\frac{\sigma_a}{\sigma_{end}} + \frac{\sigma_m}{\sigma_{UTS}} = 1 \tag{1.7}$$

$$\frac{\sigma_a}{\sigma_{end}} + \frac{\sigma_m}{\sigma_y} = 1 \tag{1.8}$$

$$\frac{\sigma_a}{\sigma_{end}} + \frac{\sigma_m}{\sigma_f} = 1 \tag{1.9}$$

where σ_{end} is fatigue endurance at a given number of cycles, σ_{UTS} is ultimate tensile strength, σ_y is yield stress and σ_f is true fracture stress

To construct 'Haigh diagram' series of SN-curves (Fig. 1.5) for different stress ratios (including R=-1) should be obtained. Based on these SN-curves the fatigue strength at a given number of cycles should be determined. These values of fatigue strength can than be used to construct 'Haigh diagram', which gives the stress amplitude as a function of mean stress [61]. Another common representation of fatigue tests with non-zero mean stress is so-called 'modified Goodman diagram', Fig. 1.6 (b). This graph is a plot of maximum stress (σ_{max}) versus minimum stress (σ_{min}). Fig. 1.6 (b) shows clearly the relation between different pairs of stress variables [62] and stress ratios.

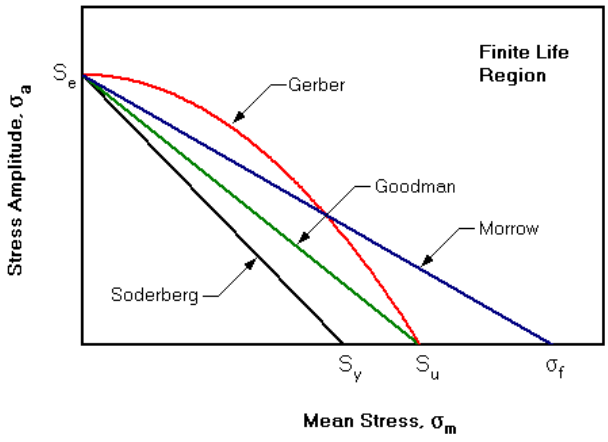

a)

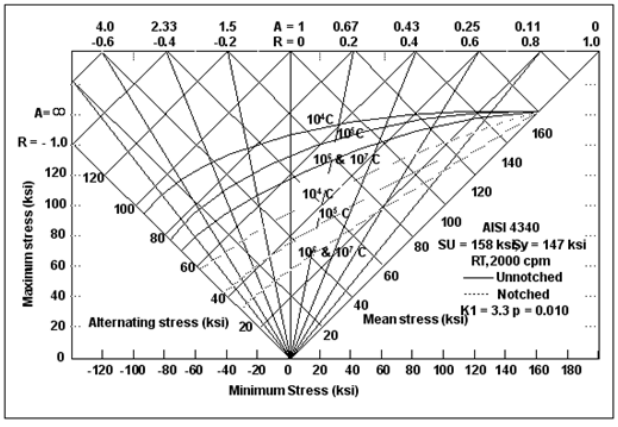

b)

Figure 1.6: The graphic interpretation of asymmetric fatigue tests results

The all presented in this section discussion are fair for majority of fatigue tests: bending, torsion, axial loading.

1.3 Regimes of Fatigue

At the beginning of systematic study on the problem of fatigue failures [21], the range of investigated fatigue life was about 10^5 - 10^6 cycles. This fact forced the first researchers of fundamental nature of fatigue to work in the denoted range [25]. Ewing and Humrey have shown, that cyclic loading produces so-called 'slip-lines' at the surface. They noted, that under higher loading amplitudes more grains show such lines, compared to the lower amplitudes. Moreover, they found, that under higher amplitudes, different systems of 'slid-lines' can be observed, while with decreasing the amplitude just strait lines in few grains can be found even below the 'fatigue limit'.

In the middle of the XXth-century, it has been understood, that not all engineering components requires a long safe fatigue life. Some engineering applications are submitted to just a few high amplitude loading cycles during their whole in-service life. Since that time works on fatigue behaviour of material under high (comparable to yield strength) loading amplitudes have been started [40, 41]. Thus, by the middle of the XXth-century two loading regimes and the first classification were introduced. The region of short fatigue life ($N_f = from\ 1\ to\ \simeq 10^4$ cycles) under high loading amplitude was called Low Cycle Fatigue (LCF). The region of 'long' fatigue life ($N_f \simeq 10^5 - 10^6$ cycles) under lower loading amplitudes was called High Cycle Fatigue (HCF).

With development of aeronautic industries, it has been found, that some components of turbojet engines are subjected to the high frequency vibrations. High frequency loading lead to very high number of cycles during a typical in-service life. 'Unexpected' fatigue failures in aircraft engines forced to investigate materials in the range of very long life ($10^7 - 10^9$ cycles). It has been found, that even below the 'fatigue limit' structural materials can failed due to fatigue [3]. Since that time a new domain of fatigue, called Gigacycle or Very High Cycle Fatigue (VHCF) region, was introduced. The Figure 1.7 illustrates the modern classification of fatigue regimes [38].

The fatigue regimes not only differs by fatigue life and stress amplitudes, but also the crack initiation mechanisms are different for these domains [3]. Initiation mechanisms can be defined by plastic strain. Under high loading amplitude(LCF), almost whole material experiences plastic deformation. In engineering terms the amplitude of plastic strain is significant (the width of hysteresis loop is large), Fig. 1.3. Several sliding systems in each material grain are involved in deformation process. Under such loading conditions, the critical state of material can be achieved almost simultaneously at different points at the material surface (the grains close to the surface are less constrained and typically plastic deformation is more preferable at the surface [63]). Thus, multiple surface cracks initiates under LCF loading.

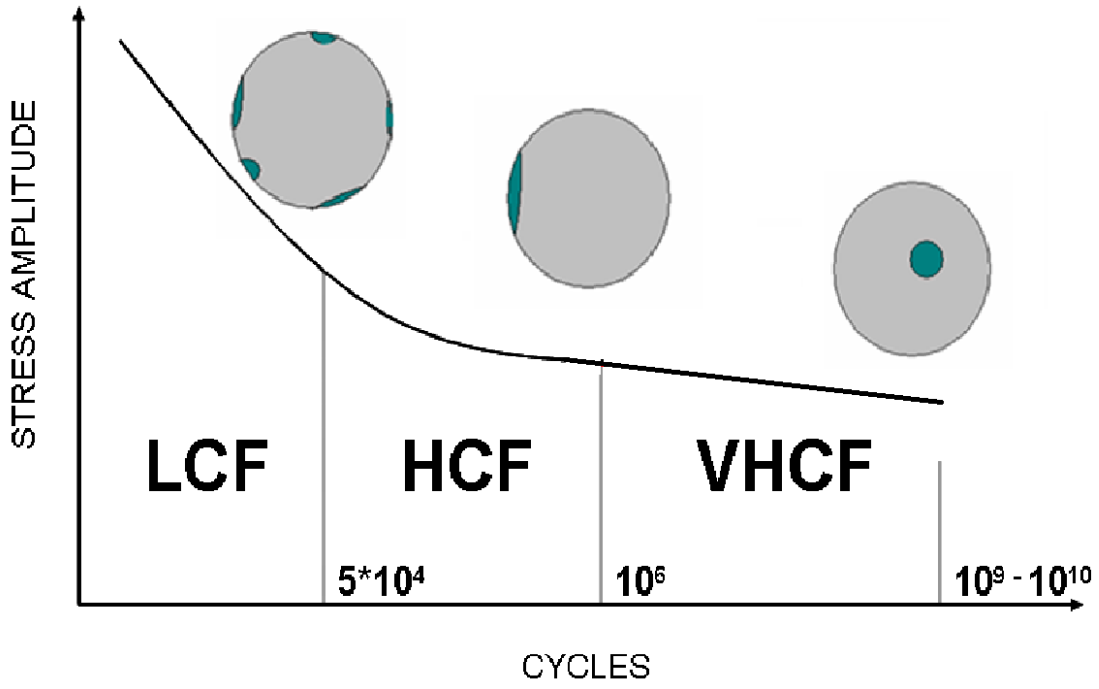

Figure 1.7: Regimes of fatigue with character position of crack initiation site [38]

With decreasing the loading amplitude, the plastic deformation becomes less important. Just a few grains are involved in plastic deformation process and the number of sliding systems activated in these grains is reducing. In engineering terms the width of hysteresis loop is diminishing with decreasing the loading amplitude, but is still finite at the 'fatigue limit' [64]. Under such loading conditions the plastic deformation is localized in so-called Persistent Slip Bands (PSBs) or near the stress concentration sites (flaws of material). The crack initiation is typically located at the specimen surface in HCF region, but there is typically a single crack [3].

The interesting things happens when the loading amplitude decrease below the conventional 'fatigue limit'. In engineering terms there is not any macroscopic plastic strain under such loading conditions and hysteresis loop is closed, point 4 on Fig. 1.3 [65]. Nonetheless, fatigue crack may occur in material under such loading and even lead to the final rupture of element. The fracture pattern under VHCF loading is usually (not always) shows an internal crack initiation site [37]. In this case fatigue is explained by plastic strain accumulation around different flaws of material (non-metallic inclusions, porosity, grain boundaries and etc.) [3].

The probability of internal position for such defects is higher compared to the surface locations. Thus, with decreasing the loading amplitude the role of micro-structural flaws

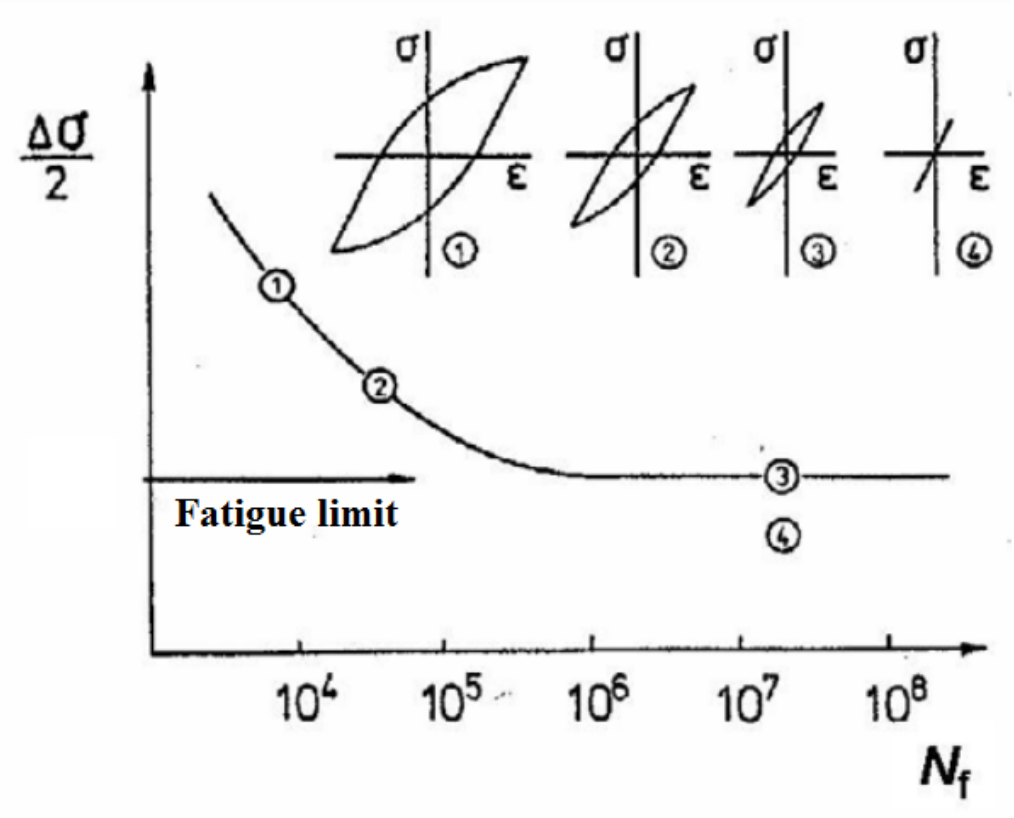

Figure 1.8: Plastic strain in different fatigue regimes [65]

increases and therefore the likelihood of internal crack initiation is increasing too. One of the more actual questions is why such internal defects does not dominate over the PSBs mechanism at high loading amplitudes and manifests themselves under low stresses? At the moment there is not any quantitative models which can explain this transition. The qualitative explanation which was proposed by C.Bathias [3] for the transition phenomena will be discussed in details in section 1.5.1.

1.4 Full SN-curve

According to the classification which was discussed in section 1.3 the full SN-curve (i.e. one single curve for all three domains) can be introduced. As usual such curves are plotted in double-logarithmic or semi-logarithmic coordinates (number of cycles is always in logarithmic scale). The full SN-curves are commonly used for fundamental investigations on the fatigue behaviour of material, because it allow a general view on material behaviour in all fatigue

domains. Thus, beside the Wohler's 'infinite life' concept (Fig. 1.5), several different full SN-curve approaches are existing nowadays.

The basic assumption for the new concepts is possible fatigue failures after the very high number of repeated loading. The more simple description is single logarithmic distribution of fatigue life. In this case the experimental data are fitted by one single permanent decreasing curve, Fig.1.9.

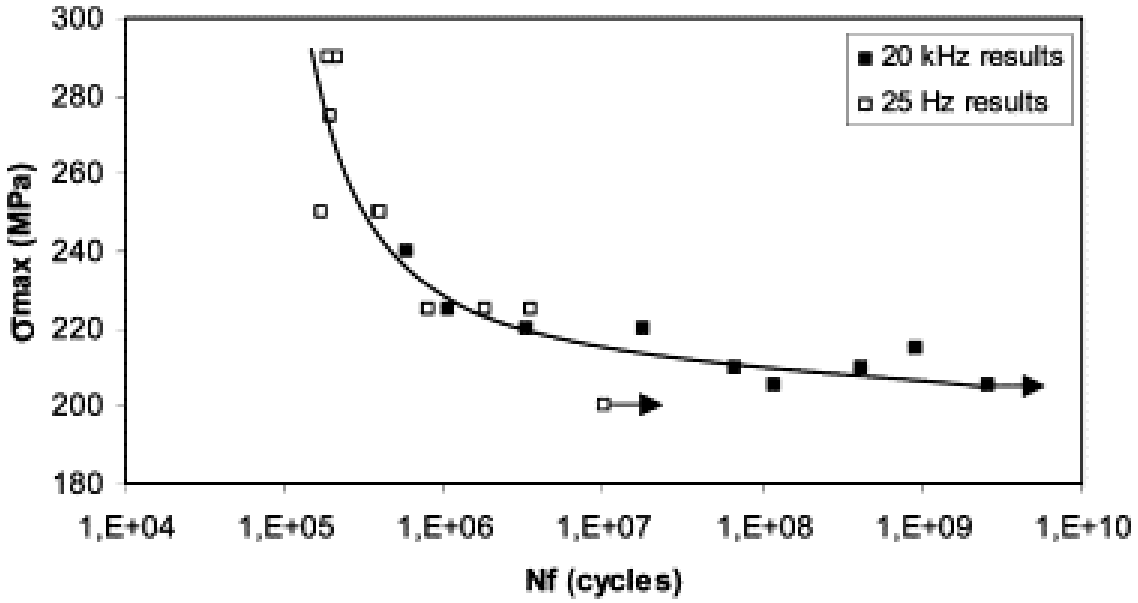

Figure 1.9: Single logarithmic distribution of fatigue life

The single curve approach is not always in good agreement with experimental data. Certain materials like high strength steels or some titanium alloys have significant scatter in fatigue life beyond 10^4 - 10^5 cycles, Fig.1.10 (a). The experimental data shows a plateau-like stage of SN-diagram. Herewith, the longer fatigue lives corresponds to an internal crack initiation. Fig. 1.10. Hael Mughrabi have summarized the main results of different research groups all over the world, so that Murakami's group [66], Bathias [37], Sakai [67], Nishijima and Kanazawa [68] on VHCF of high-strength steels and proposed the following full SN-diagram Fig. 1.10 (b). According to Mughrabi there are two fatigue limits: one is found above about 10^6 and extend only up to less than 10^7 cycles, range II on Fig. 1.10, [69]; the second-one is found at about 10^9 cycles and called 'ultimate' fatigue limit. However, available data do not permit to conclude whether, in range IV Fig. 1.10 (b), an 'ultimate' fatigue limit exists beyond $N_f \simeq 10^9$, [69]. The recent investigation in VHCF regime has shown, that there is no 'ultimate' fatigue limit [70]. Moreover, the physical explanation for plateau stage

of SN-curve is questionable. Fatigue is a continuous process of material degradation under cyclic loading. An intensity of fatigue damage accumulation can decrease with decreasing of loading amplitude, but it will never achieve a horizontal asymptote. The stepwise shape of SN-curve have a statistical character and associated with scatter of results due to changing of crack initiation mechanism. Thus, the full SN-curve presented in the Fig.1.10 (b) is not credible.

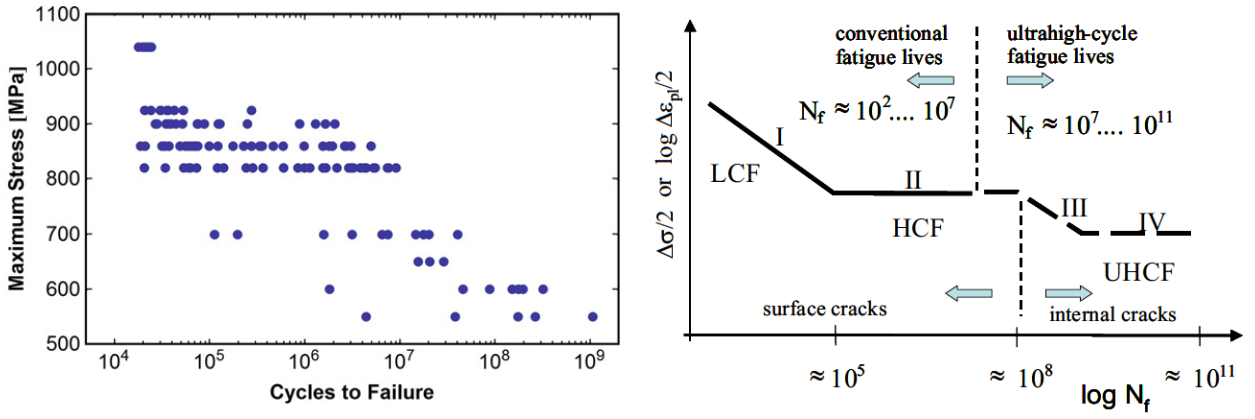

Figure 1.10: (a) Results of ultrasonic fatigue tests on two-phase titanium alloy [71]; (b) multistage fatigue life diagram [72]

Another common SN-diagram model is so-called 'bi-modal' distribution of fatigue life, Fig. 1.11. The main idea of bi-modal SN-curve is that fatigue data can be described by two individual distributions (two modes). One of the first work on the bi-modal distribution were investigations of Vera Ivanova [73]. She found that fatigue data have a significant scatter which does not fits well by one distribution. V.Ivanova proposed to use two individual (distinct) distributions for analytical description of fatigue results on steels.

The idea of bi-modal distribution was improved by A.Shanyavskiy [2]. He associated each distribution with a certain crack initiation mechanism (surface and subsurface). According to A.Shanyavskiy, probabilities (p_1 and p_2) of fatigue failure by surface and subsurface crack are stress amplitude dependent. At higher stress amplitudes the probability of surface crack initiation p_1 is higher and such mechanism is dominating over the subsurface crack. With decreasing of stress amplitude, the probability p_1 goes to zero, Fig. 1.11, while the probability of subsurface crack initiation is increasing. At certain stress amplitude the two probabilities are equal and the scatter in fatigue life become significant. This stress level is associated with the plateau part (Stage II, Fig. 1.10) of stepwise SN-curve. At low stress amplitudes the probability of subsurface crack initiation p_2 is dominating over the surface crack and internal crack appears more often.

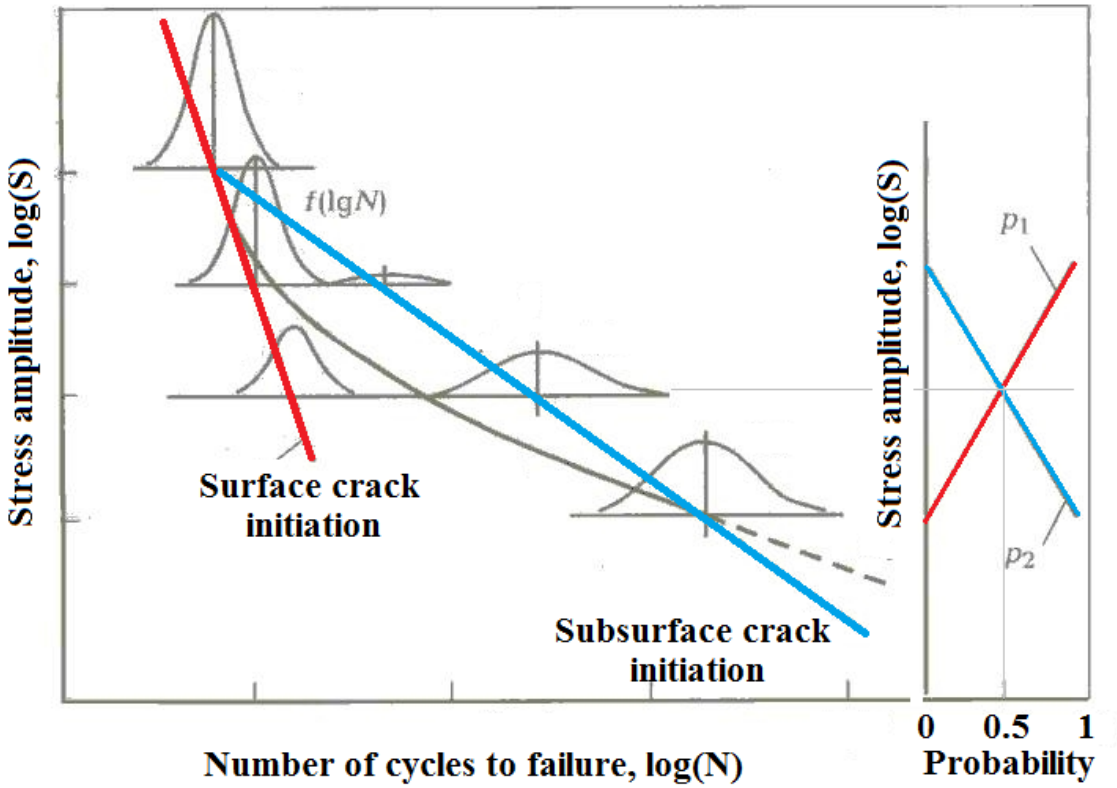

Figure 1.11: Model of bi-modal distribution of fatigue life [2]

This bi-model distribution of fatigue life was successfully adopted by American researchers for explaining the significant scatter in fatigue life of titanium alloys [71, 74]. The bi-modal distribution was also well used for explaining fatigue results on 2024-T3 aluminium alloy [56] and SUJ2 steel [75]. The bi-modal distribution is credible as for axial fatigue tests, as well for mix mode loading.

In spite on pronounceable difference in crack initiation mechanisms between different fatigue regimes (LCF, HCF and VHCF) there are no sharp limits of these domains. As usual a transition from one regime to another is realized within a certain range of stress amplitudes or strain amplitudes. This transition range was introduced by A.Shanyavskiy and called as 'bifurcation area' [76]. The bi-modal distribution of fatigue life naturally includes bifurcation area as stress amplitude range under which two possible crack initiation mechanisms may appears. In other words, above the transition area a first crack initiation mechanism is dominating, within bifurcation area two mechanisms are in competition and below this area a second mechanisms is dominating.

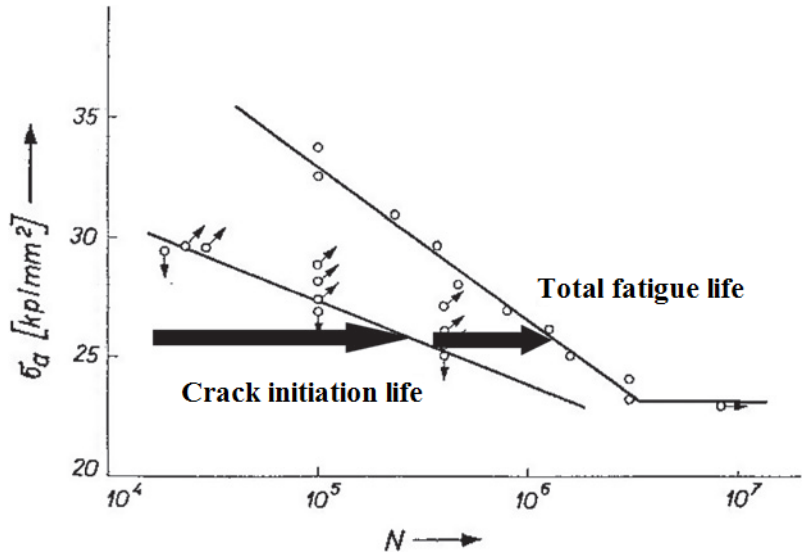

Figure 1.12: Example of French curve for low-carbon CNS 12010 steel [78]

1.5 Stages of Fatigue

Since the beginning of the 20th-century in the process of fatigue in metals several stages of fatigue has been eliminated. In 1933 H. French proposed a 'critical damage curve' [77] Fig. 1.12 late called after him.

The French curve is obtained in a two-stage fatigue experiment: first its aim is to determine a number of cycles that is necessary for the initiation of a crack with a critical length; second stage is to obtaining SN-curve up to rupture. The number of cycles which separate the French curve from the S–N curve at a particular stress level is considered to be the period of crack propagation after microcracks of critical size have been initiated. In 1937, B.F. Langer also proposed to separate crack initiation and crack propagation stages [42]. Thus, since the 1930s, the fatigue in metals became a two-stage process.

Nowadays, fatigue in metals has typically three stages:

1. Fatigue crack initiation;
2. Fatigue crack propagation;
3. Ultimate failure

The crack initiation stage is associated with forming a critical discontinuity in material structure (crack-like defect). The formation of such defect depends of numerous factors, such as loading amplitude, environment, type of material etc. When a critical size of discontinuity is reached, the crack starts to propagate. The duration of these stages is not the same and

moreover for crack initiation and propagation stages it depends of stress amplitude, Fig.1.12. The ultimate failure is very short ($\sim$ 1 cycle) and it is out of interest for determining the total fatigue life.

The period of crack propagation occupies a large fraction of fatigue life at high stress levels in the LCF (high stress amplitude) range and decreases continuously with decreasing stress level down into the HCF (low stress amplitude) range. Thus, in the long-life regime, fatigue crack initiation occupies an appreciable fraction of fatigue life, as noted by some authors [3, 79]. According to C. Bathias, the fraction of fatigue crack initiation in HCF can be more than 90 % of the total fatigue life and reach 99 % and more in case of VHCF regime.

1.5.1 Fatigue crack initiation

Fatigue crack initiation is a continuous physical process of creation of critical discontinuities in metal under cyclic loading. Since the first works of J. Bauschinger [80], Ewing and Humfrey [26], fatigue in metals was associated with changes in the internal structure of the component or specimen [81]. Founding of the permanent slip bands (PSB) at the surface of material subjected to cyclic loading show clearly, that such changes in structure are due to plastic deformation. In its turn, the plastic deformation in metals is commonly explained by dislocation motion. Up to nowadays, the fatigue crack initiation process is explained by the accumulation of plastic deformation. A general discussion on mechanisms of plastic deformation in metals under cyclic loading will be provided in present section. A particular discussion on the crack initiation in VHCF regime will be provide in the section 1.6.1.

Since the first works on the problem of plasticity in metals (Charles Coulomb, 1773; Adhemar Sain-Venant, 1870s; Maurice Levy, 1880s; Riehard von Mises, 1913 and i.e.) several theories of plasticity were developed. The two well known between them are: (1) Deformation theory of plasticity and (2) Flow theory of plasticity. The deformation theory is operated with intensity of stress σ_i and strain ε_i at a given point, Eq. 1.10 and 1.11.

$$\sigma_i = \frac{1}{\sqrt{2}}\sqrt{(\sigma_x - \sigma_y)^2 + (\sigma_y - \sigma_z)^2 + (\sigma_z - \sigma_x)^2 + 6(\tau_{xy}^2 + \tau_{yz}^2 + \tau_{zx}^2)} \tag{1.10}$$

$$\varepsilon_i = \frac{1}{3}\sqrt{2(\varepsilon_x - \varepsilon_y)^2 + 2(\varepsilon_y - \varepsilon_z)^2 + 2(\varepsilon_z - \varepsilon_x)^2 + 3(\gamma_{xy}^2 + \gamma_{yz}^2 + \gamma_{zx}^2)} \tag{1.11}$$

In particular, the well known criteria of von-Mises is the assumption, that plasticity at a given point begins when the stress intensity Eq. 1.10 reaches the yield stress of material $\sigma_i = \sigma_y$. The deformation theory can be applied just to the 'simple' loading (when all the

components of stress-strain condition are increasing proportionally to the loading parameter). Thus, the deformation theory of plasticity is not credible in case of cyclic loading. Also, it can not explain such physical phenomena as hysteresis effect, Bauschinger's effect and some others.

The flow theory of plasticity is more general than deformation theory and operates with increments of stress and strain as a function of stress. This theory can be applied for explaining the mechanical hysteresis, Bauschinger's effect, creep, relaxation process and others. Nonetheless, the models of deformation theory of plasticity is often directly or indirectly used for explanation of beginning of plastic deformation under cyclic loading.

The cyclic loading is principally differs from the monotonic tensile tests. On the Fig. 1.13 four examples of typical cyclic tension curves are presented compared with monotonic tensile curve.

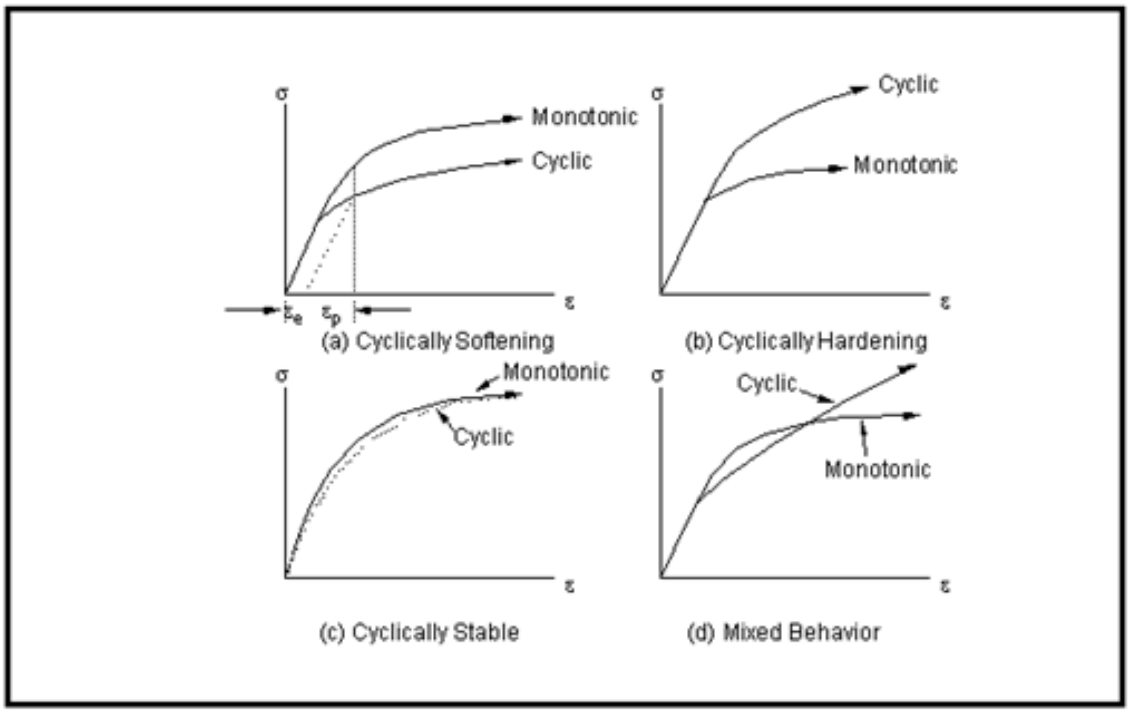

Figure 1.13: Four typical examples of cyclic tensile curves compared to monotonic tensile curve

Thus, for some materials the yield point under cyclic loading can change (Fig 1.13 (a) and (b)) or stays almost the same. The decreasing of yield point under the cyclic loading is called 'cyclic softening', and in opposite an increasing of yield point called 'cyclic hardening'. Stress softening and hardening depends on the nature of metals and can be illustrated by using stress-strain diagram, Fig.1.14.

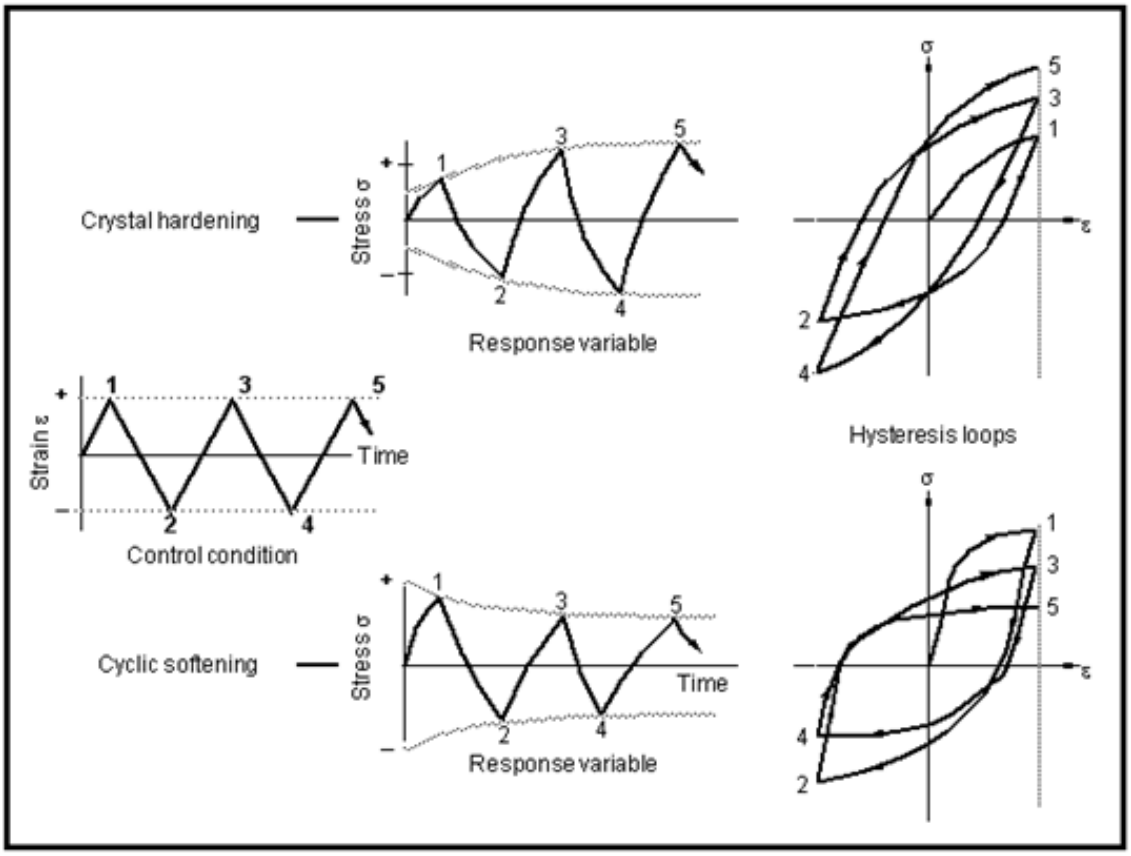

Figure 1.14: Stress-strain diagram and hysteresis loop in case of cyclic hardening and softening

Such diagram are obtained from laboratory tests on specimen subjected to constant strain amplitude cyclic loading. The width of the hysteresis loop is equal to plastic strain range. It is clear that in the case of hardening, the maximum stress reached in each successive strain cycle increases with the number of cycles, but plastic deformation is decreasing (width of the loop). In the case of softening the maximum stress decreases with the number of imposed cycles simultaneously with increasing plastic strain. This process does not continue indefinitely. In both cases, the stress will find a constant level and will remain stable at that level until the first emergence of a fatigue crack. In the case of stress softening a permanent increasing of plastic deformation in positions, where local stresses can be above yield point (yield point for cyclic softening materials is lower than quasi static value), lead to active fatigue damage accumulation and material shows a significant slope of SN-curve. In case of cyclic hardening, the plastic strain is decreasing under repetitive loading (yield point is also well above quasi-static value for such materials) and fatigue damage accumulation is less intensive (the course of SN-curve is closer to the horizontal asymptote).

All discussed above aspects of mechanical response of metals to the cyclic loading and models of plasticity are phenomenological theories. These models are based on assumptions of continuum mechanics while the nature of plasticity is associated with dislocation theory [81].

The dislocation theory describes the plasticity in crystals which is associated with sliding on crystallographic planes. The sliding process is more easy to realise on a close-packed plane along a direction with high density of atoms. The sliding lead to deformation of crystal structure and creation of dislocation. Coalescences of dislocations produce plastic deformation. The atoms near to dislocation are shifted from its equilibrium positions. Thus, the energy required for moving such atoms to the next equilibrium position is significantly less, compared to atoms in non-deformed crystal. As a result, the dislocations in metallic crystals can start to move under very small external loading ($10^{-3} - 10^{-4}G$), where G is shear modulus of metal. As usual, a real crystals initially has different types of defects in its structure: small interstitial or large substitutional atoms, dislocation, impurity phases, inclusion etc. that lead to early plasticity. Moreover, such defects of crystal leads to piling-up of dislocations. The situation becomes more complicated in case of structural metals, which are usually polycrystalline. In this case grain and phases boundaries are also playing a role of barriers for dislocations motion. Accumulation of dislocation around such barriers can lead to fatigue crack initiation.

Typically, the process of crack initiation in terms of dislocations is discussed for two types of materials: FCC and BCC materials [81] or Type 1 (Ductile) and Type 2 materials [69]. As usual, as an example of Type 1 (FCC) material is chosen single crystalline materials like cooper. Fatigue in such material is associated with forming persistent slip bands (PSB). A model of PSB formation has been proposed by Essman, Goselle and Mughrabi (EGM model). According to this model, due to dislocation motion within PSB, an extrusion appears at the material surface Fig. 1.15 (a, b). Then with continued cycling, they become roughened (i.e. "age") by gliding screw dislocations, Fig. 1.15 (c). Extrusions and roughening of the material at the surface within the PBS's are due to slip irreversibility, without which it is difficult to imagine that they could be any kind of fatigue damage. Under further cyclic loading, series of intrusions are formed within initial extrusion and by its edges. In fact, extrusions and intrusions at the surface of single crystals are areas of stress concentration at which cracks may nucleate. Thus, in a single crystal of pure FCC material fatigue crack initiates at the surface within at intrusions or permanent surface marks (extrusion+intrusion). In case of polycrystalline materials, as intergranular, as well transgranual crack initiation can be realized.

In case of pure BCC materials the sliding process is more difficult compared with FCC material. It is related to the density of atoms in sliding planes of bcc structure. It is not a

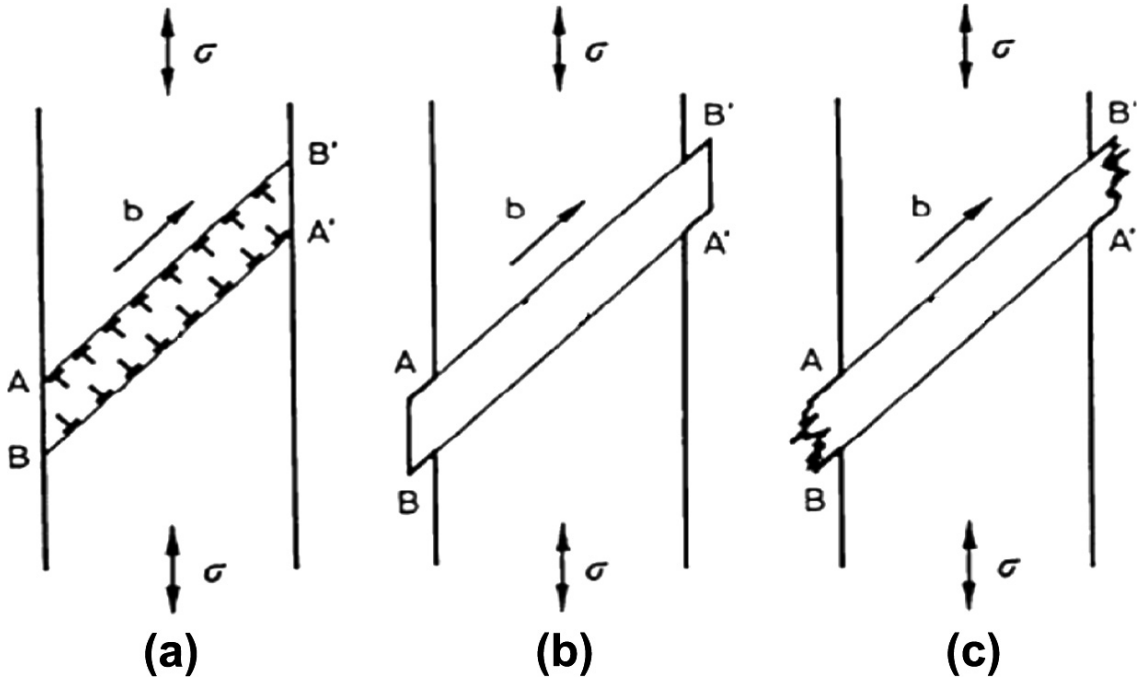

Figure 1.15: A schema of extrusion and intrusion formation at the material surface

close-packed lattice. Nonetheless, when the BCC material is alloyed by elements like C or Fe, the mobility of dislocations is increasing. The deformation mode becomes more like that seen in FCC material and PSB's form [81]. Additionally it can be noted that in materials with very low ability for sliding process another mechanism of plasticity is activated. It is twinning.

Concluding the section about fatigue crack initiation in metals it should be pointed out, that accumulation of plastic deformation is a reason for fatigue crack nucleation. The basic mechanism of plasticity in metals is the same under all the stress amplitudes - it is crystal plasticity, associated with dislocation motion. Under high loading amplitudes, numerous sliding systems are simultaneously activated, almost all the material is under plastic deformation. According to McDowell [82] this stage can be defined as 'macroscale plasticity', Fig. 1.16. Under such loading conditions it is impossible to describe each sliding system and approach of continuum mechanics should be applied for description of initiation process.

According to theory of plasticity, the grains close to surface are less constrained and plastic deformation developed first at the surface. With decreasing of loading amplitude, plastic deformation becomes more localised and developed mainly within so-called persistent slip bands (PSBs). Under such loading amplitudes the crack initiation is still preferential at the surface in case of single crystal metals, but for polycrystalline it is not always so. It is related with a limitation of continuum mechanics approach and therefore limitation of

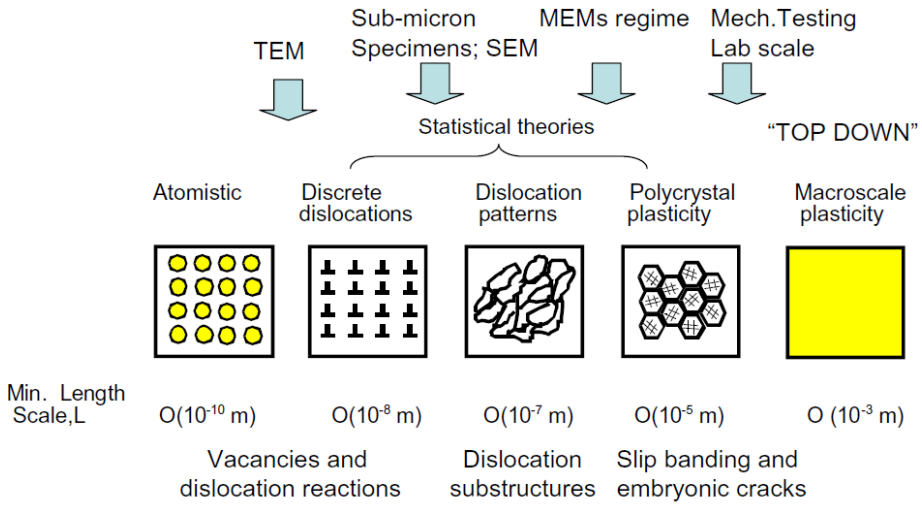

Figure 1.16: Scale levels for investigation the fatigue crack nucleation, [82]

plasticity criteria. Thus, under very low loading amplitudes, plastic accumulation is found at the dislocation scale level, where the well known criteria of plasticity (like von-Mises) can not be used. Plastic accumulation is related to the piling-up of dislocation at different structural defects like grain boundaries, impurity phases or inclusions. Of course this process is acting as under high loading amplitude, as well under medium and low amplitudes, but the process of dislocation accumulation at internal barriers or defects is time-consuming (need a large number of loading cycles). Thus, under the high and medium amplitudes, the critical state is early reaches at the surface of material. With decreasing of stress amplitude the stress-state at the surface is not sufficient to realize early crack initiation and fatigue damage accumulation is driven by dislocation motion. According to C.Bathias [3], the probability to find a defect (or barrier for dislocation sliding) is higher in the bulk of metal, that lead to the internal crack initiation. In case of single crystal of pure FFC material (barrier free material), the crack initiation is still appearing at the material surface.

1.5.2 Fatigue crack growth

The crack propagation stage follows the initiation stage. As was discussed in the Section 1.5.1, the fraction of crack propagation stage in total fatigue life under low amplitude is quite small (from 1 to 10 %). Thus, just a brief discussion about crack growth is proposed hereafter.

As mentioned in Section 1.1 there were not many works on the crack growth before the Second World War. The crack growth theories had started to develop with progress in

fracture mechanic. The very important contribution to the crack growth models development was the introduction of the Stress Intensity Factors (SIF) by Irwin [45]. This factor allows to calculate the stress and displacement distribution ahead of the crack tip, Eq. 1.12

$$\sigma_{i,j}(r,\theta) = \frac{K}{\sqrt{2 \cdot \pi \cdot r}} \cdot f_{i,j}(\theta) + ... \qquad u_{i,j}(r,\theta) = \frac{K}{\mu} \cdot \sqrt{\frac{r}{2 \cdot \pi}} \cdot g_{i,j}(\theta) + ... \tag{1.12}$$

where three dots means the negligible small members, r is the distance from the crack tip, θ is an angle with respect to the crack plane, $f(\theta)$ and $g(\theta)$ are independent from crack geometry and loading conditions functions.

In 1961 P.C.Paris proposed a model for fatigue crack growth based on the SIF [46]. This model gives a relationship between the crack growth rate and the stress intensity factor range

$$\frac{da}{dN} = C(\Delta K)^m \tag{1.13}$$

where da is crack increment for dN cycles, C and m are constant depending on the material and $\Delta K = K_{max} - K_{min}$ is the SIF range.

K_{max} corresponds to the maximum of the cyclic load and K_{min} corresponds to the minimum of the cyclic load. This model of crack growth can be plotted on double logarithmic scale graph, Fig. 1.17. As shown in this graph, the Paris law is not always in good agreement with measured crack growth rate (bold line on Fig. 1.17). Paris law is valid for the stable crack growth (Phase II).

At the very first stage (Phase I) of crack growth corresponding to short crack, the propagation speed is high. With increasing the crack length (the value of SIF is also increasing) the crack growth rate is slightly decreasing. With further increasing of crack length, the crack growth turns to unstable regime (Phase III). At this stage a crack growth rate is significantly higher compared with Paris's model prediction.

The outlined stage of crack propagation can be determined at fracture surface based on its typical fracture morphology. The final crack can be found on the fracture surface as a ductile rupture with typical dimples, Fig. 1.18.

The crack growth during the 'Phase II' for most of the ductile materials is characterized by so-call fatigue striations or beach-marks. These typical marks on the fracture surface is associated with sequences of loading cycles, Fig. 1.19.

The fatigue striations makes possible to determine the crack propagation direction, duration of growth stage and local crack rate by measuring the crack increment for cycle. Some authors assumes that the formation of such marks on the fracture surface is influenced by environment. The gazes present at the crack tip interact with a new-formed free surface

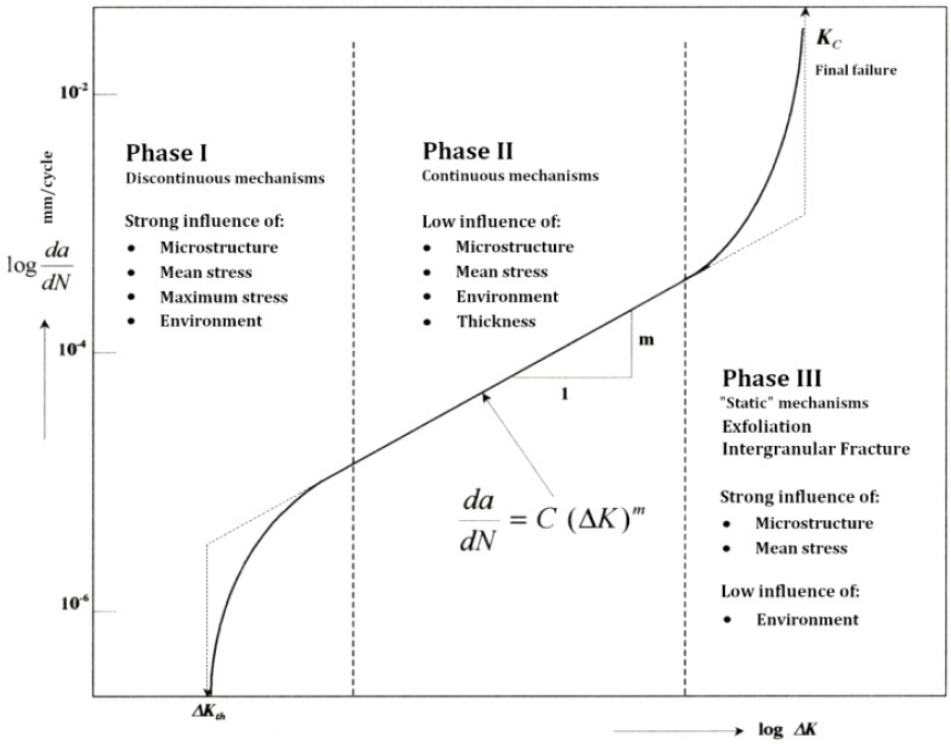

Figure 1.17: Stages of crack growth curve for ductile material

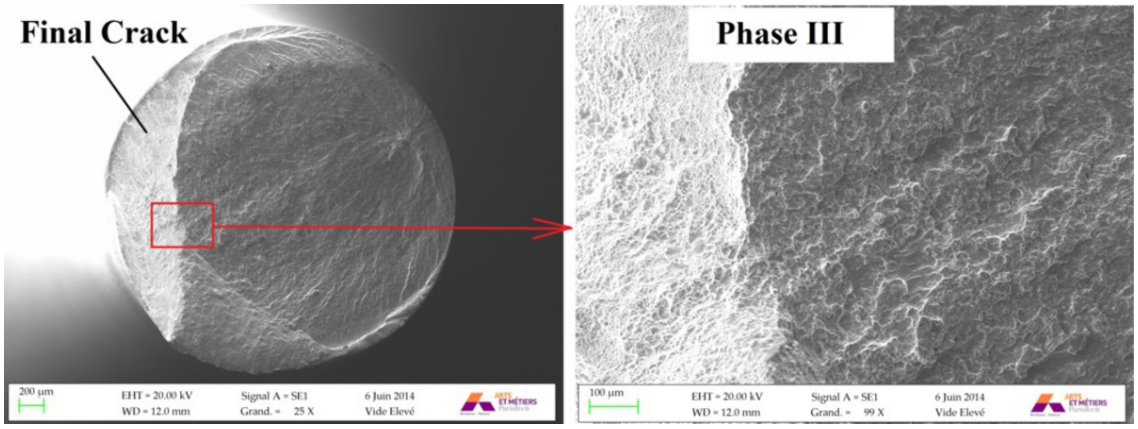

Figure 1.18: The fracture surface corresponding to phase III crack growth

during uploading stage and leaves the clearly seen marks on fracture surface.

The crack growth at stage 'phase I' is related to the problem of short crack growth. This topic of knowledge is not fully understood. Summarizing the experimental facts, it can be outlined, that crack growth rate of short-crack can exceed those of long cracks at the same applied stress-intensity range ΔK. Moreover, the short-crack can propagate at applied stress

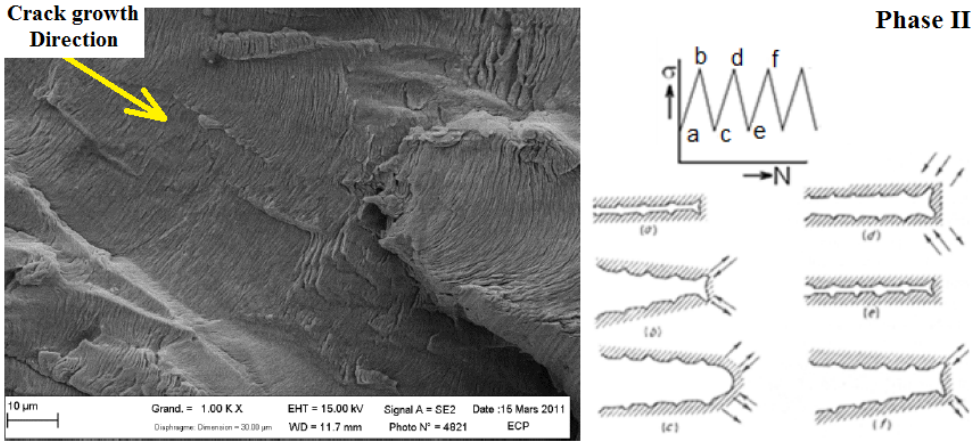

Figure 1.19: The typical for ductile materials fatigue streation during phase II crack growth

intensities lower than the fatigue threshold ΔK_{th} below which long-crack growth is presumed dormant. Thus, the problem of short crack growth should be discussed in additional suitable studies (not in the framework of the present project).

1.6 Very High Cycle Fatigue

Gigacycle or Very High Cycle Fatigue the fatigue regime corresponding to very long fatigue life (beyond 10^7 cycles) [3]. Typical loading amplitudes of VHCF range is well below the yield stress of the material and below the classic 'fatigue limit'. The problem of fatigue failures have naturally appeared with industry development in the second half of the 20th century. Developing of modern engineering applications such as cars, high speed trains, aircraft etc. led to significant increasing of in-service fatigue life due to high frequency loading. According to [38] fatigue lives for modern application varies from 10^8 to 10^{10} cycles that is VHCF range. Unexpected fatigue failures in high frequency loaded elements of aircraft's [1] engines confirmed the need of investigations in the VHCF problem.

Conventional testing methods with maximal testing frequency limited by several hundreds Hz were not suitable for experimental investigation of VHCF regime. High time-consuming and cost of such test up to 10^9 - 10^{10} cycles made conventional testing machine unacceptable for gigacycle testing. The possible solution to make fatigue tests reasonable is to increasing the loading frequency. In the 1980s, there were no standards for high frequency fatigue testing systems and several laboratories over the world had started the development of their own testing machines. These new testing systems were based on the concept of Manson's ultrasonic testing machine [41] developed in the 1950s. This machine was build based on

piezoelectric transducer working at ultrasonic frequency. The Manson's machine did not find a widespread use in the middle of the 20th century because of difficulties in controlling. The first computer controlled fatigue testing system with piezoelectric actuator was build by C.Bathias at the end of the 1980s. The high performance control of loading parameters made the machine of C.Bathias one of the best in the world.

Most of the ultrasonic fatigue testing systems are designed based on so-call 'Gigacycle concept' [3] (for details see ANNEX A). The main idea of this concept is to impose cyclic loading at a specimen at one of its own natural frequency. In this case the geometry of all the elements of the testing system including the specimen should be designed to be in resonance vibration at the same frequency. The analytical solution for this problem is built based on the theory of elastic waves in solids. The geometry of the components and specimens for gigacycle fatigue tests are presented in Chapter 2. The principal schema of the Bathias ultrasonic testing system and its operating are given in book [3] and ANNEX B.

Beside the development of new testing system and techniques, the VHCF range shows a new mechanism of fatigue cracking. In contrary to LCF and HCF with typical surface crack initiation, the VHCF is characterized by internal position of crack initiation site. The crack initiation and growth in VHCF had a particular interest. According to the work of French [77] the fraction of crack initiation in total fatigue life is increasing with decreasing the loading amplitude. But in case of internal crack initiation and growth it was difficult to experimentally prove this tendency. Just with developing of subsurface crack growth model by C.Bathias and P.C.Paris [83, 54] it became possible to estimate analytically the fraction of crack growth and initiation with regard to the total fatigue life. C.Bathias and P.C.Paris have shown, that crack initiation in VHCF can consume more than 99% of the total fatigue life. The development of non-destructive control methods (infra-red technique for instance) allowed to experimentally confirm this result.

Thus, the crack initiation stage consume most of the total fatigue life and, therefore, can be assumes as a main subject for investigations in VHCF. The two following subsections are dedicated to review crack initiation and fatigue crack growth model in VHCF regime.

1.6.1 Crack initiation in VHCF

The problem of fatigue crack initiation under gigacycle loading condition is still a widely discussed problem. According to [3], the crack initiation stage in VHCF may exceed 90% and sometimes reach more than 99% of total fatigue life. The same result was declared by Mughrabi [84] that fatigue crack initiation and slow early Stage I fatigue crack propagation are the life-controlling mechanisms in VHCF. Fatigue damage accumulation is always associated with an irreversible amount of deformation. According to Mughrabi, [64], fatigue damage is

usually related to some form of cyclic slip irreversibility. Crack initiation is not the same for all the metallic materials and it depends as of the loading conditions as well of the material type. The knowledge of the very high cycle fatigue behaviour of materials is limited up to nowadays and especially the studies on crack initiation mechanisms are rare. How it was shown by C.Bathias [38] that the crack initiation site is often located in the bulk of the material under the gigacycle regime loading. Thus, the study of the very first stage of fatigue crack nucleation is very difficult task due to absence of direct methods for in-situ observations. Nonetheless, some metallic materials, like Armco Iron shows just a surface crack initiation mechanisms, even under the VHCF loading [85]. Armco Iron is a face centred cubic (f.c.c.) material with high ability to crystal plasticity due to 12 sliding systems and high dense of atoms in sliding planes. The same crystal structure has a copper which is widely used for investigating the crack initiation mechanisms as in HCF as well in VHCF [84, 86]. In case of f.c.c. homogeneous materials the crack initiation mechanism is associated to the so-called permanent slip bands (PSB) formation. The analysis of PSB marks in LCF, HCF and VHCF [84, 87, 64] regimes and in-situ observation of PSB nucleation under the VHCF loading [85] allows to state that homogeneity of the cyclic plastic strain distribution decreases from the LCF via HCF to VHCF. As usual the surface grains are less constrained than interior grains, it can be rightfully assumed that at very low amplitudes slip occurs only in a few grains at the specimen surface [63]. This state is fair for mono-crystals of f.c.c. metals and homogeneous materials without inclusions, porosities and other defects. In case of heterogeneous materials the crack initiation is always associated with imperfections of micro-structure that lead to micro-structural changes by accumulation of cyclic micro-strains. For such crack initiation the direct observation of fatigue damage accumulation process is not possible and the initiation mechanisms are reconstructed based on the observation of fracture surfaces.

The systematic investigations on the fracture surfaces for different materials (custom iron, bearing steels, titanium alloys) made possible to distinguish the common for all materials patterns of subsurface crack which was named the 'fish-eye crack' [3, 88, 83]. It has been found, that depending on the material different micro-structural formations can be found in the centre of the 'fish-eye'. In case of steels, the more comment micro-structural formation located in the centre of 'fish-eye' is non-metallic inclusion [55, 3, 89]. Typically, the non-metallic inclusion are surrounded by a characteristic area indicating fine granular morphology [89]. Based on the significant morphology this area is called 'Fine Granular Area' (FGA). The same area was observed by Murakami and has been called 'optically dark area' (ODA) [55] and by Shiozawa [90, 91] who called it as 'Granular Bright Facet' (GBF). Thus, as the crack initiation and slow mode I crack growth are the life-controlling mechanisms of VHCF, the understanding of granular area nucleation is the cornerstone problem for VHCF behaviour of steels.

1.6.2 Crack growth in VHCF

As discussed in the previous sections, two different types of crack initiation are possible in VHCF: surface and subsurface. With decreasing the loading amplitude, usually, subsurface crack initiation dominates. Thus, two problems of crack growth exist: fatigue crack growth in VHCF with surface and subsurface initiation. These problems were successfully solved by P.C.Paris and C.Bathias. The Bathias-Paris model for crack growth briefly discussed in the following.

First the crack growth model in VHCF with subsurface initiation is discussed. This model is based on the Paris-Hertzberg- McClintock crack growth rate $\frac{da}{dN} = b\left(\frac{\Delta K_{eff}}{E\sqrt{b}}\right)^3$. Analysis of typical fracture surface, known as 'fish-eye' crack, allows to outline several typical zones, Fig. 1.20.

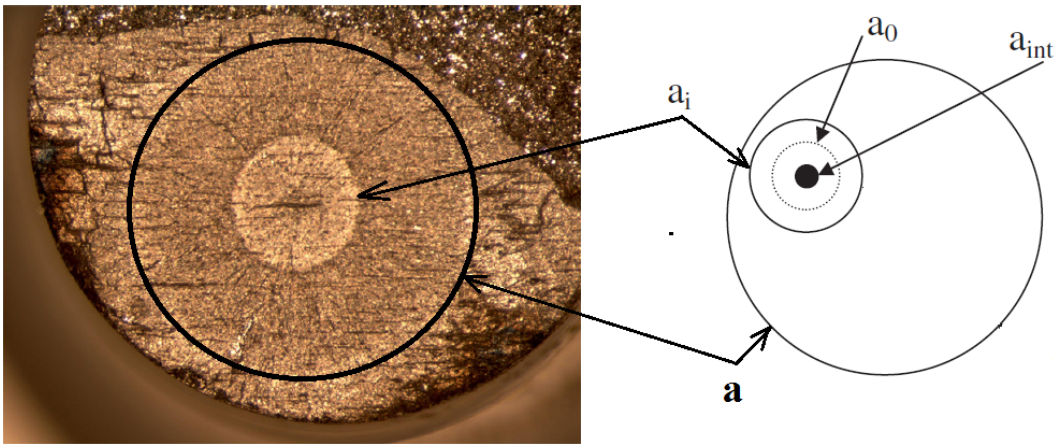

Figure 1.20: Fracture surface formed by subsurface crack, 'fish-eye' pattern and associated zones of crack [54]

According to the Bathias-Paris model, at the beginning of crack growth a small crack a_0 with no crack closure and corresponding to $\frac{\Delta_{eff}}{E\sqrt{b}} = 1$ starts from a defect of size a_{int}. This short crack becomes a long crack at a_i. According to experimental data, the growth rate of small cracks is greater compared to long crack. The schematic graph of crack growth rate versus ΔK_{eff} is shown in Fig. 1.21

The total crack growth life can be obtained by integration of the Paris-Hertzberg-McClintock growth rate model in all these ranges: from a_{int} to a_0; from a_0 to a_i and from a_i to a. The analytical solution for surface crack growth under VHCF loading follows the same logic. The difference between subsurface and surface crack initiation is in determination of ΔK. In case of subsurface circular crack it is $\Delta K = \frac{2}{\pi}\Delta\sigma\sqrt{\pi a}$. In case of surface crack, the expression for ΔK will be more complicated [88], and the total fatigue crack growth life can be calculated

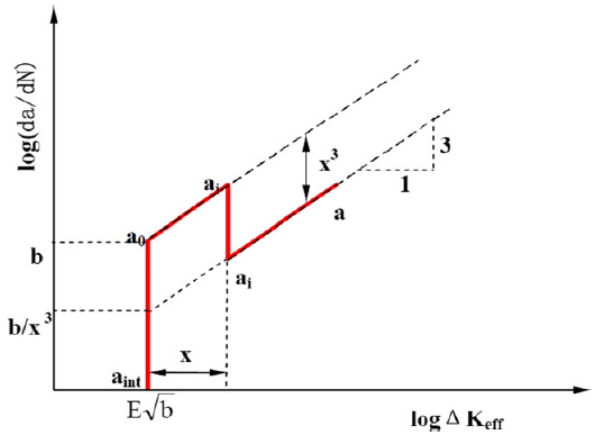

Figure 1.21: Modeling of crack growth rate in 'fish'-eye

by:

$$N_{Total} = N_{a_{int}-a_0} + N_{a_0-a_i} + N_{a_i-a} \tag{1.14}$$

The calculation of total crack growth life for subsurface [54] and for surface [88] for different materials has shown that the fraction of crack growth life is very small and often does not exceed 1 %. This confirms a tendency which was found from the French curve.

1.7 Fatigue in Titanium and Titanium alloys

1.7.1 Introduction

The problem of VHCF or Gigacycle fatigue is widespread in many different industries, such as car engine, high-speed train aeronautic and others applications[3]. Nonetheless, aeronautic industry is outstanding between others, because of several factors. First of all, the speed of rotation is much more higher for turbo-jet engine compared to car or even high-train engines. Thus, the loading frequency for aeronautic elements of motors is higher too, that led to very long fatigue life during in-service. The second point is economic reasons. One additional kilogram of weight is 'more expensive' for aeronautic application. Additional mass led to higher consumption of fuel. Thus, the ideology of design for aeronautic applications accepts fatigue crack initiation and even growth during in-service. But these cracks have to be detectable before reaching a critical length when crack growth becomes unstable. Thus, the problem of VHCF failures with its typical subsurface crack initiation and very small fraction of crack growth in total fatigue life is a very important problem for aeronautic applications.

The Gigacycle loading regime is inherent to rotating elements of turbo-jet engine. An aircraft engine (roughly) consists of three main parts: compressor, combustion chamber and turbine. The rotating parts are the first and the last. The efficacy of the whole aircraft engine is laid on the stage of design of compressor step. The common material for components of turbo-jet compressors is a two-phase titanium alloy. This second part of 'Chapter I' is devoted to: (1) brief introduction of titanium and its alloys and (2) review on fatigue in two-phase titanium alloys.

1.7.2 Titanium and Titanium alloys

Titanium is the chemical element with 22 serial number in periodic table of elements. This element has a high electro-chemical activity, that's why pure titanium never exists in nature. About 30 % (in weight) of titanium exists in the form of TiO_2 compound. Beside the dioxide of titanium, there are more than 100 minerals containing titanium, such as $FeTiO_3$, $CaTiO_3$, $CaTiSiO_5$ and others. The most commercially used sources are $FeTiO_3$ (ilmenit) from Russian Ilmen mountains and TiO_2 (rutile) from the beach sands in Australia, India, and Mexico. For industrial production of titanium, the reduction method is employed. The method of titanium extraction can be simplistically represented (example for dioxide of titanium, rutile) by the following chemical equations

$$TiO_2 + 2C + 2Cl_2 \rightarrow TiCl_4 + 2CO$$

$$TiCl_4 + 2Mg \rightarrow 2MgCl_2 + Ti$$

Initially, calcium was used instead of magnesium in the reduction method, but it was not convenient for industrial production. Justin Kroll demonstrated that titanium could be extracted commercially by reducing $TiCl_4$ by changing the reducing agent from calcium to magnesium. The process of reduction by magnesium has been called 'Kroll process' and is still widely used for industrial needs. Of course, it is not just the single chemical way to extract titanium from chemical combinations, but others methods are more complicated or (and) expensive. This extracting method is realized by batch process and also expensive, compared to the continuous methods used for other structural materials like aluminium or steels.

Pure titanium is allotropic material with two modifications: low temperature hexagonal close packed (hcp) structure, called as α-titanium and high temperature body-centred cubic (bcc) structure, called as β-titanium. The transus temperature of allotropic transformation for pure titanium alloy is $882 \pm 2C^{\circ}$. The atomic unit cell for both modification of titanium are shown in figure 1.22.

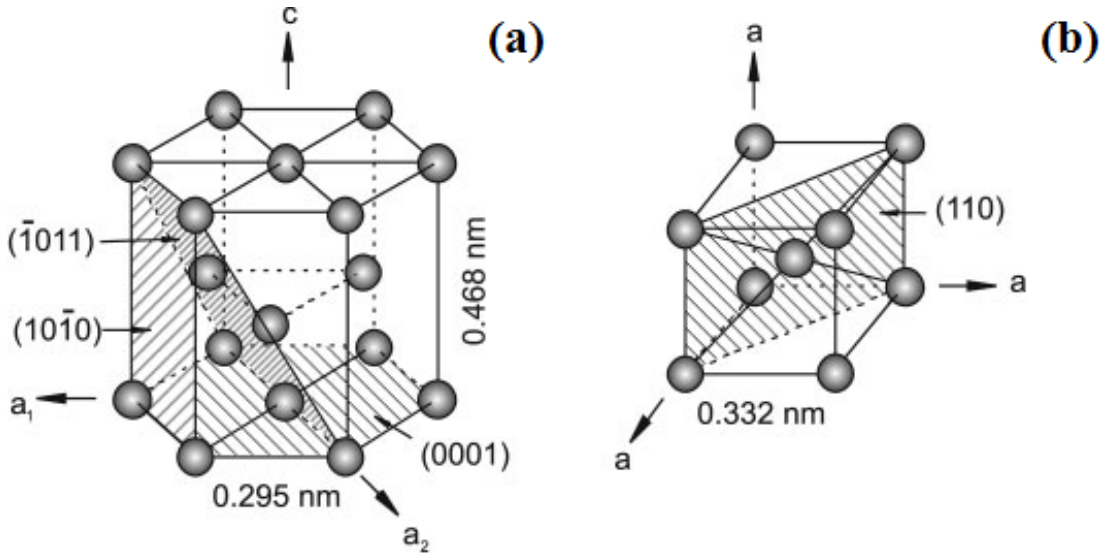

Figure 1.22: Low temperature hcp and high temperature bcc structures of titanium [92]

α-titanium with hcp crystal structure has a significant anisotropy in its lattice parameters: a=0.295 nm, c=0.468 nm, c/a=1.587 that is slightly lower than for ideal hcp crystal structure (1.633 nm). The mechanical properties of single α-titanium crystal are also different in two directions. The Young's modulus along the 'c'-direction, Fig.1.22, is 145 GPa, while in direction parallel to the 'basal' plane it is 100 GPa only. The β-titanium has a cubic crystal structure with parameter of lattice equal to a=0.332 nm at 900 LC° and isotropic mechanical

properties.

The bcc is high temperature modification of pure titanium alloy. Upon cooling from the β phase field of titanium the most densely packed planes of the bcc β-phase $\{110\}$ transform to the basal plane $\{0001\}$ of the hexagonal α-phase, Fig.1.22. The transformation from the bcc β phase to the hcp α phase was first documented in zirconium by Burgers and then later verified in titanium [93]. The corresponding transformation of the slip planes of the bcc β titanium into the basal planes of the hcp α titanium and the respective orientations of the slip directions is given by the following orientation relationship:

$$\{0001\}_\alpha \| \{110\}_\beta$$
$$\{1120\}_\alpha \| \{111\}_\beta$$

The six slip planes and the two slip directions of the β titanium unit cell give a maximum of 12 variants of orientation to the α. This variety of orientations is also reflected in the metallography micro-structure. Within the prior β grains, which can be as large as several millimetres, individual α platelets packets nucleate and grow according to these 12 orientation relationships, with the individual platelets packets having a common orientation within them. Nonetheless investigations of Stanford et al. and Bhattacharyya indicate that there is a variant selection process by which some of these α phase orientations are selected more often than others [94, 95]. Beside the orientation of forming platelets packets, the transformation from β to α titanium determines the character of future α/β grain boundaries. Initially, based on the analysis of orientation relationship it was assumed, that such grain boundaries will not be a significant obstacle for slip transfer. However, recently it was discussed that for specific orientations with respect to the loading axis the α/β interface acts as a barrier to slip transfer [96]. However, it is a special case and in general the α/β grain boundary is not expected to be an effective barrier (slight effect) to slip transfer. Thus, the α/β transformation determines the future orientation of α platelets packets and creation a slight barrier for slip transfer through α/β grain boundaries for some specific orientations.

The temperature of transition from β to α titanium alloy can be modified by incorporating impurity atoms into the chemical composition of titanium (alloying). The typical alloying elements for titanium are aluminium, molybdenum, vanadium, chromium, zirconium etc. Some of alloying elements increases the temperature of allotropic transformation, Fig.1.23 (b) and stabilise the α-phase. Such elements are named α-stabilizers: aluminium (Al), oxygen (O), nitrogen (N) and carbon (C) are typical α-stabilizing elements.

Others atoms, like Tin (Sn) and Zirconium (Zr) do not influence the temperature of allotropic transformation, Fig.1.23 (a), they are called neutral. The wide group of chemical elements reinforces the stability of β- titanium, figure 1.23 (c, d). These elements can be

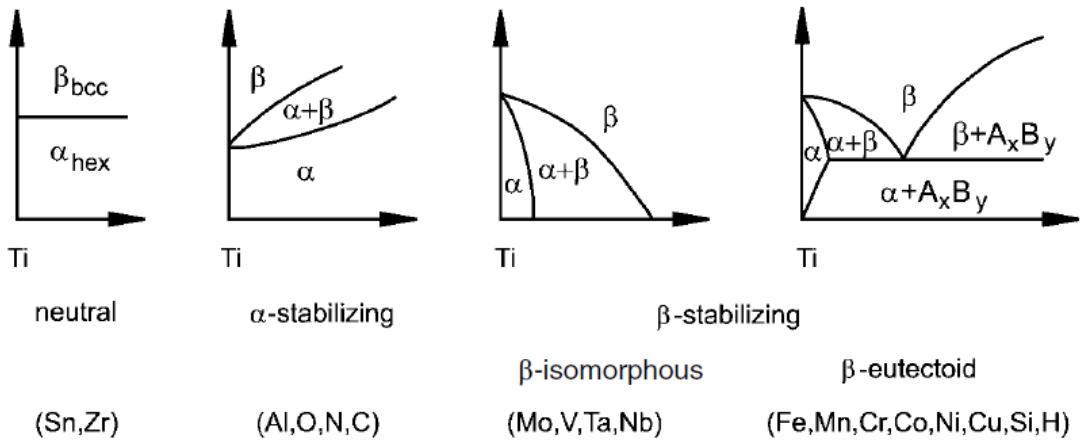

Figure 1.23: The influence of alloying elements on the transus diagramm for titanium [92]

classified as β-stabilizing elements and additionally may be separated into two groups: β-isomorphous and β-eutectoid. Molybdenum (Mo), vanadium (V), tantale (Ta) and niobium (Nb) are typical β-isomorphous stabilizers of titanium. The high concentration of such elements lead to the stability of β-titanium modification even at room temperatures. Iron (Fe), magnesium (Mn), chromium (Cr), hydrogen (H) and some others, figure 1.23 (d) are typical β-eutectoid stabilizers.

Thus, the dependence of the thermal stability of titanium modifications from the alloying elements allows to classify the titanium alloys into tree principal groups: α-alloy, $\alpha+\beta$-alloy and β-alloy. Sometimes, α-titanium alloys may be additionally classified on α and near-α alloys (concentration of β-stabilizers less than 2%). α-titanium alloys are non-heat treatable, weldable materials with poor or medium tensile strength, good ductility (equiaxed form), very good creep behaviour even at high temperatures and poor formability, that limited their usage for engineering applications. An advantage of near-α titanium alloy is increasing in heat-treatability and formability due to small amount of β-stabilizers. The advantages of near-α achieving by decreasing the creep properties of alloy. $\alpha+\beta$ titanium alloys have a high mechanical properties due to good heat-treatability. These advantages of two-phase titanium alloy makes it one of the most common structural material for numerous applications, from the aeronautic, chemical, submarine industries to the medical use. β-titanium alloy are heat treatable, readily formable materials with very high strength but low ductility.

The thermo-mechanical treatment is very important for heat-treatable titanium alloys because, it allows to manage micro-structure of material and therefore improve its mechanical properties. In the case of two-phases titanium alloy, which are commonly used for compressor elements of aero-engines, mechanical properties are very sensitive to geometrical arrangement

of two phases as well to crystallographic texture of hexagonal α-phase. In the following section, the common procedure of thermo-mechanical processes on titanium alloy will be discussed.

1.8 Thermomechanical treatment of titanium alloys

The thermo-mechanical treatment for two-phase titanium alloys is a complex sequence of solution heat treatment, deformation, recrystallization, aging, and annealing for stress relief as schematically outlined in Fig.1.24

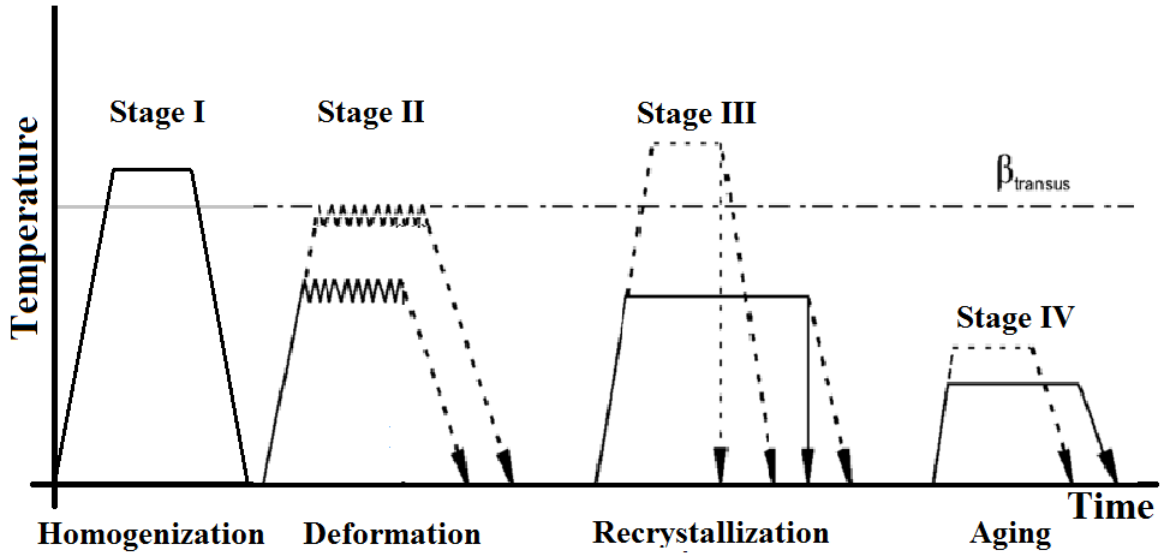

Figure 1.24: The typical termo-mechanical route for two-phase titanium alloy

The first stage of production process is homogenization in β-phase region at temperature above allotropic transformation. This step is required to homogenize β-phase grains and composition within the ingot. The most critical parameter in stage I is the cooling rate from homogenization temperature. It determines the width of α-platelets in the needle-like structure within β-grains and an extend of the continuous α-layers at β-grain boundaries [97]. Depending on the cooling rate, the alpha-platelets are either fine or coarse. Slow cooling from the β phase field results in pure needle-like micro-structures, with platelets becoming coarser with reduced cooling rate.

The next step is deformation which is commonly performed in $\alpha+\beta$-region or near to α/β transformation temperature, Fig.1.24. During the deformation process in the $(\alpha+\beta)$ phase field, the needle-like structure is plastically deformed (not broken up). The individual broken segments of the α platelets will coarsen in subsequent processing to form the equiaxed α_p

grains. This process is referred to as spherodization. The deformation at temperature near to β-transus will lead to lower fraction of α-phase and β texture will be formed (so-called transverse type of transformation texture). With decreasing of deformation temperature, the fraction of α-phase will increase and at low temperatures α-phase texture can be developed (so-called basal/transverse). The cooling rate is still a critical parameter in stage II which determine the coarseness of the α laths. Thus, during the first two stages different needle-like micro-structures can be formed.

Unlike needle-like micro-structures, equiaxed micro-structures are the result of a recrystallization process. Therefore, the alloy first has to be highly deformed in the $(\alpha + \beta)$ field to introduce enough cold work into the material. Upon subsequent solution heat treatment at temperatures in the two-phase field, a recrystallized and equiaxed micro-structure is generated. Important parameters of this recrystallization stage III are the temperature, determining the volume fraction of α_p located at the 'triple-points' of the recrystallized equiaxed β grains, and the cooling rate from the recrystallization temperature, determining the width of the individual α alpha-platelet as well as the α colony size of the needle-like structure formed during cooling within the equiaxed β grains.

The last stage IV 'ageing' is used to increase hardening of titanium alloy. During this stage Ti_3Al particles will formed within α-phase that lead to age-hardening of titanium alloys. At this stage the more important parameter is temperature, because it will determine whether age-hardening by Ti_3Al occurs in the α phase or not (if the ageing temperature is below Ti_3Al solidus temperature, there is no age-hardening of alpha-phase). Thus, the sequences of mechanical and heat treatments will determine the finale micro-structure of titanium alloys. Some typical micro-structures for two-phase titanium alloys micro-structures are introduced in the next section.

1.9 Typical micro-structures of $(\alpha + \beta)$ titanium alloys

The variation in thermomecanical proceeding lead to numerous variants of micro- structures for two-phase titanium alloys. The most common classes of micro - structural morphologies are equiaxed α, lamellar α (needle), equiaxed α + transformed (pancake) β, and Widmanstatten (basket-weave) structure, Fig. 1.26 (a), (b), (c) and (d) corresponding. Different micro-structures requires different processing route. The two extreme cases of phase arrangements are the needle-like micro-structure, which is generated upon cooling from the β phase field, and the equiaxed micro-structure, which is the result of a recrystallization process [92]. Both micro-structures can consists of fine or coarse micro-structural elements (α-platelet, α_p-grains). The mechanical properties for these extreme micro-structures are shown in Fig. 1.25. where 'O' means neutral. Thus, the fine structure provide higher strength

and ductility for titanium alloy compared to coarse structure. The equiaxed structure shows a higher strength and ductility too compared to needle-like. These features determines the better fatigue crack initiation resistance for fine structure compared to coarse and for equixed compared to needle-like. Nonetheless, the fatigue crack propagation is in opposite relation, because of worse fracture toughness properties of fine and equiaxed structures respectively. Thus, combining the geometry, size and organisation of micro-structural features of titanium alloy, different mechanical properties can be achieved.

fine	*coarse*	*Property*	*lamellar*	*equiaxed*
○	○	Elastic modulus	○	+/− (texture)
+	−	Strength	−	+
+	−	Ductility	−	+
−	+	Fracture toughness	+	−
+	−	Fatigue crack initiation	−	+
−	+	Fatigue crack propagation	+	−
−	+	Creep strength	+	−
+	−	Superplasticity	−	+
+	−	Oxidation behavior	+	−

Figure 1.25: Influence of microstructure on selected properties of titanium alloys.

The thermo-mechanical process on the two-phase titanium alloy can also influence the arrangement of micro-structural elements. In the case of fully-lamellar (needle-like) micro-structure the key parameters of final micro-structure are initial hot working in the β-phase region, homogenisation and cooling rate [97]. In the case of fully-lamellar structure the nuclei of α-phase are typically growth along primary β-grains and then the α-platelet growth into the body of primary β-grain, Fig.1.27

The size of primary β-grain will determine the size of α-platelet cluster, the cooling rate influence the α colony size and extend of α layers at β grain boundaries.

Texture. In the case of bi-modal or duplex micro-structure a texture can be developed during processing in $(\alpha + \beta)$ field. The texture is the distribution of crystallographic orientations of polycrystalline aggregate. The degree of deformation affects the intensity of the texture components whereas the deformation temperature determines the texture type. Low deformation within $(\alpha+\beta)$-phase field will produce so-called 'basal/transverse' texture. High deformation within $\alpha + \beta$-phase field will develop so-called transverse texture type.

Micro-texture. Micro-texture in titanium alloy is defined as micro-structural regions

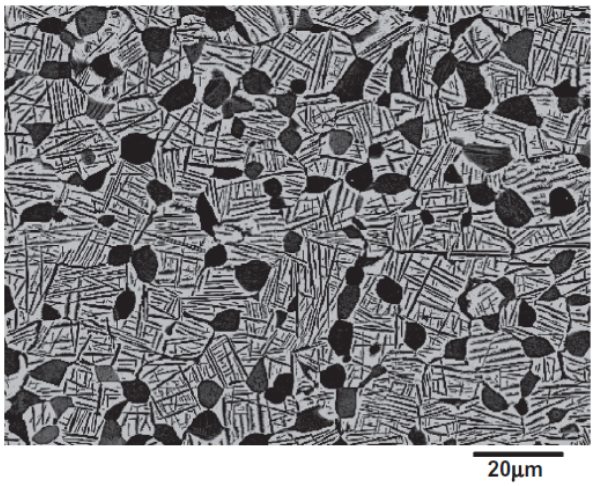

a)

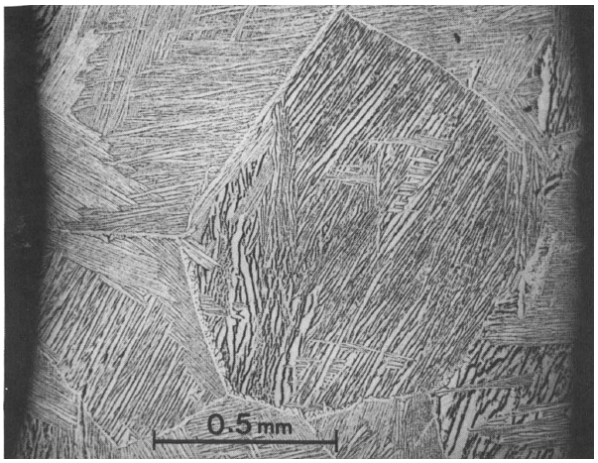

b)

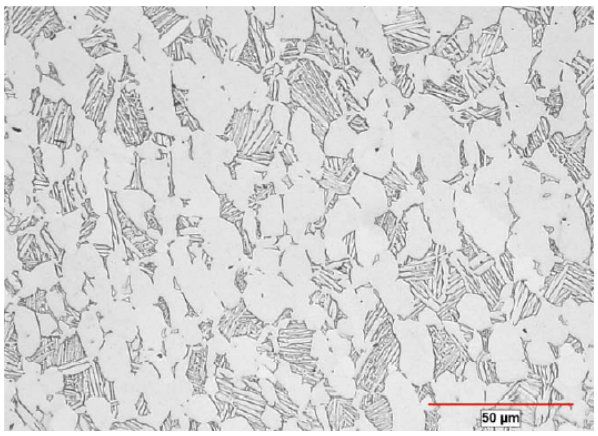

c)

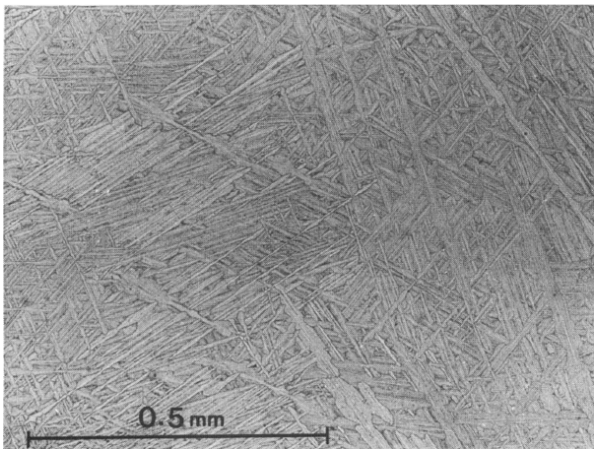

d)

Figure 1.26: Examples of two-phase titanium alloy micro-structures: a) equiaxed α [71] , b) lamellar α [98] c) equiaxed α + transformed β (pancake) [99] d) Widmanstatten (basket-weave) structure [98].

of material which comprise of grains with common c-axis texture component, Fig.1.28 [92]. These regions are commonly referred as 'macro-zones' [100]. It should be noted, that the size of such micro-textured regions can be significantly higher compared to the grain size. In the presented case the average grain size is about 25 μm while the size of macro-zone is at least several millimetres. A precise knowledge of how micro-texture is developed is not yet understood, while an influence of such macro-zones on fatigue properties of two-phase titanium alloy under HCF loading is discussed in the PhD these of Le Biavant [100].

In the present investigation, the key mechanical property is fatigue crack initiation. The following discussion about micro-structure is focused on the resistance to fatigue initiation, which is commonly explained by crystal plasticity. Thus, in the next section the crystal lattice of β-titanium (b.c.c) and α-titanium (h.c.p.) is analysed for ability to accumulate

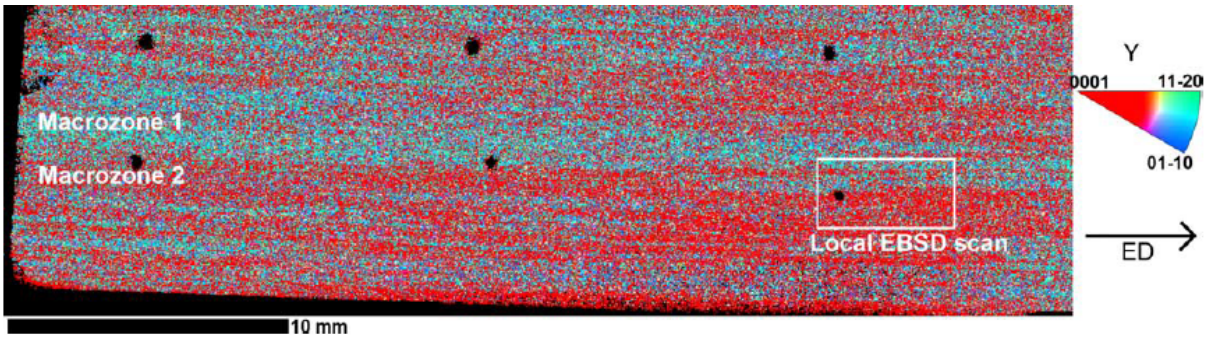

Figure 1.28: An example of two neighbouring macro-zones, [101]

plastic deformation (dislocation slips).

1.10 Slip in α (h.c.p.) and β (b.c.c) titanium

As shown in previous sections, the micro-structure of all two-phase titanium alloy consists of of α-phase and β-phase. The fraction and geometry of these phases is determined by sequences and parameters of thermo-mechanical proceeding. From the mechanical point of view each two-phase titanium alloy is a composite consisting of micro-structural elements with different chemical and mechanical properties. In case of fatigue and related to it crystal plasticity, an ability of each crystal cell should be discussed.

Figure 1.27: Example of fully-lamellar structure [97]

The plastic deformation in crystals is associated with dislocation glide by so-called 'slip planes' along 'slip direction' (the easiest way). The slip planes and directions are most highly dense packed atoms planes and directions. In case of β-titanium, the more highly dense plane is $\{110\}$, Fig. 1.22 (b). In case of α-titanium, slip planes are referred as $\{0001\}$, Fig. 1.22 (a). The number of dislocation glide opportunities in a crystal lattice is equivalent to the number of independent slip systems in this crystal. This number is determined as multiplication of slip plane number by the number of slip directions by plane. The number of slip systems for β-titanium is 12, Fig. 1.29, while for α-titanium it is equal to 3, . However, the denser slip planes are packed with atoms, the easier dislocations

can glide. Thus, the hcp lattice with a packing density of 91 % is superior to a slip plane in the bcc lattice with a packing density of only 83 %.

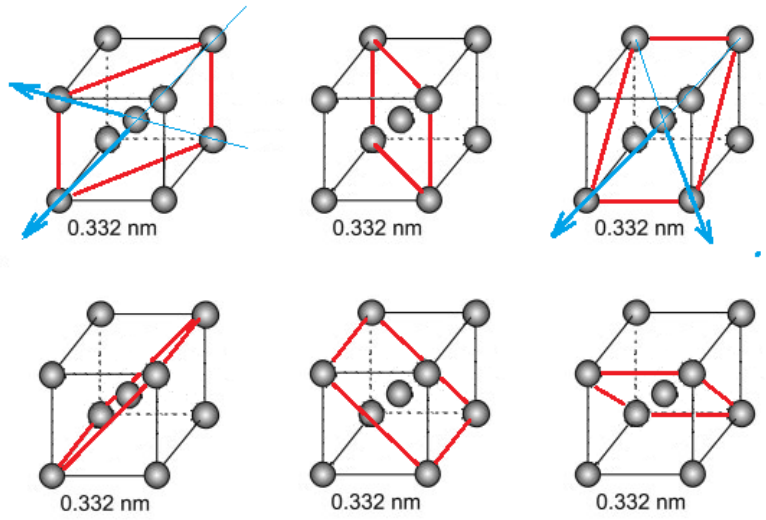

Figure 1.29: Principal slip systems in b.c.c. crystal lattice

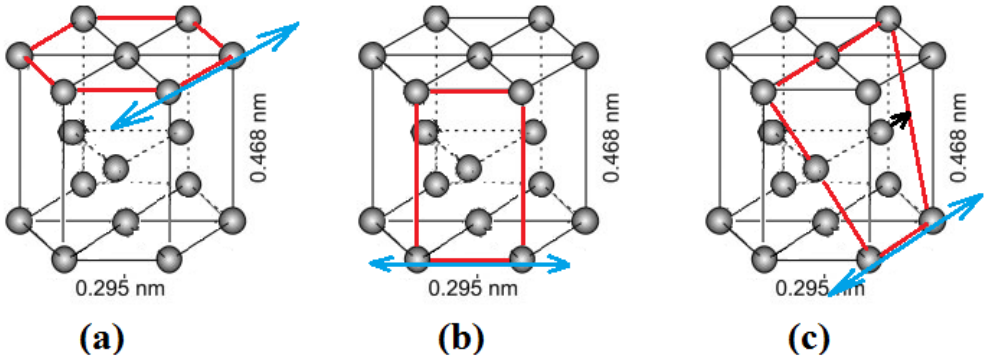

Figure 1.30: Principal slip systems in h.c.p. crystal lattice

Thus, dislocation sliding is more easy in case of single h.c.p. crystal lattice. Nonetheless, the h.c.p. structure has a limited number of independent slip systems. The basal and prism planes, (Fig. 1.30) there are three slip systems on each, but just two are independent. Slip on pyramidal planes does not increase the number further since this glide is composed of a prism and a basal component and therefore cannot be considered an independent slip system. Therefore, the h.c.p. structure has 4 independent slip systems. According to the von-Mises criterion at least five independent slip systems are required for homogeneous plastic

deformation of metals. Thus, the plastic deformation in h.c.p. crystal is anisotropic and can be easy developed just along some special direction. Beside principal slip systems, which are shown on Fig. 1.30 the h.c.p. crystal has other systems by which the plastic deformation can be accumulate, for example twinning planes, Fig. 1.31.

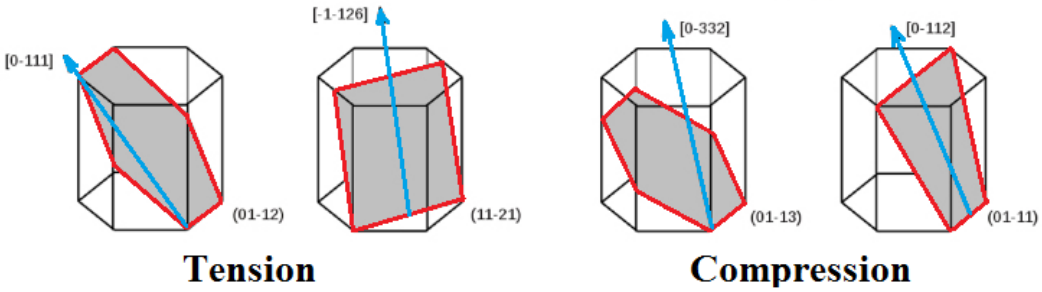

Figure 1.31: Twinning systems in h.c.b. crystal under tension and compression

Each slip system can be characterized by critical resolved shear stress (CRSS) which is required for activating them. The CRSS is quite high for twinning slip systems, that make such type of plastic deformation is more difficult. It is generally assumed that prismatic slip has the lowest critical resolved shear stress of the available deformation modes in pure titanium [102, 103]. The strong anisotropy of slip-systems makes polycrystalline of h.c.p. material extremely difficult to deform [92].

1.11 Fatigue in $(\alpha + \beta)$ Titanium alloys

The fatigue performance of titanium alloys is determined by the deformation behaviour and strength. Alloys that are likely to exhibit strain localization tend to have poor low cycle fatigue (LCF) ($< 10^3$ cycles) properties due to early crack initiation in slip bands, while alloys that exhibit higher strengths will display longer fatigue lifetimes in the high cycle fatigue range. It was also noted the ability of similarly oriented grains to transmit slip from one grain to another in these alloys. In the LCF regime, crack initiation occurs very early (in terms of life), and fatigue lifetimes are dominated by the fatigue crack growth mechanisms. At lower stresses in HCF and VHCF fatigue crack initiation occupies increasingly larger portions of the total fatigue lifetime. Thus micro-structural morphologies that exhibit improved LCF behaviour, i.e. higher fatigue crack growth resistance, generally will not exhibit superior HCF and VHCF behaviour, due to their inferior fatigue crack initiation resistance, Fig. 1.25.

From the micro-mechanical point of view fatigue damage accumulation in titanium alloy is commonly associated to sliding process in hexagonal close packed α-phase [104, 105, 106, 107].

This is fair as for high amplitude loading (LCF) [106], as well for medium amplitudes (HCF) [107]. Recent in-situ fatigue tests have clearly shown, the initiation of the crack in slip traces, Fig.1.32 [57].

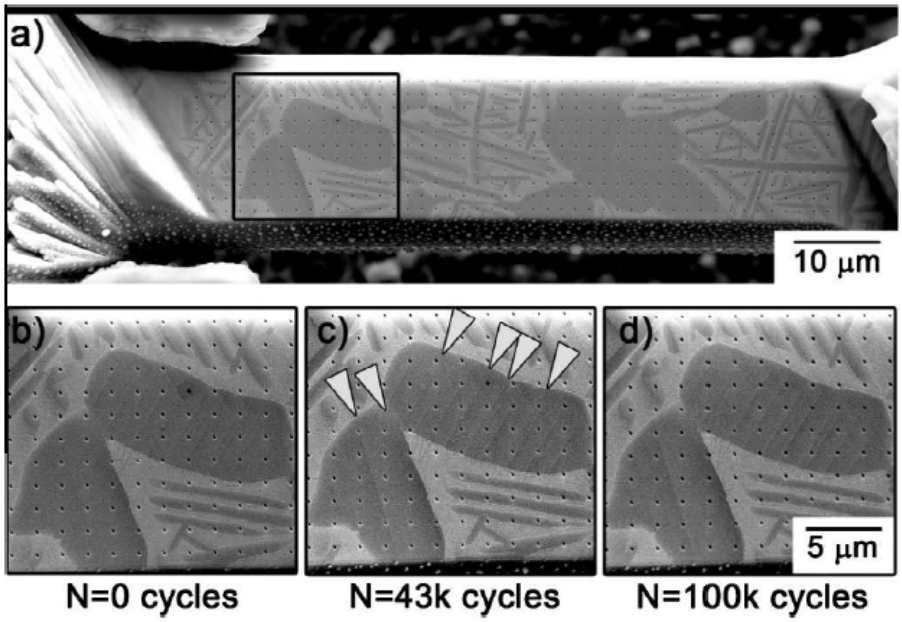

Figure 1.32: In-situ fatigue tests on two-phase titaniumù alloy showing plastic deformation by slip in α-phase, [57]

Typically, in case of titanium alloys with duplex micro-structure the fatigue crack initiates on the basal plane of α_p grains [108, 109, 110, 111, 112]. Nonetheless, the mechanisms of crack initiation depends on the initial micro-structure, texture, micro-texture and loading conditions. For example if texture or coarseness of the structure is favourably arranged for high tensile stress across the basal plane crack will initiate on this plane, otherwise slip on other panes will perform the nucleation job, although at a higher number of cycles for failure [105]. At a lower stress amplitudes the crack initiation by slip in α-phase changes to initiation at α/β interfaces [113, 114]. According to Suhua [115] the fatigue crack initiates in the interface of grains having a more high disorientation. In this case, the crack initiates as a result of relaxation of strain incompatibility between neighbouring grains. Another explication of crack initiation in inter-phase α/β is the existence of stress gradient between phases under loading [116].

With further decreasing of stress amplitude, the crack initiation site usually moves from surface to subsurface [3, 117]. Chai and Zhou [117] have investigated Ti-6Al-4V under VHCF loading by using ultrasonic fatigue testing system. They observed, that for two-phase titanium alloy crack initiation site for two-phase titanium alloy is located in the bulk of material,

that is in agreement with general scheme of fatigue crack initiation proposed by C.Bathias [3]. The analysis of crack initiation site have shown, that fatigue crack nucleated from α/β - interface, that is in agreement with results of surface initiation at low stress amplitudes. However, since 1976 when one of the first subsurface crack initiation was observed in two-phase Ti-6Al-4V titanium alloy [118], the typical subsurface crack initiation is associated with so-called 'smooth facets', Fig. 1.33 [119]

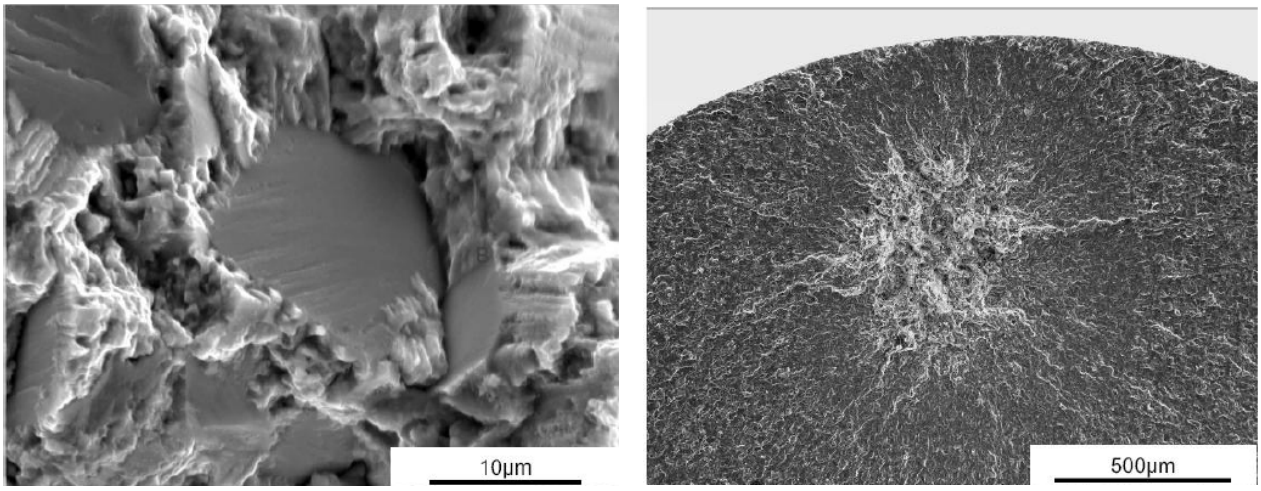

a) b)

Figure 1.33: An example of subsurface crack initiation from the smooth facet [119]

Neal [118] established, that internal crack occurs at smooth facets forming within nodules or packets of nodules. He showed that such smooth facets have an angle of about 14° by the basal plane of h.c.p lattice. The formation of such facets was explained by accumulation of plastic deformation in the α/β interface and consequently, creation a sufficient local stress for cleavage. Meanwhile, recent investigations on the 'smooth-facet' [120] has shown, that such facet-like fractures occur at one of the principal slip systems of h.c.p. (basal or prism). Herewith, it was cited that surface fatigue crack commonly occurs on basal slip plane, while in case of subsurface initiation both slip-systems are equally. Nonetheless, in case of high textured titanium alloy, the basal plane can become more suitable for crack initiation. As it was reported by Chan in 1981 [121, 100], and by Bache for Ti-6Al-5Zr-0.5Mo-0.25Si in 1998 [122] fatigue crack initiation in colonies of α-platelet occurs in long basal slip bands. These slip bands crosses several α-lath. Later, in his paper [123] Bache discusses the influence of the homogeneity of the micro-structure and grain size on crack initiation. He cited that a small grain size together with a more homogeneous structure should reduce the magnitude of the shear and tensile stresses induced in the regions where facets are likely to form [123].

Thus, summarizing the results of precise investigations on the fatigue crack initiation in titanium alloy, the following conclusions can be derived:

1. Under high stress amplitude fatigue damage accumulation leading to crack initiation is concentrated in the α-phase by developing slips at surface.

2. With decreasing the stress amplitude, fatigue damage accumulation leading to crack initiation is concentrated in the α/β interface at surface.

3. With further decreasing the stress amplitude the fatigue damage accumulation leading to the crack initiation is localized in the bulk of material. The mechanism of accumulation is strongly depended on the material micro-structure. In case of highly textured micro-structure plastic deformation can relate to sliding by the basal planes of similarly orientated α-platelet. Otherwise, plastic deformation is related to basal (or prism) sliding of individual nodule or packet of nodules. In these cases, crack initiation is explained by incompatibility in strain between neighbouring grains or phases.

In Gigacycle or VHCF there is not so many investigations on the problem of fatigue crack initiation in two-phase titanium alloy. The most deeper studies on this subject are carried out in PhD these of H.Oguma, 'Very High Cycle Fatigue properties of Ti-6Al-4V' Hokkaido University (2006), [124] and PhD these of C.J. Szczepanski, 'The role of micro-structural variability on the Very High Cycle Fatigue lifetime variability of the $\alpha + \beta$ titanium alloy Ti-6Al-2Sn-4Zr-6Mo', The University of Michigan (2008), [103].
Both authors concludes, that crack initiation in Ti-6Al-4V is related to the 'cleavage'-like cracking of the α_p-grains. J.Szczepanski carried out analysis by stereography on such 'smooth' facets and found, that the orientation of these α_p facets indicates that they form due to a slip-type process, i.e. facet poles are commonly orientated by $30 - 60^\circ$ with respect to the tensile axis [103]).

1.12 Influence of micro-structural defects on fatigue

The variability of micro-structure inherent to two-phase titanium alloys can lead to some imperfection of micro-structure at different scales. Hall presents the formalism for this approach by defining these fatigue critical micro-structural features as crack-like discontinuities (CLD). A CLD is defined as the minimum feature size at which the accumulated fatigue damage begins to behave as a fatigue crack. As Fig. 1.34 illustrates, a CLD may be related to the scale of the micro-structure and for different heats of material may be defined as α_p grains, α colonies, prior β grains, or the size of micro- textured regions (macro-zones).
where D_a is the size of α_p grain (Fig.1.34,a); D_c is the size of α-colony (Fig.1.34,b); D_b is the size of primary β-grain (Fig.1.34,c) and D_t is size of macro-zone.

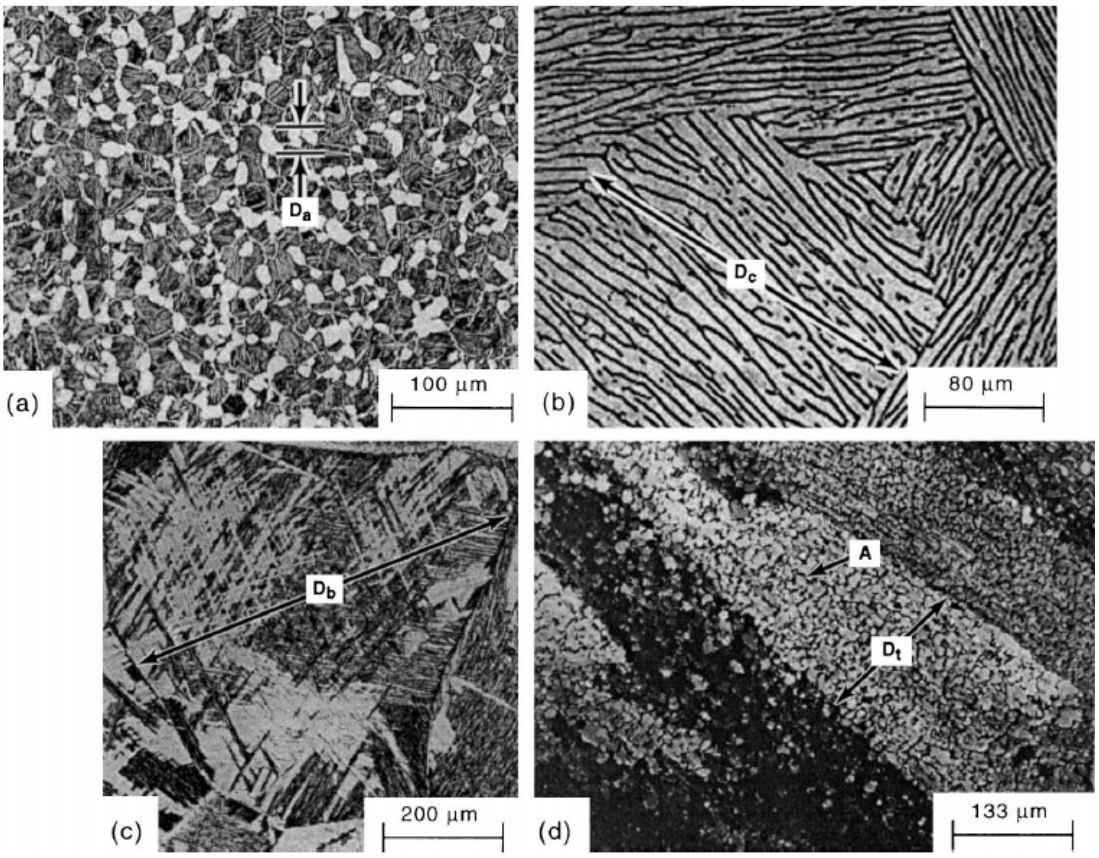

Figure 1.34: The multi-scale approach for classification of critical micro-structural features of titanium alloys, [105]

According to J.A.Hall, the existence of such micro-structural elements and their distribution will determines the fatigue life of the material. Both the micro-structure and the type of fatigue loading will ultimately determine the length scale of deformation and, hence, which micro-structural feature will be responsible for fatigue crack initiation.

Primary α_p-grains. At the smaller scale-level the crack initiation is related to the size of individual α_p grain (several micrometers). Mahajan [116] noted that bigger α_p - grains or clusters of such grains are favourable for fatigue crack initiation sites;

The α-colonies. The next scale level of fatigue damage accumulation is the α - colonies which can be several tens of micrometers. The fatigue crack in Widmanstatten micro-structure occurs across the α-colonies [125]. It can be explained by easiest transition of slip across the α-lath in transformed β-region. The size of prior β_p grain determine a region within which such α-colonies can be formed. Moreover, the α/β boundaries may also often manifest themselves as crack initiation sites [126].

Micro-textural regions. The typical size of macro-zones is vary from several hun-

dreds of micrometers up to several millimetres [100]. Experimentally it was shown, that micro-textural regions are more susceptible to fatigue crack initiation [100, 127]. Increased susceptibility of micro-textured regions to fatigue cracking is speculated to occur, since fatigue damage is accommodated nearly uniformly in these regions. The same result reported by Davitson and al. [128]. They called such micro-textural regions as 'super-grains' and suggested that super-grains were more susceptible to fatigue crack initiation, because localized deformation in one grain could be more easily accommodated in adjacent grains due to their similar crystallographic orientation leading to damage accumulation across these regions.

The denoted above features of micro-structure which becomes critical under cyclic loading shows the same tendency over the whole scale levels. Under high stress amplitudes the mechanism of slip within micro-structural element whether it is α_p-grain or macro-zone is activated. With decreasing of stress amplitude, the second main mechanisms is activated. It is slip incompatibility at an interface such as α grain boundary, colony boundary or the edge of two prior β grains. The clear relation between stress amplitude and activating mechanism does not exists as for HCF as well for VHCF, probably because of lack of systematic investigation. The data used for deriving general conclusions are captured from different studies and were obtained for different alloy. Thus, an investigation on constituencies of crack initiation mechanisms for one titanium alloy is an interesting subject for investigations.

1.13 The Very-High-Cycle Fatigue in titanium alloy

As noted above, the number of investigations on the VHCF properties of titanium alloy is limited. Moreover all available in the literature results are not dealing with deep microstructural analysis and focused on the problems of SN-curve course and scatter of experimental data. Thus, it is almost impossible to uniquely identify the main mechanisms responsible for fatigue crack initiation in two-phase titanium alloy under VHCF loading. In this section the results available in the literature will be mainly discussed in the way of correlation between mechanical properties (fatigue strength, course of SN-curve) and micro-structure.

Almost all the two-phase titanium alloys have typically a transition in crack initiation mechanism with decreasing of stress amplitudes. Under higher loading amplitudes (lower stress range of HCF) the two-phase titanium alloys exhibit single surface crack. With decreasing the stress amplitude to so-called 'fatigue limit' and slightly below, the crack initiation site is commonly observed in interior regions. The sharp transition between surface and subsurface crack initiation can not be determined for titanium alloy as well for many metals. The transition of crack initiation mechanisms depends on the micro-structural features of the alloy. The existing of defects in micro-structure as usual reduce the fatigue life at which the first transition can be observed. The next typical features of two-phase titanium alloys is

large scatter of fatigue life in VHCF. Typically, the scatter reaches 2-3 orders of magnitude [103] for most of the titanium alloys. The significant scatter in fatigue life leads to use a bi-modal distribution for reducing 'uncertainty in fatigue life' [2, 71]. According to bi-modal distribution a two different branches for surface and subsurface crack initiation can be determine. The course of the subsurface branch (typically starts at about 10^6 cycles) is also different for several alloys. In some cases, a slop of curve in VHCF region is quite important, sometimes it is almost vanished (slow decreasing in fatigue strength with increasing a fatigue life). Some explication for difference in SN-curve slop was proposed by C.Bathias [3] based on effect of cyclic softening and hardening. In case of cyclic softening the stress amplitude under the same strain amplitude is decreasing, while in the case of cyclic hardening, the tendency is reversed (stress amplitude is increasing). Thus, such cyclic behaviour of material can influence the slope of the SN-curve.

The mechanical properties (fatigue strength) of titanium alloys in VHCF is determined by their micro-structure. In the work [129] the high-strength Ti-6Al-2Sn-4Zr-6Mo titanium alloy produced in four different ways was investigated. Each process led to certain micro-structures: fine platelet, coarse platelet and two equiaxed α + transformed β structures with different phase fractions. The results, Fig.1.35 shows a significant difference in fatigue strength between different micro-structures.

The analysis of results presented in the Fig.1.35 shows, that coarse needle-like structure has the lowest fatigue strength in the VHCF region. The fine needle-like structure shows improved fatigue strength compared to the coarse structure, but it is still below the results for duplex micro-structures. Such fatigue behaviour can be explain based on general relation between micro-structure type and corresponding properties of material, Fig.1.25. In case of VHCF loading, the crack initiation is the fatigue life controlling parameter. Generally, the needle-like structure shows a lower resistance to fatigue crack initiation compared to equiaxed structure. That explains the better fatigue properties of equiaxed structure, Fig. 1.35. Herewith, the coarse structure has also a lower resistance to fatigue crack initiation compared to the fine structure. Thus, the lowest fatigue strength of coarse needle-like structure is in good agreement with general tendencies in correlation between material properties and its micro-structure. This result is very important, because it gives a reason to believe, that some general rules which are fair for fatigue in general (LCF, HCF) can be extended into the VHCF region.

The analysis of fracture surfaces of specimens fatigued in VHCF region commonly shows 'smooth' facets at the initiation site for two-phase titanium alloy. These facets are commonly called as 'cleavage facet' because of their typically brittle or quasi-brittle character. Several mechanisms have been proposed for the formation of such facets. According to Bache [122] the 'smooth' facets form by basal plane of h.c.p. structure as result of sliding process together

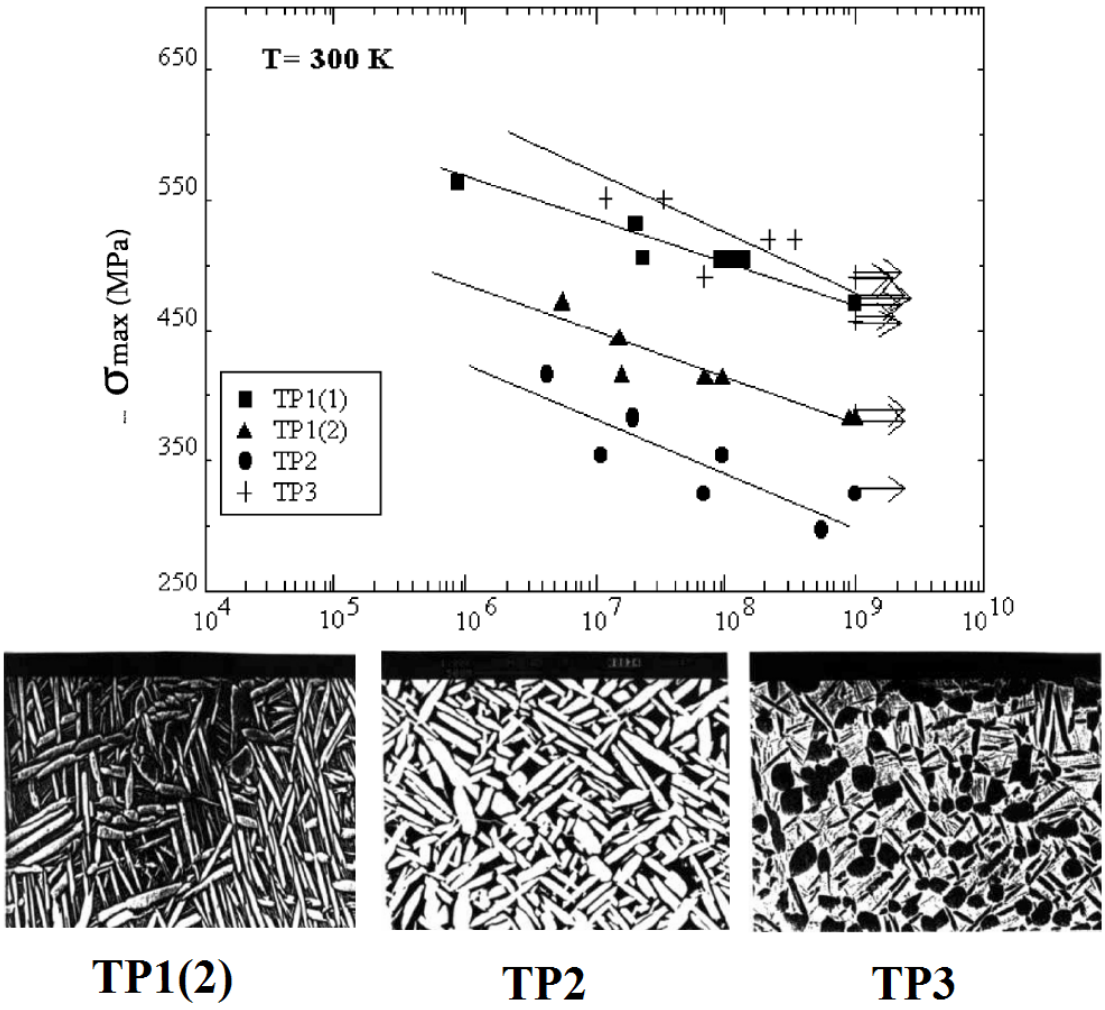

Figure 1.35: The results of fatigue tests on Ti-6Al-2Sn-4Zr-6Mo titanium alloy proceeded in four different ways, [3]

with acting a normal stress component on this plane. According to A. Shanyavskiy such smooth facets forms under local twist together with compressive component of normal stress acting on this plane [130]. The detailed analysis on the smooth facets showed that they are formed within one of two principal slip planes of h.c.p: basal or prism. However, sometimes the plane of smooth facet can have an angle by the basal or prism plane [118]. In this case the formation of brittle facet is explained by incompatibility in strain between α_p grain and surrounded β-phase. Szczepanski in his PhD has shown, that such 'smooth' facets could have different (from 30 to 60) pole orientation with respect to the loading axis, but clear correlation between fatigue life and facet's orientation can not be found [103]. Beside the facets-like crack initiation, some others reported the internal fatigue crack initiation from the

α/β interface [99].

Thus, following the classification of Hall, Fig.1.34 fatigue crack initiation under VHCF is commonly related to the α_p-grain scale-level. In this case a critical parameters becomes the size, mutual and global orientation of α_p-grain by the neighbouring grains and loading axis respectively. The results about the influence of other micro-structural features such as α_p clusters or macro-zones on mechanisms of VHCF initiation in two-phase titanium alloys is quite limited or absent.

Chapter 2

Materials and Experimental method

The problem of fatigue in aeronautical industry was briefly discussed in Chapter I. It has been highlighted that many aircraft elements are subjected to different types of cyclic loading. Engine components are often experiencing a high frequency loadings, that lead to the gigacycle fatigue life regime in-service. The two principal material for turbo-jet engine are titanium and nickel based alloys. The present research project is focused on the problem of VHCF behaviour of aeronautic titanium alloy. The specimens for VHCF tests were fabricated from the two-phase titanium alloy VT3-1 produced by two different processes: forging and extrusion. The forge technique is commonly used for turbine disks production. Thus, the specimens made from forged VT3-1 titanium alloy were machined from the compressor disk of an aircraft 'Tu-154' (Tupolev), Fig.2.1 (a). The specimens for fatigue tests from extruded VT3-1 titanium alloy were machined from bars with external diameter of 10 mm and length of 150 cm, Fig.2.1 (b). The bars of extruded titanium were provided by the All-Russian Institute of Light Alloys.

2.1 Forged VT3-1 titanium alloy

The specimens made from forged VT3-1 titanium alloy were machined from one compressor disk after being used on an aircraft (i.e. the forged Ti-alloy is not virgin). The disk was in-service for 8000 flight cycles (take-off - landing) on one of the aircraft Tu-154 made by 'Tupolev' company. The disk was a part of the D30KU-154 turbo-jet engine. After reaching the designed guaranty life, limited by around 18000 hours, the disk was removed from the turbo-jet engine and replaced by a new-one. The old disk had passed the after-service control for fatigue damage accumulation or in-service cracks. The results of control did now show any evidence of fatigue damage, any deviation in mechanical properties and any deviation in chemical composition. Thus, the disk was used for further fatigue tests. The technological

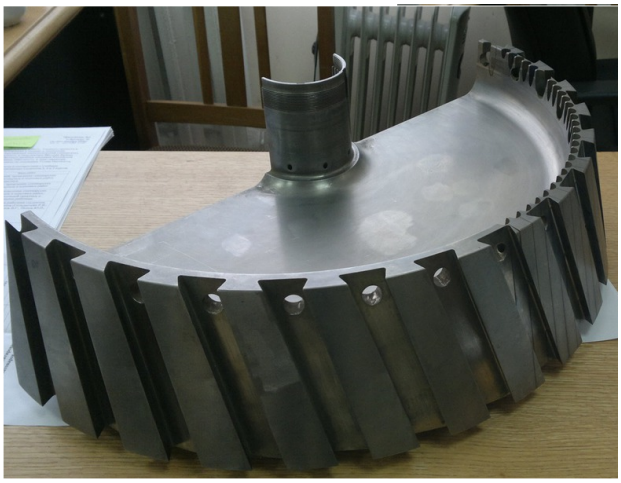

a)

b)

Figure 2.1: Forged compressor disk (a) and extruded bars (b) made from VT3-1 titanium alloy

process of turbine disk production is a commercial secret. That's why a wide spectrum of investigations on mechanical properties, micro-structure and chemical composition was required.

2.1.1 Chemical composition of forged VT3-1

The VT3-1 titanium alloy is a two phase (alpha + beta) alloy with the following main alloying elements: aluminium to stabilize the alpha phase, molybdenum and chromium to stabilize the beta phase. The standard chemical composition for VT3-1 titanium alloy series (according to the Russian State Standard [131]) is given in Table 2.1

Table 2.1: Standard chemical composition for VT3-1 titanium alloy according to [131]

Fe	C	Si	Cr	Mo	N	Al	Zr	O	H	Ti
0.2-0.7	< 0.1	0.15-0.4	0.8-2	2-3	< 0.05	5.5-7	< 0.5	< 0.15	< 0.015	Bal.

Before fatigue testing a chemical composition of the forged VT3-1 Ti-alloy was carried out in the laboratory of the Russian State Centre of Flight Safety. The results are presented in Table 2.2

Table 2.2: Chemical composition of forged VT3-1 titanium alloy

Fe	C	Si	Cr	Mo	N	Al	Zr	O	H	Ti
0.7	< 0.1	0.29	2.1	2.1	< 0.05	6.1	< 0.02	< 0.15	< 0.015	Balance

2.1.2 Micro-structure of forged VT3-1 titanium alloy

Rim part of the disk

The forged VT3-1 is a two phase (alpha + beta) titanium alloy that has needle-like micro-structure. The elongated alpha-phase platelets are separated by thin borders of beta phase (Fig.2.2).

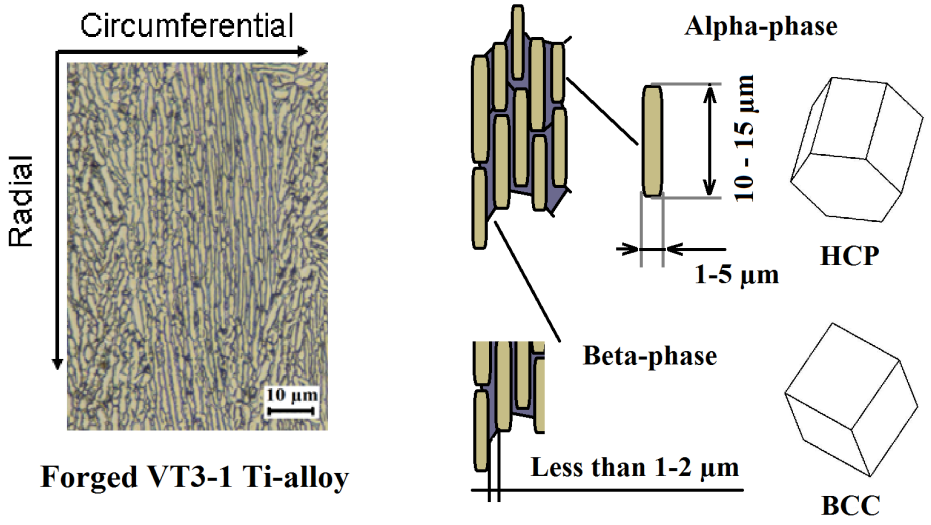

Figure 2.2: Microstructure of forged VT3-1 titanium alloy

The characteristic sizes of alpha-phase platelets are the following: length (in elongated direction) is around $10 - 15\mu m$, the width of platelets is varying from one to several micrometers. Alpha-phase has a hexagonal close packed (h.c.p.) structure. The characteristic width of borders made from beta-phase is one-two micrometers only. The fraction of beta-phase in forged VT3-1 does not exceeds 20 %. It is well known, that properties of pure titanium is not always isotropic because of features of crystallographic structure of h.c.p. [92]. Sometimes, a polycrystalline of titanium, such as two phase alloys shows anisotropic mechanical properties. Taken that into an account anisotropy of forged VT3-1 fatigue properties has been investigated in the present project. In order to have the possibility to correlate fatigue properties with respect to micro-structure the micro-structure was investigated in

three mutually-perpendicular planes, (Fig.2.3).

The cylindrical bars (blanks for specimens) were machined from the rim part of the disk in vertical direction, i.e. parallel to the rotation axis of the compressor disk. One of these bars was cut into three pieces by mutually-perpendicular planes. These planes were indexed by appropriate directions, (Fig.2.3): axial direction is parallel to the disk rotation axis; radial is direction along the disk radius; circumferential is the direction perpendicular to the radial in plane of disk's plateau part (Fig. 2.1a) .

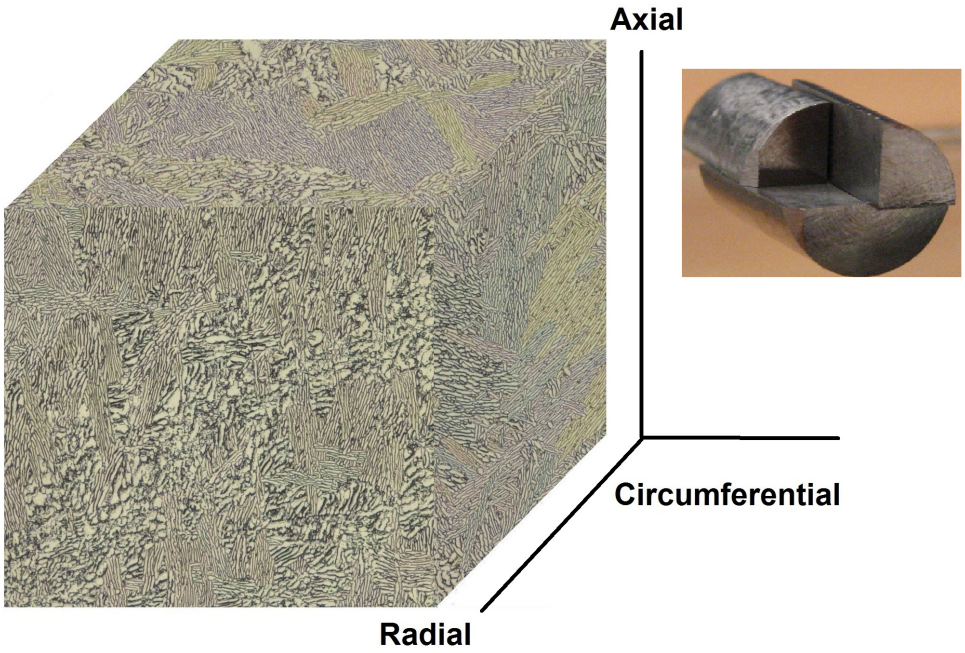

Figure 2.3: The 3D map of micro-structure of forged VT3-1 titanium alloy

The specimens for micro-structure observation were mechanically polished in three steps: (1) by SiC emeries papers with 600, 800, 1000, 2400 and 4000 grades; (2) by polishing disk with suspensions of 6 μm, 3 μm and 1 μm; (3) by OPS (Oxide Polishing Suspension). After the polishing, the specimens (micro-sections) were chemically etched by KROLL solution (distilled water 92 ml, HNO_3 6 ml and HF 2 ml) during 40 sec. The details of micro-structure observation on two different specimens are shown in Fig.2.4 for each planes.

The micro-structure morphology is almost the same within all the three perpendicular sections of one specimen, but it could be significantly different for different specimens (i.e. different morphology can be observed at different locations along the rim of the disk, see Fig. 2.4). Fig. 2.4 shows the micro-structure morphology at two different locations within the rim (specimen 1, Fig. 2.4 (a), (c), (e) and specimen 2, Fig.2.4 (b), (d), (f)). Two cylindrical bars were machined from the rim part of the disk by using the same (electro-

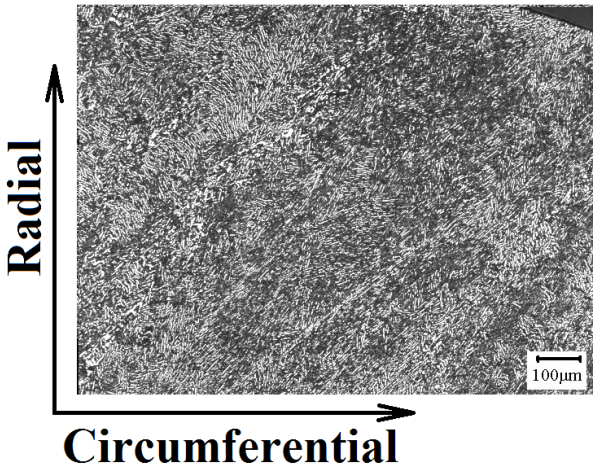

a) Axial plane, Sample 1

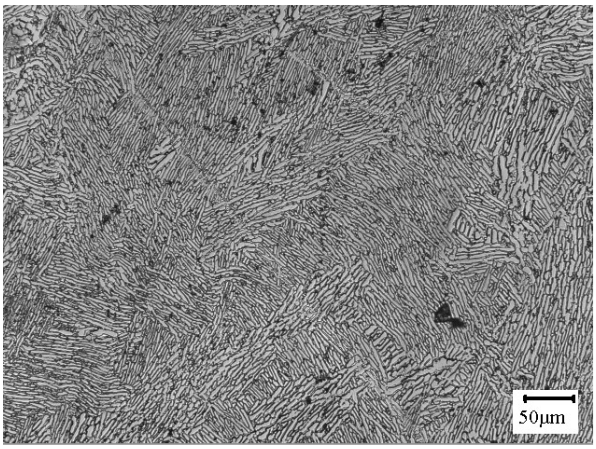

b) Axial plane, Sample 2

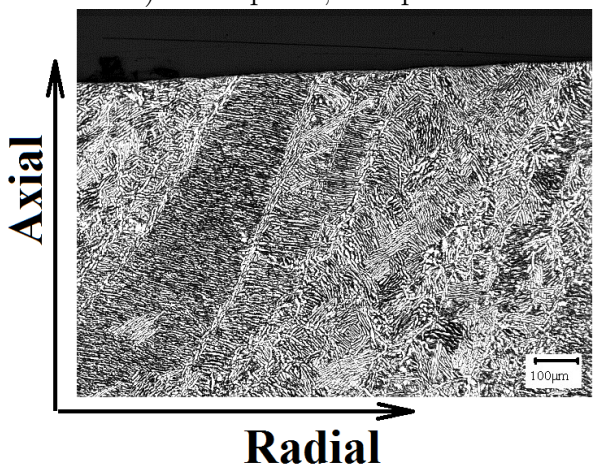

c) Circumferential plane, Sample 1

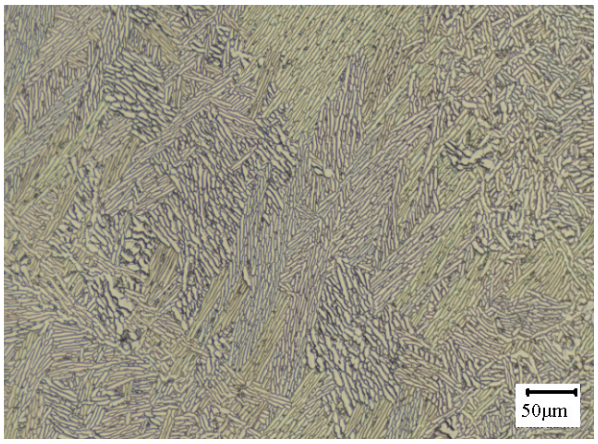

d) Circumferential plane, Sample 2

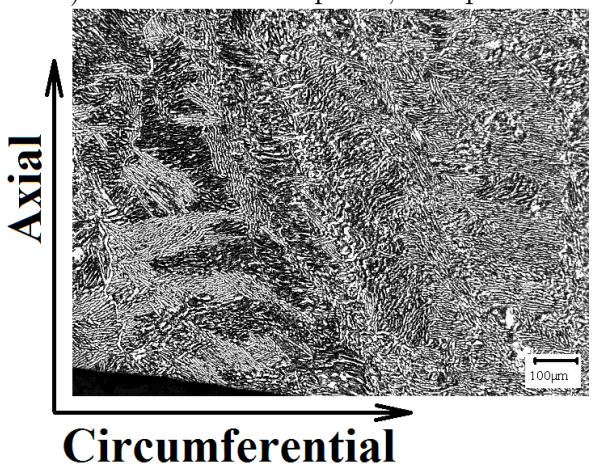

e) Radial plane, Sample 1

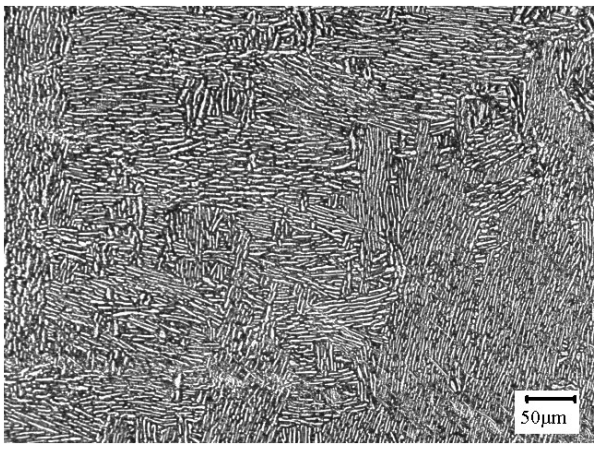

f) Radial plane, Sample 2

Figure 2.4: The micro-structure of forged VT3-1 in three mutually-perpendicular planes: (a), (c), (e)Sample 1, (b), (d), (f) Sample 2

erosion) method. The variation of the micro-structure morphology along the circumferential direction can be explained by either in-service loading effect on the material or by an initial micro-structure state due to fabrication process. Anyway, the micro-structure of forged two phase VT3-1 titanium alloy shows a significant variability in the rim part of the disk along the circumferential direction. However, the morphology of micro-structure in local zones is quasi isotropic. In order to simplify further discussion the planes of micro-section will be named by the normal vector (direction) of the corresponding section. Thus, the 'axial-circumferential' plane is named radial, the 'axial-radial' plane is circumferential and 'radial-circumferential' plane is named axial, Fig.2.4. This classification will be use all over the following sections and PhD report chapters as for micro-sections indexation as well for the specimens sets names. Comparing the images taken for the same specimen in three mutually perpendicular directions, just slight difference between radial and circumferential planes can be outlined. The slight difference can be noted for axial plane in several locations. The axial plane differs from two others by less perturbed morphology of the micro-structure, Fig.2.4 (a). For another location the difference between all the three planes is almost vanished, Fig.2.4 (b-d-f). Thus, the variation of micro-structure is quite high from one location to another within the rim part of the disk, but not everywhere consequently the micro-structure is heterogeneous.

Plateau part of the disk

As it was mentioned above, the mono-crystal of titanium and even poly-crystalline, could have a significant anisotropy of mechanical properties. In order to study a fatigue properties anisotropy within titanium disk, several sets of specimens were machined from the rim part and some sets were from the plateau part of the disk. The micro-structure of titanium alloy taken from the plateau part was studied in the similar way to the rim. The micro-sections for observations were cut from the 'queue' part of specimen, where an influence of ultrasonic fatigue testing is negligible, Fig.2.5.

The specimens from the plateau part were cut along and perpendicular to the radius of the disk. Such cut allows to study the fatigue properties and the micro-structure in two mutually-perpendicular directions (planes). The procedure of micro-section preparation for plateau part specimens (polishing and etching) was kept the same with the rim part specimens (see the subsection 'Rim part of the disk'). The analysis of 'radial' and 'circumferential' micro-sections shows that there is not any noticeable difference in micro-structure morphology between micro-sections from the plateau part, Fig.2.6.

Within both, radial and circumferential micro-sections, several different types of micro-structure morphologies can be observed. At some locations zones filled by needle like alpha-phase platelets are surrounded by coarse alpha-phase nodules that have a near to globular

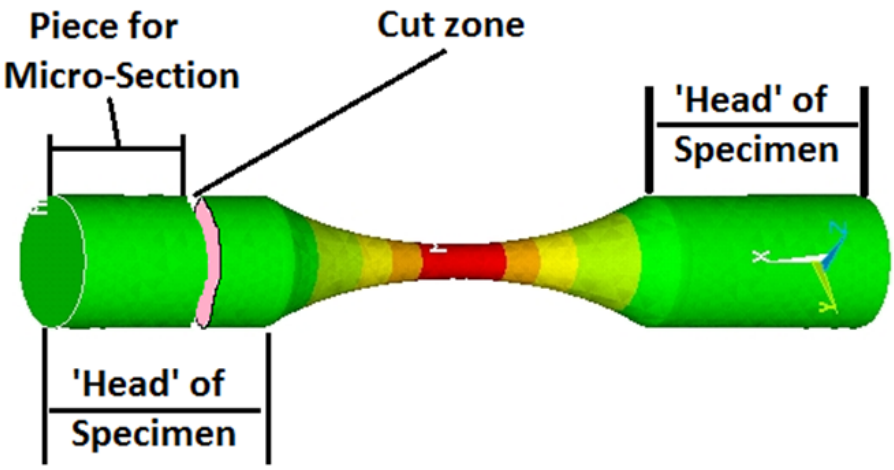

Figure 2.5: Dynamic stress distribution along specimen's axis with denoted plane of cut for micro-section

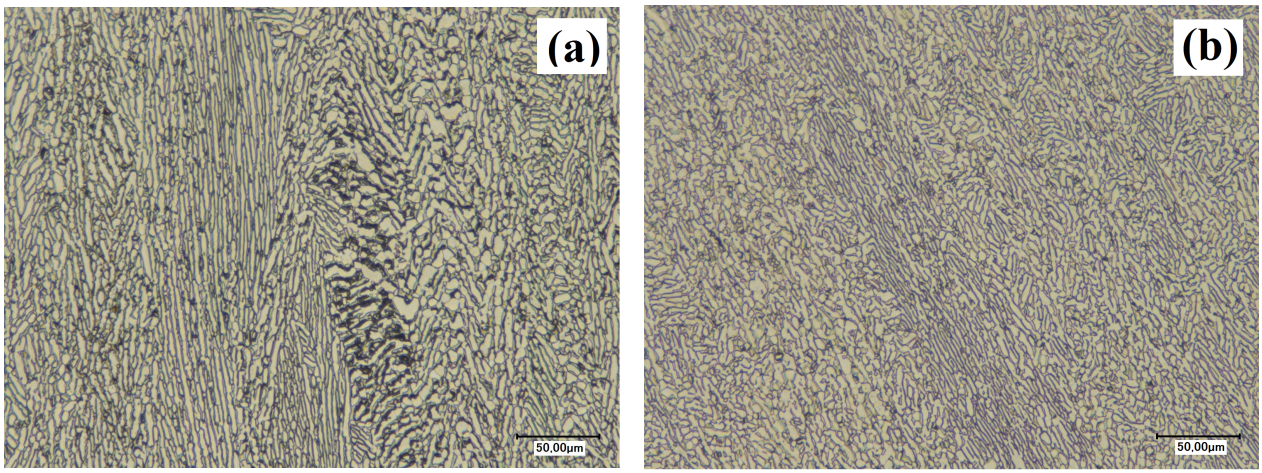

Radial plane Circumferential plane

Figure 2.6: Micro-structure of VT3-1 titanium alloy in plateau part: (a) radial plane, (b) circumferential plane

shape. At another location some zones filled by identically orientated elongated alpha-phase platelets are surrounded by areas with randomly orientated alpha-platelets. Sometimes 'cheese-board' morphology of micro-structure can be found. All these features are micro-structure were observed on several micro-sections. Thus, these variations of micro-structure morphology at radial and circumferential micro-sections can be associated with local changing of structure within micro-section and is not clearly related to the orientation of micro-section in the disk.

Table 2.3: Micro-hardness of VT3-1 in three mutually perpendicular planes

Plane	Axial	Circumferential	Radial
HV500	366	363	362

Concluding the results of observation on forged VT3-1 Ti-alloy micro-structure the following key points should be outlined: (1) micro-structure of forged titanium shows significant variation of morphology within the rim part of the disk while in the plateau part it is more homogeneous; (2) the changing of micro-structure has a local character and is not related to the orientation of the specimen ('axial', 'radial' or 'circumferential' direction). Thus, small difference of micro-structure morphology can be stated for rim and plateau parts of the disk, while no important local anisotropy was found.

2.1.3 Micro-hardness measurements

The micro-hardness measurements were carried out on the micro-sections in the three mutually-perpendicular planes. All the measurements were carried out on circular micro-section cut from the queue part of specimen machined from: (a) rim part of the disk; (b) plateau part along the radius; (c) plateau part perpendicular to the radial direction. The micro-hardness was measured in the plane, parallel to the fatigue crack growth plane for all investigated sets of specimens. The measurements were realized according to the Vickers method with the following parameters: weight is 500 grammes, time of indention is 10 sec. The average Vickers hardness was obtained for each direction through 15 measurements at respectable micro-sections. The measurement step parameters were determined from a single measurement. The distance from the edge of micro-section (more than 2.5 times the indent mark diagonal) and the step of measurement which is the distance between two indent marks (not less than 3 times the diagonal). The characteristic size of pyramidal dimple is 50 - 55 μm. Thus, the micro-hardness was measured at constant intervals of around 600 - 650 μm (10 times the diagonal) along the diameter of circular micro-section. The first point spaced from the edge about $200\mu m$ (4 times the diagonal). The results of micro-hardness measurements in the three mutually perpendicular directions are almost the same. The average value within each plane is around $360 \pm 10 \quad HV_{500}$, Table 2.3

Despite the average homogeneity of micro-hardness, the local values shows a significant scatter along the micro-section diameter, Fig. 2.7. For some specimens, the difference between maximum and minimum values of micro-hardness reach 45 HV_{500} (maximum is 399 HV and minimum is 344 HV). There is no correlation between orientation of specimen and

the scatter. The same results were obtained in the three mutually-perpendicular planes.

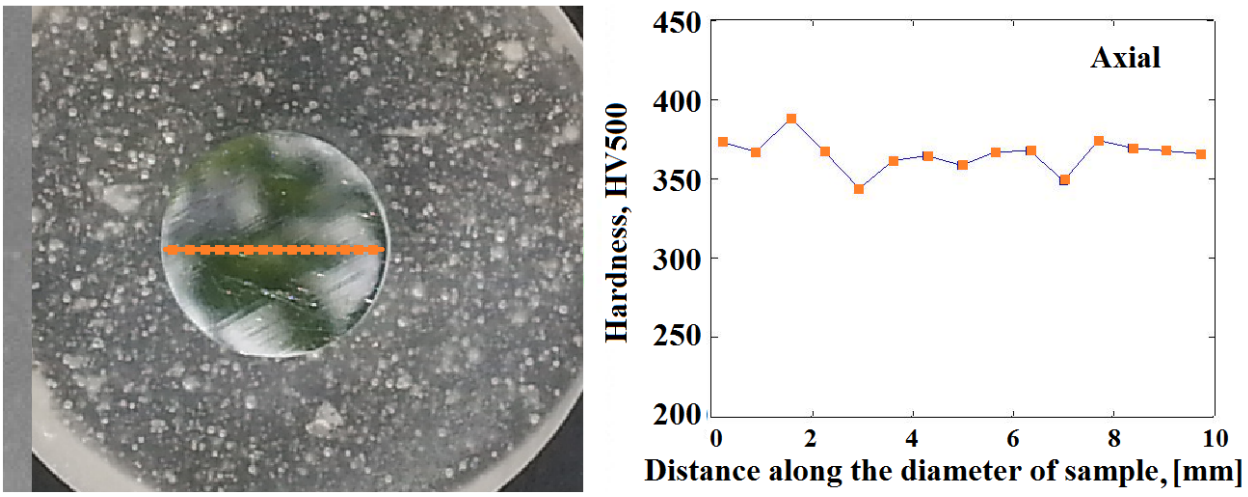

Figure 2.7: Microhardness of VT3-1 along the diameter of sample

These results can be explained by local variation of material micro-structure. The observation of micro-section has shown that the micro-structure of forged VT3-1 titanium alloy consists of clear zones or clusters of grains with quite different morphology of alpha platelets. Sometimes, the very fine alpha-platelets with the similar orientation can be grouped in clusters with the linear size of several hundred micrometers, Fig. 2.8 (a). Sometimes, the micro-structure consists of zones with rough, quasi globular, alpha-phase platelets, Fig. 2.8 (b).

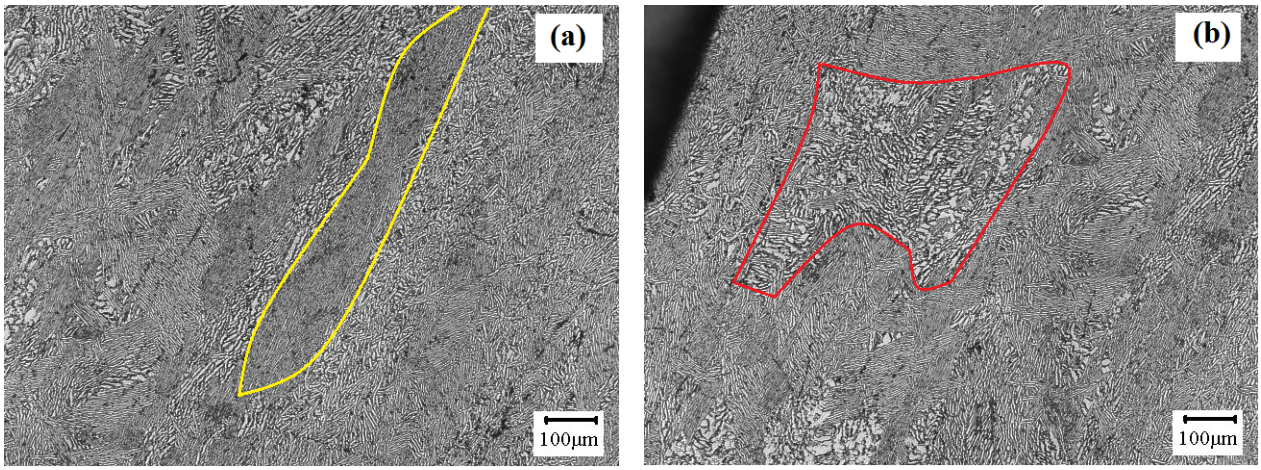

Axial plane Axial plane

Figure 2.8: Clusters of α-grains (a) fine α-grains (b) coarse α-grains

In order to study the influence of such zones on the local value of micro-hardness, addi-

tional investigations were carried out within one of such clusters, Fig. 2.9. The measurements were performed by using Roxwell machine with the next loading parameters: the weight is 200 gr, the time of indentation is 10 sec. The results of micro-hardness measurements within the fine alpha-platelets cluster show a significant drop of micro-hardness within such areas. Almost all the values of micro-hardness were found being lower than 300 HV_{200}.

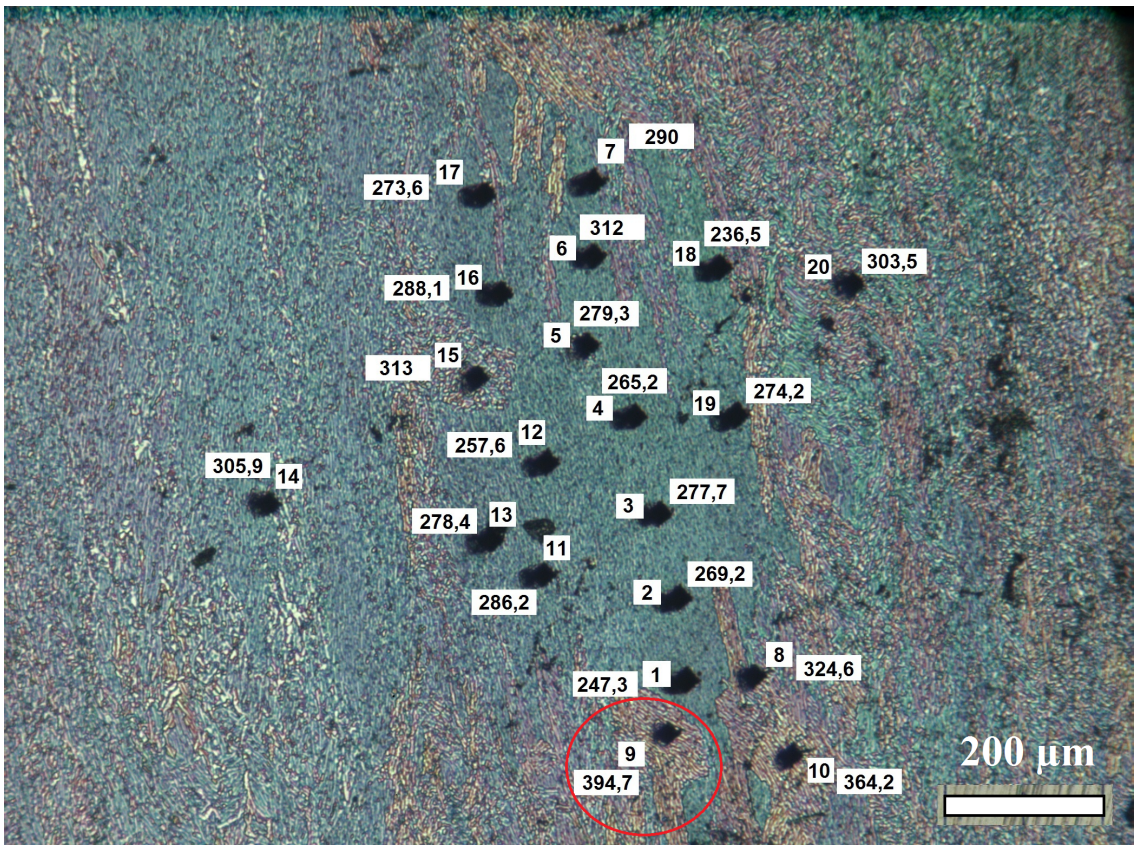

Figure 2.9: Microhardness of VT3-1 within the cluster of fine alpha-phase platelets

In contrary, the small area with rougher alpha-phase platelets, point 9 on Fig. 2.9, shows a considerably higher micro-hardness that is about 395 HV_{200}. Thus, the micro-hardness of forged titanium alloy is depending on the local characteristics of the micro-structure. In case of regular organisation of alpha platelets with characteristic size represented on Fig. 2.2 the value of micro-hardness correspond to the state standard and is about 360 HV. If the micro-structure consists of alpha-platelets clusters with deviated size, the micro-hardness is also varying within such zones. Wherein, the fine alpha-platelets clearly orientated along the same directions, Fig.2.8 (a) shows the lower value of micro-hardness compared to the randomly orientated rough alpha-platelets, Fig.2.8 (b). The same zones of local heterogeneity of micro-structure were found in all mutually perpendicular planes, therefore the variation in micro-hardness values can be explained similarly for all the investigated micro-sections.

The micro-structure of titanium alloy was carefully investigated for the inclusion. Specially for the TiN inclusion that is a common defect of ingots made from titanium. More than 15 micro-sections cut from different positions were investigated. Some specimens were re-polished after observation in order to remove the observed layer. Based on the results of this analysis, it can be outlined, that no one inclusion was observed in forged VT3-1 titanium alloy.

2.1.4 Quasi-static monotonic mechanical properties of forged titanium alloy

The mechanical properties of forged VT3-1 titanium alloy were investigated by using small tensile specimens. The specimen were shaped from the thin rectangular sheets of titanium alloy. These blanks were cut from the plateau part of the disk, Fig.2.10. The specimens were designed according to the ASTM standard, Fig. 2.11 (a) with a characteristic size d = 5 mm. The geometry of tensile specimens is shown in Fig. 2.11 (b).

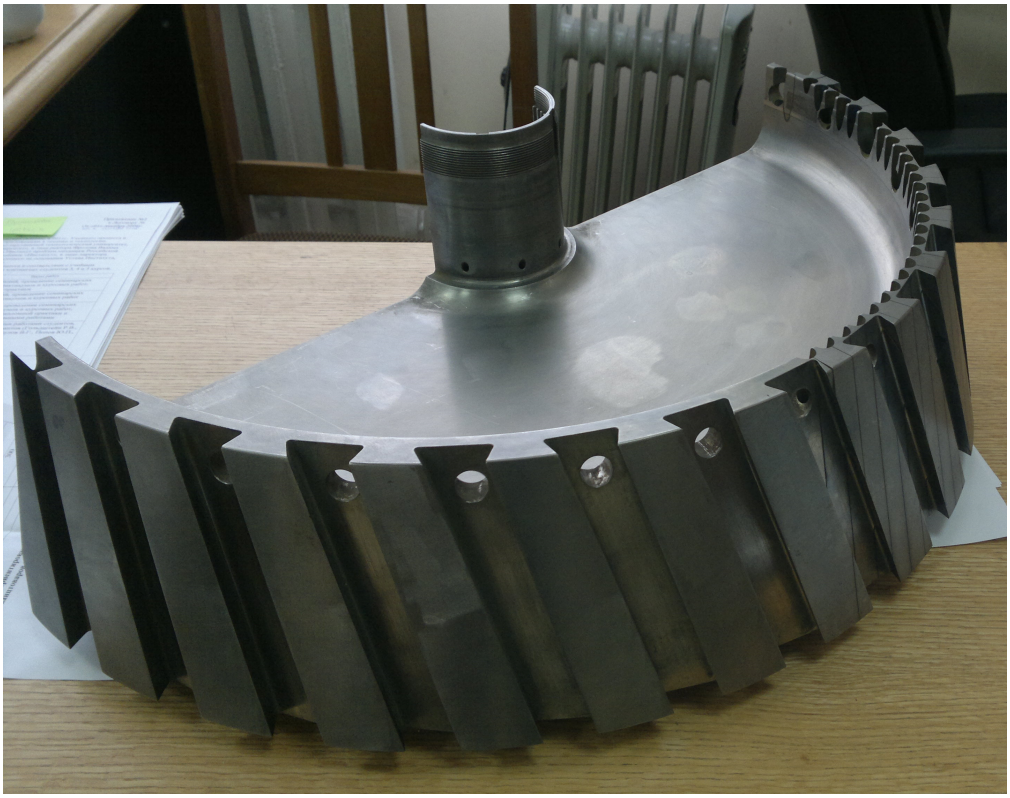

Figure 2.10: The position of blanks for tensile tests in the disk

The specimen was mechanically polished by emery paper of 600 grade in axial direction to vanish the influence of crack concentration due to surface scratch. The specimen was tested

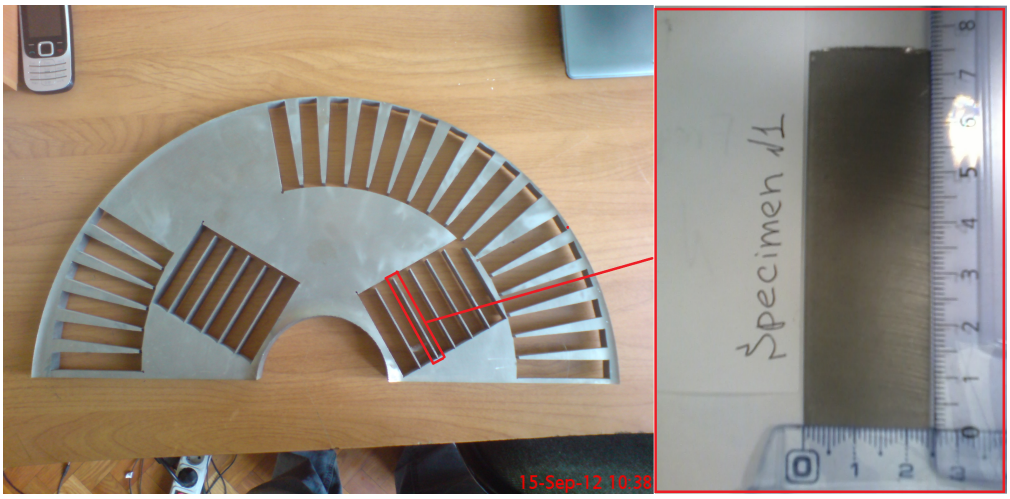

Figure 2.11: The standard for tensile specimens and actual geometry for VT3-1

by using a tensile electro-mechanical machine (INSTRON 5969) on open air. The tensile test was controlled in displacement with loading speed of $V_d = 0.075$ mm/min. In order to measure the deformation of specimen during the test, an extensometer with reference length of 25 mm was used, Fig.2.12. As the specimen's surface was polished the risk of extensometer's knife sliding is appearing. In order to avoid this sliding, shorter and more rigid elastics were used to clamp the extensometer.

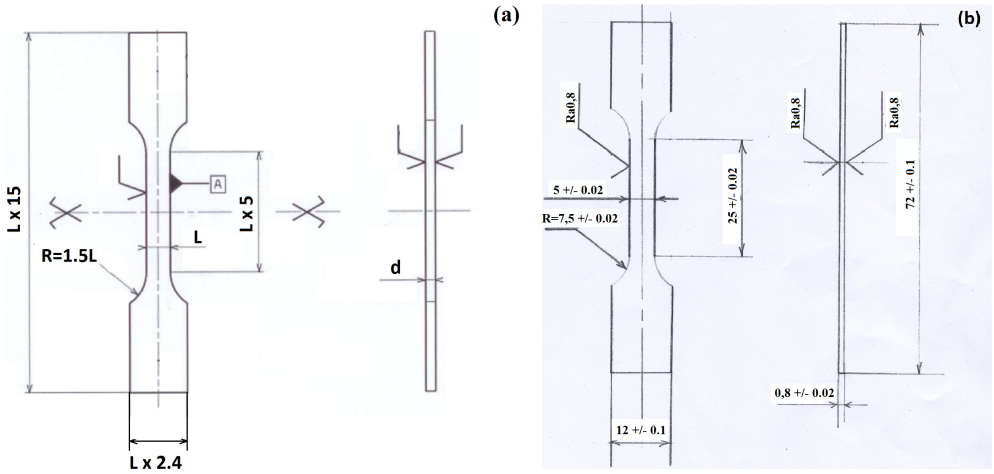

Figure 2.12: The tensile specimen with attached extonsometer, reference length 25 mm

The result of investigation on mechanical properties of forged VT3-1 titanium alloy are listed in table 2.4. The Young's modulus was found to be $E = 116GPa$. The yield stress is 940 MPa and the ultimate tensile strength is 989 MPa.

Table 2.4: Mechanical properties of forged VT3-1 titanium alloy

Parameter	E (GPa)	E_{dyn} (GPa)	$Rp_{0.2}$ (MPa)	Rm (MPa)	ϵ_R (%)	σ_f (MPa)
Value	114	116	960	989	6	978

In the case of gigacycle fatigue testing procedure an additional need for dynamic Young's modulus measurements is arising. Usually, the Young's modulus is sensitive to loading frequencies and at elevated deformation rates may be different from its quasi-static value. The dynamic Young's modulus for VT3-1 titanium alloy was determined by measurements of acoustic wave propagation rate in the bar of VT3-1 titanium alloy. The frequency of this wave was adjusted to 20 kHz that allows to get dynamic Yound's modulus at the same frequency. The result of the measurement is also presented in Table 2.4. The mass density of VT3-1 titanium alloy is 4500 kg/m^3.

The tensile curve for forged titanium alloy shows a very clear stage of plastic deformation, Fig. 2.13. The maximal engineering deformation at rupture is 6 %.

2.2 Extruded VT3-1

The extruded titanium alloy was shaped in bars of 1.5 m in length and three different diameters. The specimens for fatigue tests were machined from the bars with diameter of 10 mm. The specimens for torsion fatigue tests (Chapter IV) were machined from bars with diameter of 14 mm and the specimens for tensile tests were machined from bars with diameter of 16 mm.

2.2.1 Chemical composition of extruded VT3-1

The normal chemical composition for extruded titanium alloy is the same that for the forged VT3-1, Table 2.1. The main alloying elements are aluminium, molybdenum and chromium. The precise analysis of the chemical composition for extruded Ti-alloy was similarly done in the laboratory of the State Centre for Flight Safety. The results are listed in Table 2.5

Table 2.5: Chemical composition of forged VT3-1 titanium alloy

Fe	C	Si	Cr	Mo	N	Al	Zr	O	H	Ti
0.46	< 0.1	0.32	1.25	2	< 0.05	6.3	0.1	< 0.15	< 0.015	Balance

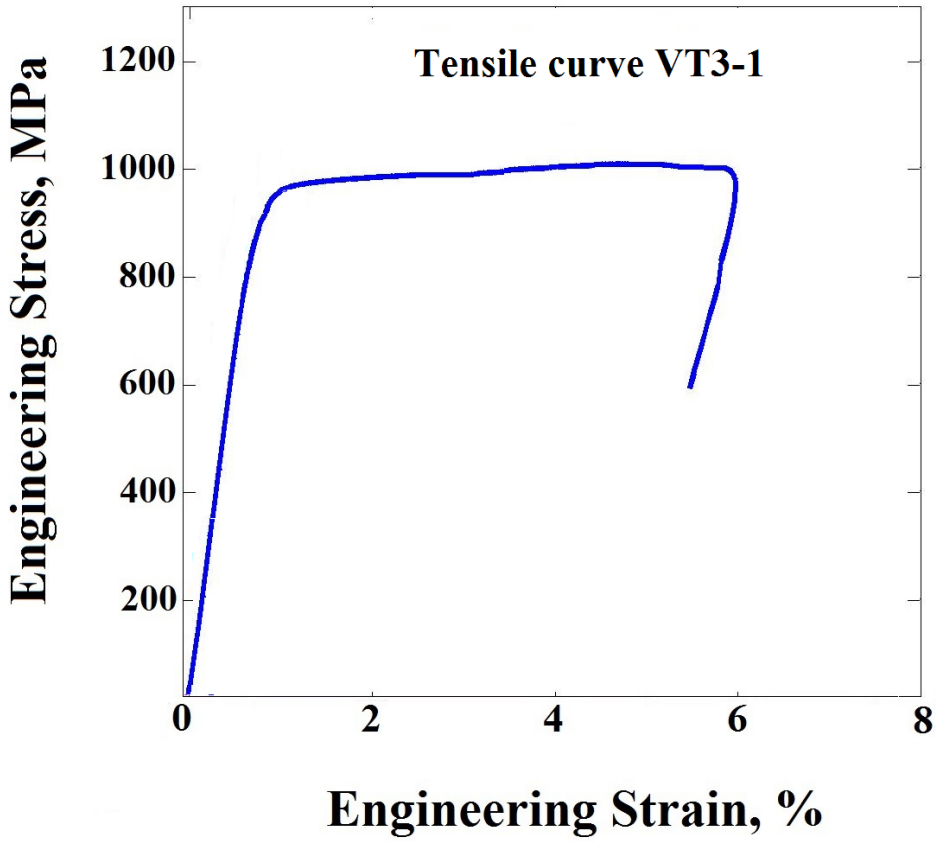

Figure 2.13: The tesile curve for forged VT3-1 titanium alloy

2.2.2 Microstructure of extruded VT3-1 titanium alloy

The micro-sections for micro-structure observations on extruded VT3-1 titanium alloy were cut from bars of diameter 10 mm. The specimens were machined along the extrusion direction. Theoretically, extrusion should produce a micro-structure with axial symmetry around the bar longitudinal axis. In order to confirm that, the two perpendicular micro-sections were cut along the extrusion direction. The observations on these planes show, that the material has a clear axial symmetry. The 3D map of micro-structure for extruded VT3-1 titanium alloy is shown in Fig.2.14.

The micro-structure of extruded VT3-1 titanium alloy is clearly changing from the core of the bar to the lateral surface of the bar. In the centre of the bar, the micro-structure is more rough, the geometry of primer beta-phase can be easily identified, Fig. 2.15. The alpha-phase formed at the borders of primary beta-phase, that can be easily recognized as white contour lines on Fig. 2.15 and grew into the body of beta-phase. The needle structure of alpha-phase platelets is extremely fine within the body of primary beta-phase. The morphology of

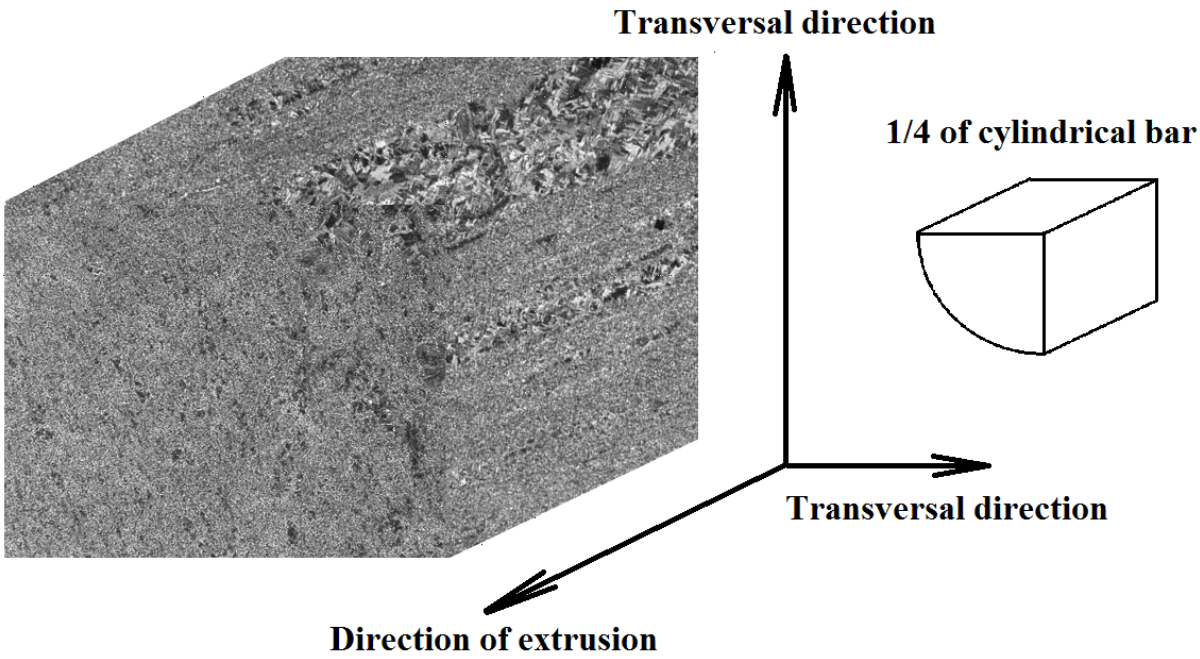

Figure 2.14: The 3D map of microstructure for extruded VT3-1 titanium alloy

micro-structure changes with increasing the distance from the core of the bar. The perturbed micro-structure morphology is localized just near to the bar core and can not be found at distance about 2 mm from the centre. Far from the centre the micro-structure becomes more homogeneous and fine close to the bar edge, Fig. 2.16.

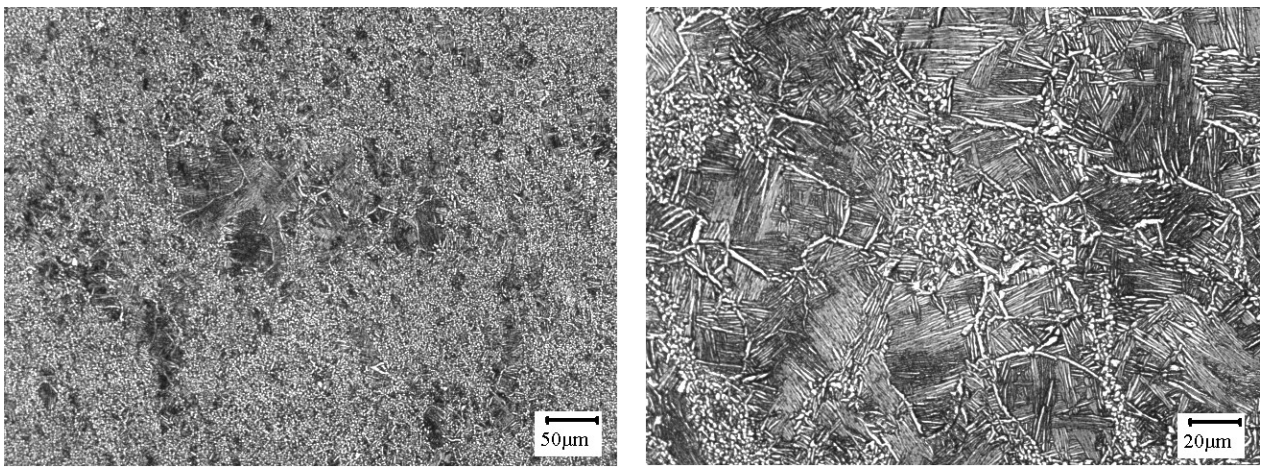

a) b)

Figure 2.15: The microstructure of extruded VT3-1 in the core of the bar

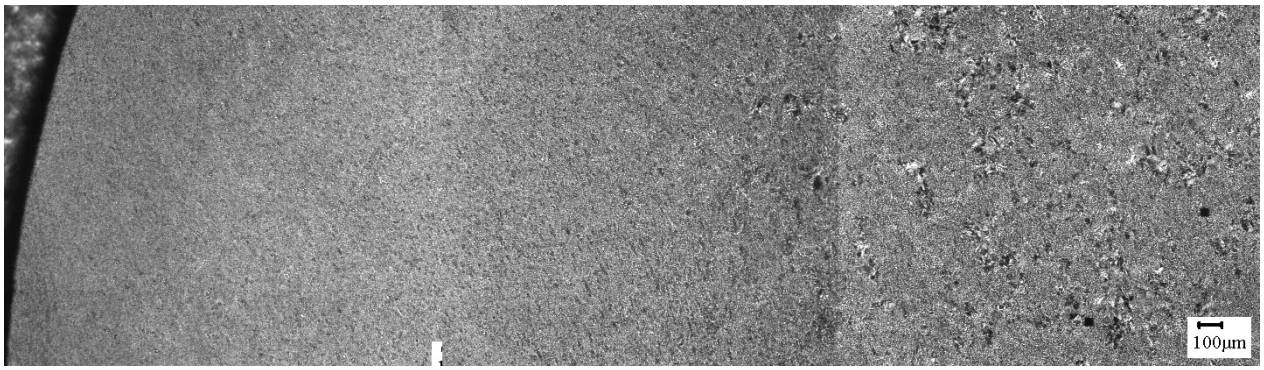

Figure 2.16: The changing of microstructure along the radius of the bar

The characteristic size of alpha-phase platelets close to the lateral surface of the bar does not exceeds 2 μm. The alpha-phase is shaped in ellipsoidal platelets, extra fine particles, but in contrary to the forged titanium alloy, the alpha-phase in extruded material is not grouped in clusters.

The micro-structure within the plane, cut along the direction of extrusion shows very clear traces, which are formed due to the material flow during the technological process. The perturbation of micro-structure in the core of bar is also clearly represented in the transversal section (Fig.2.17). Far from the core, the intensity of perturbation in micro-structure is decreasing. The micro-structure becomes more regular and fine. Nonetheless, the lines of fibering can be found even close to the lateral surface of the bar, Fig. 2.17 (c). The zone of perturbed micro-structure may have a length as less than 1 mm as well elongated up to several millimetres. It suddenly appears in the area of regular micro-structure and also unexpectedly vanishes. Except these elongated zones of perturbed micro-structure, including the traces of primary beta-phase, the micro-structure observed on transversal section also includes some chain-like lines of alpha-phase particles, elongated in the direction of extrusion. It seems that these chain-like structures are the centres of crystallisation for extruded titanium alloy, similar to the borders of primary beta-phase. The space between such chains is often filled by needle shape alpha-plates.

The alpha-phase in the area close to the lateral surface of the bar is also elongated in the direction of extrusion. The size of elongated plates is extremely small, like in the case of cross-section plane (perpendicular to the bar longitudinal axis). The typical sizes of alpha-platelets are: the length of platelet in elongated direction: around 2-3 μm, the width of the plane: around 1 μm. The micro-structure is extremely fine compared to the forged VT3-1 titanium alloy.

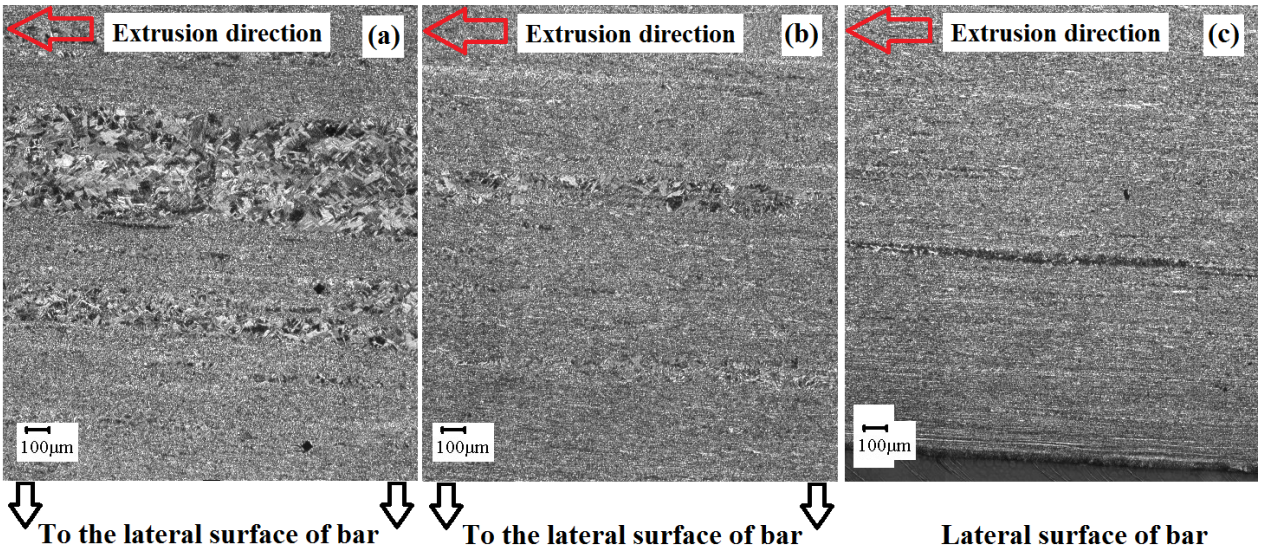

Figure 2.17: Variation of microstructure along the radius of the bar within transverse section

2.2.3 Micro-hardness of extruded VT3-1 alloy

The micro-structure of extruded VT3-1 titanium alloy has a clear symmetry axis that is the axis of the bar. Thus, the micro-hardness of extruded VT3-1 was studied within two mutually-perpendicular directions: perpendicular and along the bar axis. The measurement was realized like for the forged VT3-1. The Vickers method was used with the following parameters: weight 500 gr, time 10 sec. The measurements were carried out automatically in 15 different points along the diameter of the section. The distance between two neighbouring points was around $600 - 650\mu m$. The result of measurements within two sections shows, that there is just a small difference in micro-hardness between the two micro-sections. The average micro-hardness values within the plane perpendicular to the bar axis is 374 HV_{500}, the hardness within the micro-section along the axis is 371 HV_{500}. The values of micro-hardness of extruded VT3-1 titanium alloy is less dispersed and almost has no dependence on the position at the plane perpendicular to the axis of extrusion, Fig. 2.18.

In case of plane along the direction of extrusion, some deviations from the average micro-hardness was observed in the core of the bar, Fig. 2.19. The deviated values within the section are 364 HV (point 6) and 354 HV (point 8)

In order to study the reason of such fluctuation, the micro-section was etched by KROLL solution for 30 sec. and the micro-structure along the micro-hardness measurement line was observed. The results shows, that significant decreasing in micro-hardness is related to the bands containing the beta grains with thin needle-like alpha-platelets, Fig. 2.20.

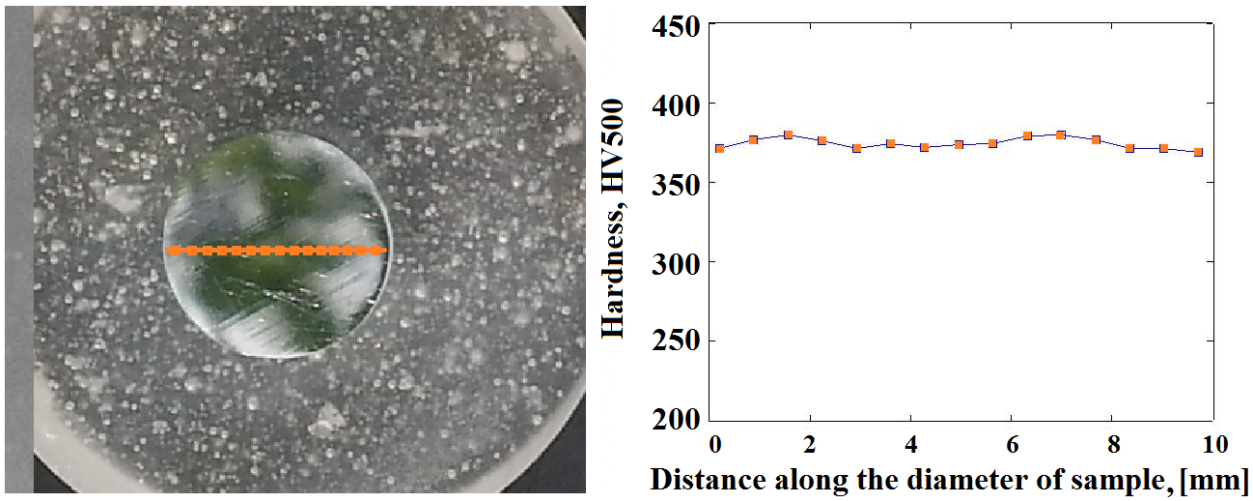

Figure 2.18: Micro-hardness of extruded VT3-1 alloy along the diameter in a section, perpendicular to the bar axis (diameter is 10 mm)

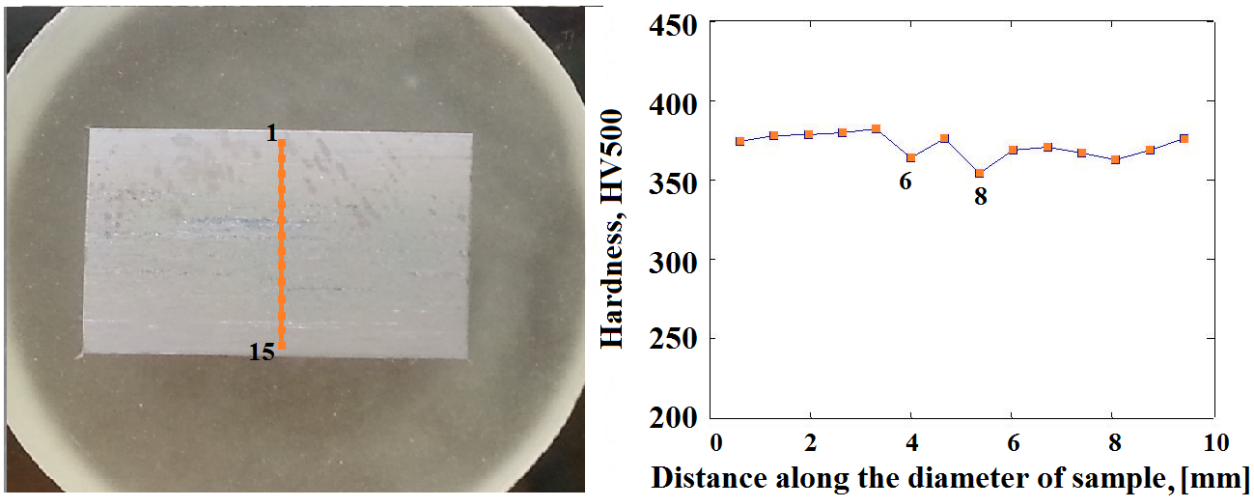

Figure 2.19: Micro-hardness of extruded VT3-1 along the micro-section's diameter, transversal to the bar's axis section

Thus, the micro-structure of extruded VT3-1 has very clear traces along the direction of extrusion represented as by the areas of thin alpha-platelets within beta grains as well by chain-like lines of alpha-phase particles. The zones with beta-grain filled by needle like platelets are dominating in the core of the bar and when moving far from the centre the intensity, the size of such zones are decreasing. Close to the lateral surface of the bar these

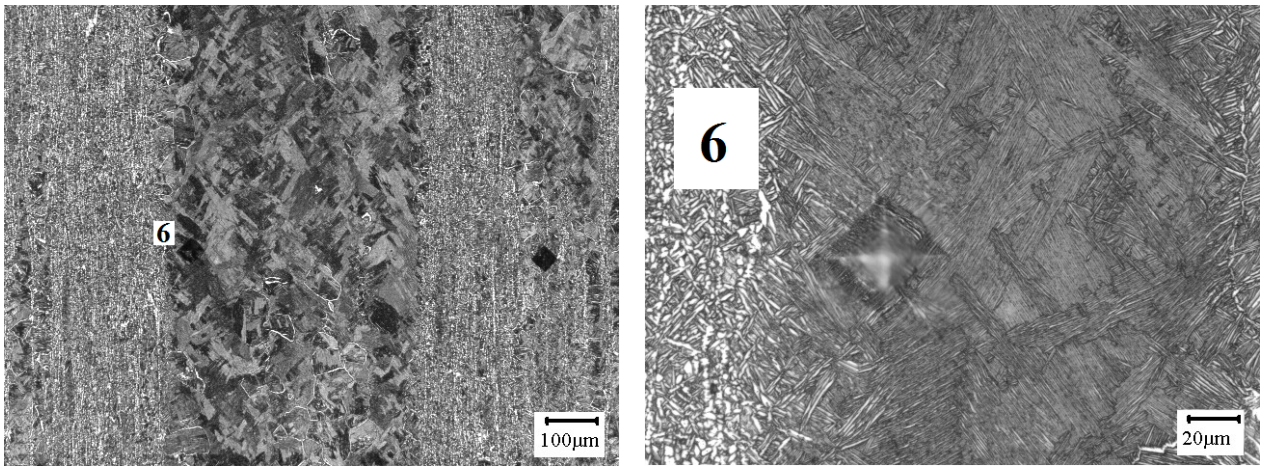

a) b)

Figure 2.20: The point of microhardness measurement within bend of non-crystallized microstructure

structures vanish. Even along the direction of extrusion these zones are not permanent. They suddenly appear in the zones of regular micro-structure, and exist within several millimetres and similarly suddenly disappear. The micro-hardness measurements within the micro-sections show, that in such zone the value of micro-hardness is lower, compared to the average value. The morphology of perturbed zones shows clear traces of primary beta-phase borders. The alpha-phase forms along these borders and growth into the body of beta-phase [97]. The formed alpha-phase needles are extremely thin and its width is often less than 1 μm. It is remarkable, that the micro-structure of extruded VT3-1 is extremely fine and the characteristic size of micro-structure components is about 1 - 2 μm only.

2.2.4 Mechanical properties of extruded VT3-1 titanium alloy

The blank for the tensile specimen made from extruded titanium alloy was cut from the end of the cylindrical bar, Fig.2.21. The blank is similar to the forged titanium alloy plate with thickness of about 3 mm. The tensile specimens from extruded titanium were machined according to the same standard, which was used for forged specimen, Fig. 2.11.

The tests were carried out by using the same electro-mechanic tensile machine under the same loading conditions: air, room temperature ($\simeq 20°C$), displacement control, loading speed was $V_d = 0.075 \quad mm/min$. The real deformation of specimen was measured by using the same type of extensometer, Fig. 2.12. The results of tensile tests on extruded VT3-1 titanium alloy shows the higher mechanical properties for material from bars. The yield stress of extruded titanium alloy is 1050 MPa, the ultimate tensile strength is 1107 MPa, the maximum deformation at rupture is 13 %. The Young's modulus for extruded titanium

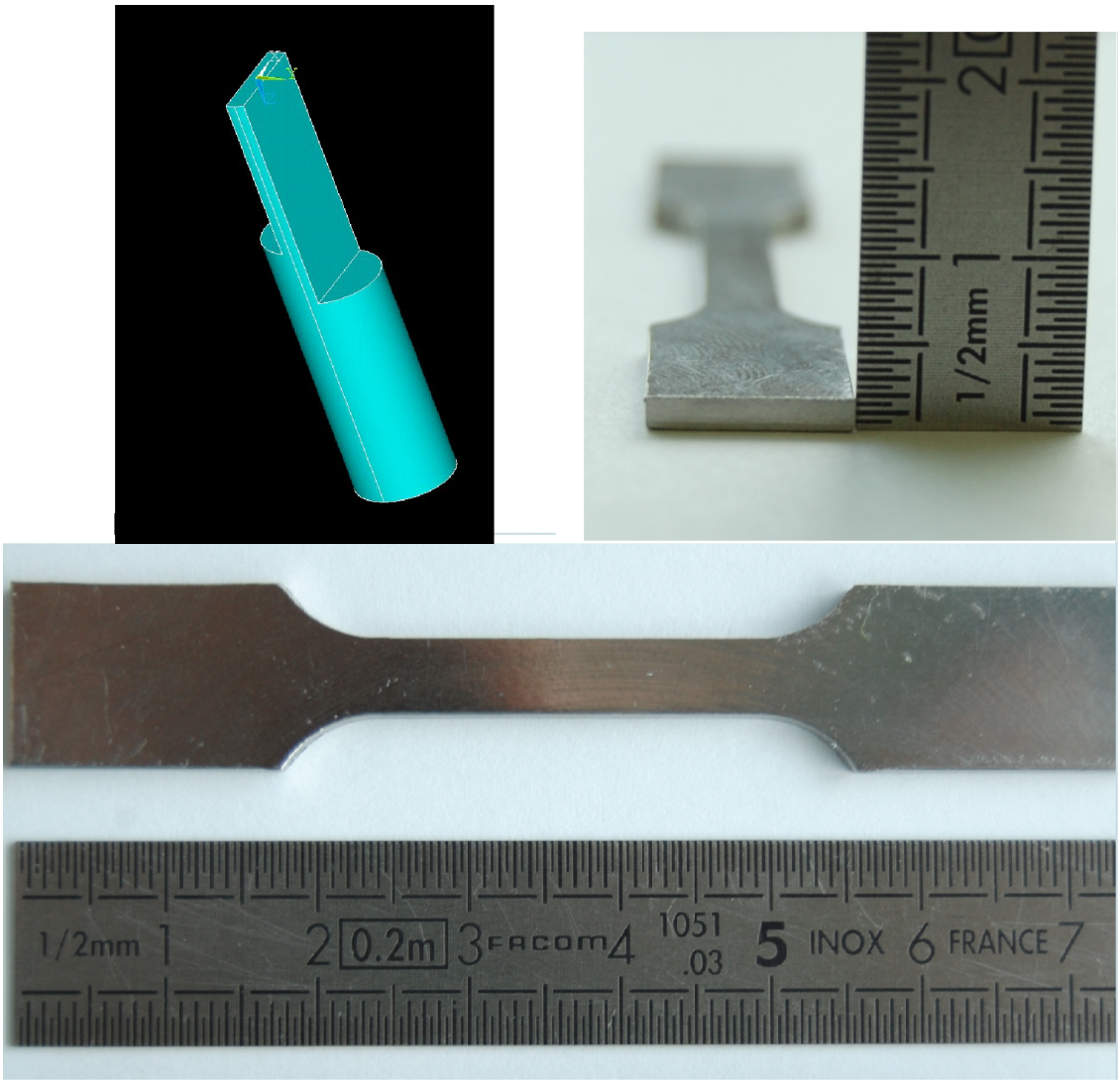

Figure 2.21: The extruded tensile specimen and schema of its position in the bar

alloy is lower, compared to the forged VT3-1 and equal to $E = 106\ GPa$. The dynamic Young's modulus is also lower compared to the forged Ti-alloy and equal to 110 GPa. The mass density is 4500 kg/m^3. Extruded VT3-1 titanium alloy is more ductile, compared to the forged-one, that can be clearly seen from tensile curves for both alloys, Fig. 2.22

The mechanical properties of extruded titanium aloy are shown in Table 2.6. The mechanical properties of the investigated material are in good agreement with technical information from state standards for extruded bars.

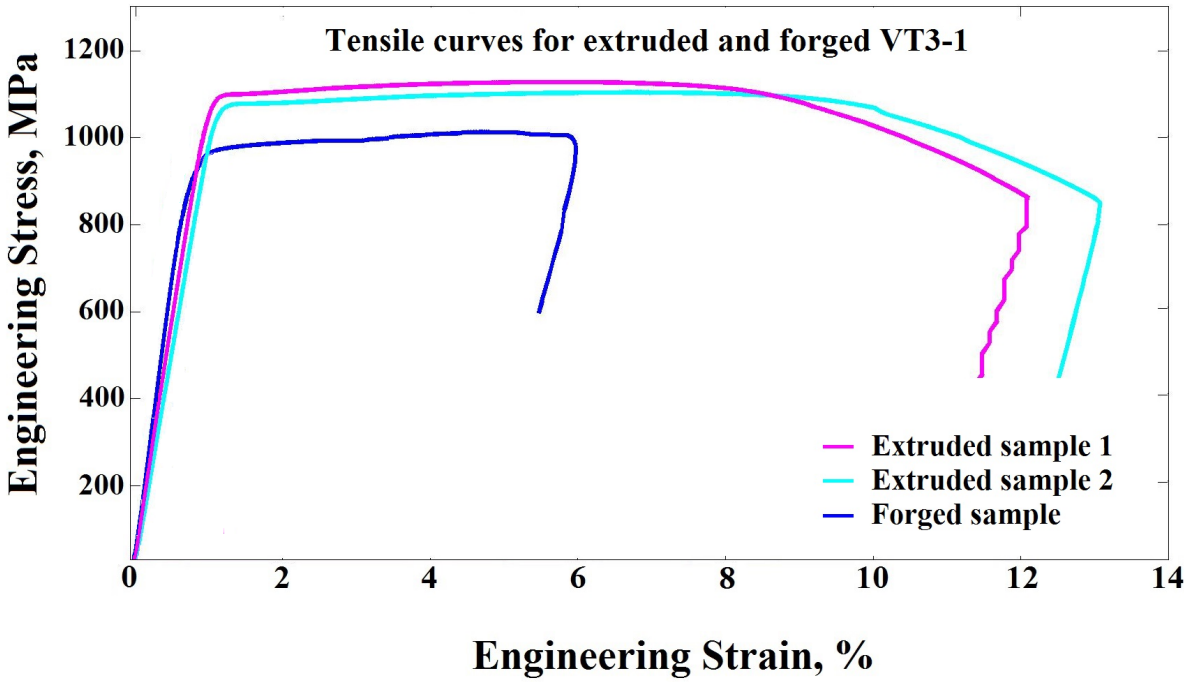

Figure 2.22: Tensile curves for extruded and forged VT3-1 titanium alloy

Table 2.6: Mechanical properties of extruded VT3-1 titanium alloy

Parameter	E (GPa)	E_{dyn} (GPa)	$Rp_{0.2}$ (MPa)	Rm (MPa)	ϵ_R (%)	σ_f (MPa)
Value	106	110	1050	1107	13	850

2.3 Specimens from forged VT3-1 titanium alloy

The fatigue specimens in forged VT3-1 titanium alloy were machined from different locations of the disk. The specimens were machined in different directions axial, radial and circumferential. That was done in order to investigate a possible anisotropy of the fatigue strength of the forged titanium alloy of the turbine disk. The first set of 22 specimens for R=-1 tests was taken from the rim part of the disk in the axial direction,(i.e. parallel to the rotation axis of the disk), Fig. 2.23(a). The specimens with such orientation (along the axis of the disk) are named 'axial specimens' in the present work and named 0AXX, where '0' is the series number, 'A' means axial and 'XX' is the number of each specimen in series (from 1 to 22). When the first tests were finished, the second set of 10 axial specimens for R=-1

tests from the rim part was machined. This series of specimens was named as 1AXX series, where A means 'axial' and 'XX' is the number of specimen in series number. These two sets of specimens were used to investigate fatigue properties of material under fully reversed tension loading (R=-1). The next series of 10 specimens for (R=-1) tests was machined from the plateau part of the disk in the radial direction (the axis of specimen is along the radius of the disk), Fig. 2.23 (c). These specimens were named as 2RXX, where 'R' means radial and 'XX' is the number of the specimen in the series. These specimens were also tested under fully reversed tension loading and allows us to compare the fatigue strength of the material in different locations and different orientations. The next set of specimens were machined to investigate the influence of mean stress on the fatigue behaviour of titanium alloy in gigacycle regime. The 10 specimens for tension-tension tests (R>0) from the plateau part of the disk were machined in the radial direction. These specimens were named as 3RXX, where 'R' means radial and 'XX' is the number of the specimen in the 3rd series. Comparing the results of fatigue tests on 2RXX and 3RXX series allows to determine the influence of mean stress on the fatigue strength and crack initiation mechanisms in forged VT3-1. The next series of specimen was also machined from the plateau part of the disk in circumferential direction (perpendicular to the radius in the plane of the disk). The 10 specimens for tension-tension tests (R>0) were named as 4CXX samples, where 'C' means circumferential and 'XX' is the number of the specimen in the series. The total number of specimens made from the forged VT3-1 titanium alloy is 62. Table 2.7 contains generalized informations about the specimens manufacturing from the forged VT3-1 titanium alloy.

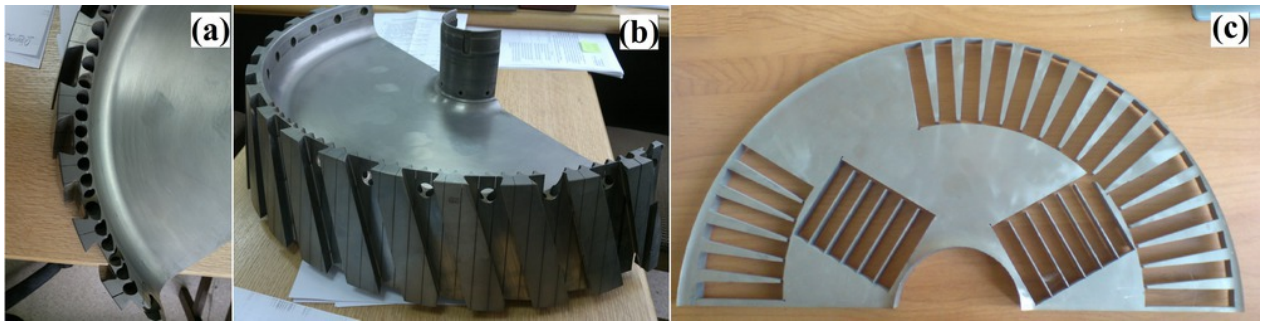

Figure 2.23: Tensile curves for extruded and forged VT3-1 titanium alloy

2.3.1 Specimens for R=-1 tests

The specimens for fully reversed fatigue tests were cut from the rim part of the disk in axial direction (0AXX and 1AXX) and also from the plateau part of the disk (2RXX). The

Table 2.7: The list of specimens from forged VT3-1

Series	Position	Direction	Ratio	Number
0AXX	Rim	Axial	R=-1	22
1AXX	Rim	Axial	R=-1	10
2RXX	Plateau	Radial	R=-1	8
3RXX	Plateau	Radial	R=0.1	7
4CXX	Plateau	Circumferential	R=0.1	7

geometry of the specimens was computed based on dynamic Young's modulus of VT3-1 and requirements of gigacycle concept (ANNEX A). The gauge section was kept the same than the typical shape of ultrasonic specimens used in the laboratory of C. Bathias [3]. The diameter of the working cross section was 3 mm, the radius of reduced profile was 31 mm. The resonance length was calculated in order to have a natural first-mode longitudinal vibration at frequency of 20 kHz. The final geometry of ultrasonic specimens made from forged VT3-1 titanium alloy is presented in Fig. 2.24.

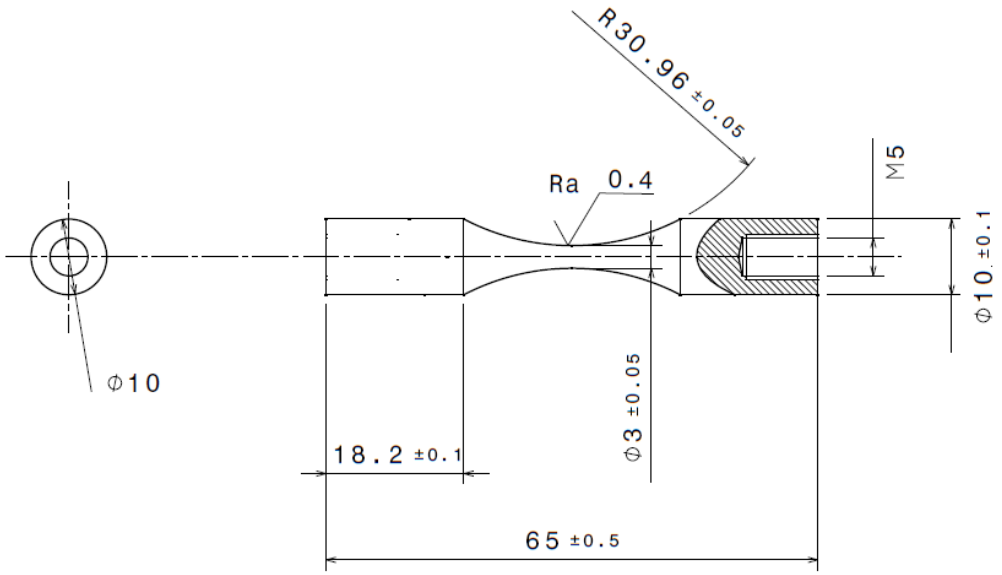

Figure 2.24: The geometry of ultrasonic specimen for longitudinal fatigue tests at R=-1, made in forged VT3-1 titanium alloy

The important parameter for each ultrasonic specimen is the relation between the applied excitation (amplitude of vibration) and the response of the specimen (stress amplitude in the working cross section). This relationship may be measured by strain gauge or calculated

analytically by using equations derived by C. Bathias [3], or numerically by using the finite element method with ANSYS, ABAQUS or any other software. The analytical solution was obtained in the following form

$$\sigma(x) = E_d A_0 \phi(L_1, L_2)[\beta_1 cosh(\beta_1 x) - \alpha_1 sinh(\beta_1 x)]e^{-\alpha_1 x} \tag{2.1}$$

where

$$\phi_1(L_1, L_2) = \frac{cos(kL_1)e^{\alpha_1 L_2}}{sinh(\beta_1 L_2} \tag{2.2}$$

$$\alpha_1 = \frac{1}{2L_2} \log \frac{R_2}{R_1} \tag{2.3}$$

$$\beta_1 = \sqrt{\alpha_1^2 - k^2} \tag{2.4}$$

$$k = \frac{\omega}{c} \tag{2.5}$$

L_1 is the resonance length, L_2 is the length of reduced cross section, R_1 is the minimum radius in gauge section, R_2 is the radius of the cylindrical part, ω is the angular frequency ($2\pi f$) and c is the longitudinal wave rate in titanium, E_d is the dynamic modulus and A_0 is the amplitude of applied vibrations. Based on this analytical solution the relationship between applied vibration and dynamic stress in the working section can be obtained. In the case of forged VT3-1 titanium alloy, the result of calculation gives the following ratio

$$\sigma_a = 14.94 \cdot A_0 \tag{2.6}$$

where σ_a is the stress amplitude (in MPa) in the working section of the specimen and A_0 is the amplitude of vibration (in μm), applied to the specimen top. In other words, the applied vibrations of 1 μm induces the dynamic stress amplitude of about 15 MPa in the centre of the specimen. Almost the same value was obtained from numerical simulation. The procedure of numerical simulation is the following: first the modal analysis should be carried out in order to find the resonance frequency of the specimen for first-mode of longitudinal vibrations; second, a harmonic analysis should be performed at the resonance frequency of the specimen. This problem is assumed to be linear because of VHCF regime, that can be easily checked by solving it under two different amplitudes of vibration. Numerical solution Fig.2.26 is quite close to the analytical solution.

2.3.2 Specimens for R > 0 tests

The specimens for tension-tension tests (positive stress ratio) were cut from the plateau part of the compressor disk in radial (3RXX) and circumferential (4CXX) directions. The specimens for both series were designed identically. Parameters of the working sections for tension-tension (T-T) specimens are the same than these for the tension-compression (T-C) ones: the cross-section diameter in the working part was 3 mm and the radius of harmonic profile R was 31 mm. The resonance length L_1 was also designed so that provide there was a resonance longitudinal vibration at the frequency of 20 kHz. The geometry of T-T specimens is illustrated on Fig. 2.25.

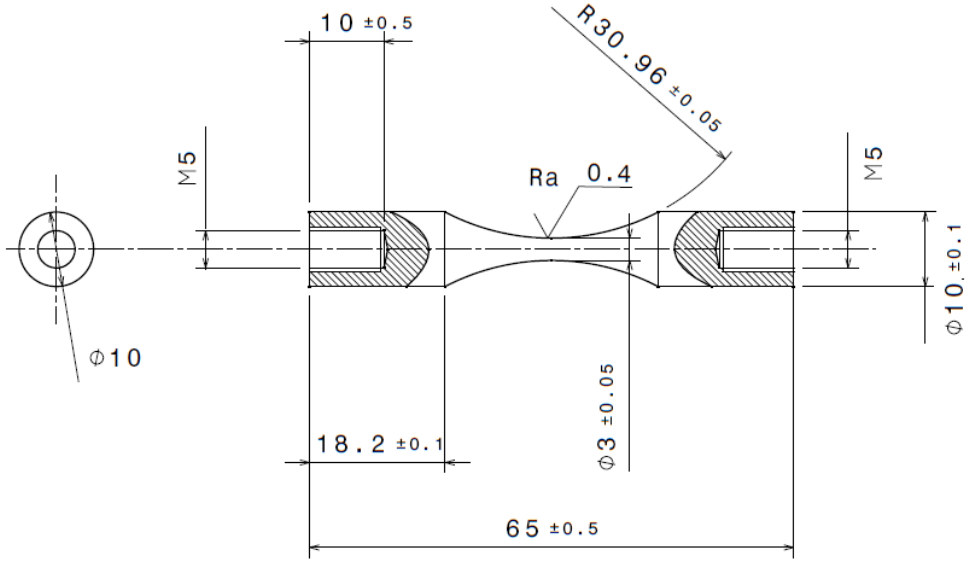

Figure 2.25: The geometry of ultrasonic specimen for R>0 tests, made from forged VT3-1 titanium alloy

The geometry of T-T specimen is similar to the T-C one, except the second hole for fixing the second horn to apply the static force. Therefore, the stress distribution under vibration loading will be the same for both T-C and T-T ultrasonic specimen (Fig.2.26).

2.4 Specimens from extruded VT3-1 titanium alloy

The ultrasonic specimens from extruded VT3-1 titanium alloy were machined from the bars along the extrusion direction. Their geometry was also designed based on ultrasonic fatigue concept and results of dynamic modulus measurements. The extruded VT3-1 titanium alloy was investigated under several loading conditions: fully reversed tension-compression with

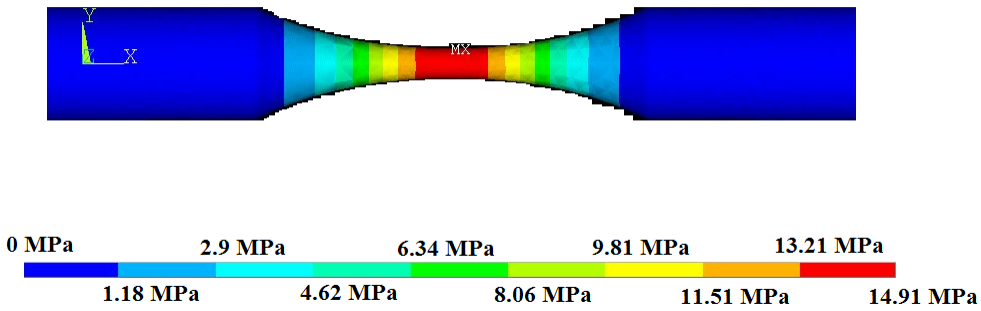

Figure 2.26: The numerical calculation of stress amplitude distribution for specimen in forged VT3-1 under a vibration amplitude of 1 μm

Table 2.8: List of specimens from extruded VT3-1

Series	Regime	Number
Ext-1XX	Tension-Compression, R=-1	20
Ext0.1XX	Tension-Tension, R=0.1	20
Ext0.5XX	Tension-Tension, R=0.5	20

R=-1, tension-tension tests with R=0.1 and tension-tension tests with R=0.5. The series of specimens were named as Ext-1XX, Ext01XX and Ext05XX respectable, where 'Ext' is extruded, '-1', '0.1' and '0.5' means the loading ratios and 'XX' is the serial number of specimen in the set. The list of ultrasonic specimens machined from the extruded bars is given in Table 2.8

The geometry of ultrasonic specimens from extruded VT3-1 is close to the specimens from the forged titanium alloy. The difference is that diameter of cylindrical part ('head' of specimen) is 1 mm smaller for extruded samples. That's why, some correction in designed was realized. The cross section in the gage section was kept the same (3 mm), the radius of reduced section was also the same (31 mm) and just the length of reduced section was made shorter, Fig. 2.27. After that, the resonance length of 'head' part was adjusted to get a natural frequency of 20 kHz.

Thus, such modification allows to keep the working section for all the specimens machined as from forged as well from extruded titanium alloy, that is very important in case of ultrasonic testing for better test result comparison. The geometry of specimens from extruded VT3-1 for T-C and T-T tests is shown in Fig. 2.28 - 2.29.

The relationship between the applied amplitude of vibrations and stress amplitude in case

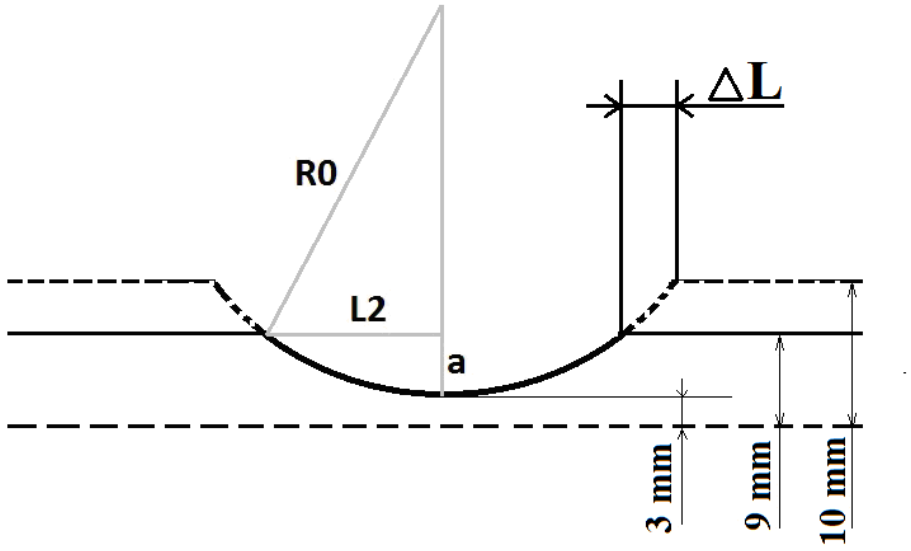

Figure 2.27: The scheme of modification in geometry for $R_2 = 9mm$ specimens

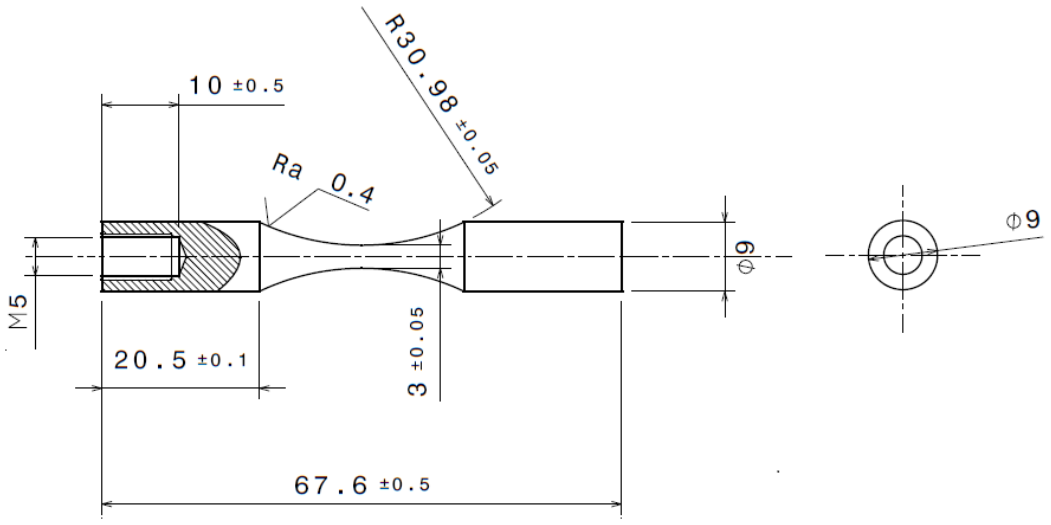

Figure 2.28: The geometry of specimen from extruded VT3-1 titanium alloy for R=-1 tests

of extruded VT3-1 titanium alloy shaped in the specimens with geometry presented on Fig. 2.28 and 2.29 is $\sigma_a = 14.8 \cdot A_0$. The small difference between relationships for forged and extruded VT3-1 titanium alloys is related to the difference in dynamic modulus for these materials, 116 GPa for forged VT3-1 (Table 2.4) and 110 GPa for extruded alloy (Table 2.6).

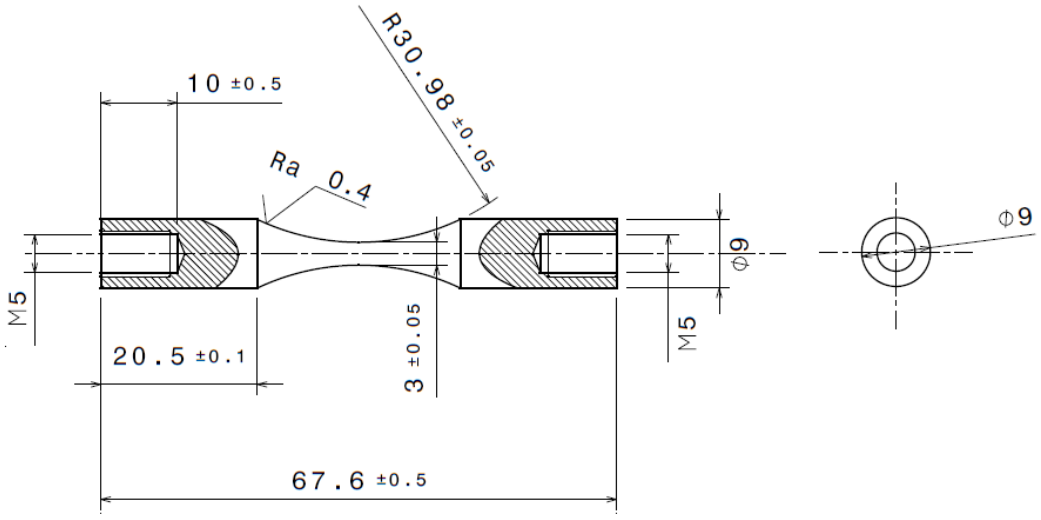

Figure 2.29: The geometry of specimen from extruded VT3-1 titanium alloy for R > 0 tests

2.5 Ultrasonic fatigue testing systems

In the framework of the present research project several types of ultrasonic fatigue testing systems were used to investigate the properties of VT3-1 titanium alloy in gigacycle fatigue regime under different loading modes. The first tests were carried out under axial loading under different R ratios: fully-reversed tension-compression with constant amplitude; tension-tension tests with two different ratios, R=0.1 and R=0.5; torsion loading mode with constant amplitude and R=-1. The axial ultrasonic fatigue testing machines were developed and installed well before present research project and these machines will be briefly described in this chapter. The calibration process and some improvements in installation will be also discussed hereafter. The torsion ultrasonic fatigue testing machine was developed and installed during this PhD project and, therefore, will be presented in details later in Chapter IV.

2.5.1 Tension-compression testing system

The axial ultrasonic fatigue testing system which was used for the tension-compression tests was developed in the laboratory of C. Bathias [3] and consists of the following principal parts: (1) personal computer with integrated multifunction board for communication; (2) control box that perform the correct connection between PC and ultrasonic generator; (3) ultrasonic generator, that modulates and amplify the high frequency sinusoidal signal based on the control electric signal from the PC; (4) piezoelectric transducer, which converts the

high frequency sinusoidal signal from generator into the mechanical vibrations at the same frequency; (5) ultrasonic horn which transfers to the specimen and amplifies the mechanical vibrations generated by the piezoelectric transducer; (6) the specimen. The specimen is also included into the system, because all the mechanical elements, including specimen, should be designed so that to be in resonance vibrations at a frequency of 20 kHz [3]. The appearance of the system is shown in Fig. 2.30.

The typical range of ultrasonic vibration amplitudes generated by the piezoelectric transducer is varying between 0.5 μm and 10 μm. Thus, without ultrasonic horn the maximal stress amplitude which can be applied to the specimen made from titanium alloy is less than 150 MPa. Therefore, in the case of typical two-phase titanium alloys, the ultrasonic horn should be capable to amplify the vibration at list for four times. In the case of high strength steels the required amplification factor should be almost twice higher (about 8 times).

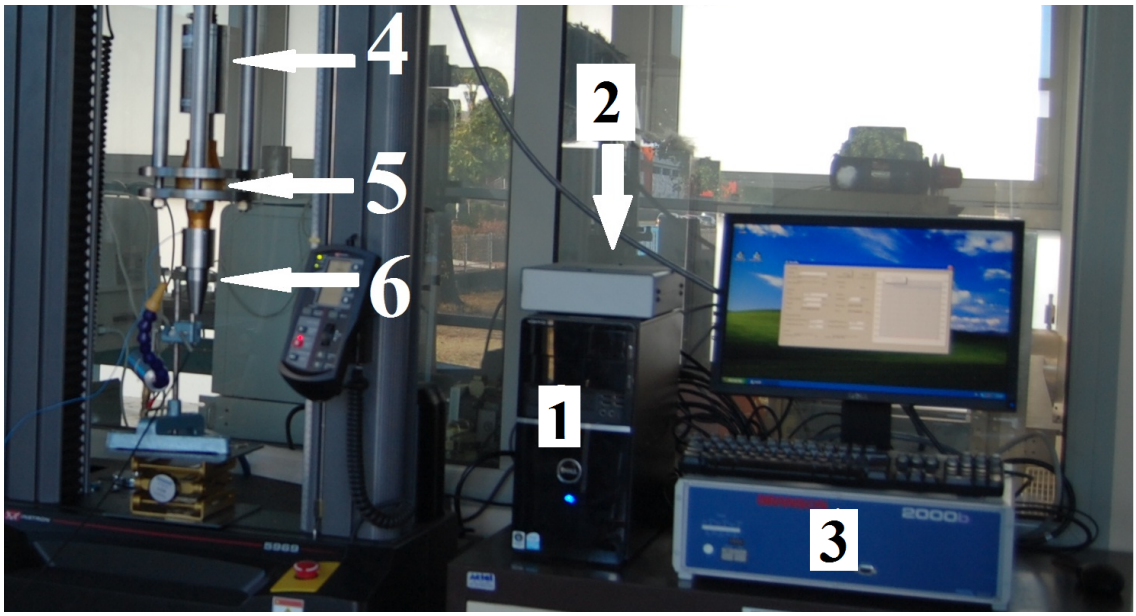

Figure 2.30: The tension-compression ultrasonic fatigue testing system

In order to apply ultrasonic testing methods to the all the spectrum of structural materials from soft aluminium to hight-strength steels, the system can be completed by one of the two different ultrasonic horns: TC horn with low amplification factor and TGD horn with high magnification factor (Fig. 2.31). In some additional case a booster with amplification factor of 1.5 can be installed between piezoelectric transducer and one of ultrasonic horns. As usual, TC horn is used for materials with fatigue strength below 450 MPa and TGD horn for material with fatigue strength beyond 450 MPa.

The horn is fixed at the bottom of the piezoelectric transducer by connecting screw. The surface of contact should be covered by special ultrasonic grease which allows a good surface

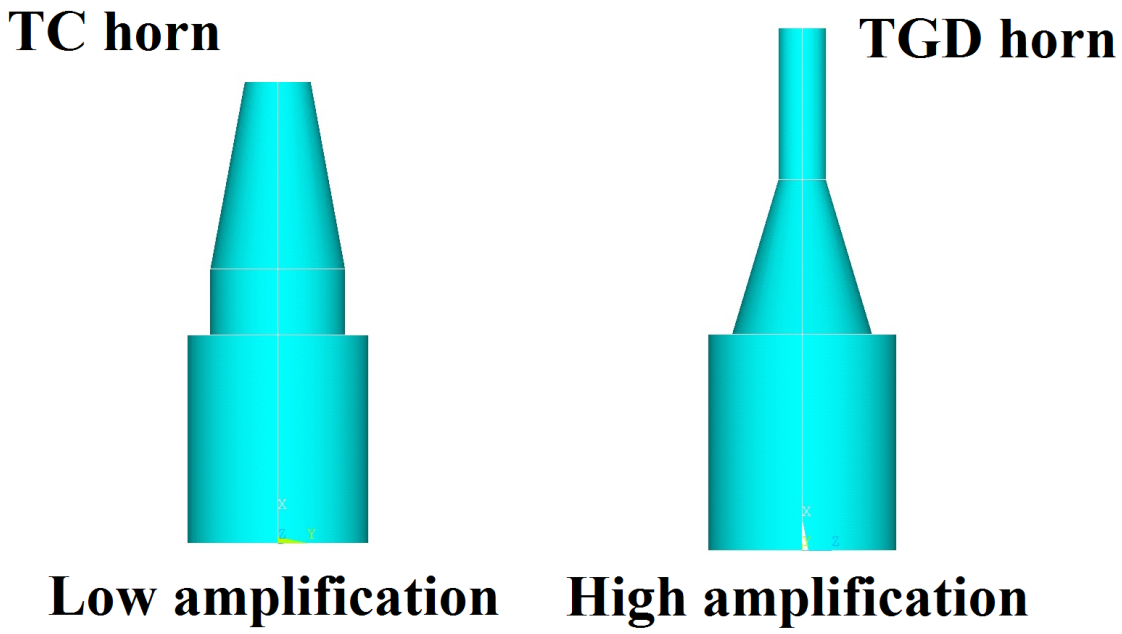

Figure 2.31: Low amplification TC horn and high magnification TGD horn

contact during the ultrasonic vibrations. In this work most of the results were obtained by using low amplification TC-horn and just few specimens were tested with TGD horn.

2.5.2 Calibration of the system for R=-1 tensile tests

The calibration of the ultrasonic fatigue testing system can be carried out with contacted measurements methods as well by non-contact one. The first type of calibration may give more accuracy results, but it needs a quite complicated ins non-contact method provides a measurement of displacements by light or laser at bottom of horn. The non-contact method need additional analytical or numerical calculations to get the stress amplitude, while contact method provides direct strain measurement. Within the present PhD project the two methods were used and the results of calibration are compared and discussed below.

Non-contact calibration method

The non-contact calibration technique was realized by using a MTI-2100 fotonic sensor (Fig. 2.32). The principle of such method is the measurement of the intensity of reflected light by vibrating surface light. The system consists of electronic part, that analyses the in-coming signal and fotonic probe with different configuration of fibres. Some of such fibres transmit the light and others capture the reflection. The intensity of measured in-come

signal depends on from the distance between the probe and the vibrating surface. Thus the pick-to-pick displacement can be measured.

Figure 2.32: The fotonic MTI-2100 sensor for measurements of displacements

The calibration may be carried out by measurement the displacement in two locations: bottom of the horn (TC or TGD depends on the required for tests range of amplitudes) or at the bottom of specimen. As usual, the measurement of displacement at the bottom of the specimen is required just to check the vibration conditions. In case of vibrations under proper gigacycle conditions the amplitudes of vibrations are the same at the bottom of the horn and specimen. Therefore, the typical ultrasonic calibration method requires the relationship between excitation voltage of piezoelectric transducer and amplitude of vibration at the bottom of ultrasonic horn. Based on amplitudes of vibrations the stress in the gage section of specimen can be calculated either by analytical method or by finite elements method. Using additional calculation to get the stress amplitude in working section of the specimen and the sensibility of the method to the surface quality are the weak points of such calibration technique. Nonetheless, these points are not critical. In case of well cleaned or polished surface where the displacements are measured, the accuracy of fotonic sensor is about 0.1 μm that is very high. In case of more rough and not clean surface, the accuracy of the method will be lower. Thus, the surface for calibration should be not damaged and well cleaned. The elastic stress is a mechanical parameter that is calculated based on measured strain and dynamic modulus. Therefore, even for contact methods the use of some assumptions and analytical calculations are obliged.

The results of calibration may be presented as a relationship between excitation tension and displacement at the bottom of ultrasonic horn or stress amplitude versus excitation tension for the specimen made from a given material. Usually the first type of calibration is used to characterize the ultrasonic horn and the second-one is used for fatigue tests. The calibration lines for low amplitude TC-horn, TC-horn with booster and high amplitude TGD-

horn obtained by non-contact method are presented in Fig.2.33.

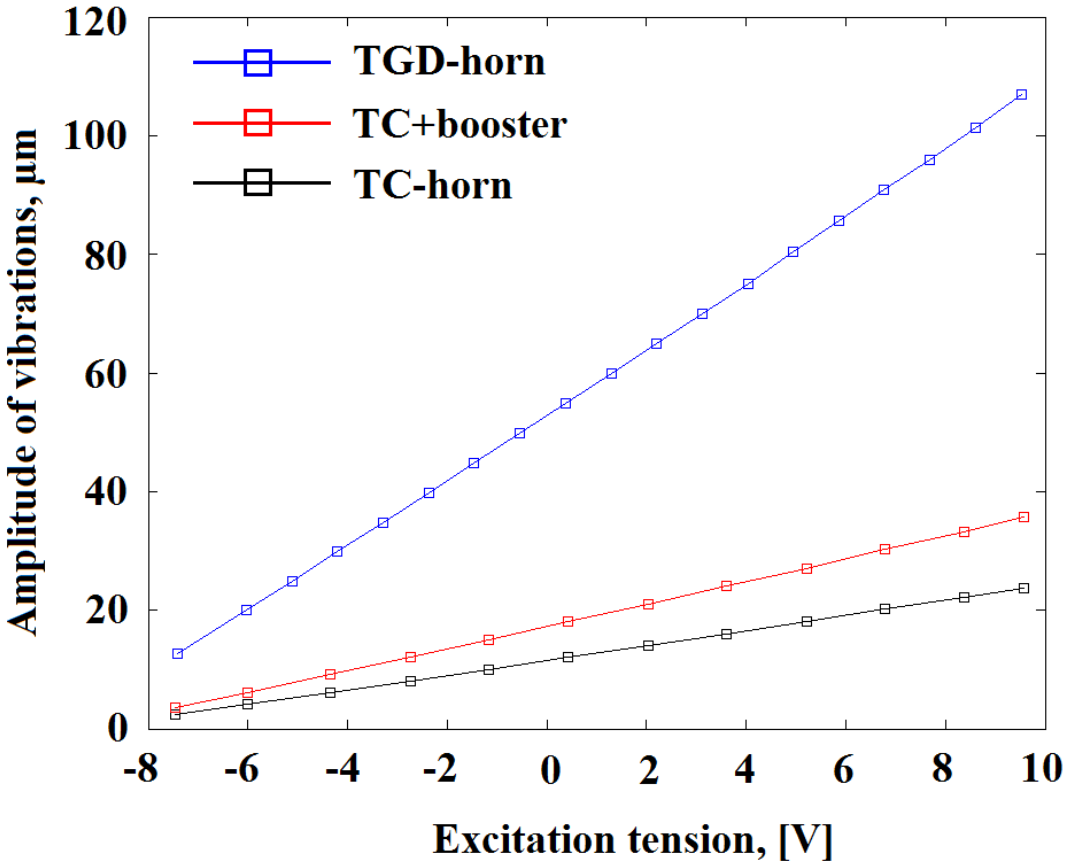

Figure 2.33: The calibration line for TC and TGD horns

As it can be seen from the calibration lines, the piezoelectric fatigue testing system can operate in wide range of amplitudes, from several μm up to more than 100 μm, that makes this method applicable for all structural metals. The stable regime of operation for the ultrasonic testing system is between '-7' and '9' volts.

Contact calibration method

The contact calibration method is based on using a strain gauge glued on the specimen surface in the area where the strain measurement should be performed. The system for contact calibration used in present research project is presented in Fig. 2.34. The strain gauge has an electrical resistance of 120 Ohm in not-deformed conditions. It was included in Wheatstone bridge as one of four resistance and the three other resistances are in the conditioning electronic device. The voltage is measured by a high accuracy multimeter with a wide bandwidth (0 to 100 kHz) and the shape of the electric signal is monitored by oscil-

loscope. The calibration allows to measure directly the strain in the specimen work section. The principle of calibration is to obtain the relationship between excitation tension that is applied to the piezoelectric transducer and the strain in working section of the specimen. Further, the strain can be recalculated into the stress amplitude by using dynamic modulus and Hooke's law.

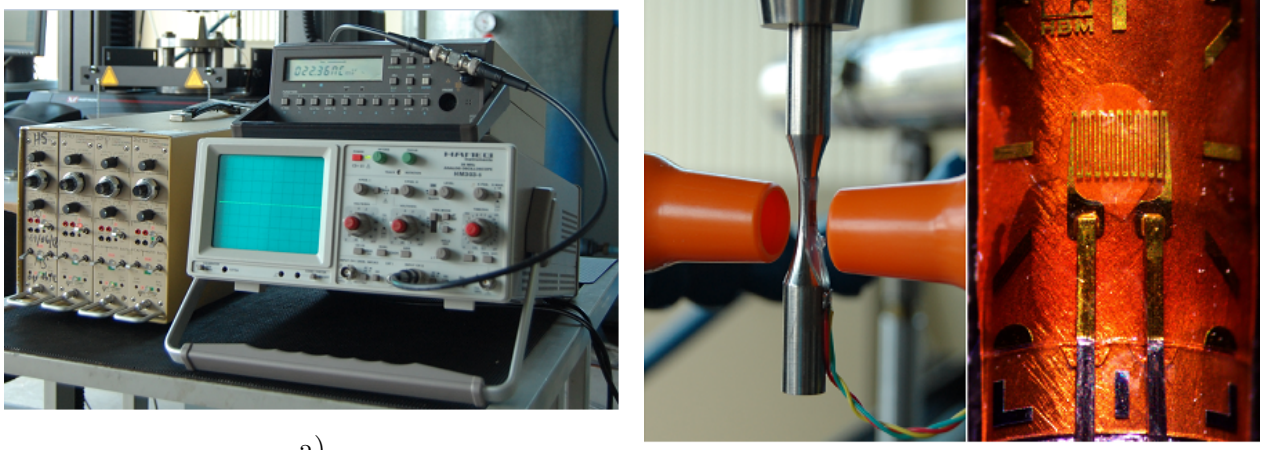

a) b)

Figure 2.34: Read and correct this notation (a) and extruded bars (b) made from VT3-1 titanium alloy

This method has a high accuracy but instrumentation of specimen can be difficult because of hyperbolic profile of the specimen and small minimum diameter in work section of specimen (D = 3 mm). Thus, the instrumentation of sample by strain-gauge required a good experience. During calibration the specimen work section should be cooled by the compressed air. In case of contact calibration method the problem of fatigue is also actual for the grid of the stain-gauge that is why the calibration should be performed under small stress amplitudes compared to the fatigue strength of the material. After that the full calibration line can be interpolated based on the data from low amplitude range by Least Squares Method. The calibration can be used just for a given material and specimen geometry that is why it is little bit more limited compared to non-contact method. The calibration lines for ultrasonic tension-compression specimen made from forged titanium alloy obtained by the two methods (contact and non-contact) are given in Fig.2.35.

The comparison of calibration lines, obtained by contact and non-contact methods shows, that within the accuracy of experimental equipments the results are the same. Thus, both methods gives the correct calibration lines with good accuracy. Each method have its own benefits and limitations. In case of non-contact method the benefits are the following: (1) the method of measurement is almost automatic that makes it more 'friendly' and very

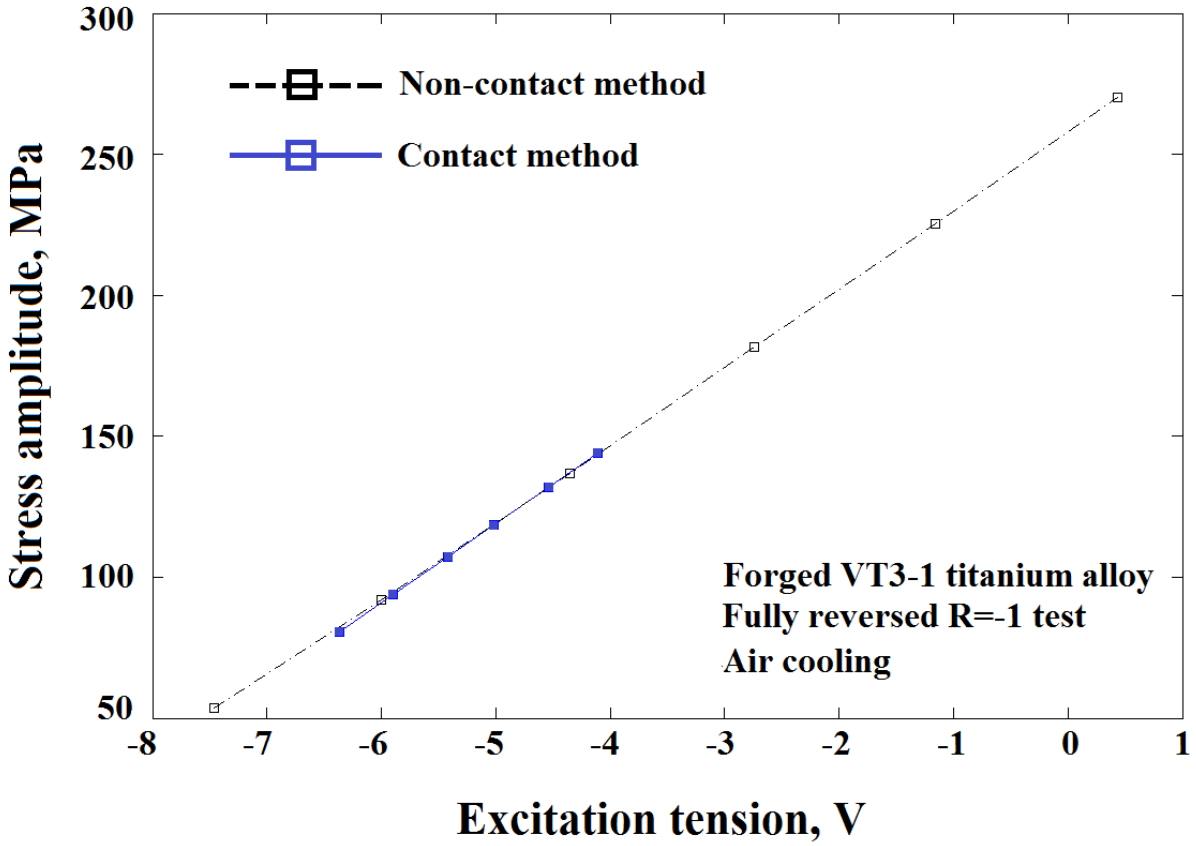

Figure 2.35: The specimen with attached strain gauge in work section

easy to use; (2) allows to make calibration of the ultrasonic horn, that can be used for specimens with different geometries and made from different materials; (3) allows to check the proper conditions of natural vibrations. The limitations of the non-contact method is high sensitivity to the quality (roughness) of vibrating surface, that may lead to scatter in calibration lines. The benefits of contact method is a very high accuracy. The strain gauge technique has a good repeatability. Moreover, the same procedure of strain gauge glueing allows to uniform the calibration process for all specimens. The limitation of this method is time and material consuming. Each new specimen has to be the instrumented with a new strain gauge. The typical time for preparation of one specimen for calibration is not less than 1 hour (glue polymerization) and the usual recommended time for fixing is 24 hours. Moreover the method is very sensitive to the electric noises which should be eliminated. Thus, in case of requirements with very accurate calibration the contact method can be suggested. In case of time saving requirements the correct line can be obtained by non-contact method.

2.5.3 Tension-tension testing system

The tension-tension loading consists of two components: cyclic and static load. In case of ultrasonic tension-tension tests the cyclic load is applied by using the same to the tension-compression piezoelectric fatigue testing system (ANNEX B). The static load is applied by using an electro-mechanic or servo-hydraulic tensile machine. In this study an electro-mechanic tensile testing machine INSTRON 5969 was used. A special frame (or support) was designed in order to install the ultrasonic testing system on the tensile machine (Fig.2.36). This frame allows to apply static load at a node of displacements of the ultrasonic fatigue testing system (horn node).

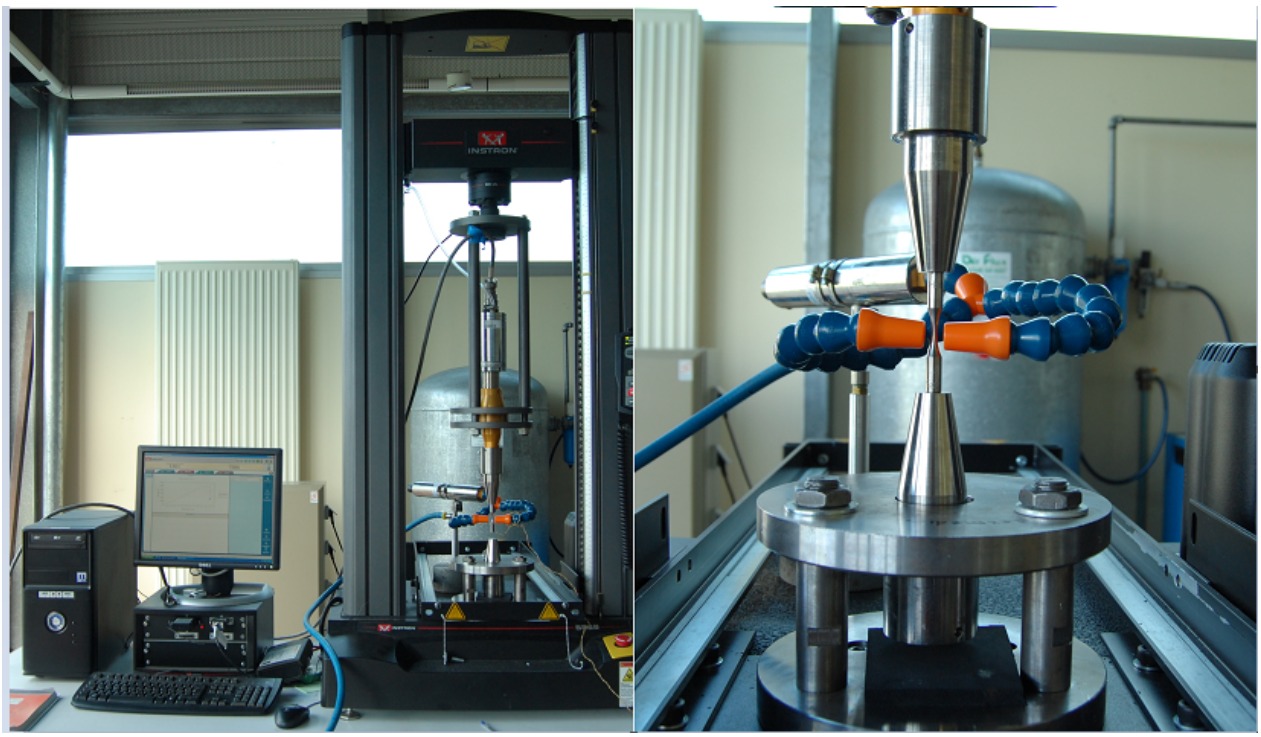

Figure 2.36: The specimen with attached strain gauge in work section

As usual the static tension is needed for tests with different positive stress ratios. The parameters of static load are controlled by the 'BlueHill' software designed by INSTRON. The cyclic loading parameters are ordered in ultrasonic fatigue testing software.

The configuration of the mechanical part for tension-tension fatigue tests should be chosen so that to keep the symmetry by the plane passing through the gauge section of the specimen. The TC-horns (typical minimum amplitude is about 3 - 4 μm) are capable to serve the range of the required stress amplitudes to fail VT3-1 titanium alloy at different stress ratios. The features of ultrasonic fatigue testing technique requires a minimum stress ratio being above

0 for asymmetric loading (to guaranty a permanent contact between support and ultrasonic horn). The loading configuration is schematically shown in Fig. 2.37.

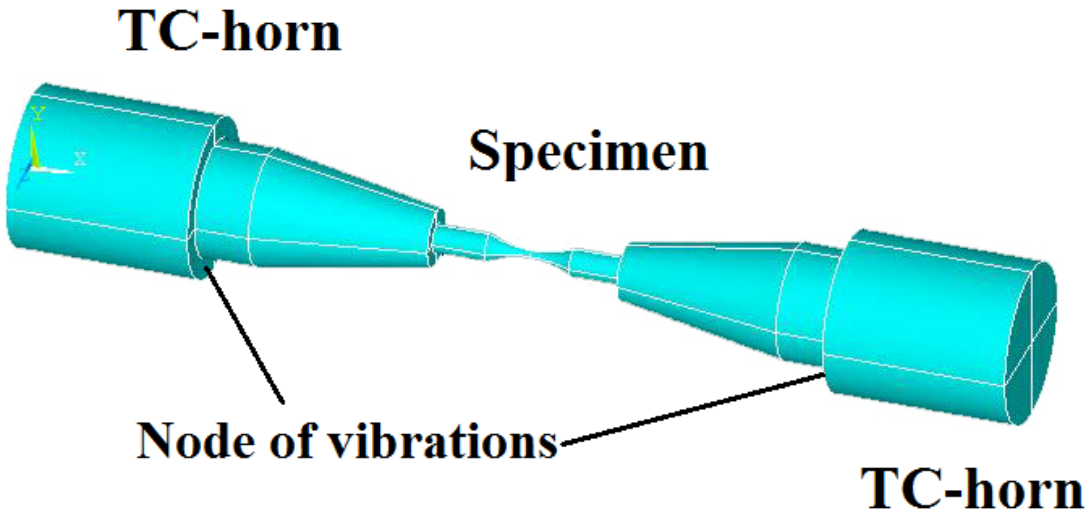

Figure 2.37: The specimen with attached strain gauge in work section

This loading system has two planes where the nodes of vibrations are found. Theoretically, the node of vibration is a point where the displacements equal to zero. In reality, planes of ultrasonic horns, Fig.2.37 could experiences any small vibrations, but they are considerable lower compared to other points of the horn. In order to determine the maximal value of displacements within these planes the non contact method was used. The results shows, that the maximum amplitude of vibration at 'node' plane can reach 2 μm at extreme operating conditions of testing system. Thus, in a normal operating regime these vibration are between 0 and 2 μm. In order to avoid the effect of small ultrasonic displacements at the 'node' plane, two lays of elastomer were introduced between the horn and static support.

2.5.4 Calibration of system for R>0 tests

The calibration of system for R>0 tests consists of two steps: calibration of dynamic and static load. For the cyclic loading the relationship between excitation and amplitude of vibration can be found in a similar way than for the tension-compression. The calculation of static load can be done as analytically based on the static force measured by INSTRON load sensor, as well by using strain-gauge. The stain gauge method allows to find the relationship

between the applied displacement and static elastic stress in the working section of the specimen. The difference between strain-gauge calibration and analytical calculation is negligible. That is important to note, that calibration of cyclic stress and static were done separately. It is assumed that there is no mutual influence of static and dynamic stresses. Thus, the principle of linear superposition can be used. This assumption has been verified by using the strain gauge calibration technique. This technique allows us to measure in operating conditions the real strain versus time (its mean and altering components).

Chapter 3

Experimental results and discussions

• Very-High-Cycle Fatigue is usually characterised by the domination of crack initiation stage over the crack growth. As this was shown for a lot of structural materials, crack initiation in VHCF can consume more than 99 % of the total fatigue life [3]. That is why the objective of present PhD project is to investigate the crack initiation process in aeronautic titanium alloy produced by: forging and extruding technologies. Moreover, crack initiation in gigacycle fatigue is related to some features of micro-structure and different types of defects (inclusion, porosity etc.).However the micro-structure of investigated titanium alloys does not include any non-metallic inclusion, as shown in Chapter II. Nonetheless, the micro structure of the studied two-phase titanium alloys consists of two phases with different latices: b.c.c. beta-phase and h.c.p. alpha-phase that involve some complex features of micro-structure ($\alpha - \beta$ borders, formation of α-colonies, macro-zones etc. The stable at low temperatures alpha-phase has a clear anisotropy of its mechanical properties in basal and prismatic directions. Sometimes this mechanical anisotropy may be found for the ingots made from such titanium alloy. For this reason, the specimens were cut from the plateau part of the compressor disk in different directions (along and perpendicular to the radius). These specimens were tested under the same loading conditions (tension-tension tests with R=0.1). Moreover, some specimens from the plateau part were investigated under tension-compression with R=-1 loading conditions in order to compare with rim part of the disk. Therefore, based on these results, the difference in fatigue strength and crack initiation mechanisms may be discussed with respect to both the position and the orientation of the specimens in the disk. The crack initiation mechanisms are investigated based on fractorgraphy analysis done by scanning electron microscopy (SEM) and EDX-analysis. The results of studying the micro-structure and EBSD maps are also used to link the features of crack initiation patterns with micro-structure of material. The first part of Chapter III deals with the forged VT3-1 titanium alloy, the second part includes the results and discussions for the extruded one.

3.1 Results of fatigue tests on forged VT3-1 titanium alloy at R=-1

• The first set of ultrasonic tests were carried out on axial specimens (0AXX series) machined from the rim part and tested under fully reversed ultrasonic tension loading(R=-1). The tests were performed at room temperature in air environment. The surface of specimens was cooled by compressed air with an air gun. The constant amplitude loading in continuous regime was used for ultrasonic fatigue tests. The tests were carried out under stress levels slightly below classical 'fatigue limit' in order to get failures in gigacycle regime $10^7 - 10^{10}$ cycles. The results of ultrasonic fatigue tests on forged VT3-1 titanium alloy are presented in Fig. 3.1

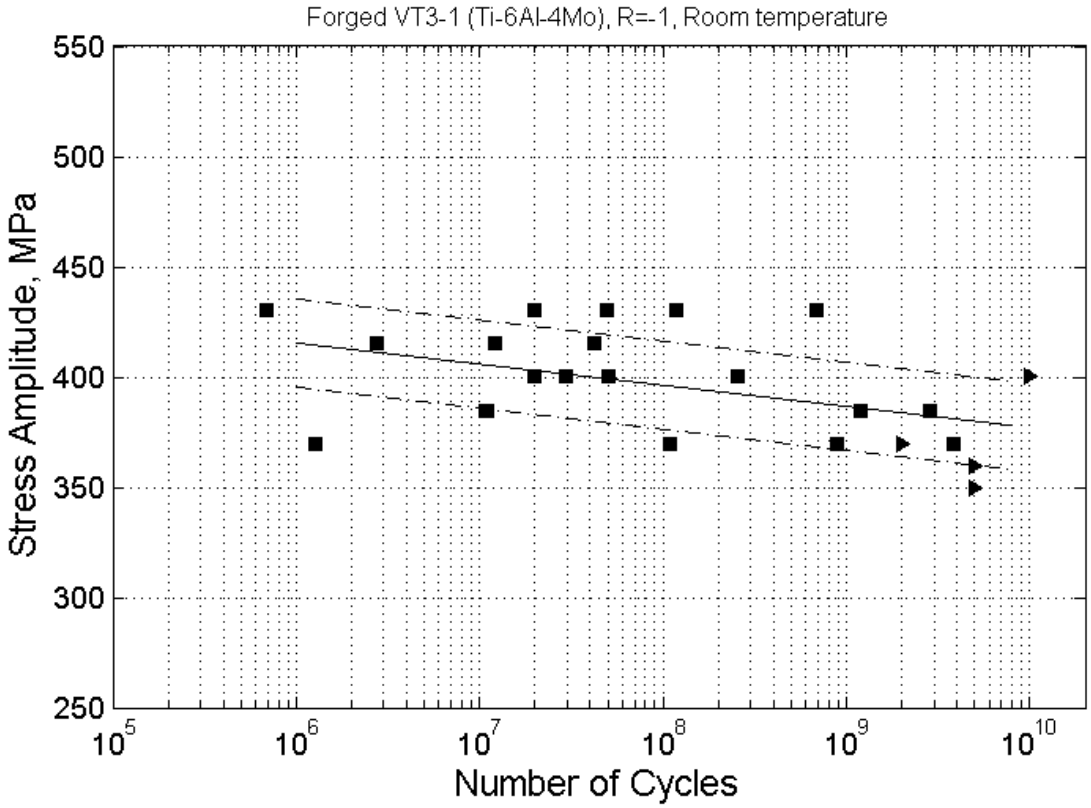

Figure 3.1: The results of tension-compression ultrasonic fatigue tests on forged VT3-1 titanium alloy

The fatigue life of forged VT3-1 titanium alloy has a large scatter in the VHCF region. Under certain stress levels the scatter reaches three orders of magnitude. At the same time, the SN-curve shows a small slope, that means a permanent decreasing of the fatigue strength

versus the number of cycles. The difference in fatigue strength at 10^6 and 10^9 cycles is around 60 MPa, that is almost 15 % of the fatigue strength. So significant decrease in fatigue strength and large scatter of fatigue life are subject for further investigation. All the fracture surfaces of forged VT3-1 titanium alloy were observed by SEM; detailed results are given in ANNEX C-2. Based on these results, the typical crack initiation sites were determined and some of them were subjected to additional EDX analysis. In the present Chapter the more representative causes of crack initiation will be discussed starting from the shortest fatigue life and moving to the longest one.

3.1.1 Fatigue life between 10^6 - 10^7 cycles

• The fatigue life between 10^6 - 10^7 cycles is usually assumed as the border between high cycle fatigue (HCF) and VHCF where the crack initiation mechanism has changed from the single surface crack initiation to subsurface crack initiation mode. It should be noted that there is not an exact or sharp border between two regions. For some materials it can be shifted or also being absent like in case of Armco Iron (80ppm carbon content) [85]. The investigation on the fracture surface of forged VT3-1 titanium alloy shows, that under the 'high' stress amplitudes and short fatigue life, crack initiates from the surface. Fig.3.2

With decreasing the stress amplitude the crack initiation site moves from the surface to the subsurface location, Fig. 3.3. The location of internal crack could be almost in the centre of the specimen.

In spite of clear fracture pattern, the location of crack initiation site is not always easy to determine for some specimens. In the case of specimen shown in Fig. 3.3 the exact crack initiation position was not found. The analysis shows that there is a sort of structural inhomogeneity close to the crack initiation site, Fig.3.4, but the reason of crack nucleation is not clear. The crack growth direction is illustrated by the arrows in Fig. 3.4. It is clear, that fatigue crack meets this structure during the propagation stage and after turns to a zone with similarly orientated alpha platelets (parallel lines at the fracture surface). These lines are not fatigue striations, because some of the fatigue crack propagation marks are aligned along these α-platelets. Thus, it seems that large clusters of similarly orientated alpha-platelets plays an important role in early stage of crack growth. Combining with the structural inhomogeneity, the clusters lead to crack branching and crack growth in different planes (split-level cracks). Such character of internal fatigue crack growth lead to form a perturbed fracture surface with strongly expressed lines of crack growth, Fig. 3.3. These clear marks are formed due to connection of cracks, growing in parallel planes at different levels ('meso-tunnel' cracking) [132]. The marks show that at the beginning, the fatigue crack growth as circular crack along the radius of cylindrical specimen. Close to the surface

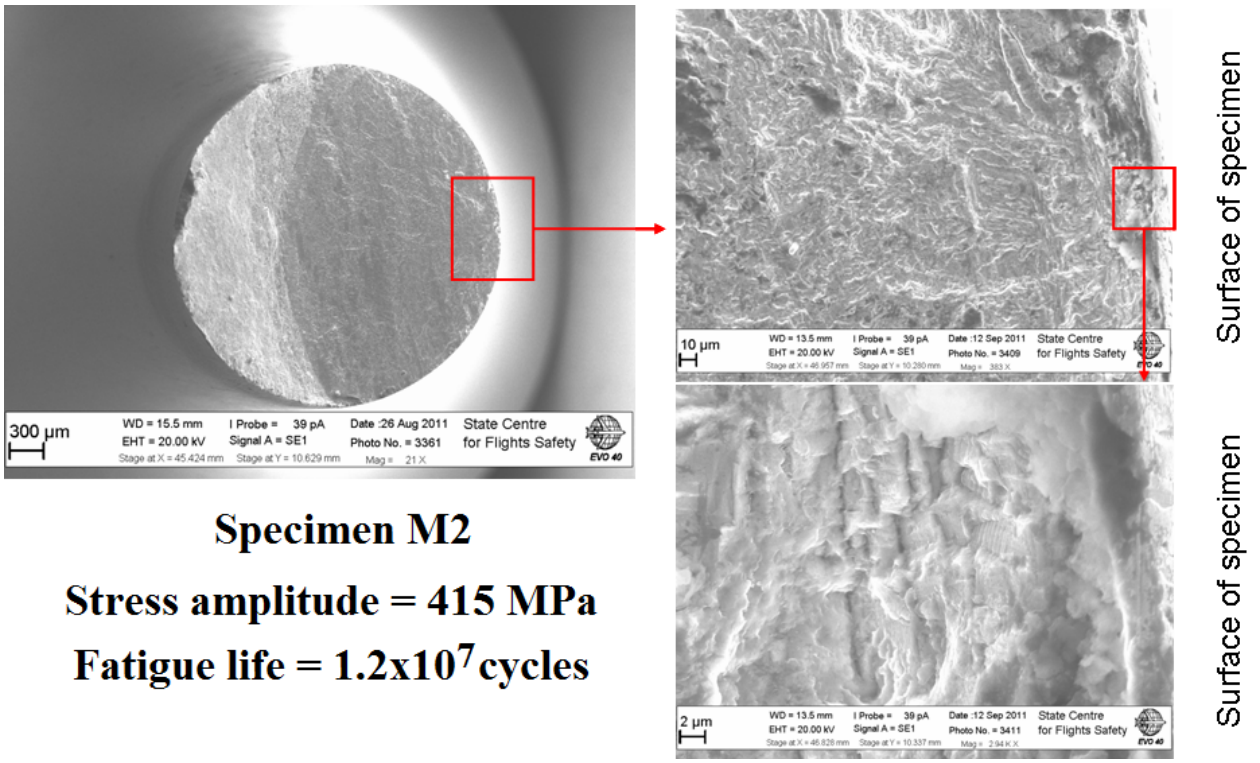

Figure 3.2: The crack initiation from the surface of specimen under high stress amplitude leading to short fatigue life.

the internal fatigue crack turn to the circumferential direction.

The analysis of crack initiation site (Fig3.5) shows that there is no clear initial area like inclusion in steels, porosity or other feature of micro-structure.

Probably, the fatigue crack was initiated from the border of two clusters adversely orientated one by another. Thus, the fatigue damage accumulation was not localized at one location but developed simultaneously at several sites along the border. Based on the analysis of crack growth marks the possible crack initiation site was found (Fig. 3.5). Thus, just the crack initiation zone within a few tenths of microns can be determined in present case of internal crack initiation. All other specimens cracked in the range of fatigue life 10^6 - 10^7 cycles show surface location of crack initiation site, Fig.3.6. Sometimes, the surface crack meets with some features of micro-structure, which influences the crack growth and crack turns to the split-level propagation.

Thus, the transition of crack initiation mechanism from surface to subsurface location exists for forged VT3-1 titanium alloy under gigacycle loading regime at fatigue life about the 10^7 cycles. Several internal cracks in forged VT3-1 were found in the range of 10^6 - 10^7 cycles. One internal crack was found after around 10^7 cycles at 385 MPa. At the same time

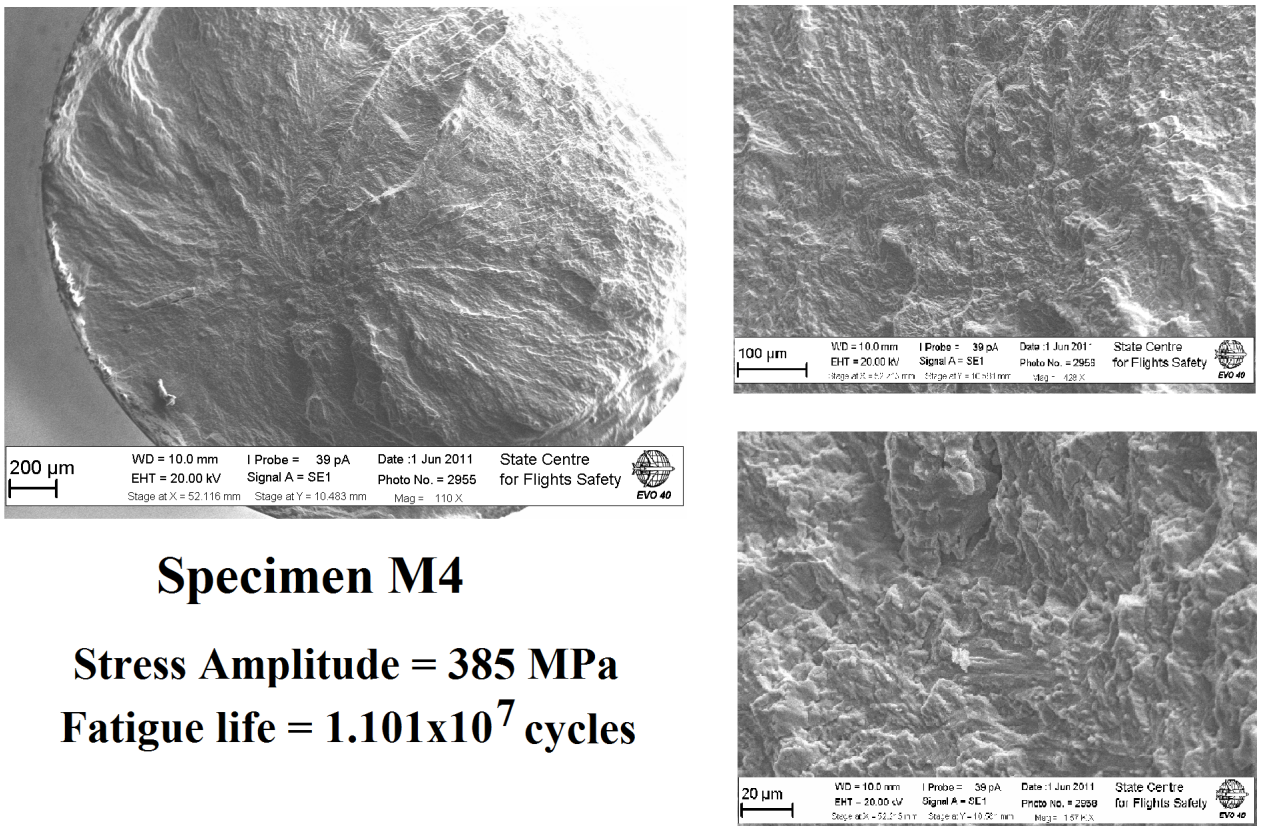

Figure 3.3: Internal crack initiation in forged specimen after $\simeq 10^7$ cycles under fully reversed tension

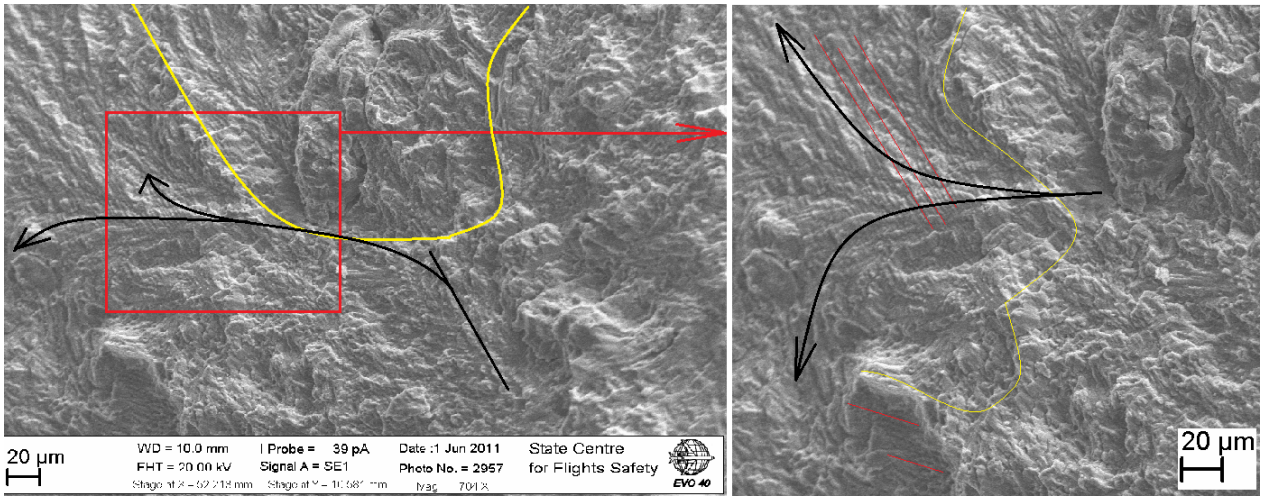

Figure 3.4: Inhomogeneous micro-structure close to the crack initiation site

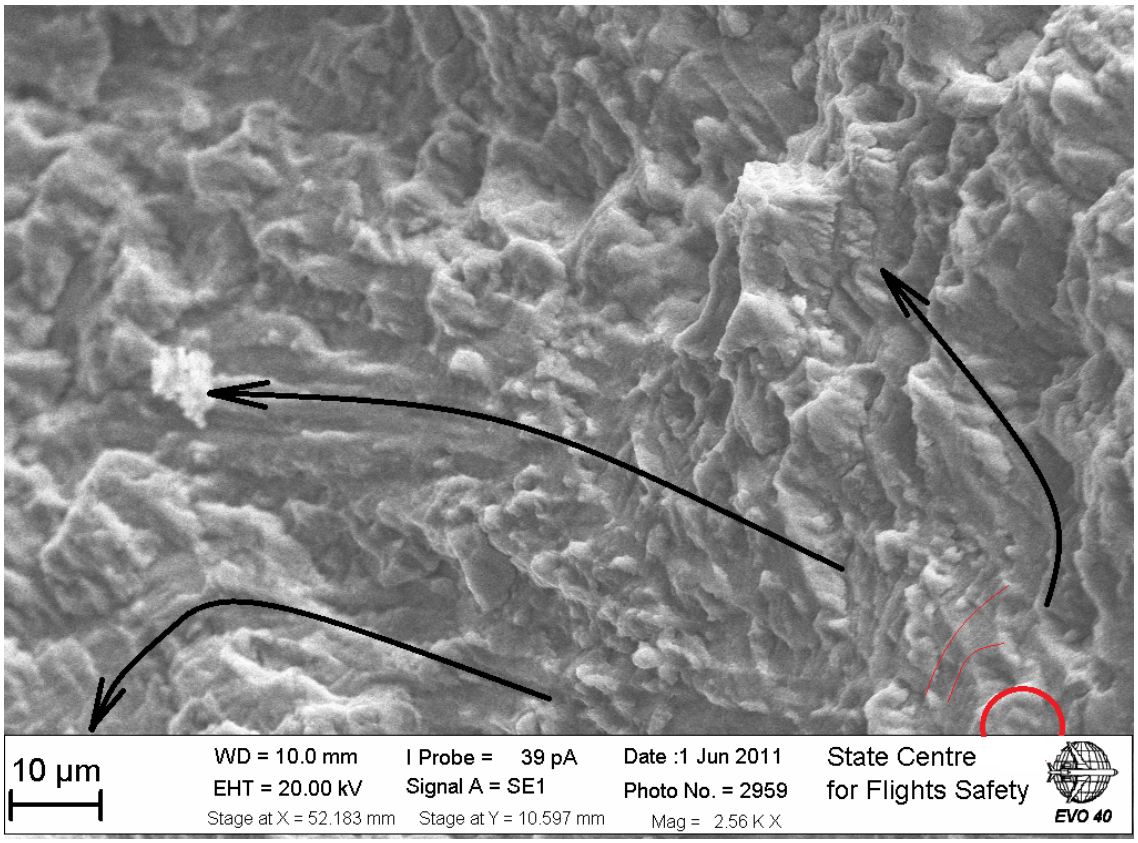

Figure 3.5: Internal crack initiation site in forged titanium alloy VT3-1 after 10^7 cycles

one surface crack was found almost after the same number of cycles to failure, but under a higher stress amplitude (430 MPa). Therefore, internal crack initiation is mostly determined by the number of loading cycles than by the stress amplitude. However, the stress amplitude should be low enough to provide so long fatigue life.

The first conclusions for the fatigue life range of 10^6 - 10^7 cycles can be outlined: (1) the internal crack initiation in forged VT3-1 is not related to clear micro-structural defects like inclusion or porosity; (2) with decreasing the stress amplitude the crack initiation mechanism changes from surface to subsurface cracking. This transition was found at around 10^7 cycles for forged VT3-1. The corresponding stress amplitude range is between 385 and 430 MPa.

3.1.2 Fatigue life of 10^7 - 10^8 cycles

• Conventionally, the SN-curve beyond 10^7 cycles is assumed to be horizontal or having a horizontal asymptote. However since the end of the 1980th this conventional assumption has been refuted by experimental investigation on different structural materials [3, 89, 70]. Based on experimental results for aluminium and titanium alloys, cast iron, high-strength steels etc.

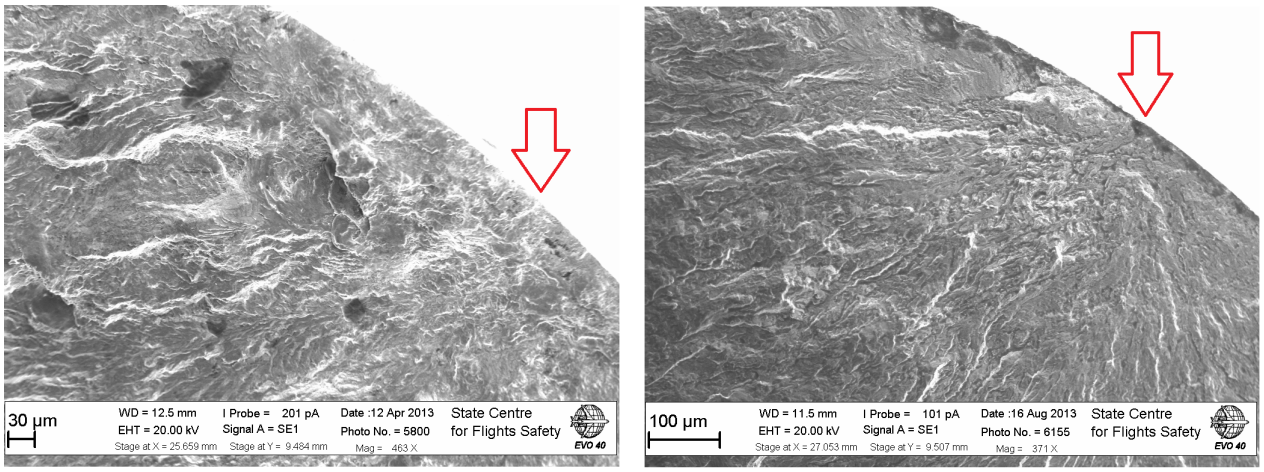

Stress amplitude = 430 MPa
Fatigue life = 6.84×10^5 cycles

a)

Stress amplitude = 415 MPa
Fatigue life = 2.75×10^6 cycles

b)

Figure 3.6: Surface crack initiation in forged VT3-1 titanium alloy under gigacycle loading regime

it has been stated that there is no horizontal asymptote on the SN-curve. The forged VT3-1 titanium alloy is not an exception from the general tendency for structural materials, Fig. 3.1. The present subsection is focused on the reason of fatigue failure of VT3-1 alloy after the fatigue life laying in range of 10^7 - 10^8 cycles. The analysis of fracture surface shows that all the specimens in this region were failed by internal cracks. No crack initiation from the surface of the samples was observed. The macro-view of typical fracture surfaces formed after 10^7 - 10^8 cycles are shown in Fig. 3.7.

The detailed analysis on the crack initiation sites have shown that at least two typical crack initiation scenarios may act in forged VT3-1 titanium alloy after 10^7 - 10^8 cycles. First of all it should be outlined that 10^7 cycles is a 'short' fatigue life for the VHCF range ($10^7 - 10^{10}$ cycles). The common reason of such decreasing in fatigue life under cyclic loading is the existence of a structural defects in the material (for example inclusions or porosities). In the case of inclusions (for steels), specimens containing a bigger inclusion show a shorter fatigue life. In case of titanium alloy there are no non metallic inclusions and typical structural defects are different heterogeneities of micro-structure. As well known it is difficult to control the micro-structure of forged titanium alloy especially when the size of ingot is so large as a landing gear or a disk of compressor. The deformation, temperature fields and their gradients can lead to forms local heterogeneities in the micro-structure. From the dislocation theory point of view, the grain, α-colony, macro-zone boundaries may discourage a dislocation movement and therefore lead to plastic deformation accumulation [105]. In the case of forged

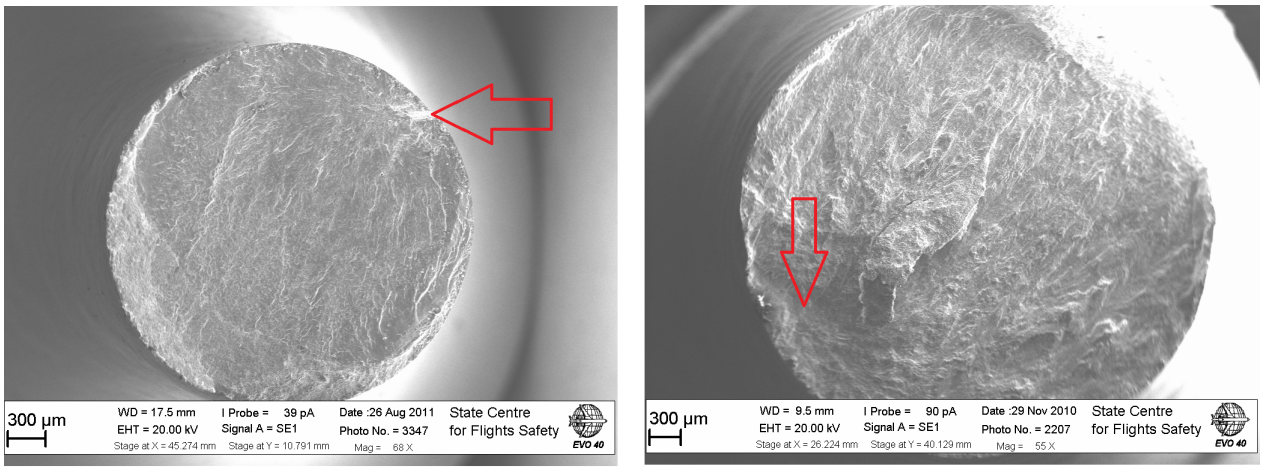

Stress amplitude = 400 MPa
Fatigue life = 2.98x10 7 cycles

a)

Stress amplitude = 370 MPa
Fatigue life = 1.1x10 8 cycles

b)

Figure 3.7: The macroview of fracture surfaces, forming after 10^7 - 10^8 cycles

VT3-1 titanium alloy, a fractographic analysis on specimens having a 'short' gigacycle fatigue life has shown a micro-structural defect at crack initiation site. It is a large agglomeration of coarse α-phase platelets, Fig.3.8.

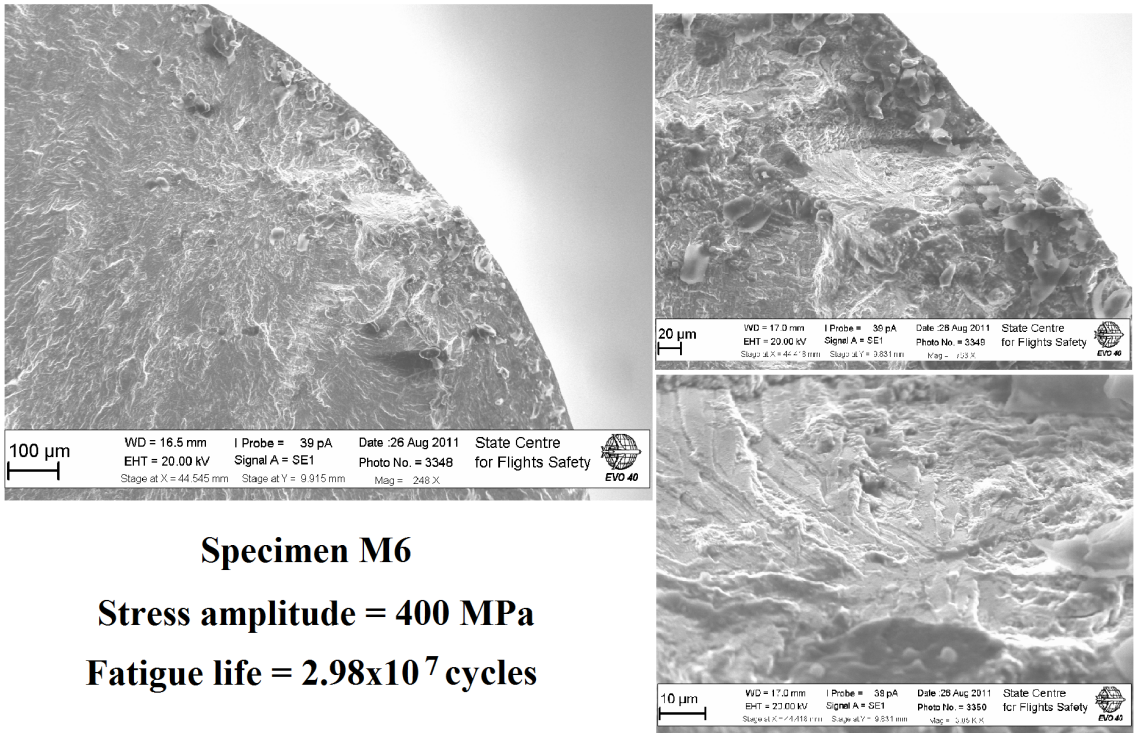

Specimen M6

Stress amplitude = 400 MPa

Fatigue life = 2.98x10 7 cycles

Figure 3.8: The crack initiation in forged VT3-1 from the defect of microstructure

The alpha-phase is mainly stabilized by aluminium in present titanium alloy which makes the material stronger and harder. The very high strength lead to a limited ductility of metallic materials. As we can see from Fig. 3.8 such agglomeration of alpha-phase shows a quasi-brittle fracture surface, that could be related to the extra content of alpha-stabilizing elements within such zone. In order to check that, EDX-analysis was performed on area with quasi brittle fracture surface. The results of analysis (Fig.3.9) shows that concentration of aluminium within brittle fracture surface is significantly higher than the normal chemical composition of the VT3-1 alloy. Moreover, the concentration of beta-stabilizing elements within the same zone is extremely low, Fig.3.9. The size of the quasi-brittle fracture surface is around 100 μm 50 μm. The local segregation of elements can lead to local increasing of micro-hardness and therefore strain incomparability between harder and normal material areas. As it was assumed by Bowen [126] an incomparability in strain even between two neighbouring grains can lead to fatigue crack initiation. In case of large agglomeration of hard α-phase platelets this effect can become more significant leading to the fatigue life reducing. The analysis of chemical composition at different locations shows that in the centre of such structural heterogeneity the concentration of beta-stabilizing elements is so low, that it could not be detected by the equipment. At the same time the concentration of aluminium exceeds the norms for the present alloy at these locations. Meanwhile, chemical composition outside of this agglomeration satisfies the standard composition, spectrum 4 (Fig. 3.9). Thus, the chemical composition anomaly within the area of about 100 μm^2 is assumed as defect of micro-structure that lead to internal crack initiation and significant decrease of the fatigue life.

The problem of chemical element segregation is very common for titanium alloy with molybdenum and niobium. The segregation of chemical elements occurs during the solidification stage. The speed of cooling is a critical parameter for this process. Some irregular structures may be formed during the solidification of alloy which are manifest themselves under the gigacycle fatigue loading, Fig. 3.10. The EDX analysis of this zone shows the segregation of alloying elements within the regular system of layer structures. The layer system in titanium alloys forms when the cooling rate is too high, that lead to the limited diffusion of 'large' molybdenum atoms to the zone of first crystallization.

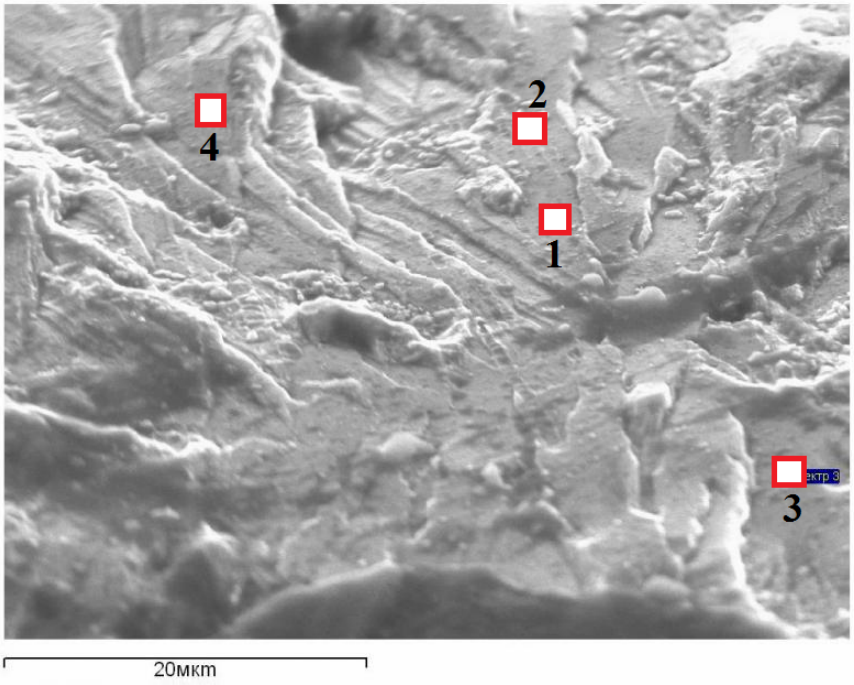

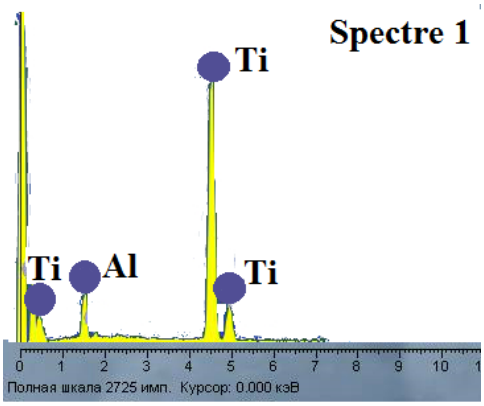

a)

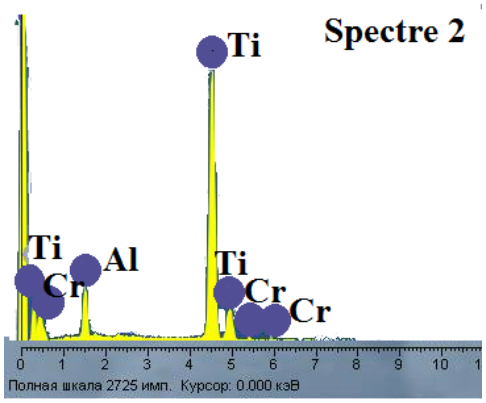

b)

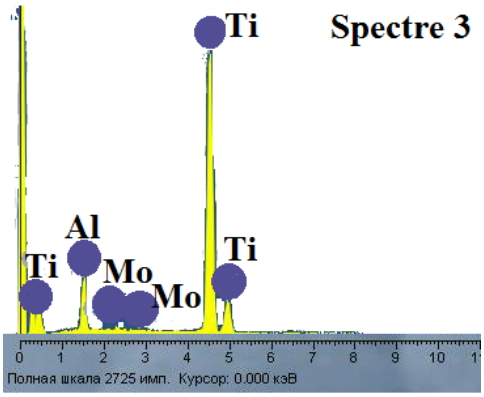

c)

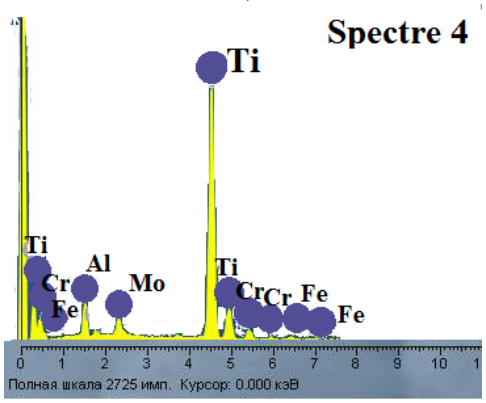

d)

Figure 3.9: Examples of two-phase titanium alloy micro-structures: a) equiaxed α [71] , b) lamellar α [98] c) equiaxed α + transformed β (pancake) [99] d) Widmanstatten (basket-weave) structure [98].

Thus, the first layer structures are formed in presence of exceeded concentration of alpha-stabilizing elements. The small atoms of Al are more mobile compared to large Mo atoms that determine its higher activity in crystallization process. The surplus Mo atoms are involved in crystallization process in locations between already formed alpha-phase layers. The analysis of chemical composition within such layers structures proves that concentration of aluminium in the layer is extremely high compared to normal composition. The results of EDX analysis shows, that concentration of molybdenum in intermediate layer is higher compare to normal composition and even exceed the concentration of aluminium.

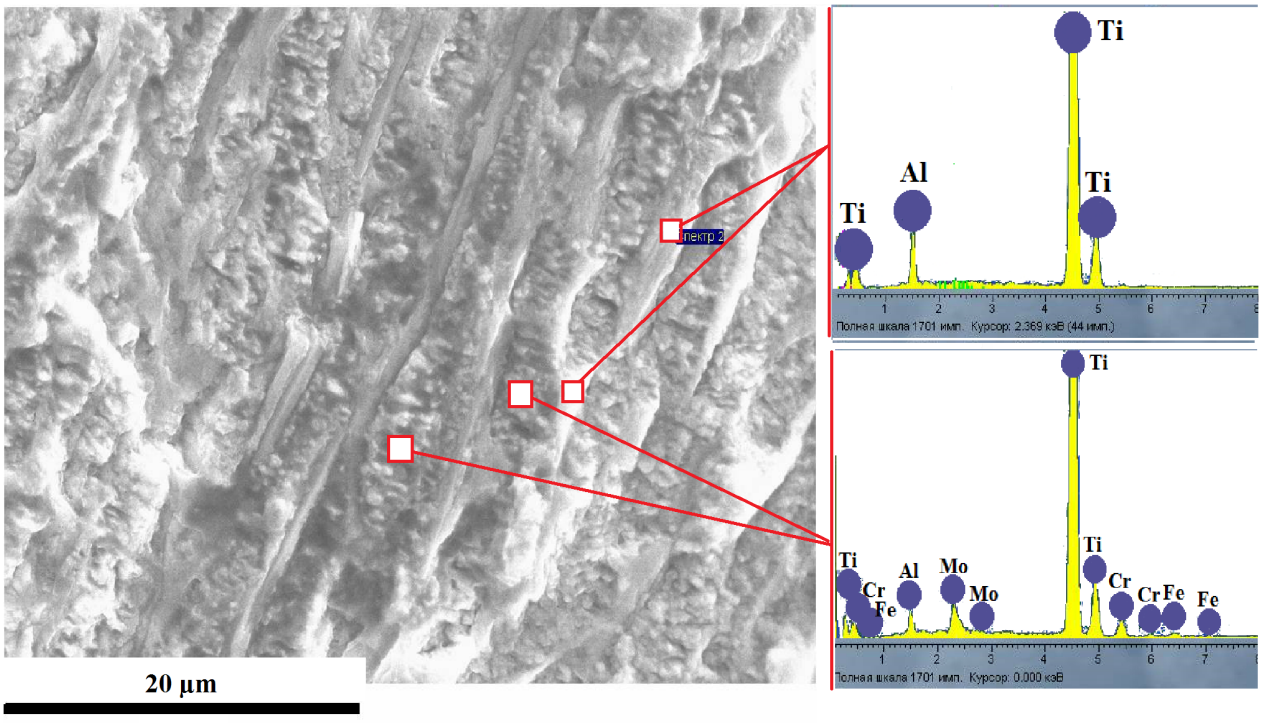

Figure 3.10: The segregation of alloying elements in regular layers

Such segregation of chemical elements leads to formation of micro-structural defect which is very inhomogeneous from the mechanical point of view. The fracture of this zone shows, that alpha-phase layers has a quasi-brittle character of fracture surface, while the intermediate layers shows a ductile type of failure. The characteristic size of zone with system of regular layer structure is similar to the size of defect presented on Fig.3.9. Such structural defects are critical elements of forged titanium alloy micro-structure, which lead to the early crack initiation under gigacycle fatigue loading and, therefore, to significant decrease of the total fatigue life.

Nevertheless, irregularities of micro-structure are not very common for forged VT3-1. In

the framework of the present research project just two specimens between all the investigated specimens have shown crack initiation from strong structural defects such as shown on Fig.3.9 and 3.10. The investigation on the specimens failed in the range of 10^7 - 10^8 cycles shows that in the absence of strong defects, the crack commonly initiates from the borders of 'macro-zones' that are large (several hundreds of micrometers) structural elements with quasi-homogeneous organisation of alpha-plates within one zone, Fig.3.11.

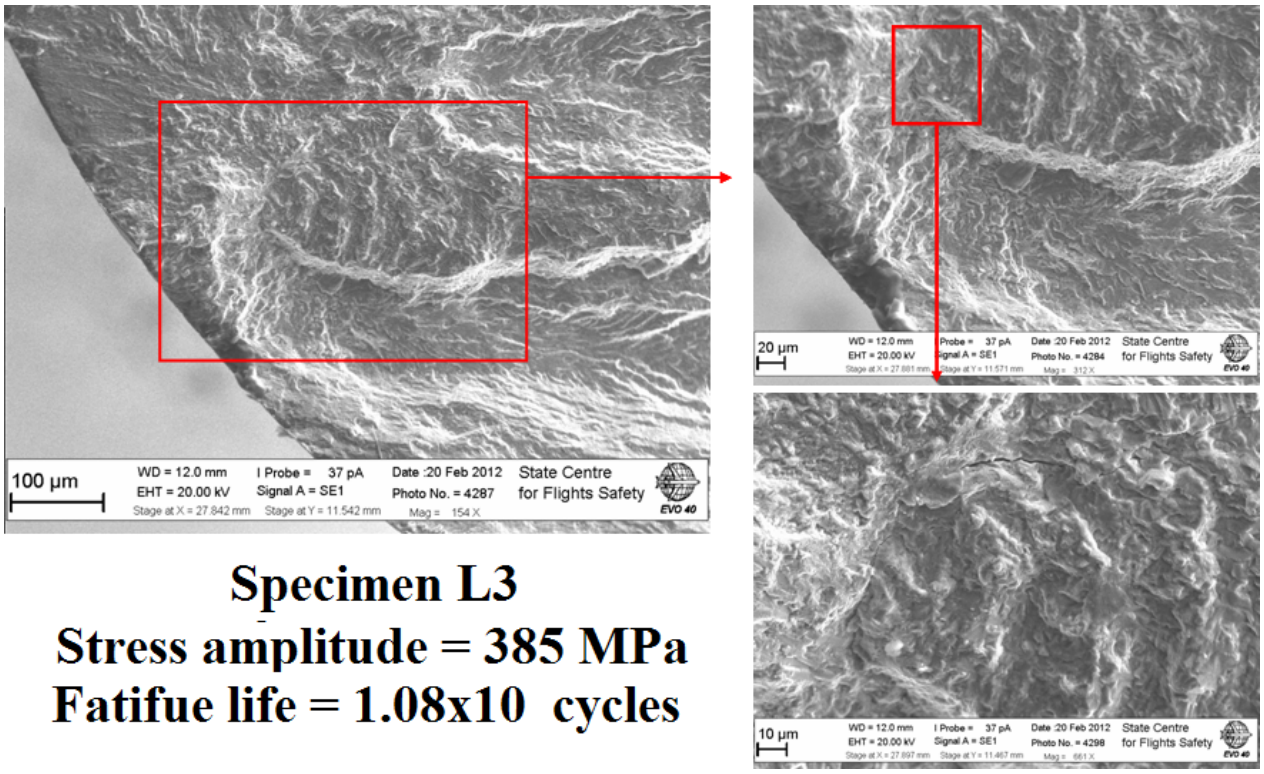

Figure 3.11: The crack initiation from the border of large structural element ('macro-zone')

The border of the large micro-structural element from which the fatigue crack has initiated is clearly highlighted by the crack, Fig. 3.11. The crack follows the border of this structural element ('macro-zone'). The presence of micro-structural elements in forged VT3-1 titanium alloy has been shown during the analysis of micro-structure in Chapter 2. It was called as macro-zones or cluster of alpha-platelets. The observation of fracture surface show that the crack often occurs at the border between such structures, Fig. 3.12. Sometimes, the alpha-plates in neighbouring 'macro-zones' are elongated along almost the same direction. In this case the border between these clusters are not clearly seen at the fracture surface. Thus, the fatigue damage accumulation at boundaries of clusters depend on both global orientation of the cluster by the axis of loading and mutual orientation of two neighbouring clusters.

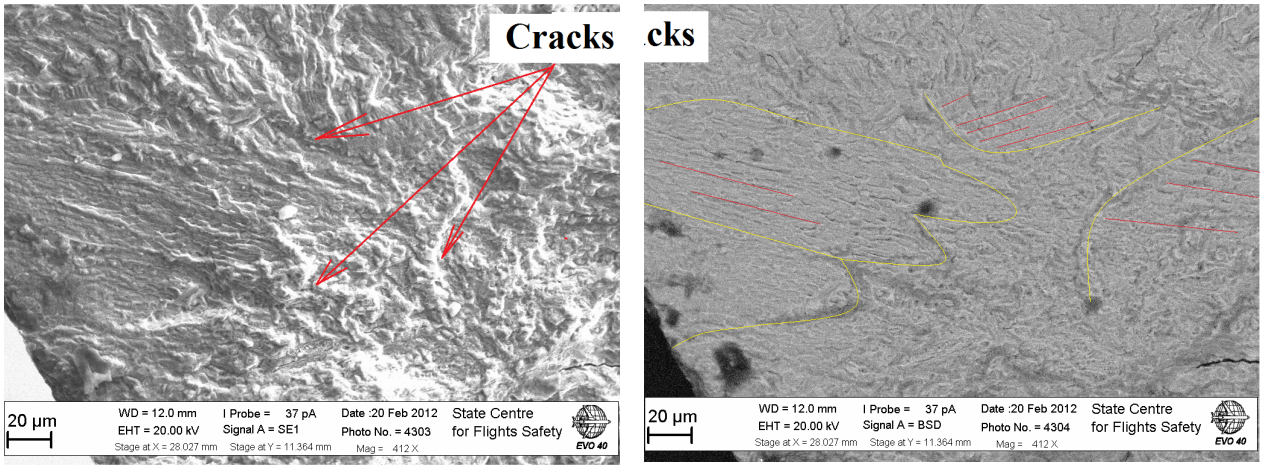

a) b)

Figure 3.12: The border of 'macro-zone' at fracture surface of forged VT3-1 titanium alloy

The crack initiates at locations where two conditions are met: the global and mutual orientations are more unfavourable. In order to study the geometry, global and mutual orientation of the clusters in forged VT3-1 alloy the electron backscattered diffraction (EBSD) analysis was carried out. The results of analysis shows, that micro-structure of forged VT3-1 titanium alloy is represented by clear clusters, Fig. 3.13. Based on the EBSD analysis it can be outlined, that neighbouring clusters could have as always similar global crystallographic orientation as well a quite different disorientation up to 85°. The size of the cluster is also very heterogeneous. The largest cluster on the presented map is about 800 μm long and 400 μm width. However, the analysis of micro-structure shows that the 'macro-zone' can reach the size of several mm for forged VT3-1. The mutual disorientation of neighbouring clusters is varying from $30° - 40°$ to $80° - 85°$. Thus, the border between some clusters may block the dislocation movements and becomes the fatigue damage accumulation sites. The variation in cluster's size, global orientation, mutual orientation of two and more clusters may lead to the significant scatter in the fatigue life of forged VT3-1 titanium alloy. Probably it exists the combination of more unfavourable factors for global and mutual orientations that lead to early fatigue crack initiation, as shown in Fig. 3.11.

Thus, concluding the result of fractography, X-ray and EBSD analysis on the specimens, broken in the range of fatigue life $10^7 - 10^8$ cycles it can be outlined the following: for all the investigated specimens, the crack initiation sites are in the bulk of material; some of the crack initiations are related to the structural defects, such as agglomeration of alpha-phase plates or regular system of layer structures with different concentration of alloying elements. The regular system of layer structures are similar to the micro-structures obtained for aluminium by laser hardening (high heating rate). These structural defects influenced on the fatigue life of forged titanium alloy leading to the early crack nucleation and reducing the total fatigue

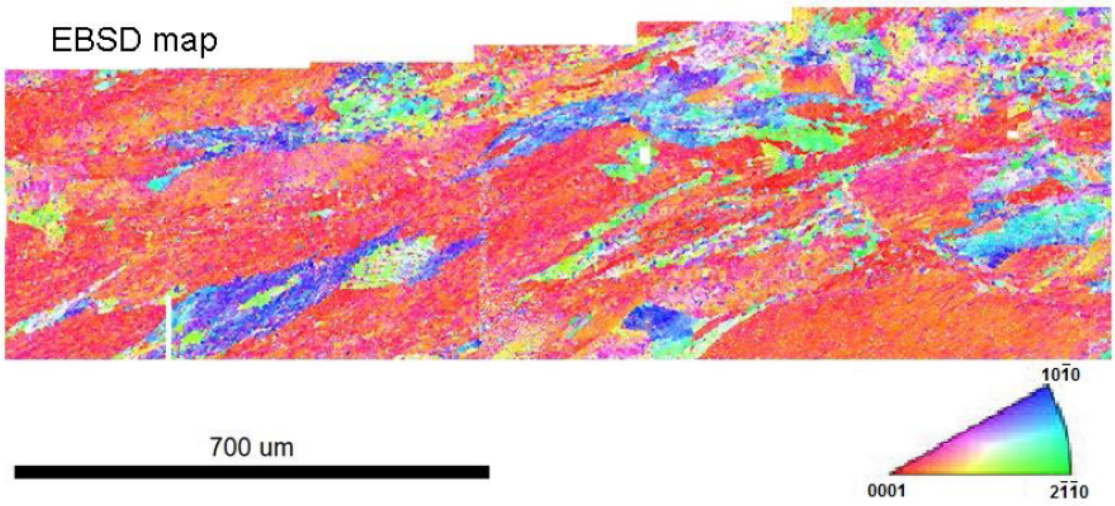

Figure 3.13: The EBSD map of forged VT3-1 titanium alloy

life. In the absence of strong structural defects, the borders of clusters becomes the sites of fatigue damage accumulation. A sort of competition between the two crack initiation mechanisms can be traced, like in case of surface/subsurface crack initiation. The analysis of EBSD map shows that large clusters of almost similarly orientated alpha-platelets exist in forged titanium alloy. The disorientation between clusters is varying in a wide range up to almost 90°. It is assumed that the combination of global and mutual orientation of the clusters may lead to early fatigue failure even compared to the strong defects.

3.1.3 Fatigue life between 10^8 - 10^{10}

• The range of stress levels which are corresponding to the fatigue life between $10^8 - 10^{10}$ cycles is not significantly lower compared to the discussed above range. Sometimes the fatigue crack at 10^9 cycles and at 10^7 cycles can be obtained under the same stress level. The reason for that is probabilistic nature of critical defect distribution in the material. The work cross-section of the specimen is 3 mm in diameter and high stress amplitude zone is very localized (along the specimen axis) in the middle of the working hyperbolic part of the specimen. Thus, the volume of material which is subjected to the high enough stresses is quite small. The probability to find the same critical micro-structural imperfection in two different specimens investigated under the same stress level is quite low. Therefore, even if the crack initiated from the same type of micro-structural defect, the total fatigue life will be different. The stress range leading to fatigue life between 10^8 and 10^{10} is from 370 to 430 MPa. The macro view of typical fracture surfaces of specimen failed in this range is shown

in Fig. 3.14.

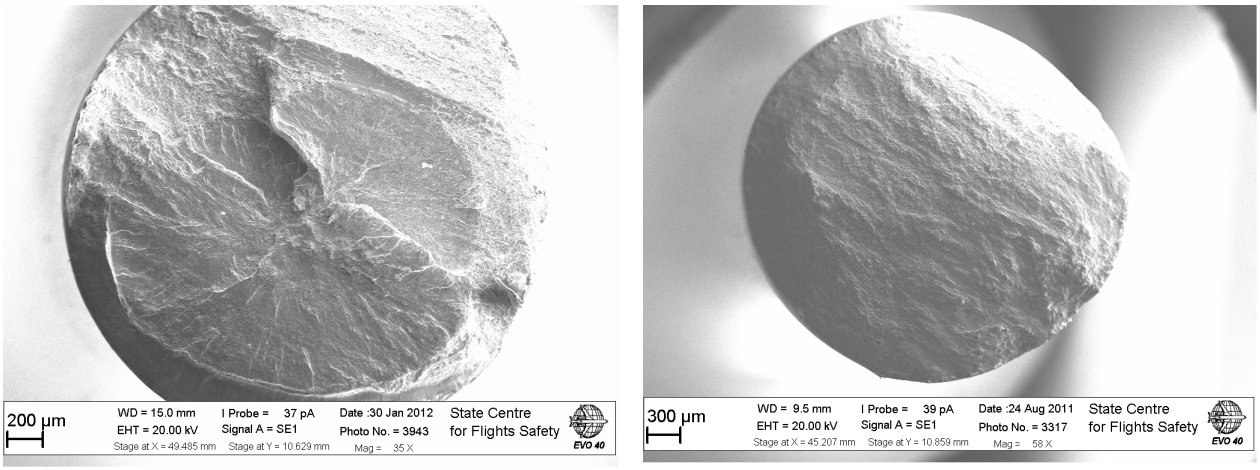

Stress amplitude 430 MPa
Fatigue life 1.18×10^8 cycles

a)

Stress amplitude 385 MPa
Fatigue life 3.84×10^9 cycles

b)

Figure 3.14: The macroview of typical fracture surface after 10^8 - 10^{10} cycles

The crack initiation sites in this range of fatigue life are also located in the bulk of the material. Sometimes the crack initiates from the core of the specimen, sometimes it originates close to the specimen surface. However, there is no link between the position of crack initiation site and the total fatigue life. The detailed analysis on the crack initiation sites for broken specimens beyond 10^8 cycles shows the competition between several crack initiation mechanisms. One specimen between all the tested ones beyond 10^8 cycles has shown crack initiation from the boundary of clusters, which was discussed in the previous section. Thus, such mechanism of crack initiation may appears even after the very high number of loading cycles, but the number of such initiations looks to be less compared to shorter fatigue life. Most of the investigated specimens have shown a new type of crack initiation sites.

The crack initiation by quasi-brittle cracking of single alpha-phase platelets were first observed on the fracture surfaces obtained after 10^8 cycles, Fig. 3.15. The characteristic size of the smooth facet is similar to the width of the typical alpha-phase platelet and equal to 2 μm. The peculiarity of the facet fracture is the absolutely flat or smooth surface within 2 μm square. All the neighbouring facets show the traces of crack propagation while the first smooth facet is absolutely flat even under the high magnification of about 18000 times Fig.3.17. The smooth facet failure is the most common crack initiation mechanism in two-phase titanium alloy under VHCF [120]. The formation of such facets is not clearly explained up to now. Some authors explain such pattern of fracture surface by sliding process in basal plane of alpha-phase [123]. Other authors proposes the twining mechanism of such subsurface

cracking [130] to explain the absolutely smooth surface formation by local twining under local compression load (at the grain scale).

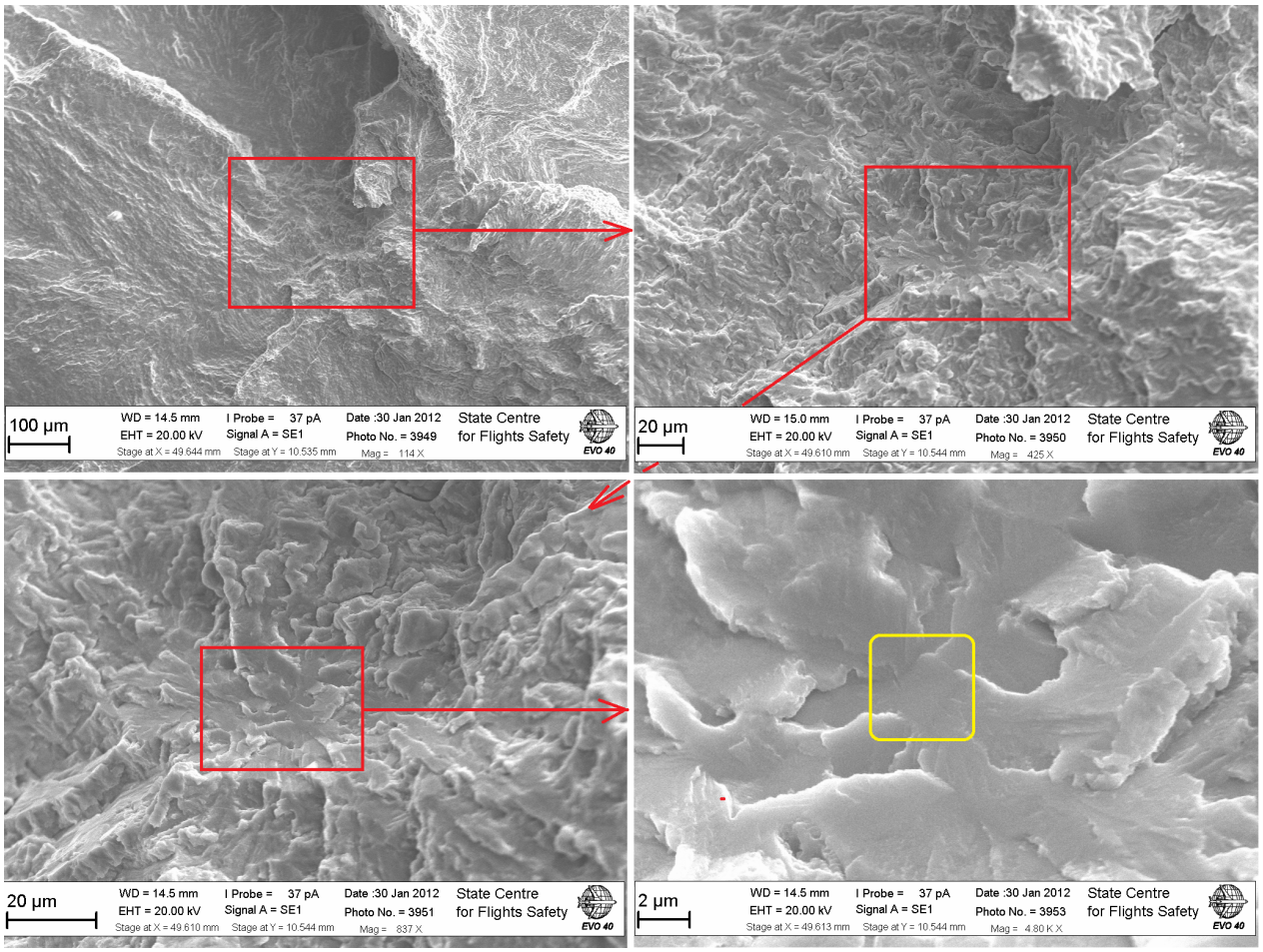

Figure 3.15: The fatigue cracking by forming the 'smooth facet'

The study of smooth facets shows, that all the investigated facets have a characteristic size of about 2 μm. The analysis of results in literature shows, that the size of smooth facets from which the crack initiates may reach up to 10 μm [71]. The comparison of fracture surface with the micro-structure of titanium alloy studied in [71], (Fig.3.16) allows to assume, that the smooth facets are formed within one of the alpha-phase location. Thus, it can be assumed that the first smooth facet forms within one the alpha-phase platelets.

The size of the first smooth facet is related to the characteristic size of the alpha-phase formation. In case of forged VT3-1 the alpha-phase shape is elongated platelets with a typical width of 2-3 μm that is in good agreement with all found smooth facets in investigated alloy. Some examples of smooth facets are illustrated in Fig. 3.17. These facets are located in different positions relative to the crack initiation site, but the characteristic size is the same.

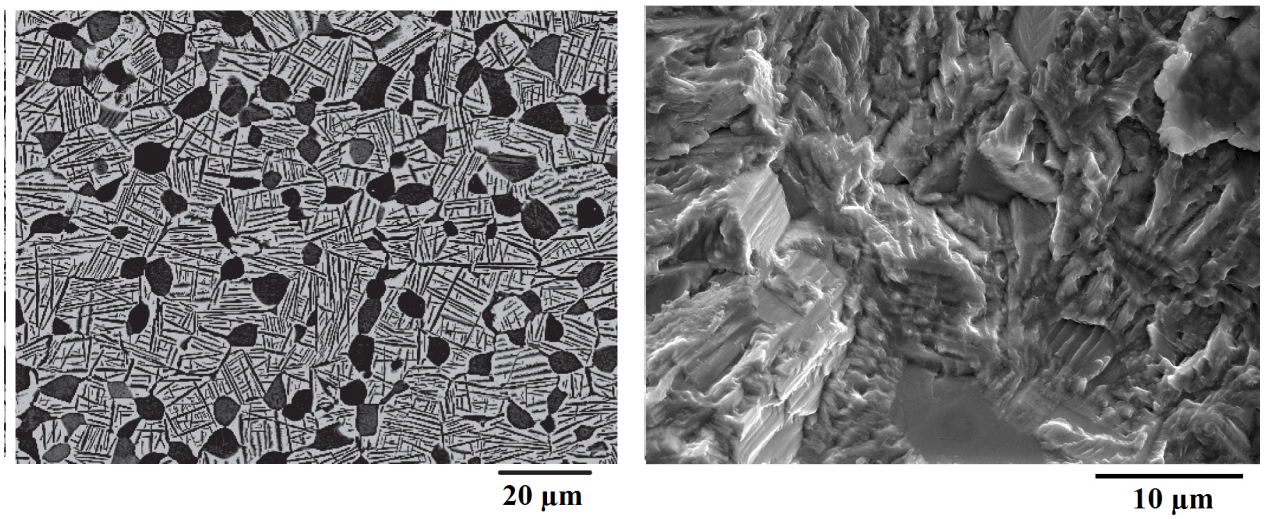

a) b)

Figure 3.16: The smooth facet in two-phase Ti-6Al-2Sn-4Zr-6Mo titanium alloy and its microstructure [71]

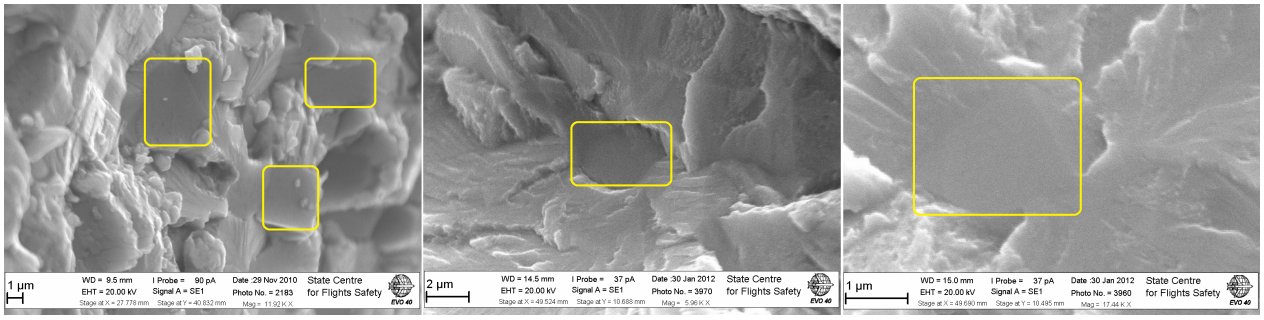

Figure 3.17: Examples of smooth facets crack initiation in the forged VT3-1 titanium alloy

Therefore, the smooth facets in two-phase α-β titanium alloys are formed within the alpha-phase. That can be proved by applying the EDX analysis within such zones. The results for different facets shows the same tendency: the local concentration of beta-stabilizing elements is quite low but still significant, while the alpha-phase stabilizing elements are present in excess. The example of EDX analysis within smooth facet is shown in Fig. 3.18. The facet cracking or cleavage-like facet of titanium alloy was found for different two-phase titanium alloys including widespread in aeronautic industry Ti-6Al-4V [124].

Although the total fatigue life is mostly related to the crack initiation stage in VHCF regime, the further works of Oguma on VHCF behaviour of Ti-6Al-4V were focused on the fatigue damage development mechanisms starting from the cleavage-like facet and not focused on the mechanisms of smooth facet initiation [119]. The internal character of fatigue

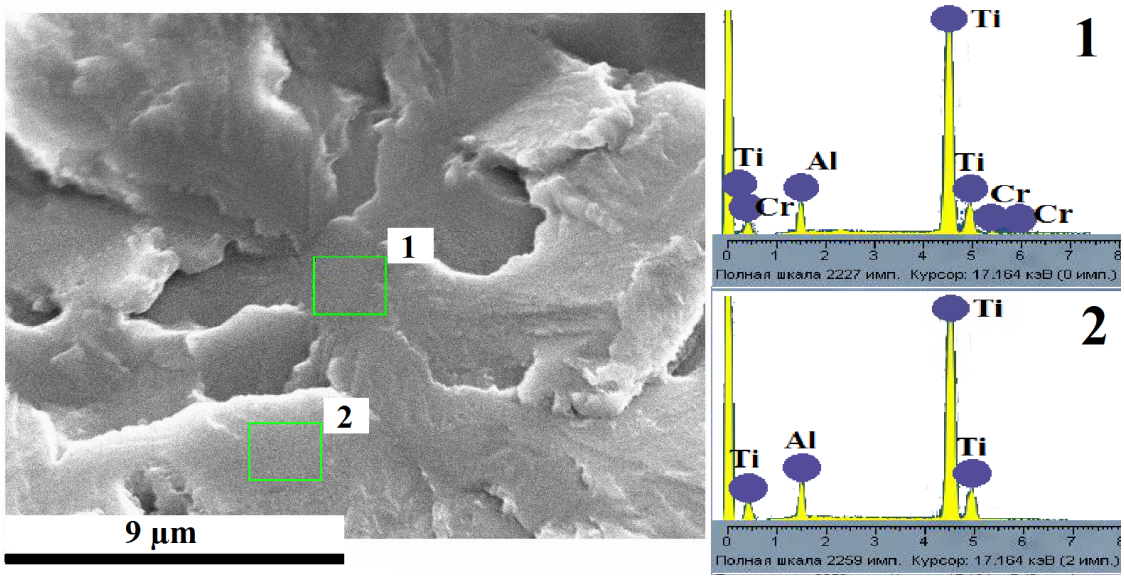

Figure 3.18: EDX analysis within two cleavage-like facets

crack nucleation in VHCF and the very localized area of the smooth facet formation makes incredibly difficult in-situ investigations on the mechanism of the first smooth facet cleavage-like formation. Thus, hypothesis only can be developed based on the results of observation on the fracture surfaces. Up to now there is not any criterion or micro-mechanical models which can predict the position or characteristics of alpha-phase formation (single platelet or agglomeration of α-platelets) that will be cracked first. Probably this criterion should be multi-parametric, like with cluster's boundary, and should operate with crystallographic orientation of the alpha-phase platelet or coarse α-platelets within large agglomerations by the axis of loading, neighbouring structures, position in the specimen, local chemical composition and others. At the moment, we can just note it like a fact, that the most common crack initiation site in two-phase titanium alloys under tension in VHCF regime is cleavage-like smooth facet. In case of forged VT3-1 titanium alloy such mechanism of crack nucleation is more typical for fatigue life beyond 10^8 cycles.

Another typical crack initiation site in forged VT3-1 titanium alloy under VHCF that manifests itself beyond 10^8 cycles is quasi-smooth facets. The nature of quasi-smooth facets looks to be similar to the smooth facets and related to the alpha-phase platelets failure. But the size of the quasi-smooth facets exceeds the typical dimensions of alpha-platelet cross-section and may reach around 10 - 15 μm. Such formation are typically elongated and remains the longitudinal section of the alpha-platelets which were observed in the micro-structure, Chapter II. The next difference between smooth and quasi-smooth facets is higher roughness of quasi-smooth facets. A typical crack initiation site with quasi-smooth facet is

shown in Fig. 3.19. The site of crack initiation shows a quasi-brittle character of fracture surface with pronounceable roughness, Fig.3.20. In a similar way, an additional analysis of the chemical composition within such zone has been carried out.

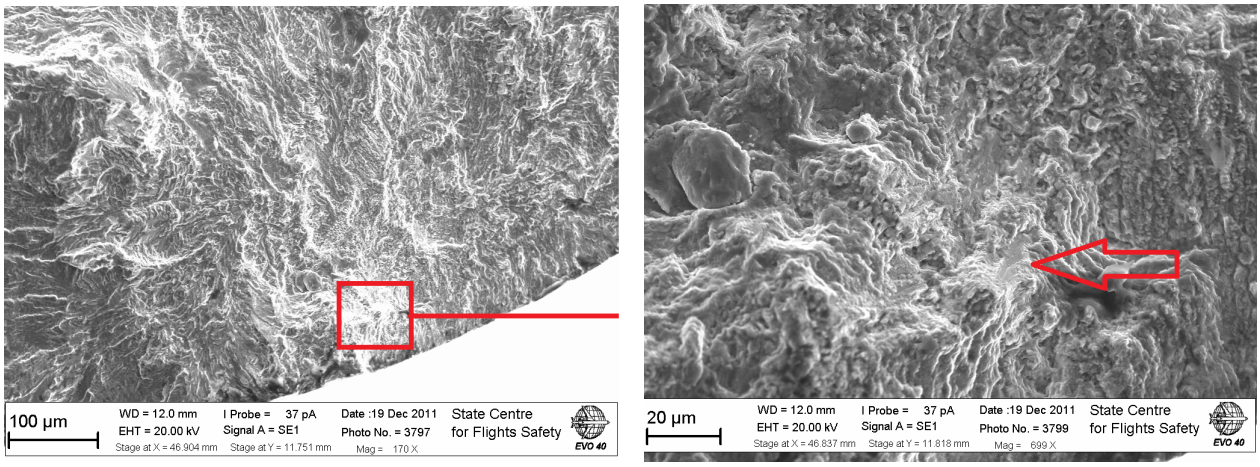

a) b)

Figure 3.19: The crack initiation from the quasi-smooth facet in fogred VT3-1 alloy after 10^9 cycles

The EDX analysis was carried out in several locations within the quasi-brittle fracture surface. A significant difference in chemical composition can be outlined. In the case of quasi-smooth facets, the fracture area is significantly enriched by alpha-stabilizing elements and does not contain any noticeable (detectable by the experimental equipment) content of beta-stabilizing elements, (Fig. 3.20). Whereas outside of this crack initiation site the chemical composition turns to normal.

Thus, such crack initiation sites were classified as self-sustained type of fatigue crack nucleation and called as initiation due to chemical inhomogeneity. It should be noted that the changing of chemical composition under the VHCF loading was already reported for metal materials. The results of observation on crack initiation sites in steel has shown a higher concentration of carbon at initiation sites, that can be early observed by optical microscope as a black or dark area. Such zone in steel is named Optically Dark Area (ODA) [55] and the carbonisation was assumed to be due to cyclic loading [89]. In the case of titanium alloy a sort of changing in chemical composition was observed too, but the question is it due to cycle loading or initial state of material is unclear. From one hand the diffusion of chemical elements is possible under cyclic loads, that is well know as Gorskiy effect. From another hand, the size of alloying elements in the case of VT3-1 titanium alloy is large. The position of Molybdenum in periodic system of elements is 42, while the titanium has the 22nd number. Thus, the diffusion of so large atoms at room temperature is quite problematic, even under the high amplitudes of loading. In order to investigate the initial chemical composition and

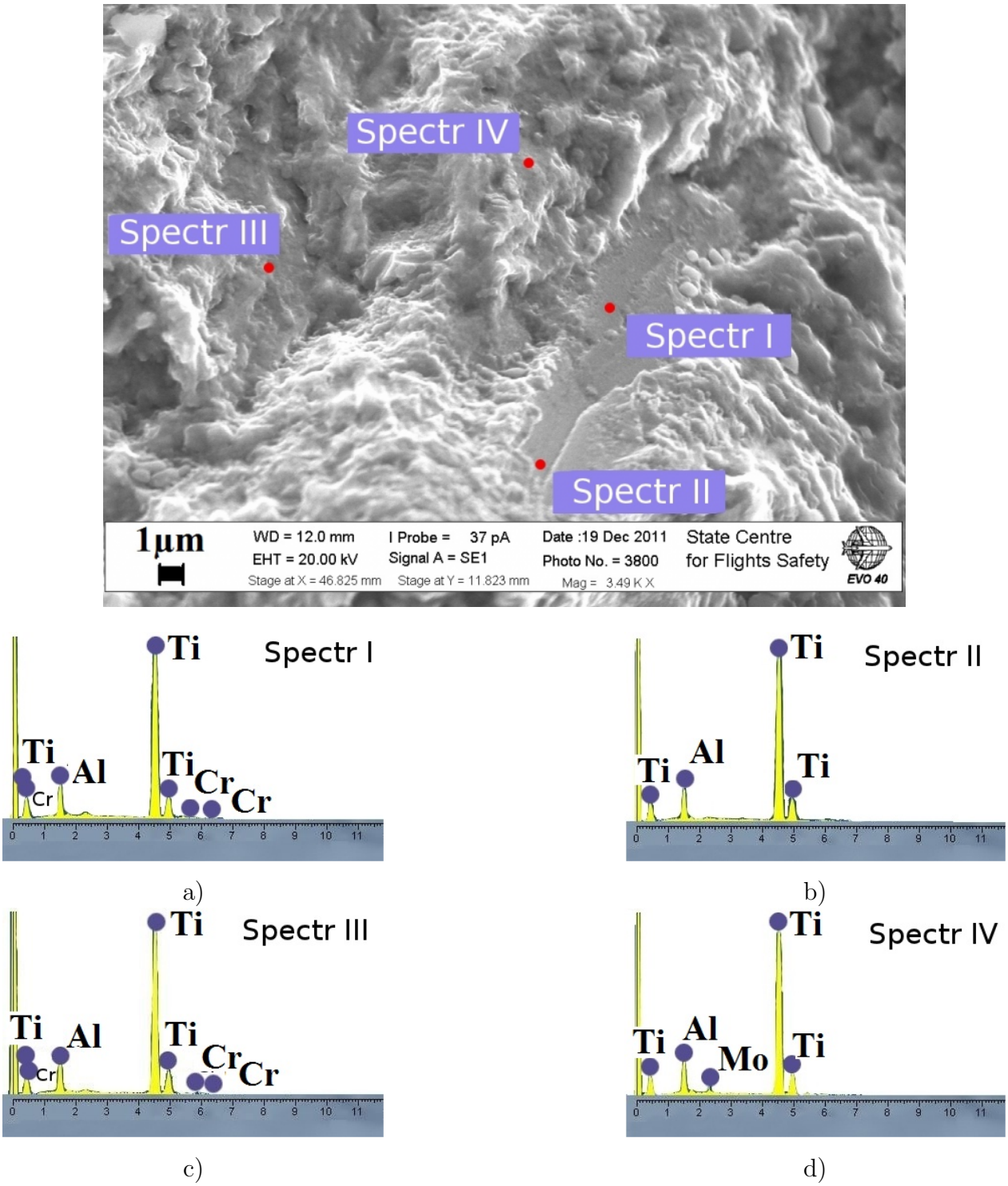

Figure 3.20: EDX analysis on the quasi-smooth facet in the crack initiation site

elements distribution of VT3-1 before fatigue test, a virgin micro-section was investigated by EDX, (Fig. 3.21).

The micro-structure was investigated for the presence of the alpha-platelets with the similar dimensions as the quasi-smooth facet (Fig. 3.20). On Fig. 3.21 one elongated alpha-

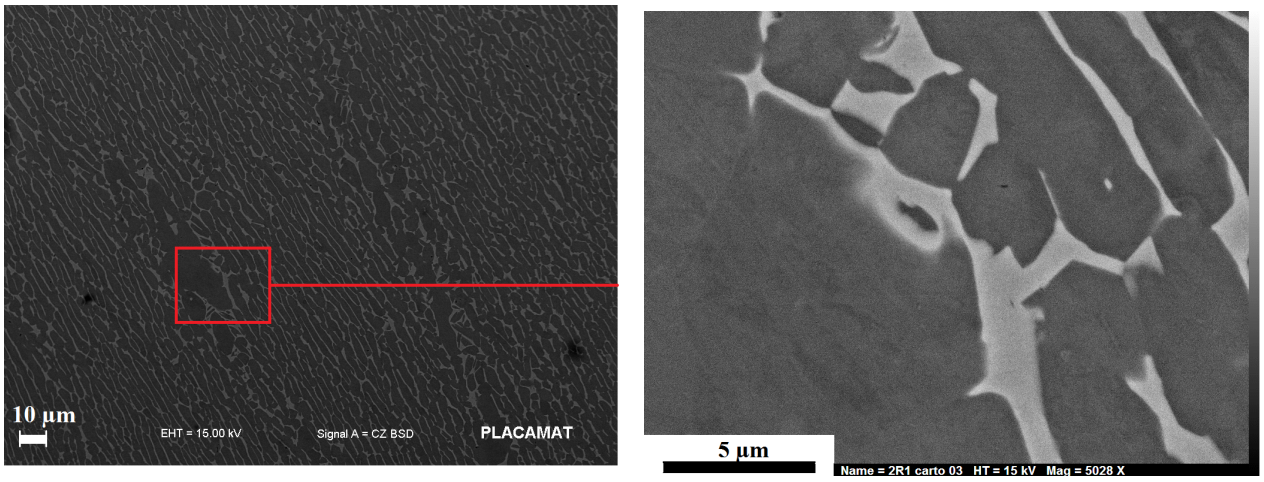

a) b)

Figure 3.21: The microstructure of vergin VT3-1 titanium alloy and area of chemical elements analysis

plate with longer side of about 10 μm is shown. The map of the following chemical elements: titanium, aluminium and molybdenum was built for a selected area. The results of chemical analysis are shown in Fig. 3.22. Comparing the maps of each element the following conclusion can be proposed: the distribution of titanium within the selected area is homogeneous and no significant segregation can be traced. The map of aluminium shows very clear segregation of aluminium in the body of the alpha-platelet, while the concentration of aluminium in the borders (beta-phase) is very low. The map of molybdenum also shows a clear segregation of this element but in contrary to the aluminium the concentration of Mo is higher in the borders between alpha-platelets (i.e. in beta-phase). In order to quantify the concentration of alloying elements in the body of alpha-platelet and in the beta-phase, an additional analysis was carried out in both locations. The result of this analysis shows a significant difference in concentration of alloying elements, especially in the case of molybdenum, Fig 3.23. The quantitative analysis in the body of alpha-plate for aluminium shows, that concentration of aluminium (7.1%) is almost laying in the range of normal chemical composition (5.5 - 7 %), while the concentration of molybdenum is very low (0.59 %). It significantly deviates from the standard (2 - 3 %). The quantitative analysis in the beta-phase shows a very high concentration of beta-stabilizing elements, in particular the content of molybdenum is two - three times higher (6.28 %) than the normal composition (2 - 3 %).

Thus, the problem of segregation of molybdenum is very important in the case of forged VT3-1 titanium alloy. Most of the crack initiation sites, except at the borders of clusters, which were found in VHCF region for VT3-1 titanium alloy are related to the chemical composition of the alloy. In the case of early subsurface fatigue crack initiation, the initiation

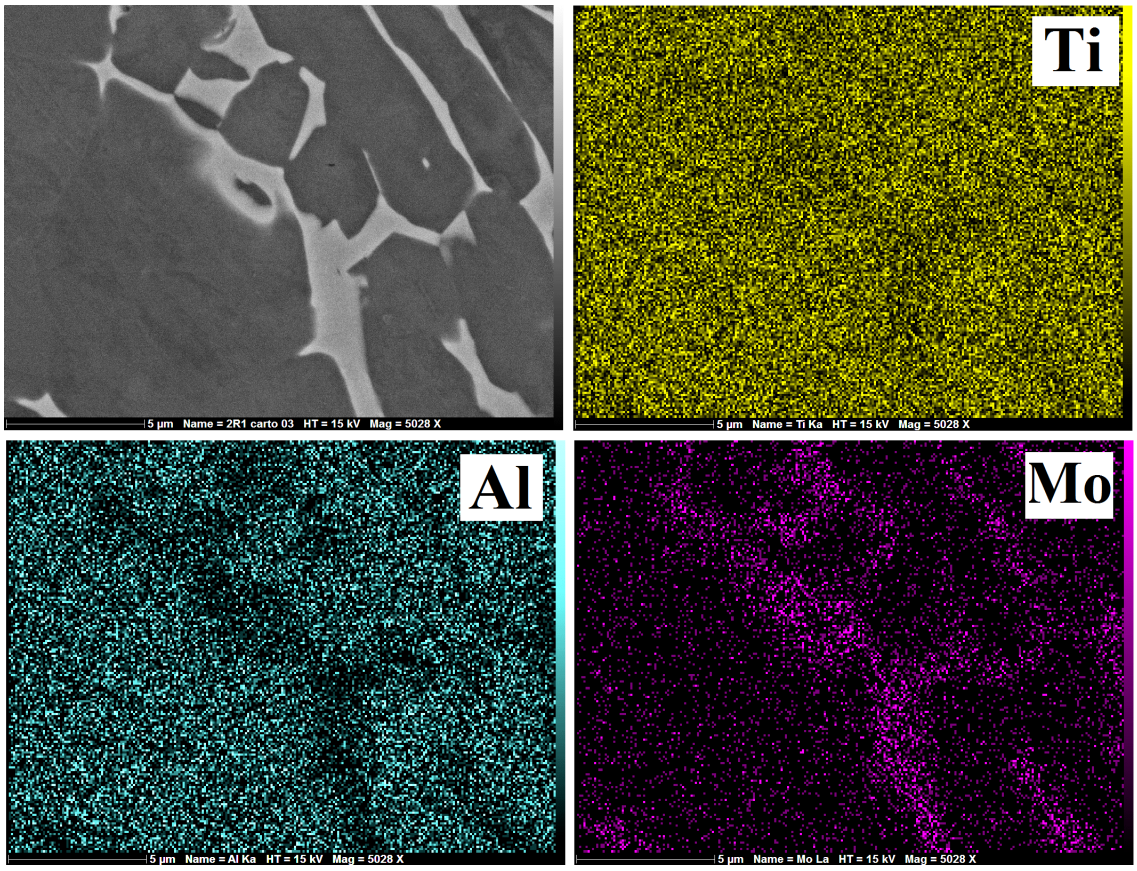

Figure 3.22: The maps of chemical compositions for titanium, aluminium, molybdenium and chromium within selected area of forged VT3-1

is related to micro-structural defects, which forms due to thermo-mechanical treatments and also shows the segregation of chemical elements at another scale level - several hundreds of micrometers. For the longer fatigue life the segregation manifests itself at another scale level: chemical inhomogeneities of tenth of micrometers leads to subsurface crack initiation. In case of absence of such chemical inhomogeneities in the plane of maximal stress the segregation manifests itself at the smaller level, it is the cleavage of alpha-platelets with cross section of about 2 μm. All these crack initiation mechanisms and crack initiation from the border of large clusters are in competition. Sometimes under the same loading condition one type of micro-structural heterogeneities becomes a crack initiation site, sometimes another feature of micro-structure breaks first and fatigue crack nucleates from it. Such feature of subsurface crack initiation may be explained by multi-parametric dependence of each mechanisms. As in case of smooth facets as well for clusters, it seems that several parameters, such as crystallographic orientation of cluster (or facet), the geometry, the parameters of neighbouring clusters (facets) could play an important role in fatigue damage accumulation at

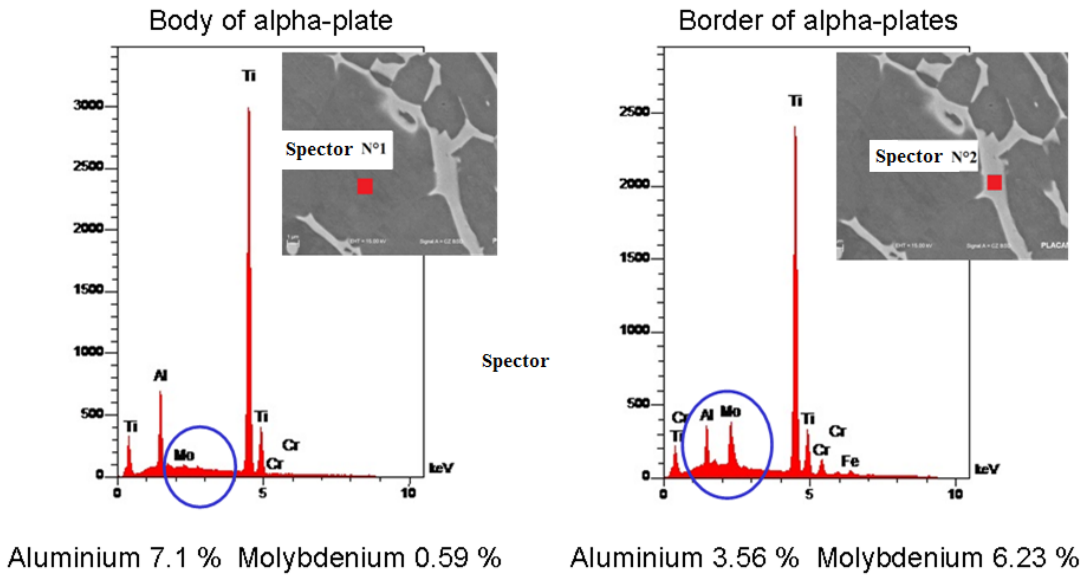

Figure 3.23: The quantitative analysis of chemical element content in the body and intermedial of alpha-plates

such features of micro-structure. In this subsection the presented results can be summarized in terms of crack initiation mechanism on a SN-curve diagram. The result of this analysis is shown in Fig. 3.24.

The interpretation of fatigue data in such form show, that with decreasing the stress amplitude, the mechanism of crack initiation is changing from surface to subsurface cracking. The same tendency has been shown many times for different materials and it allows the interpretation in terms of bi-modal distribution of fatigue life [71, 2]. According to such interpretation the competition between surface and subsurface crack origination appears in the region of transition from HCF to the VHCF. The same behaviour can be observed for forged VT3-1. In the case of VT3-1 the transition range in terms of fatigue life is between 10^6 and 10^7 cycles. Beyond 10^7 cycles the VHCF regime is mainly characterized by internal crack initiation and, in the case of two-phase titanium alloy, by a significant scatter in fatigue life. This scatter is related to the feature of micro-structure which provoke the crack initiation. The initiation from the different micro-structural defects were classified and grouped in so-call 'crack initiation mechanisms'. The analysis of fracture surfaces for all the specimens failed after 10^7 cycles has shown that there is a competition between different subsurface crack initiation mechanisms. These mechanisms mostly depends on the number of cycles than on stress amplitude i.e. under the same stress amplitude two different mechanisms may occur after different fatigue life. This is due to the probabilistic nature of the critical defects distribution in the material, like inclusions in steels. Thus, the fatigue life of forged

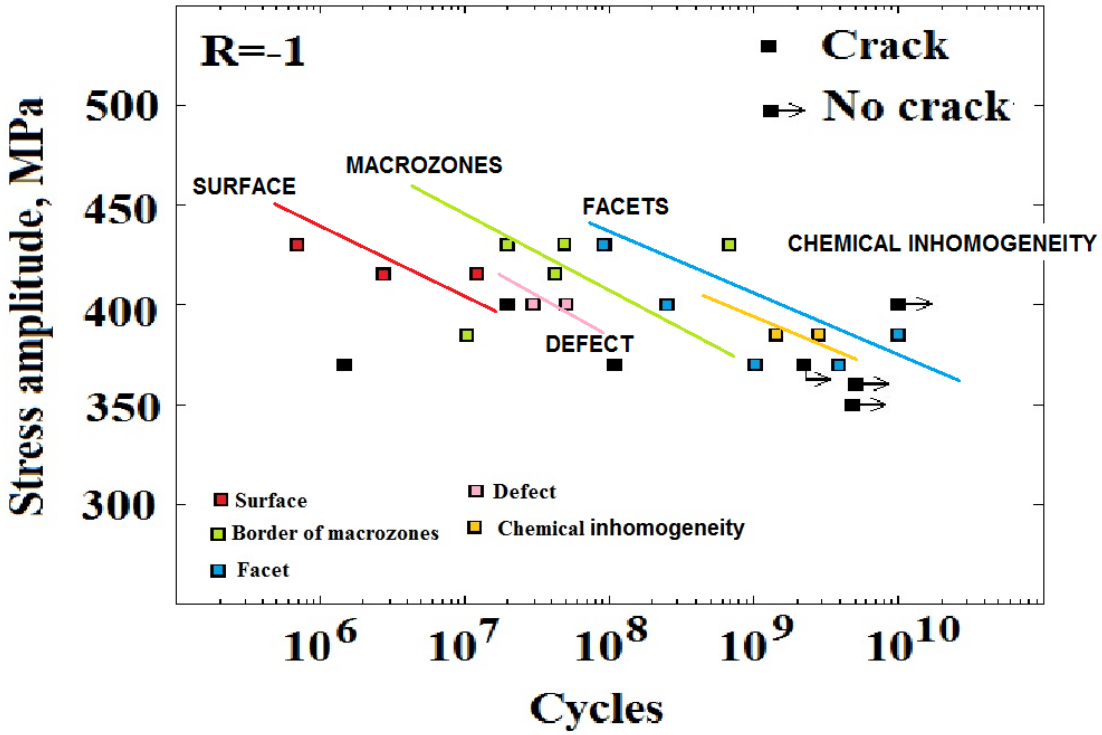

Figure 3.24: The results of tension fatigue tests (R=-1) on the forged VT3-1 titanium alloy from the rim part of the disk with indication of crack initiation mechanism

VT3-1 titanium alloy in VHCF region can be characterized by a multi-modal distribution with several curves corresponding to the different crack initiation mechanisms. The whole zone of competition between mechanisms is often called as 'bifurcation area' in the works of A. Shanyavskiy [2, 76]. This term outlines the character of material behaviour in the region of transition. Before the test we don't know which critical defect is located in the plane of maximal stress amplitudes and, therefore, the fatigue crack may initiate as from a strong defect, as well from a cleavage facet that can lead to a significant difference in fatigue life.

3.2 Results of fatigue tests on forged VT3-1 titanium alloy under tension (R=0.1)

• As it was noted in Chapter I, the high frequency vibrations loading is a very important problem for the turbo-jet engine blades and for the rim part of the disk too. Under such in-service conditions, these components experiences both the dynamic load and the quasi-static load due to the centrifugal force. Vibrations with superposed mean stress seems to

be an important problem because, usually, in-service fatigue failures occurs in the blades of the turbo-jet engines [1]. Thus, the problem of studying the fatigue behaviour of aeronautic materials in VHCF under positive stress ratios is arising. Since the crack initiation process in gigacycle fatigue consumes more than 90-99 % of the total fatigue life, the investigation should be focused on the crack nucleation process, like in the previous section, and on the identification of the typical crack initiation sites and mechanisms in forged VT3-1 under gigacycle fatigue loading with positive loading ratio.

The ultrasonic fatigue tests on forged VT3-1 titanium alloy has been performed by using the machine for tension-tension tests, Chapter II. The specimens for present study were machined from the plateau part of the disk in radial and circumferential direction (3RXX and 4CXX series). The static load during the ultrasonic fatigue tests is will be applied in the same direction (along the specimen's axis) than static force induced due to the in-service loading conditions (radial σ_{rr} and circumferential $\sigma_{\theta\theta}$). The first noticeable result of fatigue tests, is that there is no significant difference in fatigue strength between radial and circumferential specimens under the ultrasonic tests at positive stress ratio. The results of fatigue tests on radial and circumferential specimens are presented in Fig.3.25.

The results of the ultrasonic fatigue tests show a very small difference in fatigue strength for 'radial' (axis of specimen along the radius) and 'circumferential' (axis of specimen perpendicular to the radius) specimens, which may be related to the scatter of micro-structure features of the material behaviour. The noticeable features of obtained results is that circumferential specimens shows the fatigue failure in a wide range of fatigue life, while the results for radial specimens are grouped in the range of 10^7 - 10^8 cycles. An objective of tensile pull-pull fatigue tests is an investigation of possible crack initiation mechanisms under positive loading ratios. To realize this goal, all the broken specimens were observed by using SEM. The investigation on fracture surfaces are separated into two parts: fatigue life of 10^7 - 10^8 cycles and beyond 10^8 cycles.

3.2.1 Fatigue life in the range of 10^7 - 10^8 cycles

- The majority of the broken specimens shows that fatigue life is laying in this range 10^7 - 10^8 cycles. The fracture surfaces of radial and circumferential tension-tension specimens show a higher perturbed morphology (Fig. 3.26).

The perturbation of fracture surface is related to several factors. The first one is the feature of crack initiation. As shown for forged VT3-1 and some steels, the short crack growth can be realized in different planes. In this case for steel [133] the initiation at different levels lead to form so-called 'butterfly wings' however the crack growth within individual crack plane is not perturbed. For the forged titanium alloy the further crack growth is very

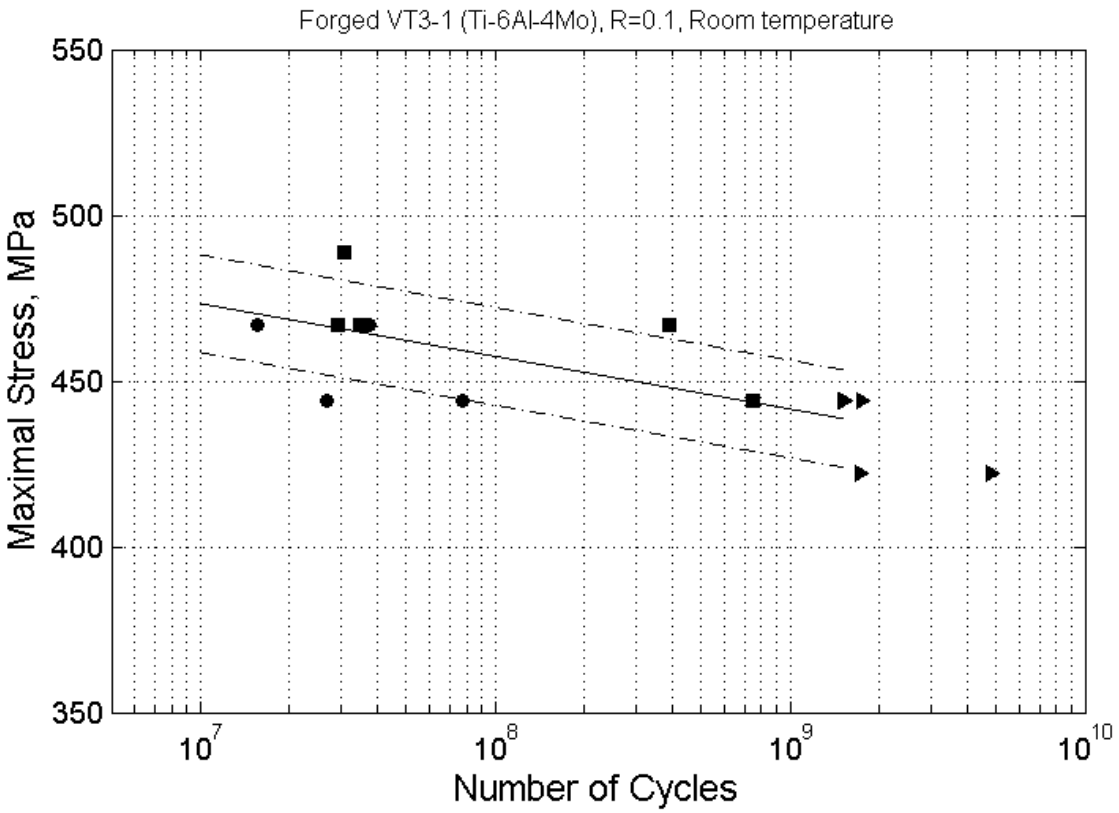

Figure 3.25: The results of ultrasonic fatigue tests at R=0.1 on specimens cut in radial and circumferential directions

sensitive to the micro-structure of the material. The analysis of fracture surfaces for radial and circumferential specimens allows us to assume, that intensive fibering processes were acting during the thermo-mechanical fabrication process of the disk. Figure 3.27 shows the 'macro-layers' on the fracture surface, which are not related to 'meso-tunnels' crack.

Sometimes the crack propagates along these macro-layers, sometimes across. In the first case, the relief of the fracture surface is more perturbed compared to the crack propagation perpendicular to the macro-layers. Moreover, the micro-structure of the forged VT3-1 titanium alloy is represented by the large clusters with similarly orientated alpha-platelets. It seems that crack growth within such formation or within its border, is more preferred. Thus, when the fatigue crack reaches the favourably orientated α-platelets cluster it turns to propagates almost in a flat plane, Fig. 3.28. The typical size of such clusters may reach several hundreds of micrometers. The intensive cluster fracture appears preferably under the fatigue tests with superimposed static load. In case of tensile fully reversed loading, clusters of α-platelets are mainly manifest themselves by cracking along the their boundaries. The

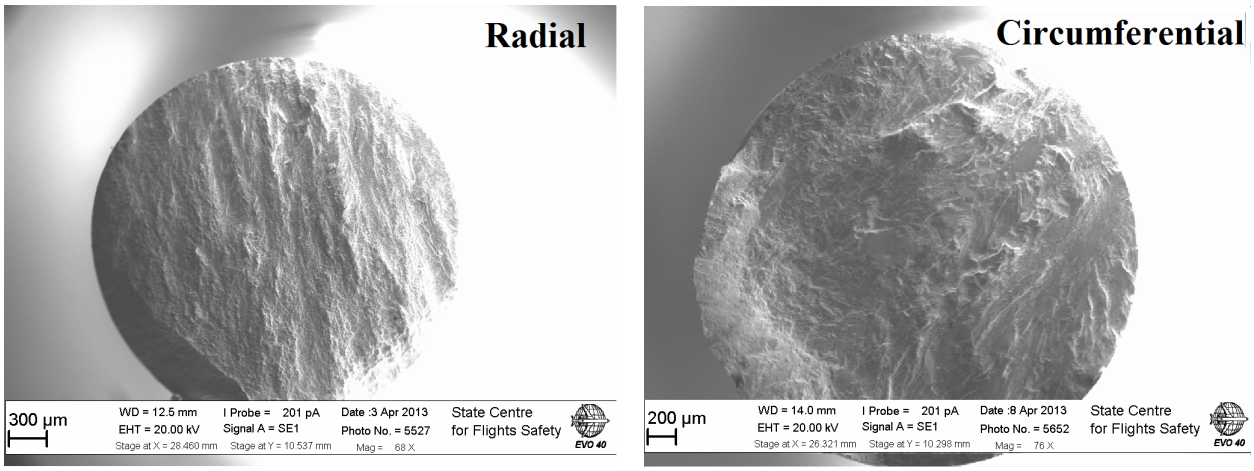

Stress (Max) = 470 MPa
Fatigue life = 3.5×10^7 cycles

a)

Stress (Max) = 470 MPa
Fatigue life = 3.8×10^7 cycles

b)

Figure 3.26: The typical fracture surfaces of radial and circumferential specimens after $\sim 10^7$ cycles at R=0.1

crack propagation under positive loading ratios within such macro-zones was observed as in direction perpendicular to the alpha-platelets elongation, Fig. 3.28 a, as well along alpha-plates, Fig.3.28 b. Perhaps, it is just a particular case, but when the crack propagates across the alpha-platelets elongation direction, the fracture surface is less perturbed. In contrary, if the crack propagates along the alpha-platelets elongation direction, some marks of crack growth can be clearly seen on the fracture surface within the cluster.

The difference in cracking morphology within the clusters is related to the different types of crack propagation. The analysis of the fracture surface within the cluster in the regime of backscattering electrons show, that the crack probably moves very close to the boundary of two macro-zones or by their border. The small micro-structural elements (like islands), which stay at the fracture surface show different from the macro-zone orientation of α-platelets, figure Fig. 3.29. In some cases the fracture surface within cracked 'macro-zone' exhibits a relativity large (about 20 μm) rest of micro-structural elements with similarly orientated alpha-platelets, Fig.3.29 and 3.30. In other cases, the cluster fracture surface has several structural elements, which are differently orientated as by the alpha-plate direction of substrate cluster, as well one by another. The question of the cluster's boundary geometry should be studied additionally, but it looks like sometimes the crack can moves through the cluster border, or very close to it, by forming almost flat fracture surfaces. Some SEM observations on the fracture surface of specimens failed under tension-tension conditions can give indirect information about the boundary of the cluster, Fig. 3.31. This figure shows

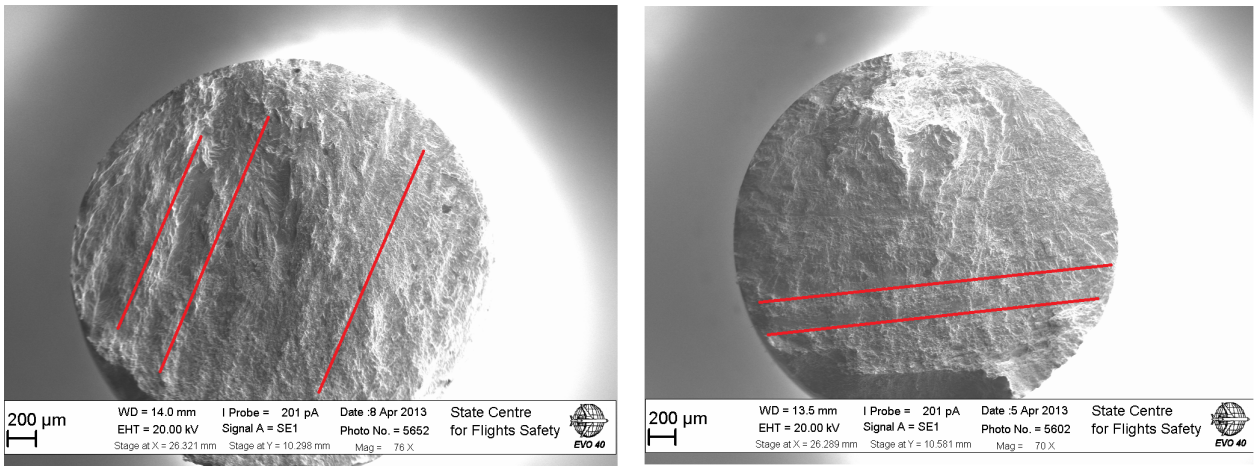

a) b)

Figure 3.27: Cracking within clusters of forged VT3-1

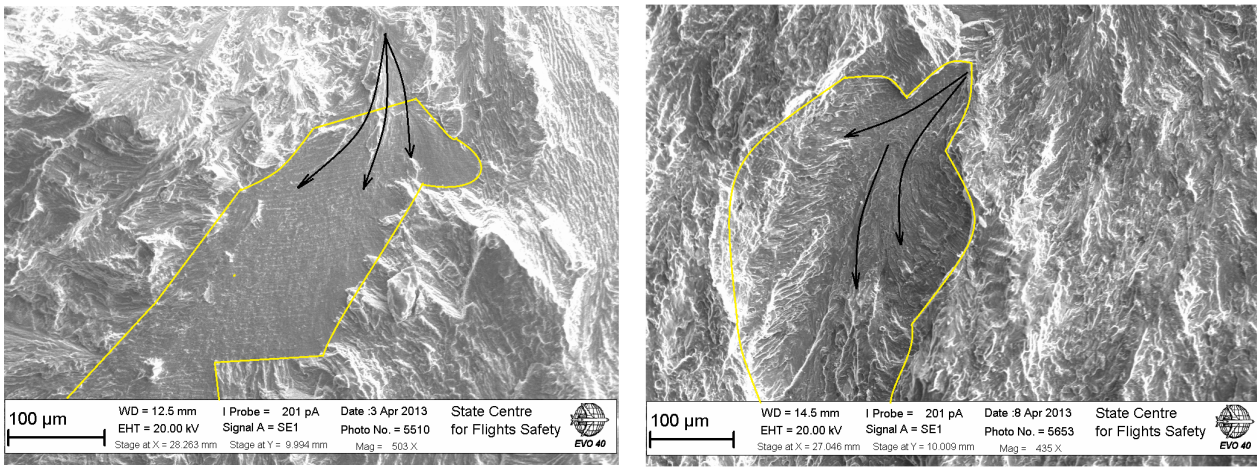

a) b)

Figure 3.28: Crack propagation within the large cluster in forged VT3-1 under R=0

the border of two structural elements with two different orientations of alpha-plates within the element. The angle between two orientations of plates within structural elements is around 90°. The distance of transition from one structural element to another is less than 10 μm with a sharp structural element border. It is interesting to note, that with changing in crack orientation, some elements of neighbouring structural element is present on the fracture surface. Therefore, not all the boundaries of structural elements are preference crack propagation planes. The conditions when the crack propagation is more preferential within the close to the boundary layers are not studied up to now. Therefore, the elements with different orientation of alpha-plates can be assumed as the rest of neighbouring structures like another cluster or series of regular colonies of differently orientated alpha-plates.

The question why the small structures were still attached to the cluster and why not

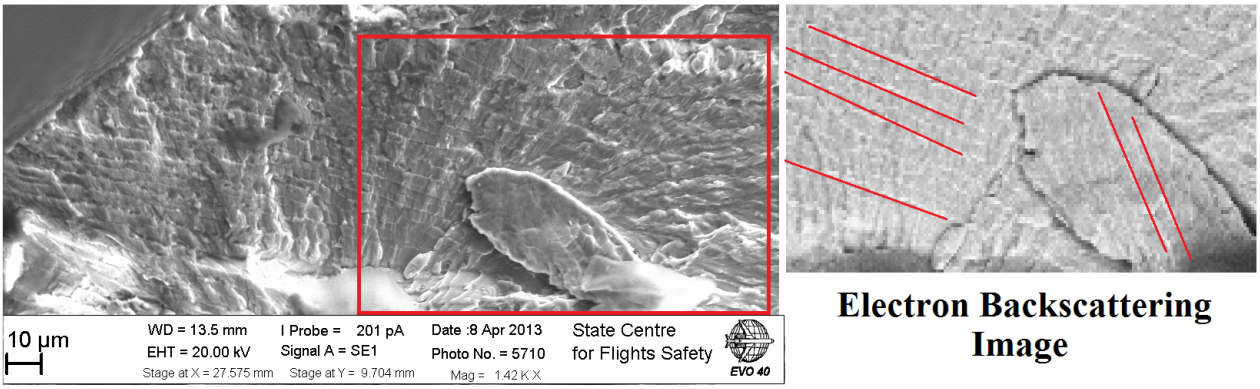

Figure 3.29: The analysis of fracture surface within a cluster by SEM in backscattering electron regime

cracked by the interface of connection is still open. In some particular cases, Fig. 3.29, it can be explained by possible split-cracking, when the crack initiated from the boundary of clusters growing in two parallel planes at the beginning and turns to one plane propagation. In other cases, Fig. 3.30, the formation of 'islands' of differently orientated alpha-platelets is still not well investigated.

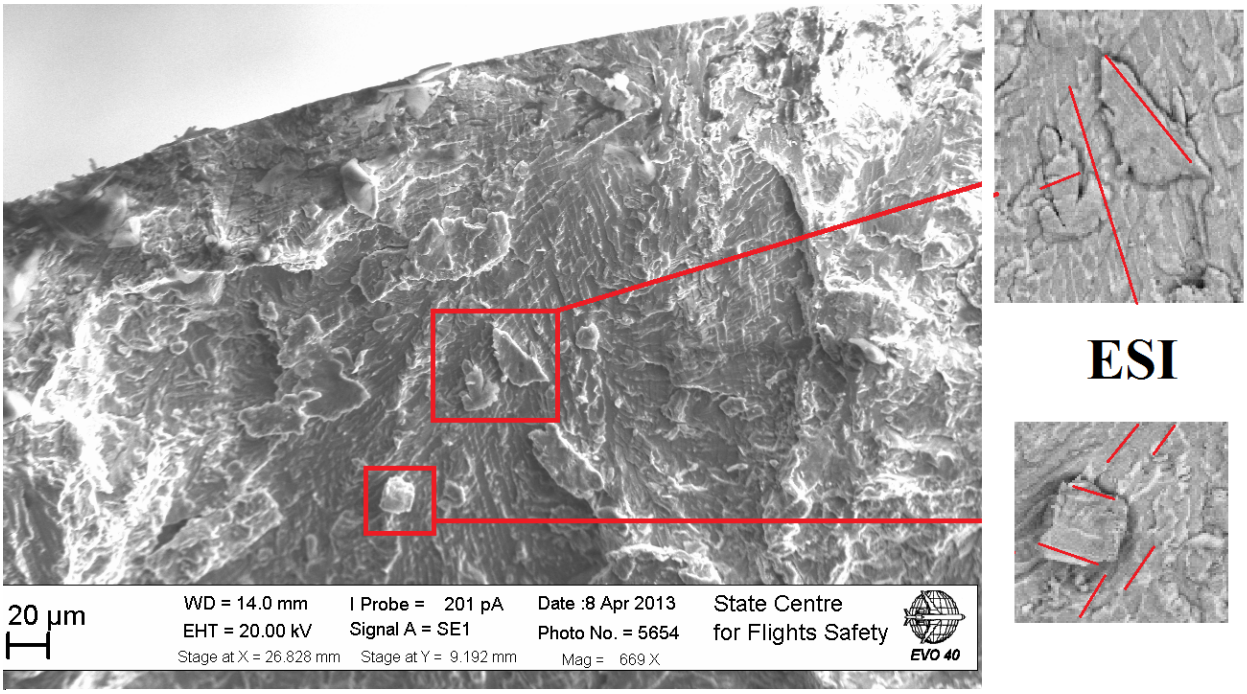

Figure 3.30: The trackes of small colony at the fracture surface of the cluster

It should be outlined, that not all the cluster fracture surfaces have some traces of the neighbouring micro-structural elements. Most of them are clearly failed by inter-granular crack, Fig. 3.31.

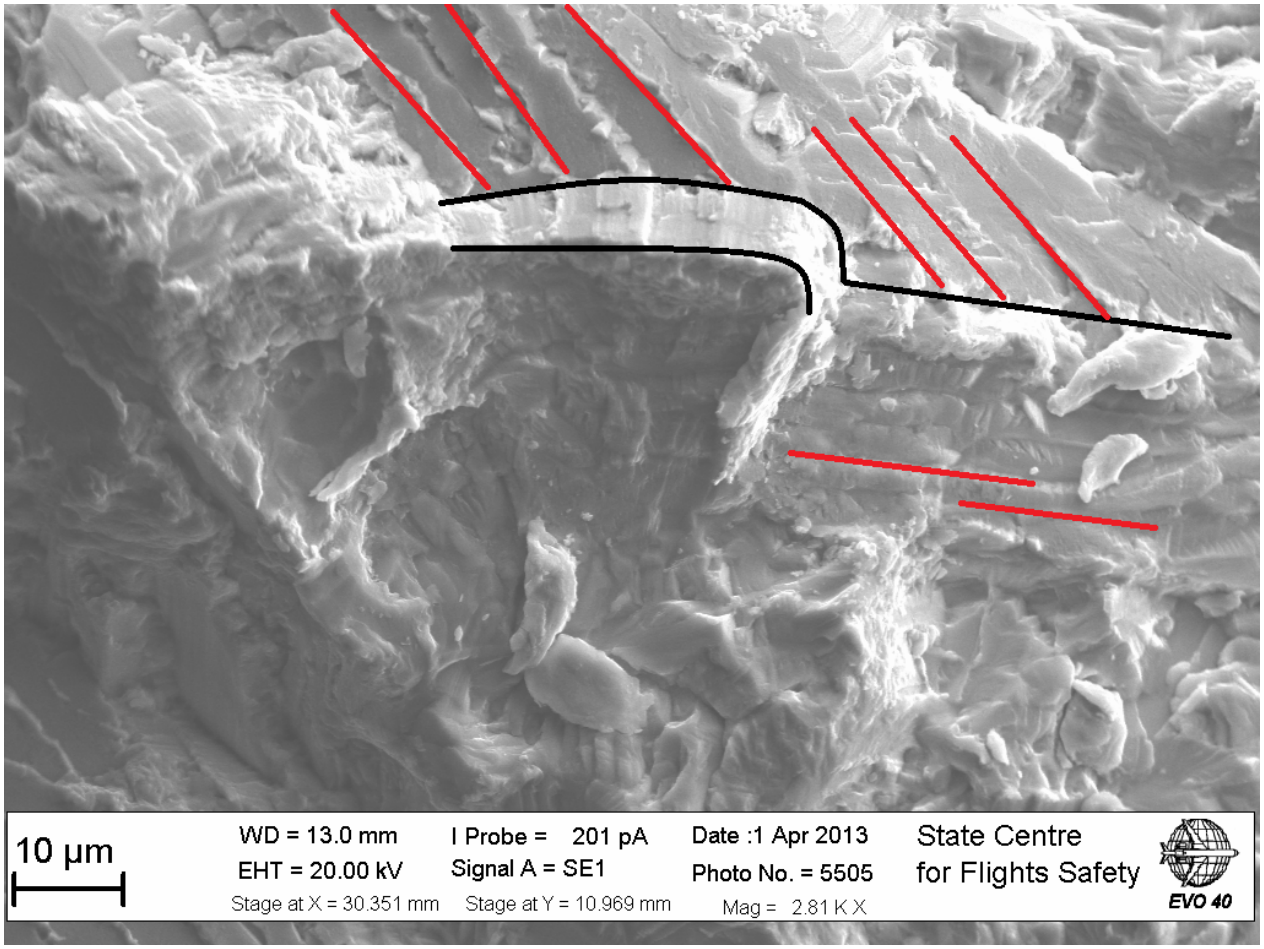

Figure 3.31: The border of the cracked cluster under tension-tension loading

The border of the cracked cluster is clearly visible in Fig. 3.31. The cluster shows several cracks perpendicular to the picture plane, starting from the cluster boundary. These cracks form a very perturbed fracture surface even within the similarly orientated alpha-platelets area. Thus, under the ultrasonic fatigue tests with superimposed static tensile stress, the borders of 'macro-zones' have a significant influence on the crack path and therefore fatigue failure morphology in forged VT3-1 titanium alloy. Some clusters show a quasi-brittle fracture surface under such loading conditions. These zones of quasi-brittle fracture are surrounded by ductile failure mode. The nature of such fracture forming needs an additional investigation and probably related to the crystallographic orientation of alpha-platelets in the cluster with regard to the loading axis.

Crack initiation under tension R=0.1 loading

- The crack initiation under tension-tension ultrasonic fatigue tests is also related to the borders of macro-zones. The fracture surfaces for almost all the specimens tested under tension-tension conditions shows a clear crack initiation from the borders of macro-zones, (Fig. 3.32). The fracture surface shows some traces of interaction between two fracture patterns or friction with typical morphology. Several cracks propagate from this boundary. The same growth feature of the fatigue crack was found in the neighbouring to crack initiation clusters, Fig. 3.33. The picture taken in back scattering electron mode give more clear position of crack initiation sites from the border of macro-zone.

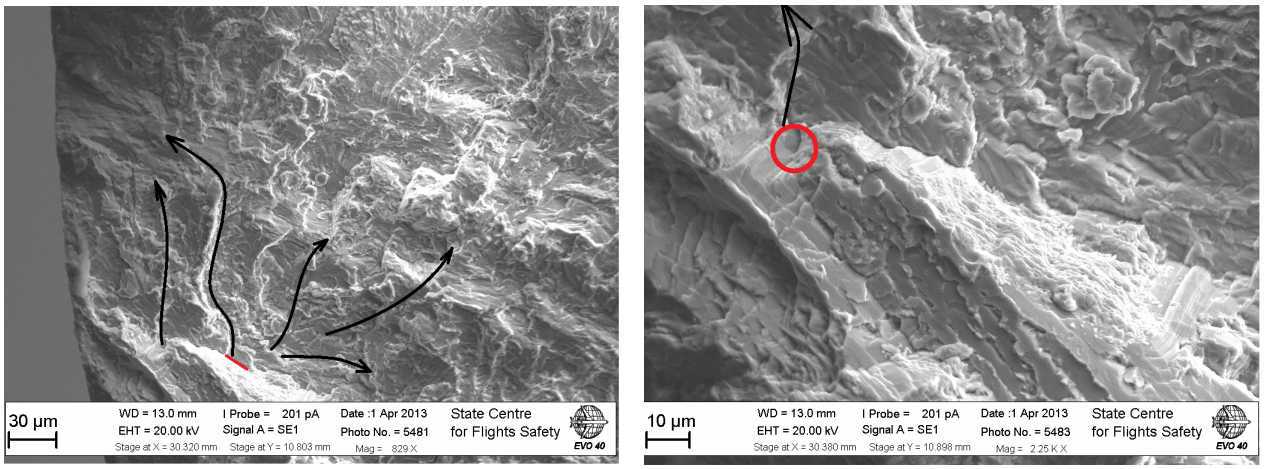

a) b)

Figure 3.32: Crack initiation from the bondary of clusters under tension-tension loading

The cracks presented on Fig. 3.33 are not all laying in the plane of the main crack. Many secondary cracks forms in the plane perpendicular to the fracture surface and propagates across the alpha-platelets. Such crack growth is probably related to split-level cracking, which is usual for the investigated forged VT3-1 titanium alloy. The analysis of fracture surface shows, that fatigue cracks in plane of the main crack, starts to propagate within the cluster from different positions.

Sometimes, the crack initiation even under tension-compression is related to a smooth facet, but the reason of such crack nucleation is also mostly related to the boundary of differently orientated alpha-platelets, Fig. 3.34. The origination of crack is located at the border of two clusters with mutually-perpendicular orientation. The smooth facet which is found in the crack initiation area is not probably a critical element of micro-structure from which crack is initiated. It means that in case of another location, without border of clusters, it will never be a crack initiation site itself.

The analysis of crack initiation sites in the forged VT3-1 titanium alloy under positive

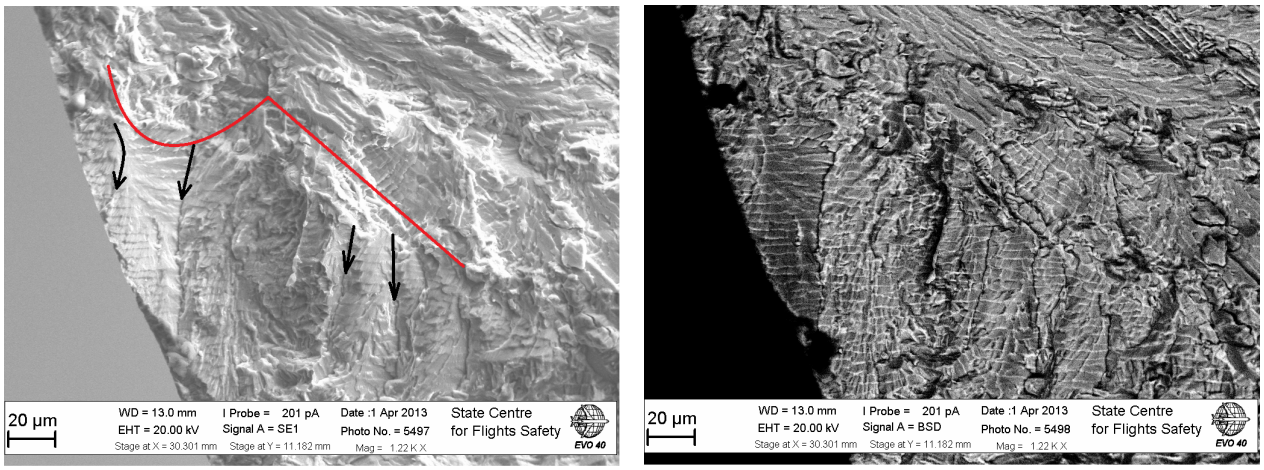

a) b)

Figure 3.33: Several crack propagating from the border of cluster

load ratio shows, that an effect of cluster boundaries is more significant in case of loading with tensile static load compared to the fully reversed loading. The crack often nucleates from the border of micro-structural elements with the different orientation of alpha-plates, that lead to form some smooth facets which are located close to the border of the cluster. The boundary between clusters are cracking first and initiates the growth of several crack from this border. These cracks growth at different levels, by forming split-level cracks and complex morphology. Moreover, sometimes during the crack propagation stage some unfavourably orientated clusters may lay in the planes of moving crack. In this case, the crack turns to propagate in almost flat plane showing a quasi brittle fracture surface. Probably these quasi brittle flat fracture surfaces are formed by inter-granular crack, propagated in the border of large cluster. Sometimes the large cluster surrounded by regular colonies of alpha-platelets, that can be assumed based on the fracture surface analysis in backscattering electron regime. Several 'islands' with different orientation of alpha-plates in it, were found at the quasi-brittle fracture surface of a cluster. The crack propagation stage is also very sensitive to the cluster borders. When the crack reaches the boundary it cracks and several secondary cracks start from this broken boundary. These cracks may lay as in the plane of the main crack (maximal normal stress), as well perpendicular to this plane. The perpendicular crack initiates due to the connection of split-level cracks, starting from the border of clusters. The total fatigue life for the majority of specimens is ranged from 10^7 to 10^8 cycles. Crack initiation under fully reversed axial loading (R=-1) is also related to the fracture from the boundaries of clusters, but it was less expressive. Therefore, the static tensile load, superimposed on high frequency vibrations may activate the role of cluster boundaries in crack initiation and propagation process in forged VT3-1 titanium alloy. In order to finally clarify this assumption, the fully reversed fatigue tests R=-1 were carried out on the specimens machined from the plateau

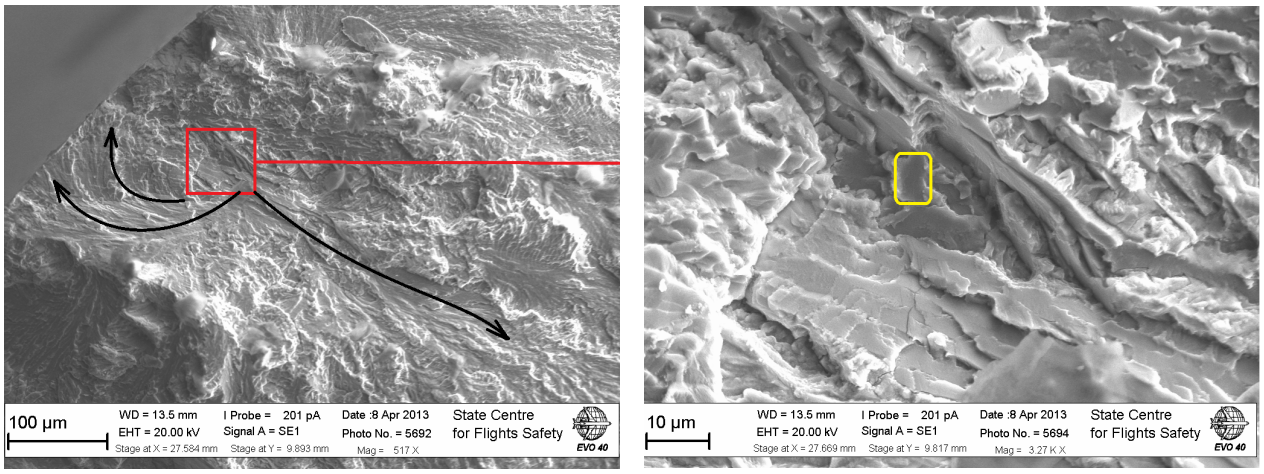

a) b)

Figure 3.34: The crack initiation from the smooth facet located between clusters of alpha-plates

part of the disk in the same direction than the tension-tension specimens.

3.3 Results of fatigue tests on forged VT3-1 from the plateau part under tension (R=-1)

• Additional fatigue tests under fully reversed tension loading were carried out on specimens machined from the plateau part of the disk in the radial direction. This series 2RXX was investigated in a similar way with tension-compression tests on 0AXX and 1AXX series, (also machined from the rim part of the disk). The significant difference in crack initiation mechanisms between tension-compression (R=-1) and tension-tension (R=0.1) tests lead us to carry out additional tests under tension-compression conditions. The 1AXX specimens were also loaded under R=-1 regime. Both series were air cooled during the fatigue tests in order to perform the tests at room temperature.

The tests were carried out up to the failure or reaching outrun lifetime, limited by around 10^9 cycles. The results of investigation on both series 1AXX and 2RXX shows that there is no significant difference in fatigue endurance as for specimens machined in radial direction, as well in axial. Therefore, from mechanical point of view there is no significant effect of anisotropy in fatigue properties between rim and plateau parts of the disk. The results of the fatigue tests on 1AXX and 2RXX series are shown in Fig. 3.35. The results show the permanent small slope of the SN-curve and fatigue failures even beyond 10^9 cycles. The difference in fatigue strength at 10^6 and 10^9 cycles is about 30 MPa ($\simeq 10\%$). The scatter in fatigue life is also large for these series of specimens, that is similar to the first tests on

0AXX specimens. The limitation of experimental points does not allows to build the SN curve for the radial and axial specimens separately. That is why just a tendency in fatigue behaviour for each series may be traced. It seems that scatter in fatigue life is slightly higher for specimens from the rim part. In case of axial specimens the scatter of fatigue life reaches 3 order of magnitude, while in case of radial specimens it is around 2 orders of magnitude. Moreover, one premature failure was found at the relatively low stress amplitude on an axial specimen. The majority of results are grouped around the same trend line and some specimens were failed after almost the same fatigue life.

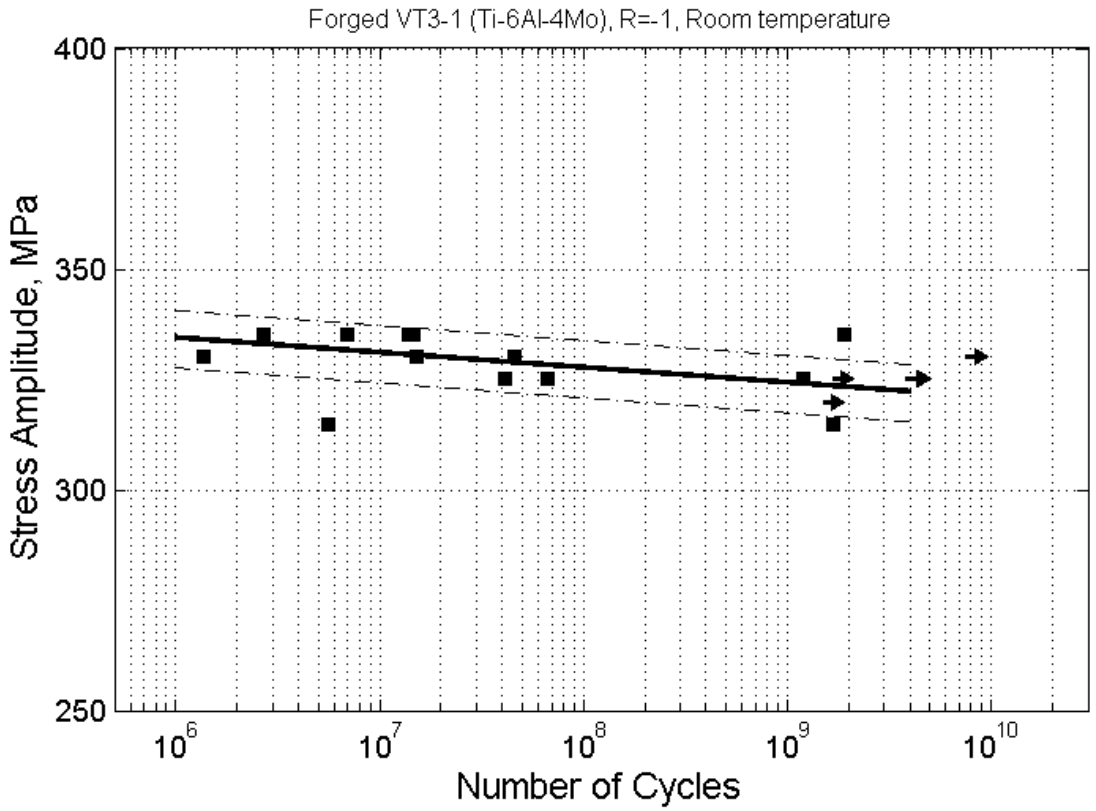

Figure 3.35: The results of fatigue tests on 1AXX and 2RXX series of forged specimens

In order to answer to the following question: 'is cracking due to the cluster borders related to the loading mode or material properties in the plateau part of the disk?', SEM observations were carried out on the fracture surfaces of all the specimens. The first noticeable features of all the fracture surfaces obtained under fully reversed tension is that no quasi-brittle fracture was observed on specimens cracked under (R=-1) conditions. The crack initiation sites were close to the specimen surface or for some of them at the surface. A typical fracture surfaces for radial and axial specimens are shown on Fig. 3.36. The crack morphology within the

whole cross section is almost the same for radial and axial specimens. In both cases the stress amplitude is about the same and the fatigue life is short, less than 5×10^6 cycles. Under such loading conditions, the fatigue crack initiated from the surface, that is in good agreement with previous results on the 0AXX series. The fracture surface is quite perturbed in case of (R=-1) ultrasonic tests and it is related to the cluster structure of forged VT3-1 titanium alloy, but an influence of it is less expressed and can be found at the crack propagated stage, Fig. 3.37.

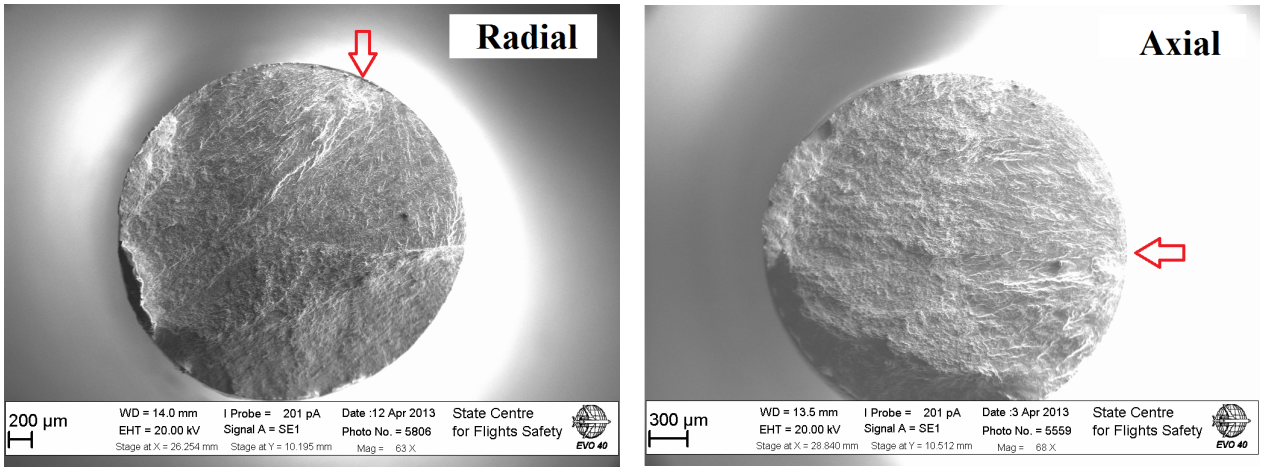

a) b)

Figure 3.36: The fracture surface of specimens machined in (a) radial and (b) axial directions

The crack nucleates from the specimen surface and propagates into the bulk of the material. Not far from the crack initiation site the zone with very clear interaction of crack lips can be found, marked by a rectangle (Fig.3.37 a). Such type of interaction leads to the destruction of the fracture surface (by friction) that is typical for tension compression regime.

Near the crack initiation area, the weakly expressed boundary of macro-zones can be found. The role of such micro-structural element is not dominant in case of tension-compression tests but it still influenced on the crack propagation process. In case of tension-compression the border of macro-zone does not produce any secondary crack, especially in perpendicular to the main crack plane. The fracture surface shows a more ductile character of failure without large quasi-brittle zones.

With decreasing the stress amplitude the crack initiation sites moves from the surface to the subsurface position, Fig. 3.38. As it was discussed above, the crack initiation in this case is related to some sorts of micro-structural imperfections, like boundaries of clusters and strong technological defects. In the case of tests on 1AXX and 2RXX series tested under tension (R=-1), this was confirmed. The example of crack initiation presented in Fig. 3.38 for forged VT3-1 titanium alloy after $N_f = 4.62 \times 10^7$ cycles shows a heterogeneity of micro-structure, where the typical pattern for investigated VT3-1 alloy structure can not

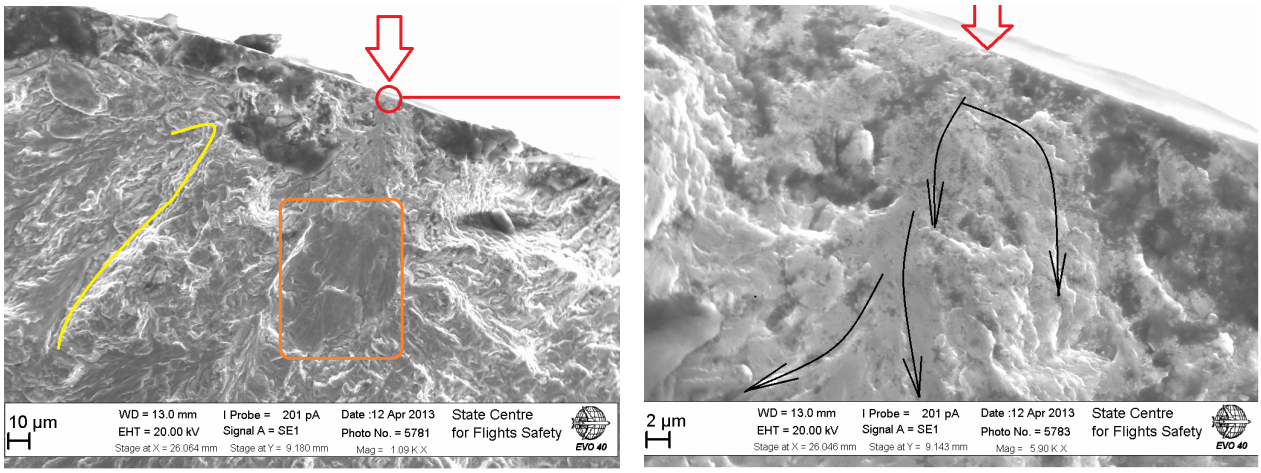

a) b)

Figure 3.37: Typical surface crack initiation after $\sim 10^6$ cycles with weakly expressed boundary of micro-structural element

be recognized. On Fig. 3.38 the type of crack initiation looks like an initiation in some steels, when the fine granular area is formed in the crack initiation site. The question about the nature of such fine granular area in titanium alloy is still open because of limitation in fatigue data. The first possible answer is that such structure forms due to the fully-reversed loading conditions which brakes the alpha-platelets up to an amorphous structure. The second possible reason is the initial state of material micro-structure which was not well crystallized.

The observation of specimens fracture surfaces from the 0AXX series can help to answer to this question. The similar no-recognized structure was found in the specimen loaded with a stress amplitude 385 MPa and which got failure after $\sim 10^9$ cycles, Fig.3.39. This figure shows the area located about 80 - 100 μm from the crack initiation site (initiation from chemical inhomogeneity). The cracked structural element on Fig.3.39 shows non-recrystallised structure between the system of layers. It seems that such micro-structure mostly results of the technological process, that loading process, because the neighbouring bulk of material shows a well crystallized structure. Probably, the final fracture is the result of both factors: the features of forming the alpha-platelets and the fully reversed loading. Thus, the crack initiation presented in Fig. 3.38 was not formed in the material during cyclic loading. Thus, the internal crack initiation after about 10^7 cycles as for axial, as well for radial specimens shows the similar tendency: it is the transition from HCF to the VHCF region the first internal crack nucleates from some sort of strong micro-structural defects. With further increasing the fatigue life, the crack initiations are still located in the bulk of material and in case of fatigue life around 10^9 cycles the initiation is related to the large cluster's boundaries and sorts of facets cleavages, which were discussed above for axial specimens (0AXX series).

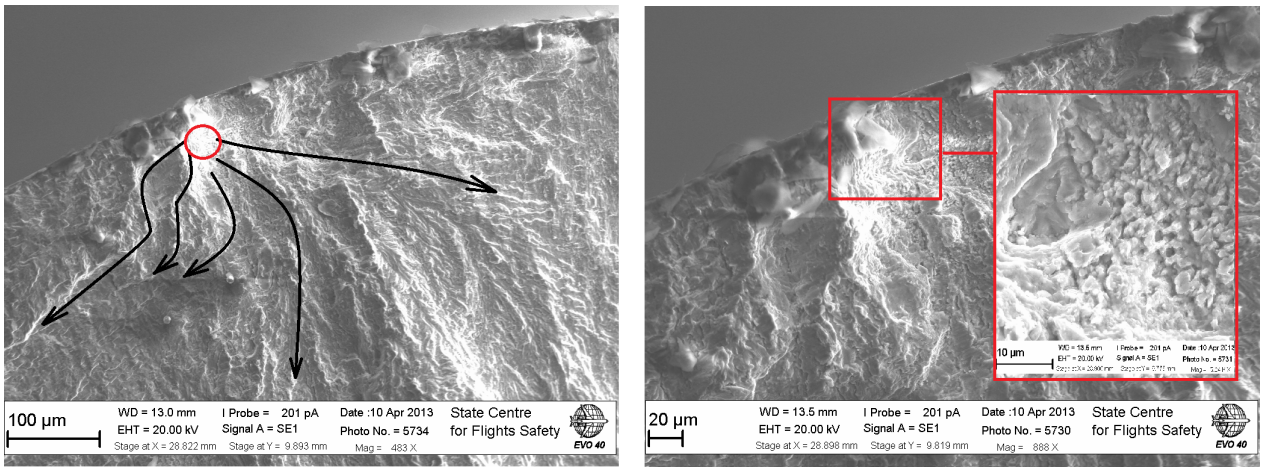

a) b)

Figure 3.38: The subsurface crack initiation after $\sim 10^7$ cycles

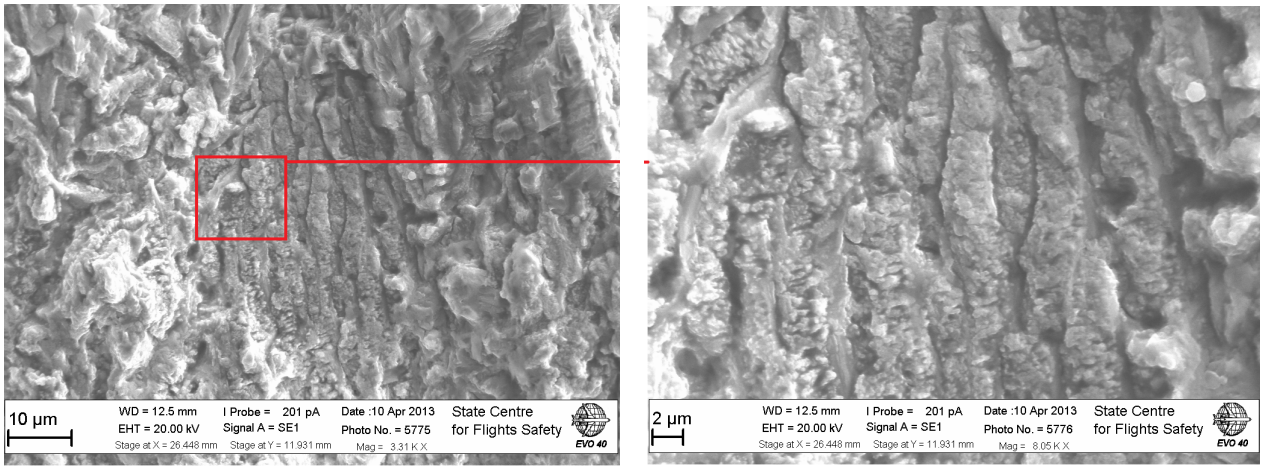

a) b)

Figure 3.39: Irregular structure in forged VT3-1 titanium alloy

Summarizing the results of fatigue tests on the forged VT3-1 titanium alloy machined in the compressor disk for turbo-jet engine it can be outlined, that under fully reversed tensile conditions, a large scatter in fatigue life was observed. The analysis of fracture surfaces by different methods shows, that such difference may be correlated with the different crack initiation sites. Under the 'high' stress amplitudes and relatively short fatigue life the initiation occurred at the specimen's surface. The same tendency was found in the all investigated series of specimens. A competition between surface and subsurface crack initiation was found near the classic 'fatigue limit' or fatigue strength at 10^7 cycles for forged VT3-1 titanium alloy. It was found, that transition from surface to the subsurface crack initiation is located in the range of 10^6 - 10^7 cycles. Moreover, the same sort of competition between crack initiation mechanisms was found for subsurface crack. As it was shown, the internal crack

initiation in forged VT3-1 titanium alloy is related to the imperfections of micro-structure, which are represented by strong technological defects due to features of thermo-mechanical process (forging), boundaries of large micro-structural elements which are the areas with almost similarly orientated alpha-platelets. The EBSD analysis on virgin titanium alloy shown that typical micro-structure of forged VT3-1 titanium alloy is represented by clusters of grains with the same orientation which an often called 'macro zone' [100]. The crack also initiates from the local zones with variation in chemical composition, that are formed due to segregation of chemical elements during forging. And finally cracking by forming smooth facets, which was noted by many authors. The explanation of such formation is associated to the cleavage of alpha-platelets by the one of more preferential sliding planes. As usual the smooth facets forms within the basal plane of alpha-lattice (h.c.p.), Chapter 1

Moreover, the fatigue behaviour of forged VT3-1 titanium alloy was investigated under positive mean tension loading. It has been shown, that under such loading conditions, the boundary of 'macro-zones' plays the dominate role as in crack initiation, as well in crack propagation process. Almost for all the investigated specimens the crack initiation was observed from the border of clusters. The observation of crack path under R=0.1 fatigue loading has shown, that some clusters are more favourable for crack growth. The crack propagation within such clusters is quasi-brittle and forms large flat surfaces with clearly seen alpha-platelets structure. The analysis on several quasi-brittle zones has shown, that fatigue crack moves through the boundary of cluster or very close to it (less than 10 μm). The rest of neighbouring micro-structures with quite different orientation of alpha-platelets were found at the fracture surface. It has been shown, that forming the fracture surface with large quasi-brittle zones is not related to the position of the specimen into the forged ingot. Several tests on specimens machined in radial and circumferential directions of the compressor disk were carried out and in each case the same tendency was noted. Additionally it has been shown, that forming of such fracture surface is related to the mean normal stress(mean tensile load). The fully-reversed tests (R=-1) on the specimen machined in the radial direction does not show significant influence of cluster boundary on the crack initiation mechanism.

Finally, the analysis of the mechanical properties of forged VT3-1 taken from different positions in the disk (rim and plateau part) and in different directions (axial, radial, circumferential) does not show any noticeable difference in fatigue properties. It seems that the scatter of fatigue life is just slightly larger in case of axial specimens machined from the rim part of the disk. The results of tests on axial specimens shows the same fatigue properties with specimens machined from the plateau part of the disk, except some specimens with significantly deviated fatigue life. Such behaviour can be explained by the noticeable difference in number of investigated specimens from the rim part and from the plateau. The number of investigated specimens from the rim part is several times greater than that from the plateau

part. As the crack initiation in case of VHCF is partly a probabilistic problem, the existence of deviation points for value with higher statistical data base looks normal. Nonetheless, the fact of existing a worse cases of premature failures combined with permanent decreasing of SN-curves for VT3-1 under the different R-ratios, should attract additional attention of industries, working with two-phase titanium alloys.

3.4 Results of fatigue tests on extruded VT3-1 titanium alloy under tension (R=-1)

• The fatigue properties of extruded titanium alloy were investigated with specimens machined from extruded bars of VT3-1 titanium alloy. The testing conditions were the same than for the tests on forged VT3-1 (Chapter 2). The fatigue tests were carried out on the same fatigue testing system in the open air, with additional compressed air cooling. The tests were run up to the specimen failure or up to reaching a out-run limit of about 10^9 cycles. The objective of present research is to determine the fatigue strength of extruded VT3-1 at 10^9 cycles by staircase method and to study crack initiation mechanisms. The results of tension-compression tests under fully-reversed loading (R=-1) on extruded VT3-1 titanium alloy are shown in Fig.3.40

The observation on the fracture surfaces of specimen broken in the range of fatigue life between 10^6 and 10^9 cycles shows internal crack initiation for all the observed specimens. Therefore, the transition from the surface crack initiation to the subsurface crack initiation is shifted to the shorter fatigue life in case of extruded titanium alloy. The same results for titanium alloy are not surprising. It has been reported [134] that sometimes internal crack initiation can occurs even under low cycle fatigue test performed on smooth specimen at room temperature in presence of defects. Additional investigations on the crack initiation sites were performed in order to identify the nature of micro-structural imperfections of extruded titanium micro-structure. It has been shown that as after the relatively short, as well after the long fatigue life the type of crack initiation site is the same, Fig. 3.41.

In both cases the crack initiates from pockets of thin α-platelets formed within primary the β-grains. The same agglomeration of α-platelets were also found during the study on a micro-structure of extruded material. It has been shown, that such micro-structures are mainly located in the core of the cylindrical bar. Moreover, such agglomerations are not always located in the exact centre of the cylindrical bar and can fluctuate from the centre. These features of micro-structure are formed during the extrusion process, and can be found almost over the whole cross section of the bar. Some axial symmetry in distribution of defects by the axis of specimen can be observed within its cross-section. In the plane parallel

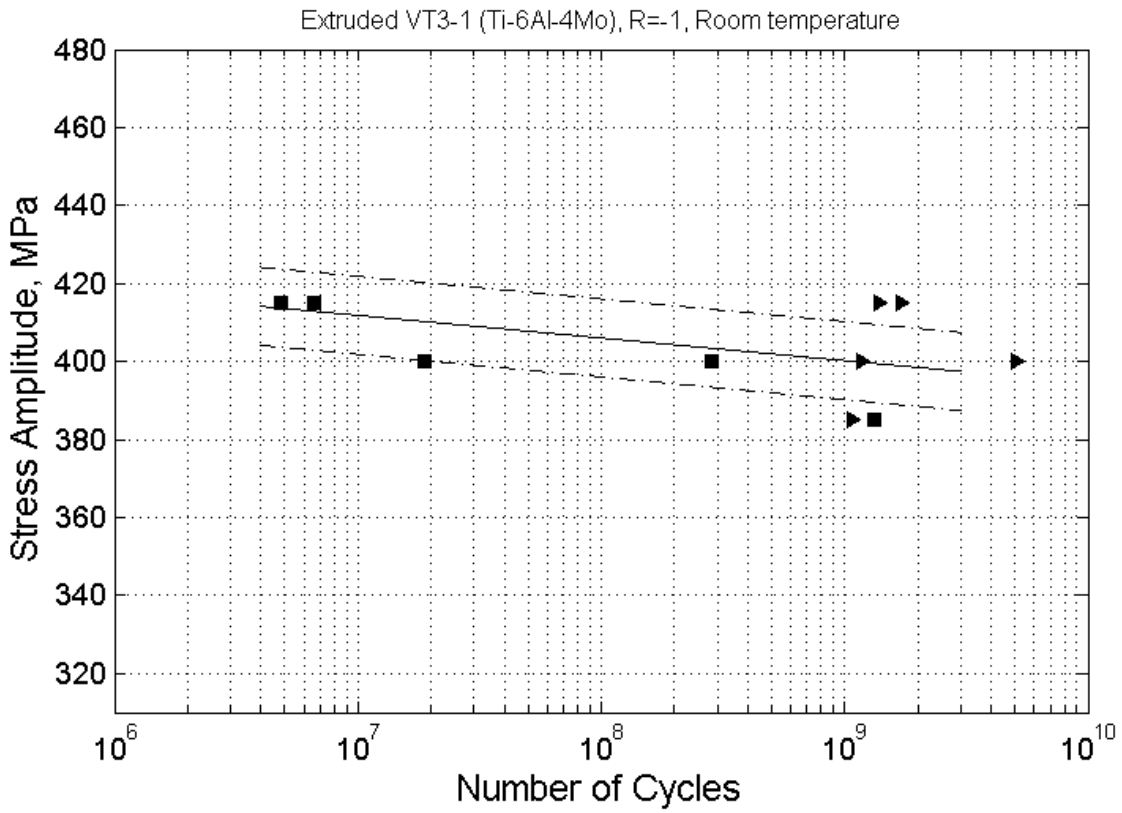

Figure 3.40: The results of ultrasonic fatigue tests on extruded VT3-1 titanium alloy under tension (R=-1)

to the extrusion direction these defects forms elongated chain-like structures. Such chain-like heterogeneities of several hundreds of micrometers long can appear from the area with usual micro-structure and after than vanish. Such features of micro-structures defines the position of the crack initiation site within cylindrical cross section of specimens (diameter 3 mm). The axis of specimens coincides with the axis of extruded bar, therefore, the cross section covers the area of maximum perturbation of extruded micro-structure in extruded bars. The analysis of crack initiation sites shows, that crack always starts from the prime β-grains containing very thin needle like α-platelets. The more interesting thing at fatigue cracking of extruded titanium alloy is 'butterfly wings' formation on the fracture surface. These typical structures were commonly discovered in steels and were explained by cracking along the grain boundaries. In the case of extruded titanium alloy, the typical size of alpha-plates is in the range of micrometers. The presented 'butterfly wings' in extruded titanium alloy are longer than 300 - 400 μm. Therefore the wings-like structures do not always appear along the grain boundaries, while the mechanism of wings nucleation is the same. As shown in Fig. 3.42, the

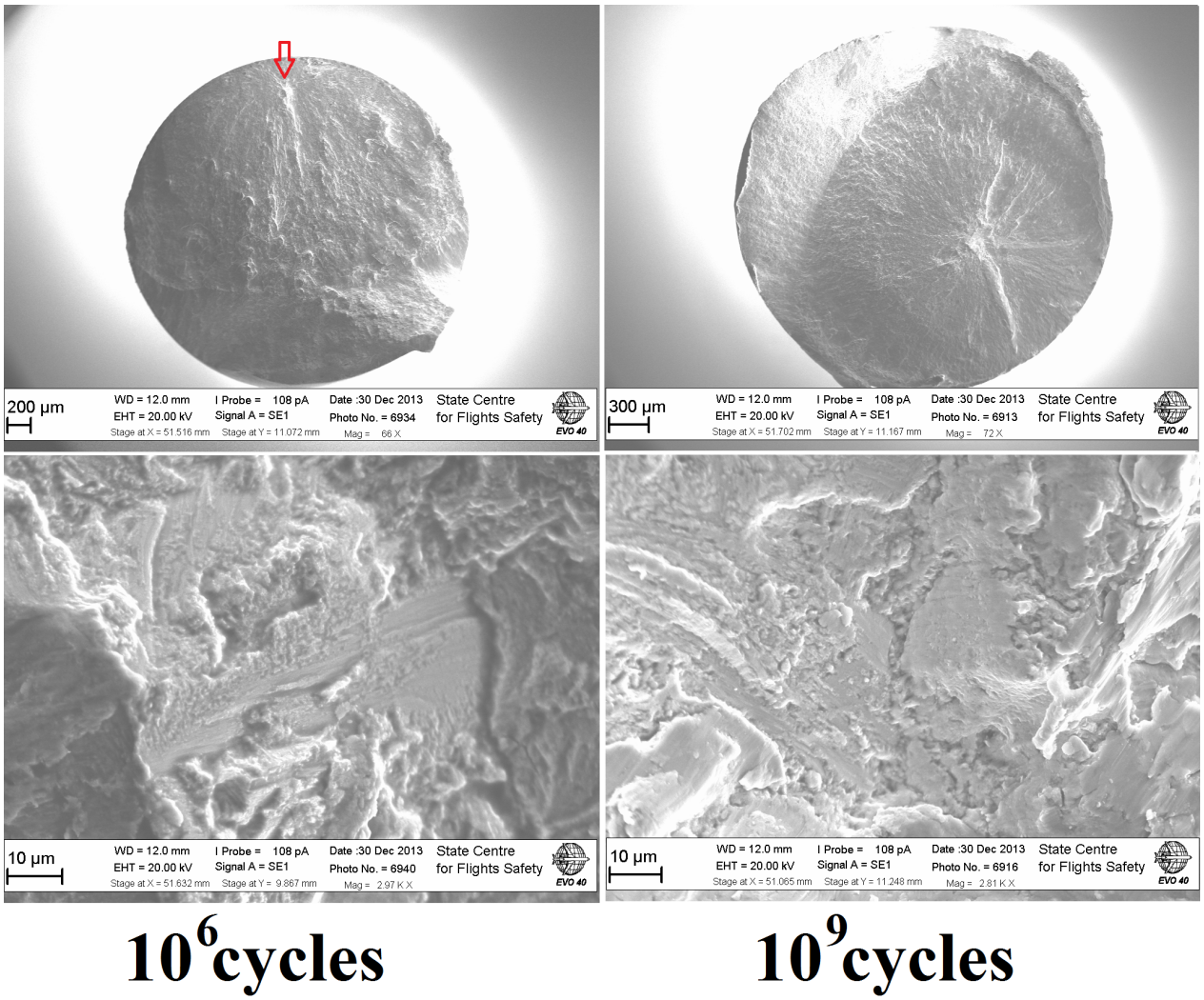

Figure 3.41: Crack initiation in extruded VT3-1 titanium alloy after about 10^6 and 10^9 cycles

crack initiates from the prime β-grain with needle α-platelets by cleavage in plane orientated of about 45° by the loading axis. Such initiation mechanism allows the further crack growth at two different levels (in different planes).

These two cracks at different levels growth simultaneously up to the moment when one of they reach the specimen surface. At the moment when crack turns from the subsurface to surface crack, the two cracks coalesce in a single crack. The material between initial two cracks at different levels is now braking by shear mode. It seems that not all the material between the two cracks was failed, because the 'butterfly wing' is still attached to the fracture surface. Just a part of connection volume was cracked to relax the shear stress between two split-level cracks. The so impressive wing length may be explain by the high capability of

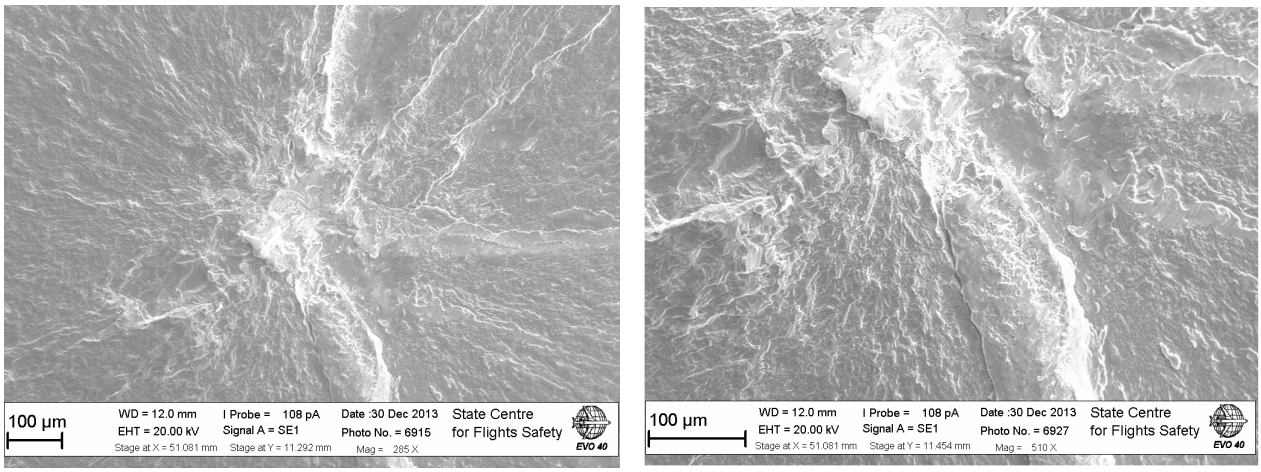

a) b)

Figure 3.42: The crack initiation with forming the 'butterfly wings' at the fracture surface

extruded titanium alloy to accommodate plasticity (see the tensile curve for extruded VT3-1, Chapter 2).

3.5 Results of fatigue tests on extruded VT3-1 titanium alloy under tension (R=0.1)

• In order to investigate the influence of positive mean normal stress on the fatigue strength and the mechanisms of fatigue crack initiation, ultrasonic tests at R=0.1 were carried out on the extruded VT3-1 titanium alloy. The experimental conditions were the same than for the tests with positive loading ratio on the forged VT3-1 titanium alloy. During the ultrasonic testing the surface of the specimens was cooled by compressed air. The results on extruded titanium alloy under R=0.1 are shown on Fig.3.43.

The observation on the fracture surfaces of specimens broken under the R=0.1 shows just an internal position of crack initiation site. Like under fully-reversed loading, the crack initiation area may be located as close to the centre of the failed cross section, as well close to the specimen's surface. The detailed analysis of the crack initiation sites for the longer and shorter fatigue life shows the same tendency that was observed for tension-compression loading. The crack initiates from the prior β-grain with needle α-platelets, Fig. 3.44.

The morphology of cleavage structural element at the centre of fatigue crack initiation is not the same for different specimens, but one typical tendency can be found for the majority of the tested specimens under R=0.1 conditions. The initiation site for samples subjected to a positive mean stress often shows some elements with trans-granular fracture (Fig. 3.45). It means that under the positive mean tensile stress conditions the role of micro-structural

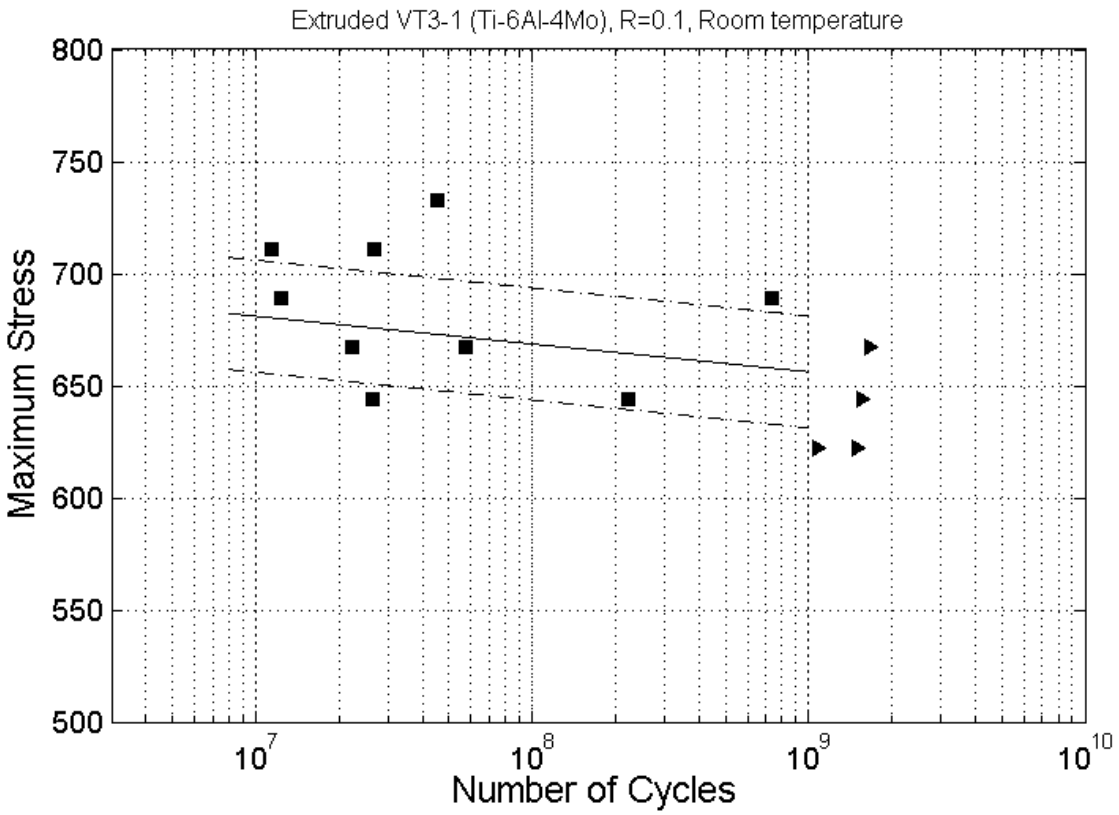

Figure 3.43: The results of ultrasonic fatigue tests on extruded VT3-1 titanium alloy under tension (R=0.1)

boundaries becomes more significant in fatigue cracking. The characteristic size of microstructural elements in case of forged and extruded titanium alloy differs in tenths or hundreds times, but the tendency is the same. Fatigue crack initiates at the borders of primary microstructural element (marco-zone and prime β-grain).

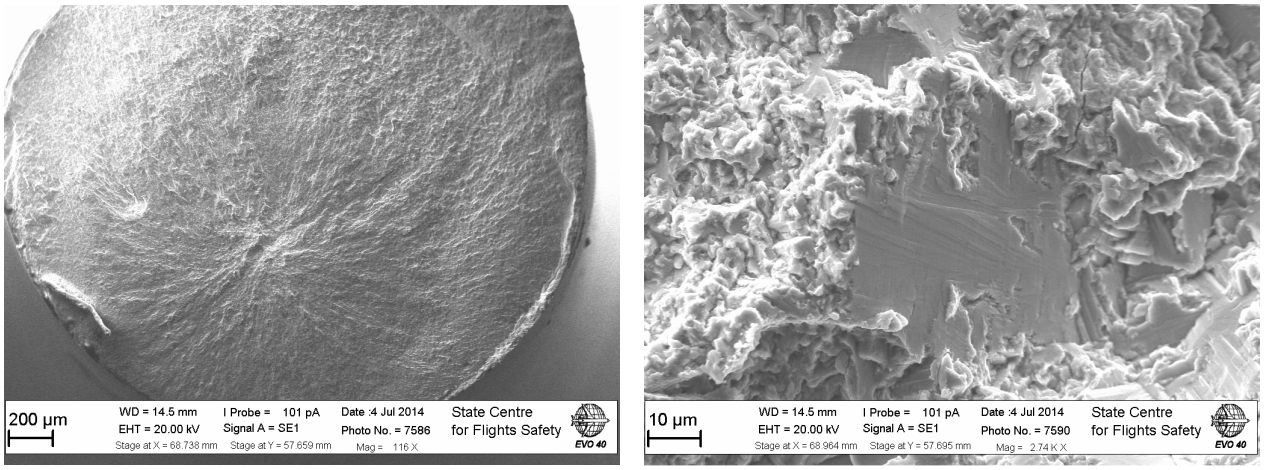

a) b)

Figure 3.44: The fracture surface of extruded VT3-1 titanium alloy under R=0.1 at fatigue life below 10^8 cycles

3.6 Results of fatigue tests on extruded VT3-1 under tension (R=0.5)

• As it is well known, aeronautic titanium alloys are often used for applications, subjected to high loading ratio. In order to investigate the fatigue strength of VT3-1 titanium alloy under different ratios, the series of tension-tension tests with R=0.5 was carried out on smooth specimens. The results of investigation are shown on Fig. 3.46.

The low number of extruded specimens were available for fatigue tests under R=0.5 loading conditions does not allows to make any assumption about the scatter in fatigue life of extruded VT3-1 under such loading ratio. Nonetheless, the tendency which can be noted through the experimental data shows a slight slope in fatigue strength curve. Moreover, all the specimens were broken in the range of 10^8 - 10^9 cycles, i.e. in the range, where the fatigue crack should not appears, according to the concept of infinite fatigue life. Therefore, in case of extruded VT3-1 titanium alloy under R=0.5 the 'fatigue limit' was not found and the fatigue strength at the given number of cycles (10^9) was found by using staircase method.

All the investigated specimens were broken by subsurface crack, Fig.3.47.

The location of crack initiation site is varying from one specimen to another and can be found as close to the centre of broken cross section, as well close to the surface of specimen. The analysis of crack initiation site shows the same crack initiation mechanism than it was observed under tension-compression (R=-1) and tension-tension (R=0.1) loading. In the centre of initiation zone the cleavage of prime β-grain with needle α-platelets were found. Thus, it seems that such defects of micro-structures in the extruded VT3-1 titanium alloy are

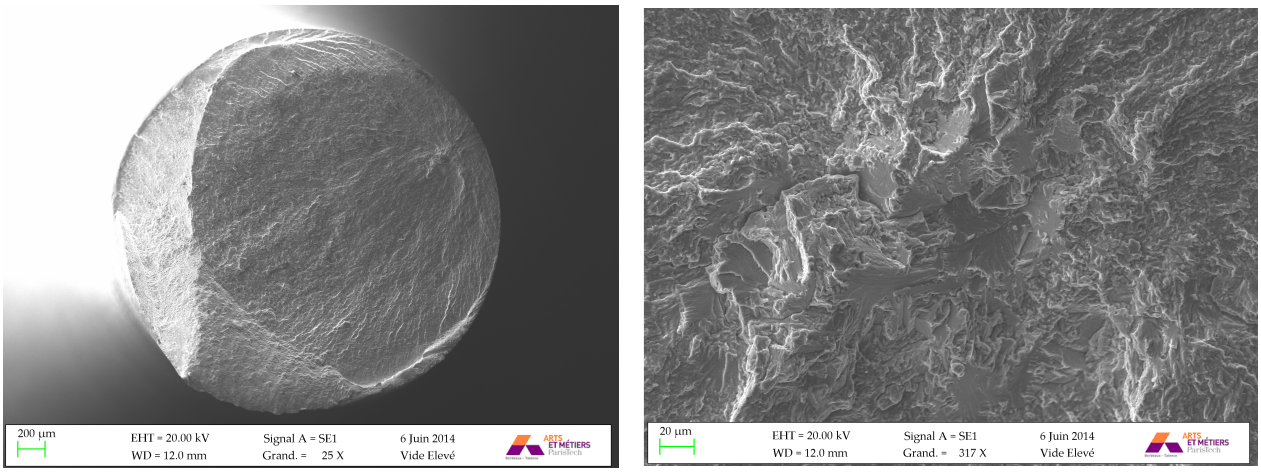

a) b)

Figure 3.45: The fracture surface of extruded VT3-1 titanium alloy under tension (R=0.1) at fatigue life beyond 10^8 cycles

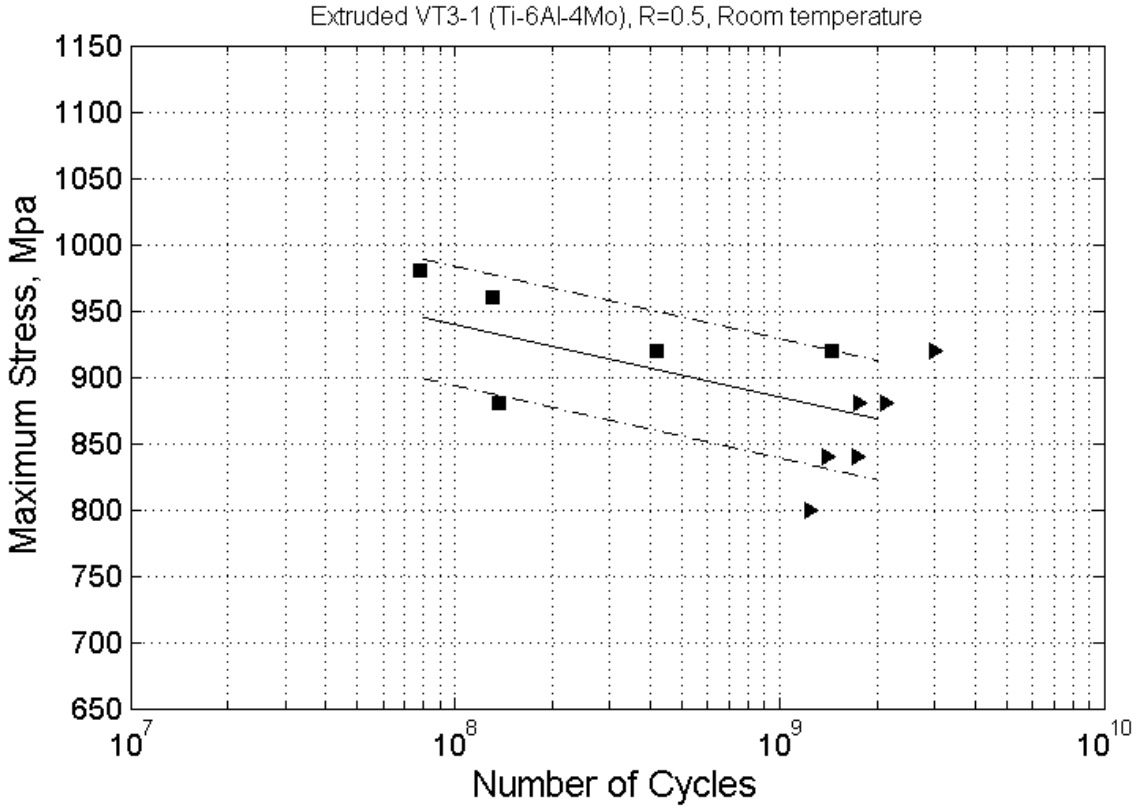

Figure 3.46: The results of fatigue tests on extruded VT3-1 titanium alloy under, R=0.5 loading

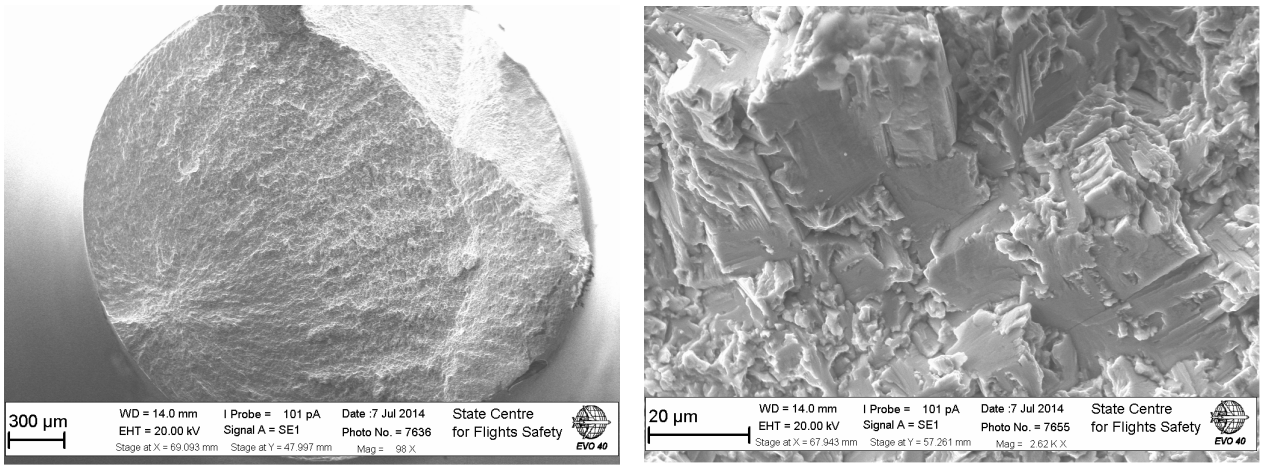

a) b)

Figure 3.47: Typical fracture surface and crack initiation site in extruded VT3-1 titanium alloy under R=0.5 loading

fatigue life controlling features of micro-structure. They lead to the crack initiation in the similar way under the different loading ratios, starting from R=-1 up to the tests with R=0.5. Moreover, the existence of such structural homogeneities lead to internal crack initiation even under the stress amplitudes, corresponding to 10^6 cycles.

3.7 Influence of the fabrication process on the gigacycle fatigue behaviour of VT3-1

• Based on the results of fatigue tests (R=-1) on 'axial' and 'radial' specimens it can be stated that there is no significant difference in fatigue strength between specimens machined from the rim and plateau part of the disk, Fig. 3.48 (a). Moreover, the tests on 'radial' and 'circumferential' specimens (both machined from the plateau part) show almost the same fatigue strength under ultrasonic loading, Fig. 3.48 (b). Thus, it can be stated that there is no significant anisotropy in fatigue properties under ultrasonic loading for the forged VT3-1 alloy.

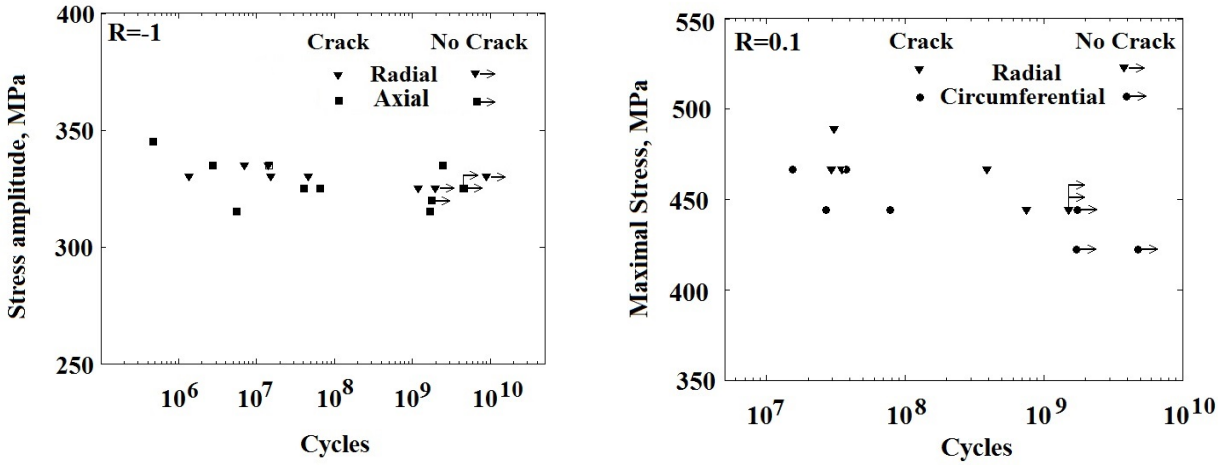

a) b)

Figure 3.48: The results of ultrasonic fatigue tests on (a) axial and radial specimens at R=-1 and (b) on radial and circumferential specimens at R=0.1

The analysis of fracture surfaces obtained under R=-1 and R=0.1 loading shows a noticeable difference in crack initiation mechanisms. In the case of R=-1 loading, several initiation mechanisms can be observed: initiation from surface; from agglomeration of coarse α-platelets; borders of macro-zone; chemical inhomogeneity and smooth facets. Each of such mechanism dominates over the others at different fatigue life that lead to 'competition' between initiation mechanisms. In the case of R=0.1 loading, only one mechanism of crack initiation was found. It is crack initiation from the border of macro-zone. The large clusters of similarly orientated α-platelets are very sensitive to the static mean stress. The interpretation of the results on the Haigh or Goodman diagram, Fig. 3.49 shows that such fatigue behaviour of forged VT3-1 lead to significant reduction of the fatigue strength. The results of tests under positive stress ratio are localised well below the both Gerber and Goodman lines. In order to compare the gigacycle fatigue behaviour of VT3-1 titanium alloy obtained by different production technologies, the series of fully-reversed (R=-1) and pull-pull (R=0.1 and R=0.5) were carried out on extruded VT3-1.

The results of fully-reversed tests (R=-1) on extruded VT3-1 titanium alloy show almost the same fatigue strength with the forged alloy, Fig.3.50. It is unexpected result, because the UTS of extruded alloy is about 200 MPa higher, compared to the forged VT3-1. The analysis of fracture surface of extruded VT3-1 have shown, that fatigue cracks initiate at the same type of micro-structure defect independently of the fatigue life. This type of defect is primary β-grain filled by ultra fine α-platelets. The size of such β-grain is ranged from 40 to 60 μm. The only subsurface cracks were observed for extruded VT3-1 under R=-1 loading condition.

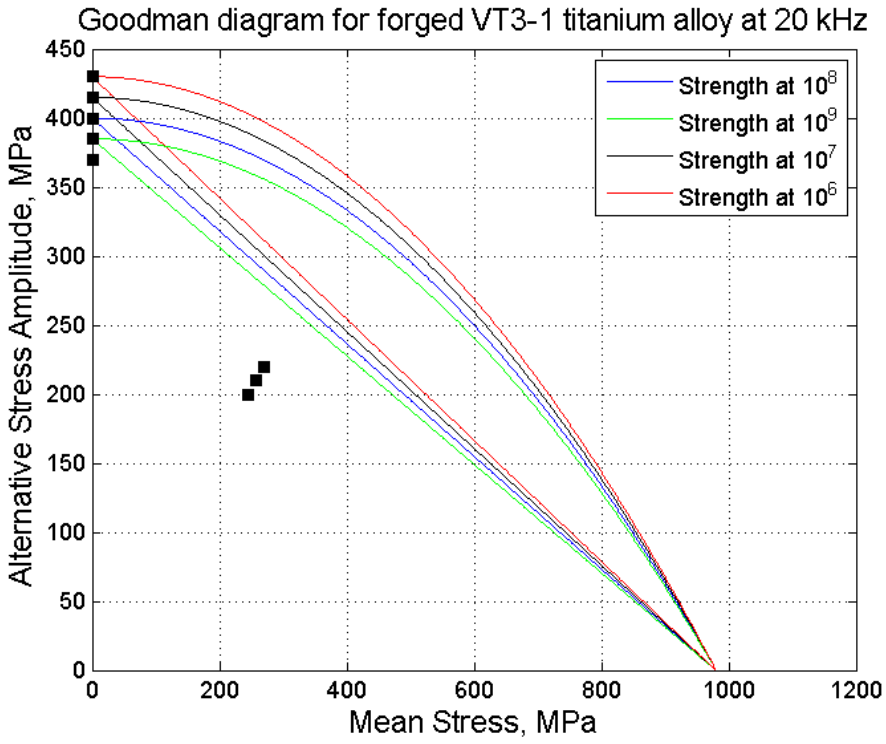

Figure 3.49: The Goodman diagram for forged VT3-1 titanium alloy at 20 kHz

The fatigue tests on extruded VT3-1 under positive stress ratios (R=0.1 and R=0.5) has shown the same crack initiation mechanisms than under R=-1 loading. Similarity to fully-reversed tests, just an internal crack were observed. The internal crack were always nucleated from the primary β-grain fitted by thin α-platelets. Unlike in the case of forged VT3-1 the fatigue behaviour of extruded VT3-1 is in good agreement with models for positive mean stress loading, Fig. 3.51. In-spite on clear micro-structural defect of extruded VT3-1 the fatigue strength under higher mean stresses seems to me improved compared to tension-compression regime (mean stress $\sigma_m = 0$). Comparing the results for forged and extruded VT3-1 under positive mean stress it can be stated, that large clusters of α-platelets (up to several hundreds of micrometers) are more sensitive to static normal stress (tensile) compared to small defects of micro-structure (the size of primary *beta*-grain is about 40 - 60 μm).

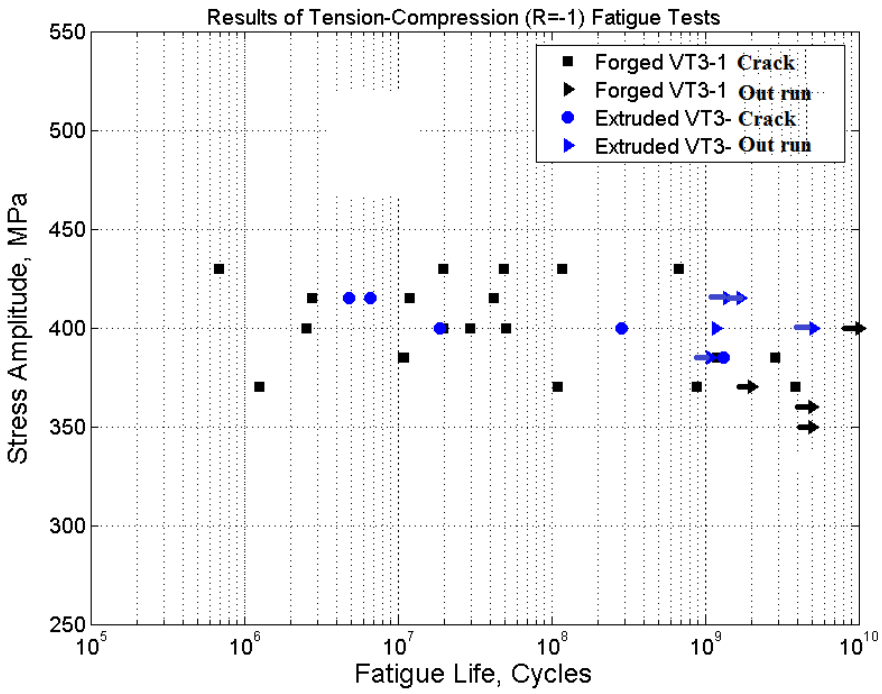

Figure 3.50: Results of fully-reversed (R=-1) tension fatigue tests on forged ('axial' specimens) and extruded VT3-1 titanium alloys

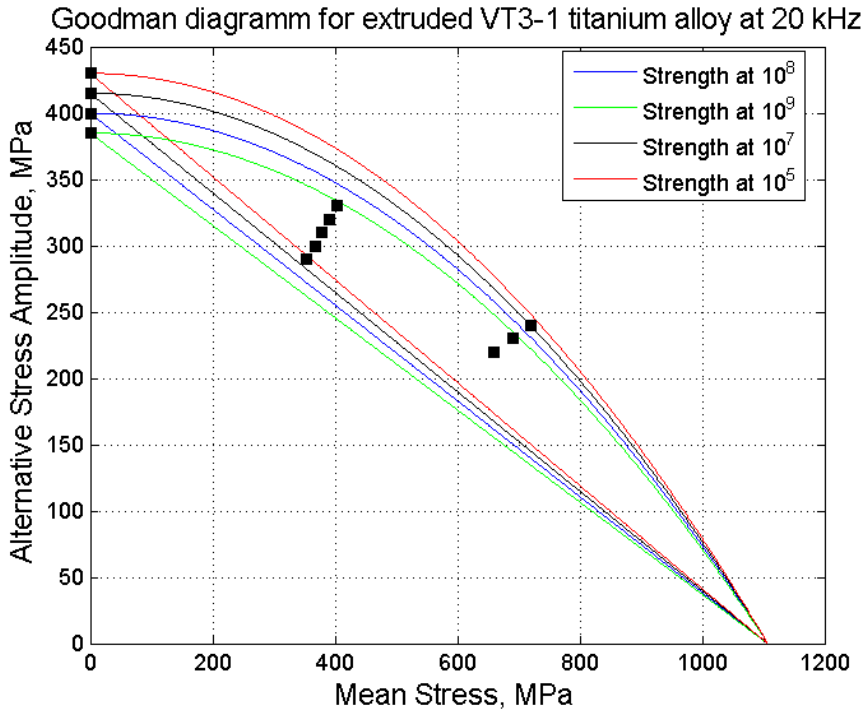

Figure 3.51: The Goodman diagram for extruded VT3-1 titanium alloy at 20 kHz

Chapter 4

Ultrasonic Fatigue Torsion Testing System

4.1 Introduction

Many elements of modern machines are subjected to very high number of loading cycles. It has been noted that for certain industries like car, high-speed train, airspace and others in-service fatigue life ranges from 10^8 to 10^{10} cycles [3]. Fatigue strength of most structural materials has a tendency to decrease even beyond 10^7 cycles [56]. Thus all the material properties, such as fatigue strength can not be extrapolated from measurements at lower number of cycles [135] and have to be experimentally established. Conventional fatigue testing techniques are not suitable for investigations in VHCF regime because they need long testing time. Usual an ultrasonic fatigue technique is employed for such investigations. Real operating conditions for materials combine different loading modes, such as longitudinal, bending, torsion and its combinations. That's why over the last two decades different ultrasonic fatigue testing machines were developed for investigating fatigue behaviour under tension-compression, tension-tension, bending, fretting fatigue and torsion loads in VHCF region [53]. Some of such testing systems are commercially used (for example piezoelectic tension-compression machines), others are laboratory used prototypes. This chapter describes the development of one laboratory used prototype: an ultrasonic torsional fatigue testing system.

Even the first ultrasonic fatigue testing system for longitudinal tests was developed by Mason and Wood in 1956, the first ultrasonic machine working in torsion appeared more than 30 years later and further progress in ultrasonic torsion methods was related to the development of direct piezoelectric converters. However, one of the first ultrasonic torsion fatigue testing system was constructed based on longitudinal piezoelectric activator by Telsonic company in 1990. The first torsion testing machine based on direct torsion converter

was designed in Japan in early 1990th. Both types of torsion machines were initially controlled by analogic system and had not high-performance feedback that allowing permanent correction of the loading parameters. The first machine with a high-performance computer control feedback was developed in 1989 by the research group led by Claude Bathias in laboratory ITMA. The permanent control of loading parameters was initially applied just to the longitudinal piezoelectric transducers, that led to the appearance of two different designs for ultrasonic torsion fatigue systems: (1) direct torsion system guided by analog pulse control without feedback; (2) indirect torsion system with computer control of the loading parameters. The direct torsion machine was employed for tests on high-strength aluminium [136] in cooperation with Ueha (Tokio) and K.Ohya (Nagoya). This machine had a relatively low power supply of 300W. Direct torsional transducer provides a transformation of sinusoidal electrical signal into mechanical angular vibrations at the same frequency. This ultrasonic torsion machine was design to work in resonance at frequency of 21 kHz. All the mechanical parts including mounting part, horn and specimen were also designed to be in resonance at 21 kHz. All the connections between the mechanical parts were realized by coupling screws [136]. Loading was performed by pulses with working block of 500 cycles at normal amplitude and pauses between blocks from 50 to 1000 ms. The results on high-strength aluminium alloy 2024 under pure ultrasonic torsion loading have shown that the fatigue strength of Al2024 is continuously decreasing from about 160 MPa at 10^6 to 97.5 MPa at 10^9 cycles. It has been shown, that fatigue crack initiation under ultrasonic torsion may occur as on perpendicular to the specimen axis plane as well along the loading axis on one of the maximum shear stress planes. After the initiation stage, the torsion fatigue crack growth was observed on one of the maximum normal stress planes. Thus, the angle between crack propagation direction and specimen axis is 45°. Moreover, it has been noted that under higher stress amplitudes numerous fatigue cracks occurred near the crack initiation site; with decreasing of loading amplitude no crack branching were observed. Although the results of ultrasonic investigation on aluminium alloy are qualitatively similar to previous torsion investigation on mild steel at low loading frequency of 1 Hz [137], the problems of cumulative fatigue damage accumulation are limited to use pulse-pause method. In this case the determination of the total fatigue life is uncertain. Indeed, due to the pulse-pause technique the loading condition is close to be variable amplitude, requiring the use of a fatigue damage accumulation concept that is not yet developed for ultrasonic loading and very long life. These difficulties of fatigue data interpretation have activated works on creating a torsional ultrasonic fatigue testing system working continuously.

The first continuous torsional ultrasonic fatigue testing machine was built in France by research group led by Bathias [138]. This machine was constructed based on longitudinal piezoelectric transducer working at resonance frequency of 20 kHz. A special system of

longitudinal and torsional ultrasonic horns provides to transform axial displacements into torsional vibrations, Fig.4.1 [53].

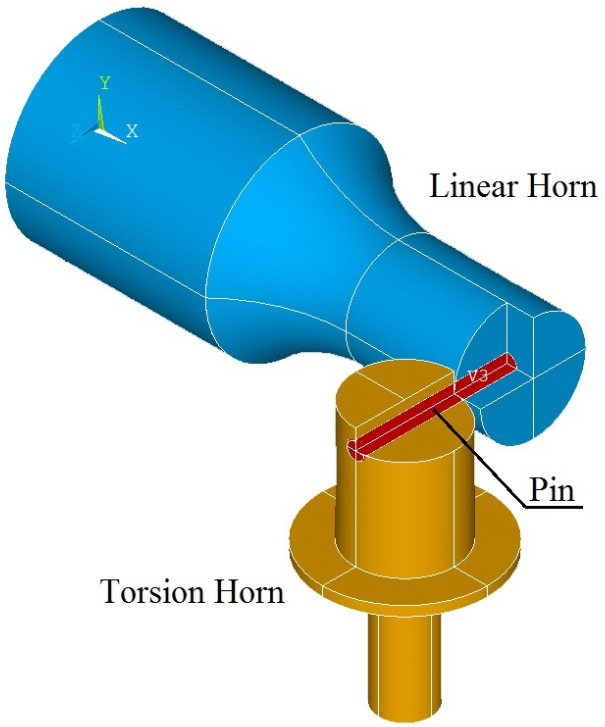

Figure 4.1: System of special ultrasonic horns of continuous torsion testing system

All the elements of the machine have been designed to be in resonance at 20 kHz. In additional to continuous loading regime this fatigue system has another important advantage: the power of longitudinal piezoelectric converter is significantly higher compared to direct torsion transducer and reaches 2000 W. This features of continuous torsion system allow to test materials with a high mechanical properties, such as high-strength steels. The first results under ultrasonic torsion on two different steels (D38MSV5S, 100Cr6) and aluminium 2-AS5U3G-Y35 were obtained by using the continuous torsion testing system [139, 140, 141]. It has been shown for the first time, that even under torsion loading internal cracks could initiate from inclusion in 100Cr6 high-strength steel [140]. It was outlined, that the location of fatigue crack initiation in 100Cr6 steel is strongly depends on number of cycles to failure: the internal crack initiation is often observed for longer fatigue life exceeding 10^7 cycles. In case of D38MSV5S steel and 2-AS5U3G-Y35 aluminium alloy just surface crack initiations were observed for all the fractured specimens even at very long fatigue life (beyond 10^9 cycles). Surface fatigue crack initiation appears on one of the maximum shear stress planes while the further crack growth appears on the maximum principal stress plane (45°). Such,

these results are qualitatively similar to torsion behaviour of steels at low loading frequency. Moreover, in order to investigate an influence of loading frequency the results of ultrasonic investigations were compared with results for the same steel (D38MSV5S) obtained at 35 Hz. It has been shown that fatigue data at two different frequencies are in very good agreement [140].

Thus, over the last 20 years, the two different ultrasonic torsion fatigue testing concepts were developed based on direct torsion and longitudinal piezoelectric transducers. Both machines operates in resonance mode at frequencies lying in the range from 20 to 21 kHz. Both techniques allows to investigate as relativity soft materials like aluminium, as well a high-strength alloys like 100Cr6 [140] or SWOSC-V [142] steels. Fracture surfaces and torsion crack initiation mechanisms investigated in VHCF regime by using ultrasonic techniques are in good agreement with tests results at lower frequencies (1Hz and 35 Hz). However, an additional subsurface crack initiation mechanisms under torsion loading was found for inclusion containing materials. Summing up the development of torsion ultrasonic machines, it should be noted that high performance torsion systems has been built by Japanese and French researches. But, although the obtained good results, each technique has its own shortcomings: direct ultrasonic machines operates with small pauses that involve the problem of total fatigue life calculation; Bathias's machine has a complex connection between ultrasonic horns that subjected to ultrasonic bending and sometimes gets a fatigue failure in connection pin. Thus, in spite of good results obtained by using presented above machines and their high performances, a new ultrasonic fatigue testing machines have to be designed in order to eliminate the shortcomings of both systems.

4.2 Gigacycle Torsion Fatigue concept

The ultrasonic torsion fatigue testing concept is quite similar to longitudinal tension-compression method. In contrary to conventional fatigue torsion testing method which uses a forced vibration, an ultrasonic one operates in free vibration conditions at the natural specimen frequency [3]. In the case of torsion testing, the ultrasonic vibrations are angular, that provide to excite a pure torsion motion within the specimen. To better understand this phenomenon, it is worth briefly recalling the elastic wave theory. The solution of differential equations for general three-dimensional isotropic elastic body shows that two types of elastic waves may exist in an infinite isotropic elastic body: longitudinal and transverse waves. Longitudinal tension-compression method is based on theory of longitudinal wave propagation, while the torsion ultrasonic concept is related to transverse wave theory. In the case of torsion motion, the derived equation, or equation of motion, can be written as the next

$$\rho J_p(x)\frac{\partial^2\varphi(x,t)}{\partial t^2} = G\frac{\partial}{\partial x}(J_T(x)\frac{\partial\varphi(x,t)}{\partial x}) \tag{4.1}$$

where $J_p(x)$ - polar moment of inertia, $J_T(x)$ - torsional strength and φ is twist angle

Based on Eq.4.1 an analytical solution for all the mechanical parts of ultrasonic torsion testing system can be derived. As usual a loading part of torsion machine consists of one or several ultrasonic horns. These horns consists of both constant cylindrical sections and reduced along horn's axis cross section. Generally it is assumed that increasing the number of connection elements or connection surfaces leads to increase energy dissipation because of the real contacts between mechanical elements are not perfect. Thus, it is better to use a minimum number of ultrasonic horns when designing a fatigue testing machine. Ultrasonic torsion fatigue testing system, introduced in the present paper, consists of unique horn, which is connected directly to piezoelectric transducer (Fig.4.2). Analytical solution for such horn may be built by 'cross- linking' of analytical solutions for tagged on the figure 4.2 parts: part $N°1$ is a cylinder with length L_1 and constant radius; (2) part $N°2$ is a cylindrical bar with reduced cross section; part $N°3$ is similar to part $N°1$. Since all the three parts of the ultrasonic torsion horn have an axial symmetry, their polar moment of inertia is equal to torsion strength $J_p(x) = J_T(x) = \frac{S^2(x)}{2\pi}$ where $S(x)$ is the cross section along x axis. Substitution of moment of inertial and torsion strength into Eq.4.1 gives the following equation

$$\frac{\partial^2\varphi(x,t)}{\partial t^2} - \frac{G}{\rho}\frac{1}{S^2(x)}\frac{\partial}{\partial x}S^2(x)\frac{\partial\varphi(x,t)}{\partial x} - \frac{G}{\rho}\frac{\partial^2\varphi(x,t)}{\partial x^2} = 0 \tag{4.2}$$

Eq.4.2 consists of two parts, which are one-argument derivative, that admits the representation of analytical solution as multiplication of two functions, each of which is depending from just one argument (time or coordinate)

Let us introduce a new interpretation of function $\varphi(x,t)$ which consists of one part depending from position x and the second part is a time depending function

$$\varphi(x,t) = \xi(x)\cdot e^{i\omega t} \tag{4.3}$$

In this case the equation of torsion motion can be written as

$$\frac{d^2\xi(x)}{dx^2} + \frac{d}{dx}Ln[S^2(x)]\frac{d\xi(x)}{dx} + K^2\xi(x) = 0 \tag{4.4}$$

where $K = \frac{\omega}{c}$, $\omega = 2\pi f$, $c = \sqrt{\frac{G}{\rho}}$, f is a frequency

Assuming a constant radius of cylinders for parts 1 and 3 and hyperbolic profile for part 2, an analytical solution for each part can be found as:

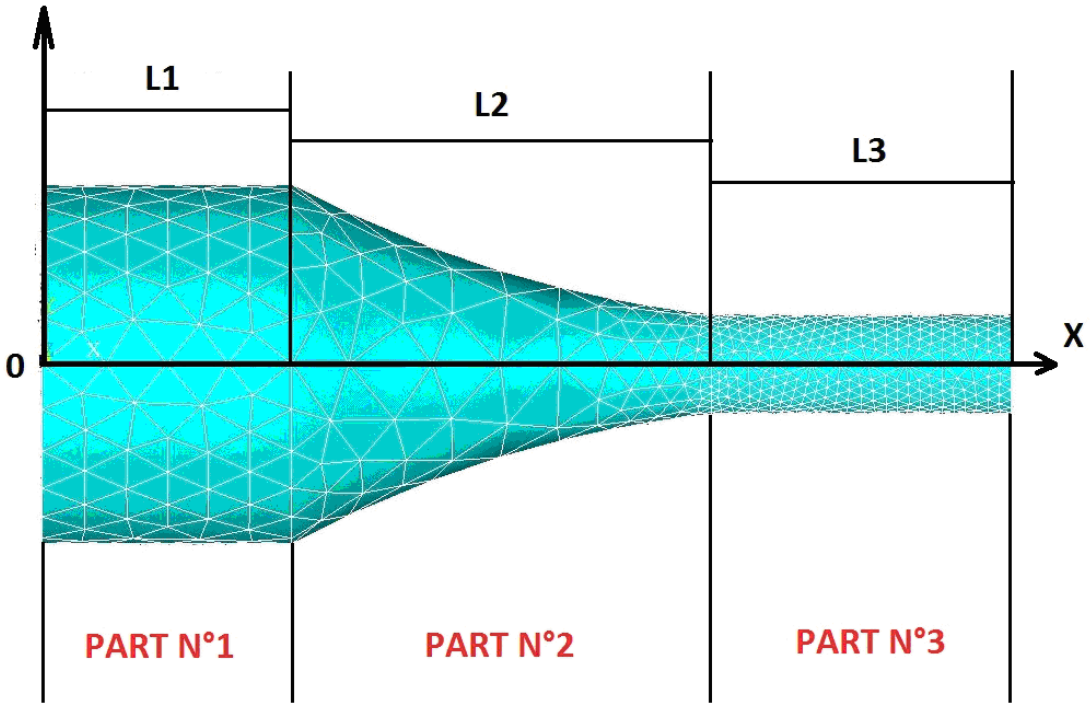

Figure 4.2: Relation between wave speed and ratio r/λ for cylindrical bar

$$\xi_1(x) = C_1 Sin(\omega t) + C_2 Cos(\omega t) \tag{4.5}$$

$$\xi_2(x) = \frac{C_3 e^{\beta x} + C_4 e^{-\beta x}}{cosh[\alpha(L_1 + L_2 - x)]} \tag{4.6}$$

$$\xi_3(x) = C_4 Sin(\omega t) + C_5 Cos(\omega t) \tag{4.7}$$

$$where\ \alpha = \frac{1}{L_2} acosh\left(\frac{S_{max}}{S_{min}}\right)\ and\ \beta = \sqrt{\alpha^2 - K^2}$$

Constants C_i should be determined from the boundary conditions. In case of ultrasonic torsion testing an angular vibration is assumed as free vibration, thus the following boundary conditions and cross linking restrictions are used

$$\xi_1(x) \mid_{x=0} = \xi_0 \qquad \xi_1'(x) \mid_{x=0} = 0 \tag{4.8}$$

$$\xi_1(x) \mid_{x=L_1} = \xi_2(x) \mid_{x=L_1} \qquad \xi_1'(x) \mid_{x=L1} = \xi_2'(x) \mid_{x=L_1} \tag{4.9}$$

$$\xi_2(x) \mid_{x=L_1+L_2} = \xi_3(x) \mid_{x=L_1+L_2} \quad \xi_2'(x) \mid_{x=L1+L2} = \xi_3'(x) \mid_{x=L_1+L_2} \tag{4.10}$$

$$\xi_3(x) \mid_{x=L_1+L_2+L_3} = 0 \tag{4.11}$$

Thus, obtaining of the analytical solution of equations (4.5 - 4.7) satisfying these boundary conditions is not a difficult task.

4.3 Design of torsion loading components

The Design of the torsion horn was realized in order to several main objectives, namely to amplify angular vibrations; to get a resonance frequency of horn being in the work range of the piezoelectric converter (from 19500 Hz to 20500 Hz); to obtain a long life in-service conditions. For this new torsion testing system the excitation in ultrasonic angular vibrations was realized by using direct torsion piezoelectric transducer. This converter was fully developed by BRANSON ultrasonic company for commercial use, thus its performances should be assumed as given parameters. The power of such direct torsion transducer is limited to 300 W and the maximum twist angle is 0.25 mRad. The torsional ultrasonic transducer used for ultrasonic testing machine developed in this PhD project is shown on Fig.4.3.

The properties of direct torsion converter gives some initial parameters and limitations for ultrasonic torsion horn design. The key parameter is the maximum amplitude of twist angle of the piezoelectric converter. The design of horn should satisfy to the following key requirements: (1) the ultrasonic torsion system should be capable to perform continuous fatigue tests on high-strength materials, such as titanium alloys and high-strength steels (for example 100Cr6 bearing steel) ; (2) the natural frequency of ultrasonic torsion horn should be in the work range of piezoelectric testing system (from 19'500 to 20'500 Hz). In order to match the first requirement, it is necessary to determine a maximum twist angle that allows to get failure of specimen made from a given high-strength material. The shape of

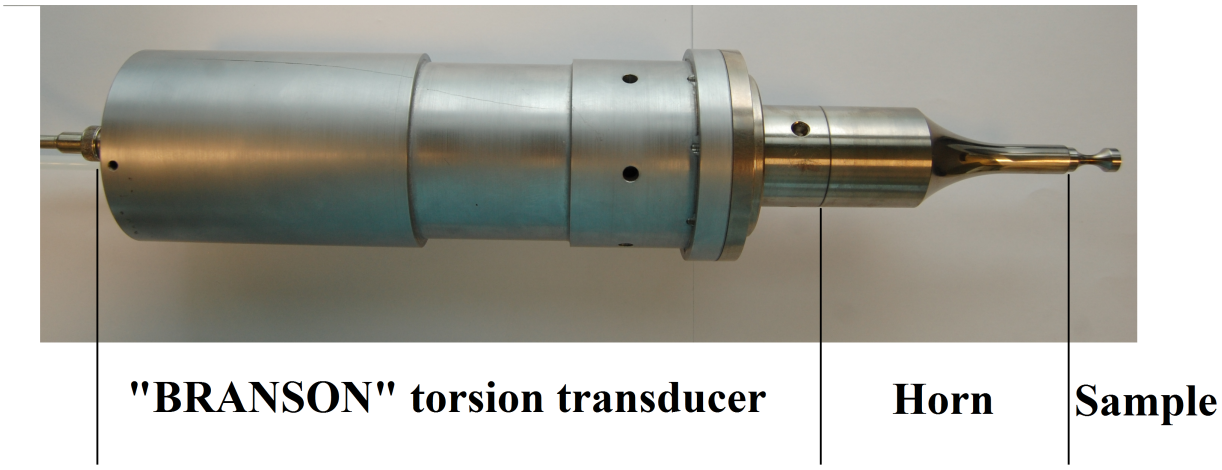

Figure 4.3: Torsion ultrasonic transducer made by BRANSON

ultrasonic torsion specimens was developed based on elastic waves theory in solid bodies [3]. The geometry of specimen for present tests was kept the same than geometry used for previous investigations [138]. Taken into account the mechanical properties of material used for investigations, a range of required twist angle amplitudes can be determined. Based on this range of required twist angles, the magnification factor of ultrasonic torsion horn can be calculated. The magnification factor of ultrasonic horns is determined by its geometry, namely by difference in diameters of 'input' and 'output' parts of the horn. Therefore, to increase the magnification factor of horn, the difference in diameters should be increased. However, such an increase leads to increase stress amplitude in horn and lead to higher risk of fatigue failure. Classical examples of fatigue failures in locations with diameter change can be found in literature about trains wheelset failures, dated by 1850. Thus, to match the requirement on magnification factor, an optimal solution should be found, which will allow to obtain long life for the horn and, at the same time, to get failure of specimens.

The first limitation of the torsion converter (relativity small twist angle) can be overcome by choosing a good geometry and material for ultrasonic horn. An important point for design is also a relatively low power of direct torsion piezoelectric actuator (300 W). The decreasing of power consumption under the same resonance conditions could be achieved by decreasing the total mass of the horn. In order to better understand how to decrease the mass of the ultrasonic horn, let us have a look on typical ultrasonic horn geometry, Fig.4.2. It consists of three parts : 'input' part, part of reduce cross-section and 'output' part. The length of 'output' part (resonance length) is strongly determined by geometries of two previous parts and it is used for adjusting the resonance frequency. Thus, we can not easily modify this part. The second part is responsible for transfer of angular vibration from part with big diameter

to the part with small diameter. Thus, the geometry of this part should be design to minimise the stress concentration due diameter change. If parameters of this part should be changed, a quite high attention should be paid to stress amplitude analysis at minimum diameter. So, it is not recommended to change these settings. The 'input' part of horn is less critical part for modifications between all three sections. It is responsible for proper vibration mode and usually its length should be equal to 1/4 of elastic wave length. Nonetheless, based on numerical simulation it was shown, that this length could be decreased and resonance frequency could be corrected by changing the parameters of the following two parts (length of reduced cross-section and resonance length). As a prototype, the first ultrasonic horn was designed with an 'input' part length of 1/8 elastic wavelength. The schema of this prototype and numerical simulations of this horn are shown in Fig.4.4. Based on numerical simulation it has been shown, that the plane where the shear stress reaches the maximum values is located at plane of connection between part with reduced cross-section and 'output' part, Fig.4.4.

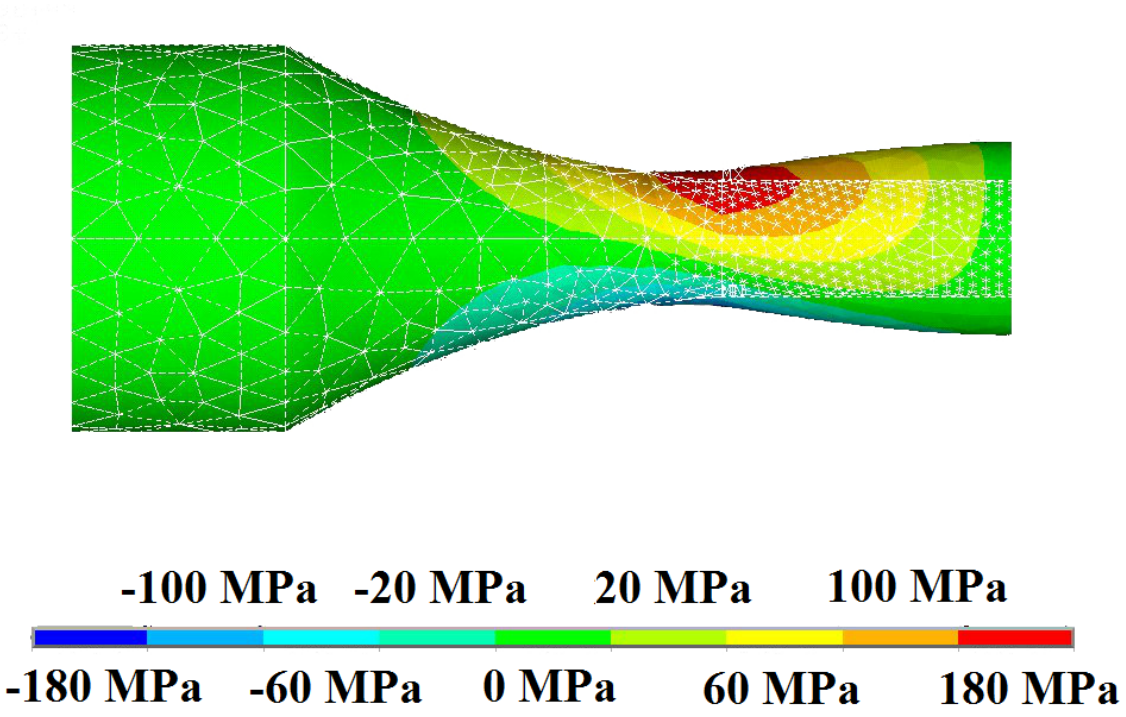

Figure 4.4: Shear stres distribution within torsion ultrasonic horn

The torsion ultrasonic horn with shorter 'input' part has some advantages: (1)the mass of such horn is small compared to typical ultrasonic horn with 'input' part length equal to 1/4 elastic wavelength; (2) the shorter L_1 length needs to increase the length of reduced section in order to realize a first mode torsion vibration within ultrasonic horn. Increasing

of L_2 length allows to use a bigger radius for hyperbolic profile, that led to reduce the stress concentration factor in the area of connection between part with reduced cross-section and cylindrical part. The stress field plotted on Fig.4.4 is corresponding to the maximum twist angle of direct torsion transducer. The weak point of this prototype is the small magnification factor compared to ultrasonic horns with smaller radius of their reduced part. Nonetheless, in spite of less significant effect of stress concentration the first prototype of direct ultrasonic torsion horn was cracked, Fig.4.5. This failure was studied and it has been shown, that crack had initiated from surface defect introduced during the manufacturing process. This fatigue failure have forced us to include additional treatment in the manufacturing process of torsion horn. Since the surface quality in transition area is a critical parameter, the connection zone should be polished up to mirror-like condition. Except mentioned above features of torsion horn design, the procedure of design is typical for ultrasonic horns and briefly discussed below.

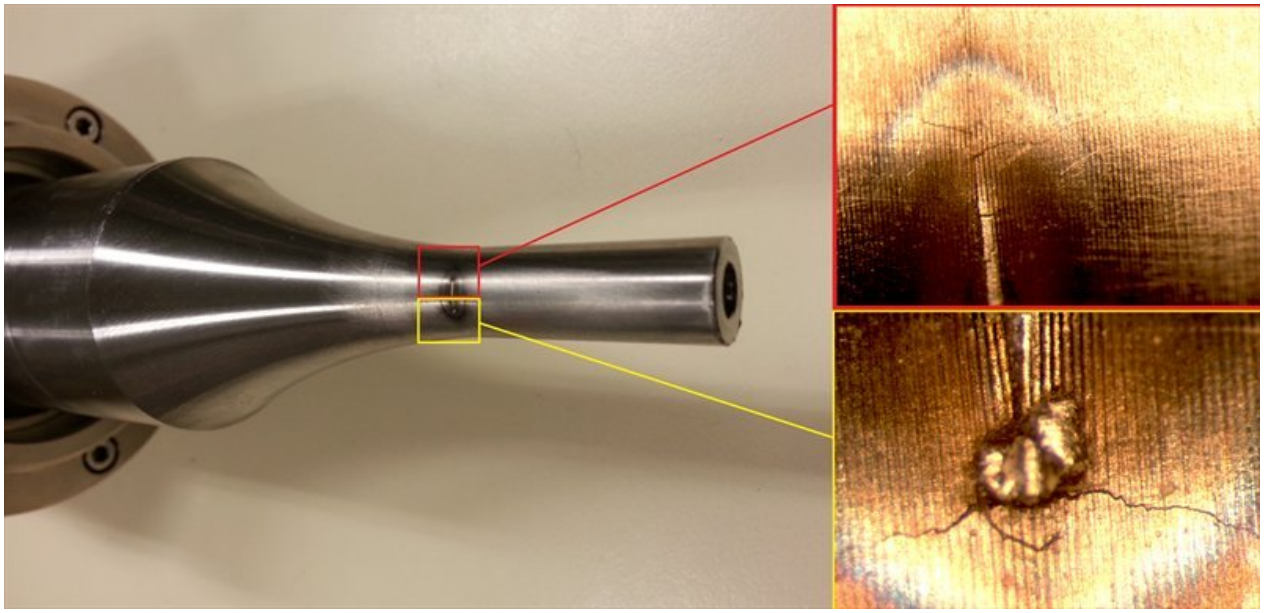

Figure 4.5: Torsion fatigue crack in zone of transition from hyperbolic to cylindrical part

Design of an ultrasonic torsion fatigue testing horn as usual consists of two steps: the first step is an analytical first order approach of horn geometry based on equation given in section 4.2 and the second step is an optimisation of horn geometry by using finite element analysis. On the first step some key dimensions, such as length of head part L_1 (Fig.4.2), length of reduce section L_2 and resonance length L_3 (part $N°3$) may be determined. According to ultrasonic concept, developed by C. Bathias, the length of head part for all types of ultrasonic horns should be equal to one-fourth of the elastic wavelength whatever the excitation mode

(tension-compression or torsion). The length of the reduce part is calculated based on simple geometric considerations that allows to reduce a stress concentration effect. The resonance length is a function of all the dimensional parameters (L1, L2, both diameters and constants of hyperbolic profile) and the mechanical properties of material (Dynamic modulus, density and Poisson ratio). On the second step an optimisation of horn dimensions can be carried out in order to get a more precise value of required natural frequency. During the optimisation process some correction of reduced section geometry can be introduced in order to reduce the effect of stress concentration. At this stage two important problems should be solved: to reach a high enough magnification factor and to reduce the maximum stress that always exists in zones of diameter changes, Fig.4.4 and Fig.4.6. The amplitude of angular displacement for direct transducer as usual does not exceed several mRad and has to be amplified by increasing the difference in diameters of 'input' and 'output' parts. The material for ultrasonic horns should be chosen so, that its fatigue strength must be significantly higher than acting cycle stress in transition zone.

The second prototype of ultrasonic torsion horn was designed according to C. Bathias concept. The length of 'input' part of torsion horn was equal to one-fourth of torsional elastic wave. The radius of reduced section was smaller, compared to the first prototype and resonance length adjusted to get the required natural frequency, Fig.4.6

The smaller radius of reduced part lead to increase shear stress amplitude in transition zone, but at the same time makes the horn more rigid that is a favourable factor for ultrasonic elements. Higher rigidity of horn provides to obtain a clear spectrum of natural frequencies and escape spurious modes of vibrations. Moreover, the configuration presented on Fig.4.6 provides a higher magnification factor, that is almost 15 % higher for more rigid horn. In spite of increased horn mass of horn, the difference in power consumption is not so significant, because of resonance character of vibrations. Thus, comparing all the benefits and weak points of both designs, the final design was realized according to more usual (classical) concept of ultrasonic fatigue testing systems [3].

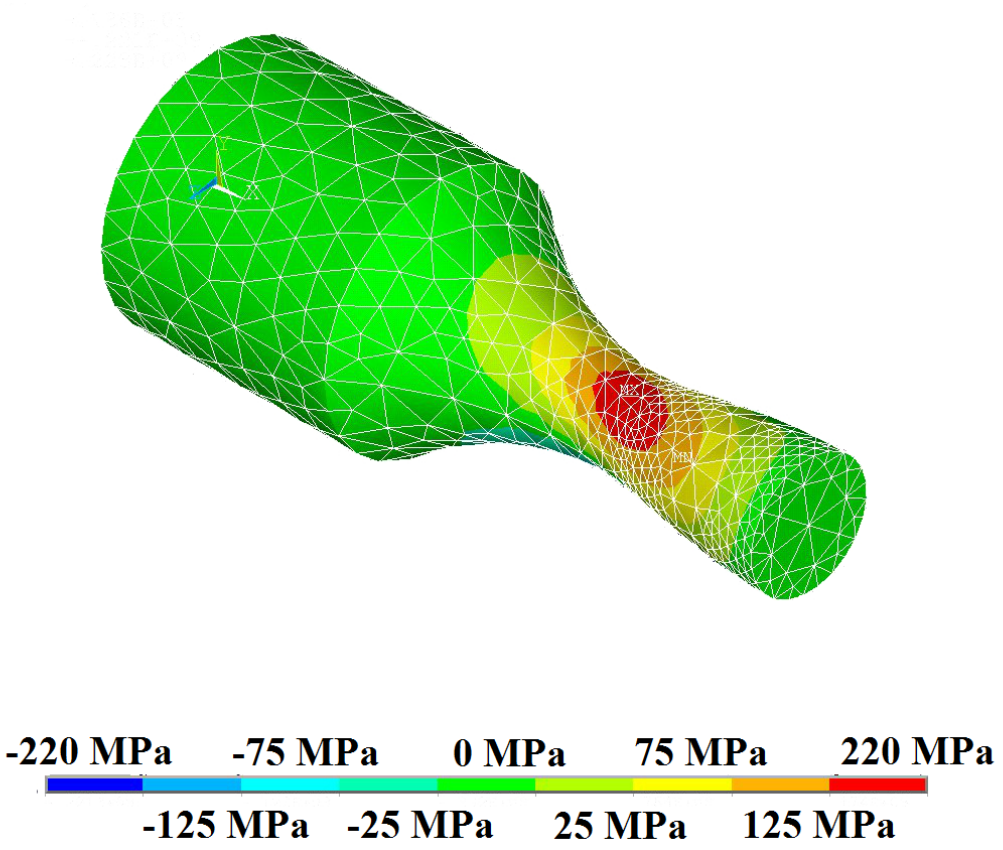

Figure 4.6: Shear stress distribution within torsion horn with 'input' length of 1/4 wavelength

4.4 Calibration of the torsion system

The principle of ultrasonic torsion testing system calibration is the same than for tension-compression testing systems. It is a determination of the relation between stress amplitude in gauge section of specimen and applied tension of controlling signal. However the procedure of torsion system calibration has its own nuances and difficulties. First of all, the ultrasonic vibrations are angular, that makes almost impossible to use optical linear displacement sensor that is used for longitudinal horns calibration. Nonetheless some efforts were made to use the optical (laser) sensor for torsion machine calibration. The main idea is to attach a small plane sheet of metallic material to lateral surface of torsional ultrasonic horn where are a maximum displacements are expected (minimum stress amplitude), Fig.4.7.

This sheet of material will have a longitudinal component of displacement due to rotation, which can be measured by optical sensor and recalculated into twist angle. This method can be used just to determine the order of magnitude of vibration but it is not accurate enough. Thus, another calibration technique should be used. The modern measurement techniques of ultrasonic vibrations can be classify into two principal groups: (1) non-contact

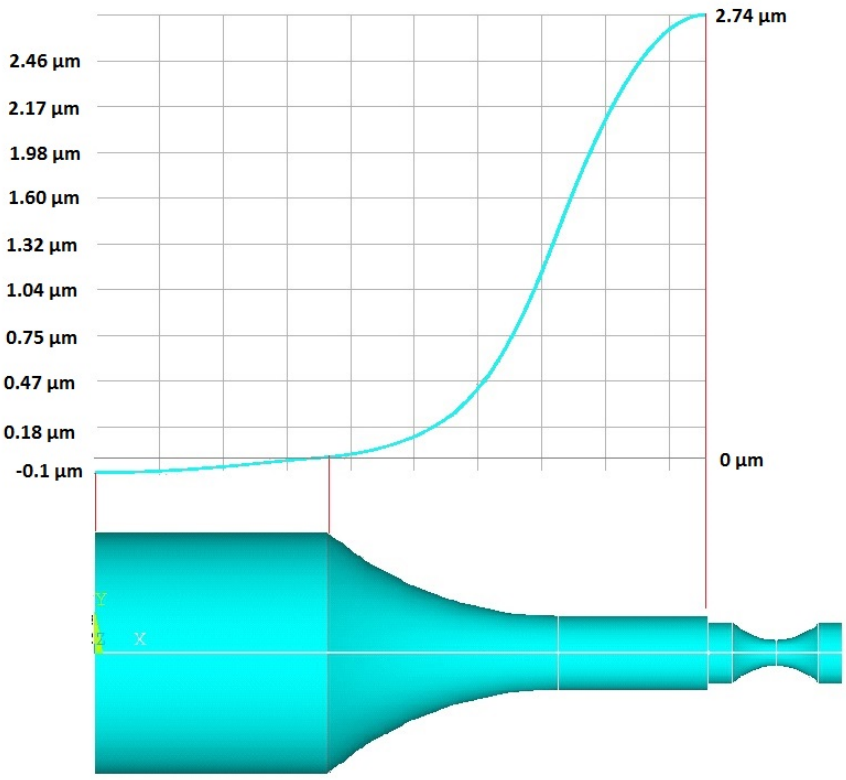

Figure 4.7: Distribution of torsion displacement along the ultrasonic horn axis

methods and (2)contact methods. The first non-contact group contains several techniques, from relativity simple, based on analysis of captured images at horns bottom or 'head'-part of specimen before vibration and during the oscillation [143], as well high-tech 3D laser scanning vibrometry [144]. The contact method is based on strain-gauge measurements which provides the measurement of deformation at surface in specimen working section. In the present study two (not-contact and contact) methods were used. The non contact method was realized by using specially designed microscope with portable USB camera [85] in the similar way than [143]. A small vertical scratch was plant at the specimen cylindrical 'head' part. Under stationary conditions this mark is a more or less straight line. When the vibrations starts, this line transforms into an area in the USB camera with low capture rate, Fig.4.8

The half of this area width is equal to the amplitude of torsion displacement which can be recalculated into twist angle by using a simple relationship between twist angle and radius of cylindrical part and torsion displacement $D_{tors} = R \cdot \varphi$. After getting an amplitude of torsion displacement, the stress amplitude in the gauge section of specimen can be calculated by using numerical methods, as well analytical solution. Even based on results presented on Fig.4.8, it is clear that this method has a limited accuracy and does not work very well

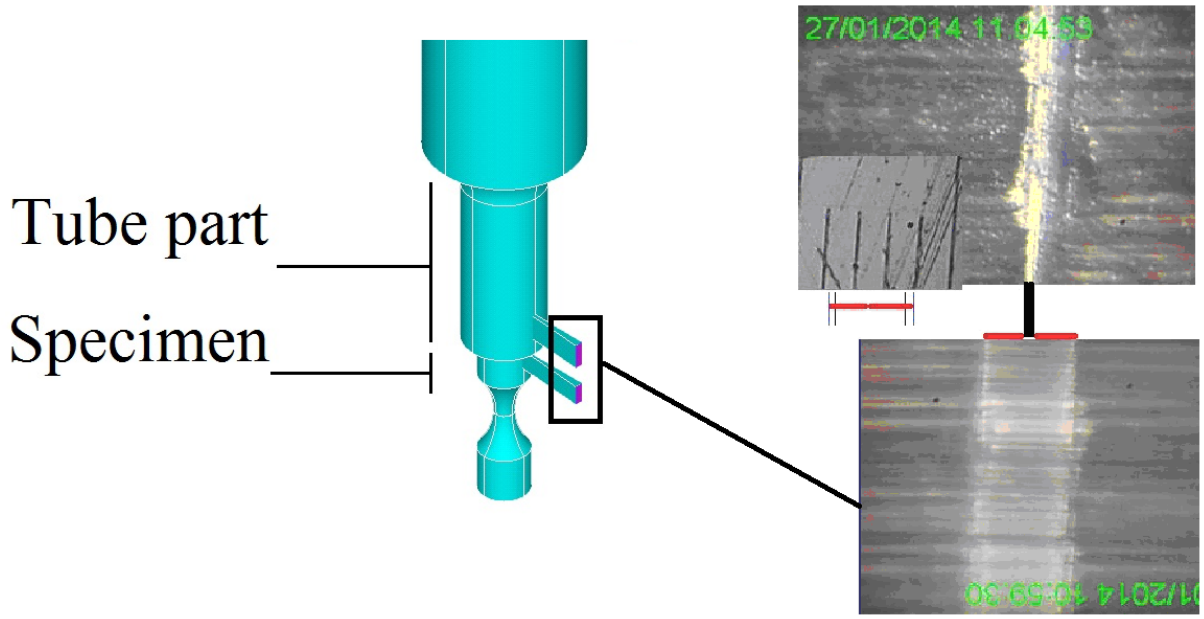

Figure 4.8: Scheme of non-contact calibration method for torsion system

under high twist angle amplitudes, because borders of illuminated area becomes less clear and sharp.

The contact calibration method was realized by using Vishay 2210 Signal Conditioning Amplifier System, oscilloscope to control the shape of the loading cycles, multimeter and strain gauge 1-XY40-0.6/120 HBM, Fig.4.9. The measurement technique is based on 1/4 Wheatstone bridge where the gauge is one of four resistances of 120 Ohm.

The calibration with a strain gauge was carried out for both forged and extruded titanium alloys. The results of calibration are shown in Fig.4.10.

The interest of non-contact method is that it does not require a special preparation of specimen. In case of strain gauge calibration the result is more precise, but individual calibration line should be obtained for each investigated material that needs a new instrumentation of gauge for each material.

In this study, the same VT3-1 titanium alloy but obtained by two different ways: forged technology and extrusion. That's why two specimens equipped by strain gauges were used for calibration. The results of piezoelectric torsion testing machine calibration are shown in Fig.4.10. Also, the result of calibration by the non-contact technique is presented in the same graph to compare two types of calibration methods (non-contact and contact). The non contact method is available for low amplitude measurements but in the case of high values of twist angle it should be improved to increase an accuracy or replaced by strain-gauge

Figure 4.9: Vishay System 2210 and strain gauge used for contact calibration

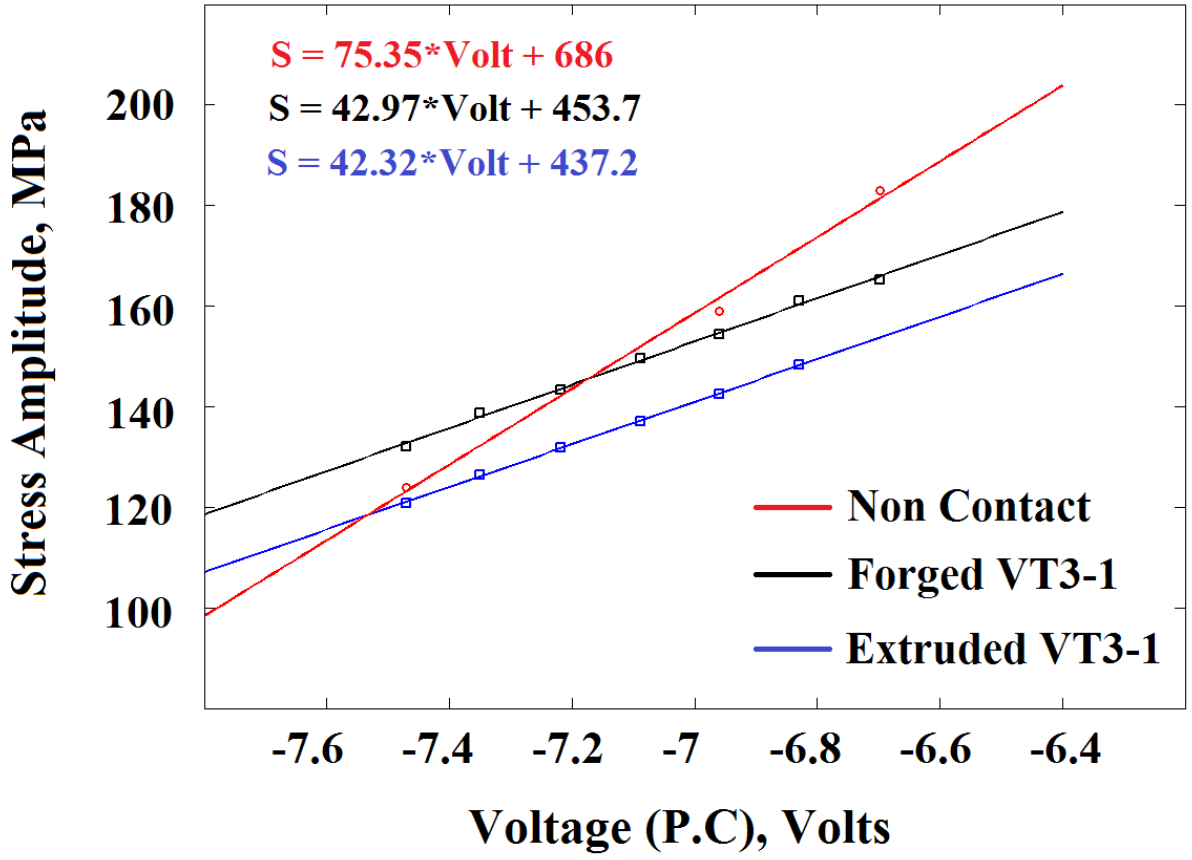

Figure 4.10: Calibration lines for torsion specimens: non-contact and strain-gauge methods

technique. In the present work all the calibration lines were obtained by using strain-gauge calibration method, because it gives more precise results.

4.5 Specimens for torsion tests made from VT3-1 titanium alloy

As noted above, the VT3-1 titanium alloy was produced by two different ways (forging and extrusion). The set of forged torsion specimens (6 samples) was machined from the rim part of the real compressor turbine disk used in this study to specimens. First, the cylindrical blanks were cut from disk by electro-erosion method and after the specimens were shaped by turning. The orientation of the specimen longitudinal axis was parallel to the compressor disk rotation axis. The extruded titanium alloy specimens were machined from bars of length 1.5 m and diameter 14 mm. The axis of extruded torsion specimens was parallel to extrusion direction. The extruded specimens were machined directly from cylindrical bars by turning. The blanks of forged and extruded titanium alloy are shown on Fig.4.11.

Figure 4.11: The blanks of VT3-1 titanium alloy: forged disk and extruded bars

The mechanical properties, micro-structure and chemical composition for both materials are discussed in Chapter II. The geometry of torsion specimens for ultrasonic tests, Fig.4.12, was developed based on results of dynamic modulus measurement by using analytical and numerical methods. The numerical simulation was used to adjust the resonance length of specimens.

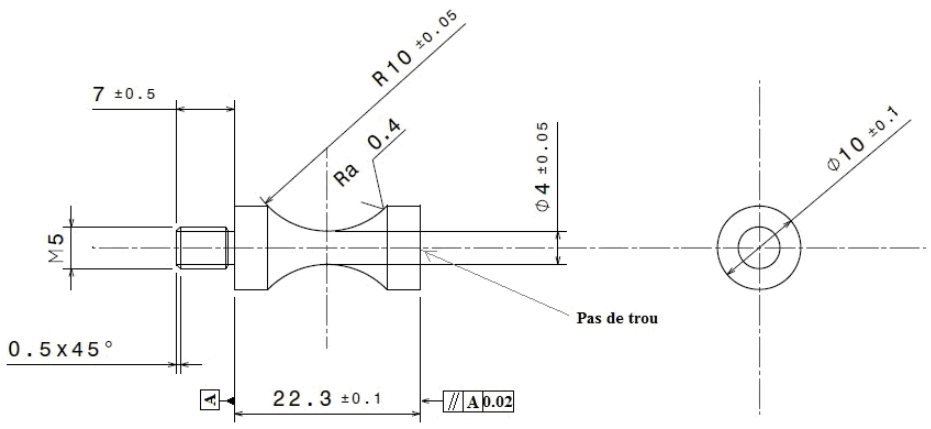

Figure 4.12: The geometry of ultrasonic torsion specimens made from VT3-1

4.6 Results of torsion tests on VT3-1 titanium alloy

4.6.1 SN-diagram for extruded and forged VT3-1

Fatigue tests on forged and extruded titanium alloys were carried out up to fatigue failure or run-out limit of 10^9 cycles in air. An air gun device was used to keep the temperature at the specimen's surface that is allowable for fatigue testing on titanium alloy. All the results were obtained by using the ultrasonic testing torsion machine described previously. The loading frequency of the machine is lying between 20200 and 20400 Hz, depending on the investigated material. All the investigated specimens were cracked at fatigue life being beyond of 10^6 cycles. The results of torsion tests in VHCF regime shows, that the SN-curve has continuously decreases with increasing the number of loading cycles beyond 10^6. This tendency is the same for both materials forged and extruded, Fig.4.13.

The resistance of extruded VT3-1 to torsion loading is higher compared to forged titanium alloy. This fact can be well explained by difference in mechanical properties which are also higher for extruded titanium alloy. Nonetheless, the slopes of both curves are quite the same. The scatter of fatigue life in the case of torsion loading is smaller compared to tension-compression (R=-1) regime that is probably due to limited series of tests.

4.6.2 Macroscopic view of torsion crack in VT3-1 titanium

In case of VT3-1 titanium alloy, the torsion specimen is never broken into two parts, because of high enough ductility of the material. As usual, fatigue crack detected automatically by the ultrasonic testing machine based on the frequency. In some cases, the torsion crack can

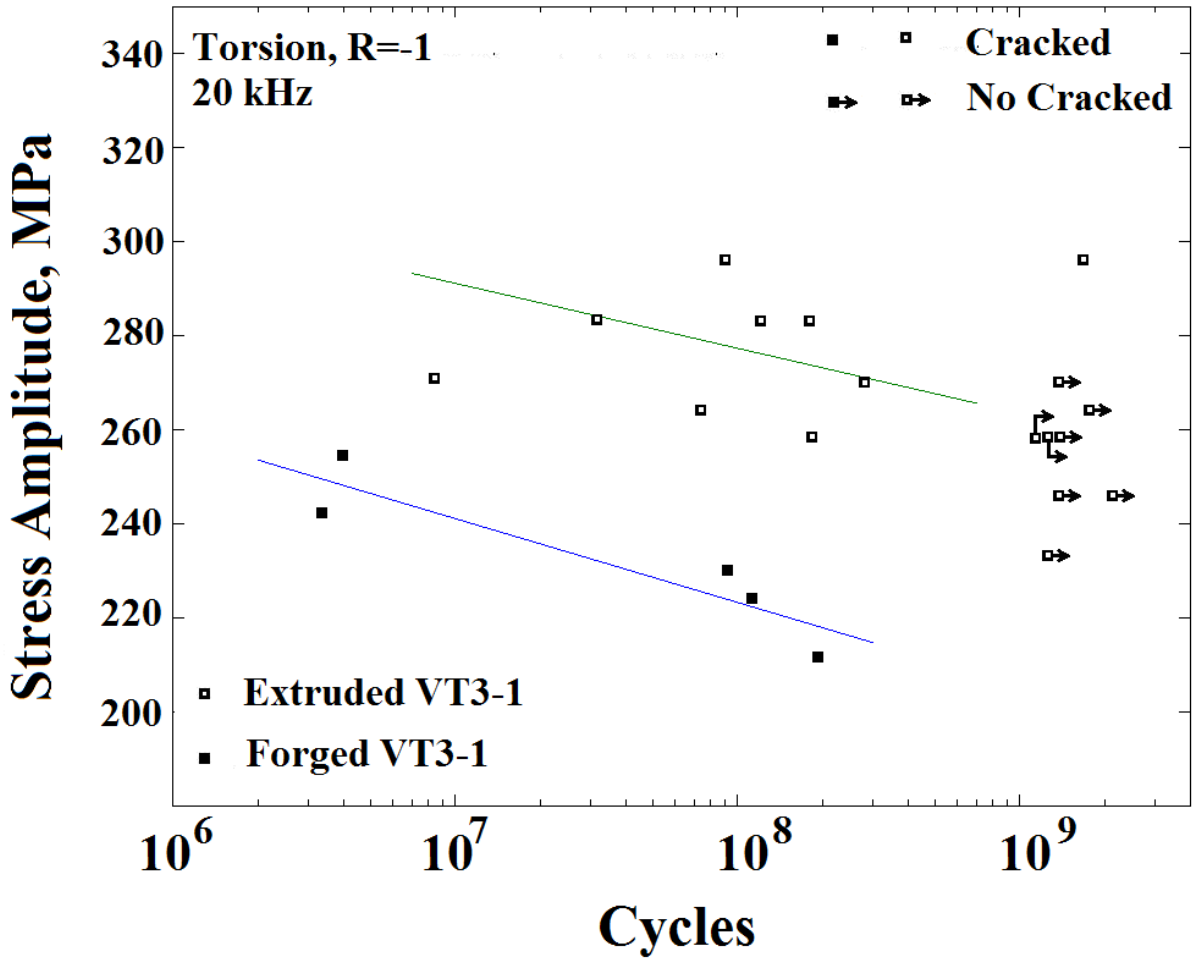

Figure 4.13: Results of ultrasonic fatigue tests on VT3-1 under pure torsion

be observed just by using optical microscopy. In all the observed specimens the fatigue crack or cracks have an angle by the specimen's axis about 45°. The specimen could be cracked as by one main crack, as well by two almost equivalent cracks, Fig.4.14.

Under a higher magnification it is clear, that crack growth on 45° plane is typical for long enough torsion fatigue crack. The small crack initiates in one of the maximum shear planes, which are shown on Fig. 4.15. Therefore, the initial crack starts in perpendicular or on parallel to specimen's axis plane and growth up to a critical length. After reaching this length, the crack turns in the plane of maximum normal stress, which are mutually perpendicular and have the angle of 45° by the specimen's axis. Further, the developed torsion fatigue crack may have some branches, which are starting from the main crack and moves about the parallel to it. The same sequence of torsion fatigue crack growth under ultrasonic loading

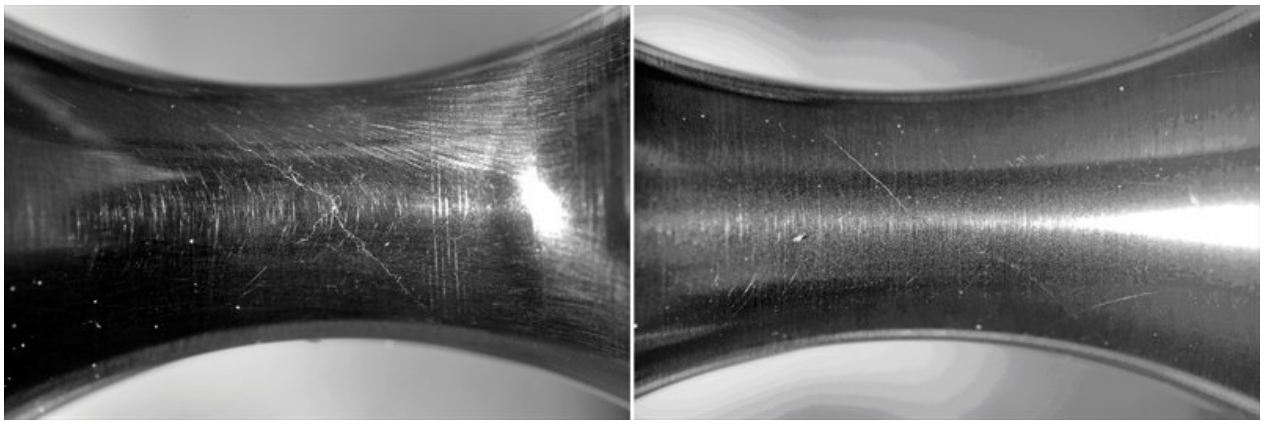

Figure 4.14: Results of ultrasonic fatigue tests on VT3-1 under pure torsion

was outlined for different structural metals such as steels, aluminium [137, 139].

4.6.3 Procedure of torsion specimen 'opening'

The combination of two factors: high enough ductility and relativity small size of torsion crack, does not allow to obtain the torsion specimen broken into two parts, Fig.4.14. In all investigated cases the torsion crack have changed significantly the stiffness (and therefore resonance frequency) of sample before the final failure. Consequently, the problem of specimen opening is appearing. There is several ways to open the torsion crack. In some laboratories an additional torsion cycles are applied to get specimen broken into two parts. It seems that such method can lead to introducing some additional damages at the fracture surface because of shear. An alternative solution is cyclic loading in longitudinal direction with positive stress ratio up to the final failure of torsion samples, but this is not always easy to realise, because of small specimen's size. Moreover, the torsion cracks have a very complex crack path with branching at the later stage of propagation. The cyclic loading, even under positive stress ratios in longitudinal direction can produce some friction between crack lips and therefore damages the fracture surface.

So, in order to open specimen and minimization the risk of introducing damage on the fracture surface, the new method of opening was introduced. The principle of this technique is the following: first, the crack tips should be marked by visible points (for example by spots of marker). The side with visible crack we will call 'face' and the other side is 'back'. When the position of crack is outlined, the specimen should be installed on the electro-erosion machine by the 'back' side to the thread and its position to be around 45 degree to the vertical. After, the position should be adjusted so, that two marked points at the crack tips were at

the same line with electro-erosion thread. The cut length should be little bit longer, that a half of specimen's cross section. The cut specimen is presented on figure 4.15.

Figure 4.15: The torsion specimen with 45 incision prepared for openning

Such procedure allows to reduce the non-cracked cross section (life section) of torsion specimen and therefore decrease the plastic deformation under tensile opening. The final specimen opening was realised manually in the way, allowing to keep the specimen under tension. This technique allows to avoid the cyclic loading which can damage the fracture surface as for crack propagation stage, as well for crack initiation. All the specimens were opened by this way. In the case of two fatigue cracks on the lateral surface, Fig. 4.14 (left), the longer crack was chosen as opening plane. The results of investigations on the crack path in torsion is given in the following section.

4.6.4 Microscopic view of crack initiation area: SEM observations on fracture surfaces

From a microscopic point of view, all the fracture surfaces can be separated into two main groups: crack initiation from surface and crack initiation from the bulk of material (subsurface crack). The torsion loading conditions are so, that surface crack initiation is more preferred due to maximum stress amplitude being at the specimen surface. However, as for forged, as well for extruded VT3-1 titanium alloy, the subsurface crack initiations were observed at

the long fatigue life. The crack initiation and crack propagation stages are sensitive to the micro-structure of material, the results for extruded and forged specimens will be presented separately.

Extruded VT3-1 titanium alloy

The crack initiation in extruded titanium alloy under pure torsion is depending from the number of loading cycles. The shorter fatigue life is characterized by surface crack initiation, while with increasing number of cycles the subsurface crack initiations were also observed. For all the specimens with surface crack initiation it can be stated that fatigue crack is always initiated on the plane of maximal shear stress (along or perpendicular to the specimen's axis). The shear mode crack is small and does not exceeds 30 μm. The typical torsion fatigue crack in extruded VT3-1 titanium alloy is shown on Fig. 4.16. The fracture surfaces for all specimens are presented in annex.

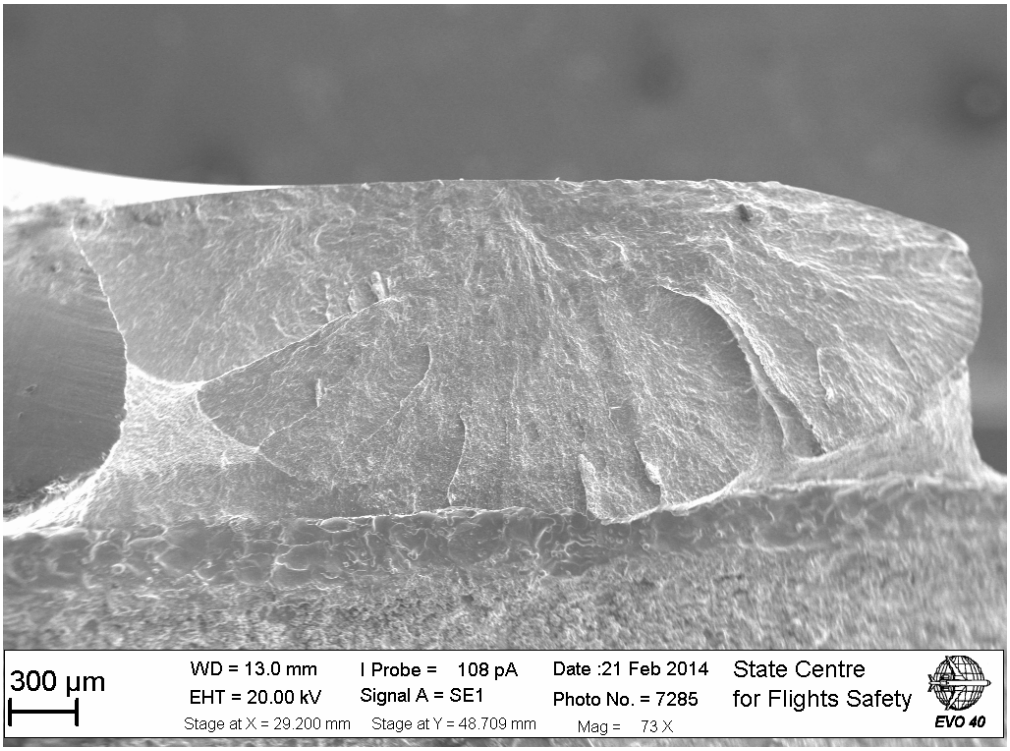

Figure 4.16: Torsion fatigue crack in extruded VT3-1 titanium alloy

Torsion fatigue crack starts from the surface and propagates in the bulk of material to the centre and along the specimen surface. The crack nucleates under the shear mode loading, that's why very often the initiation site is damaged by friction. Thus, there is no clear explanation of the crack initiation mechanism in extruded VT3-1 titanium alloy under pure

torsion, fig.4.17.

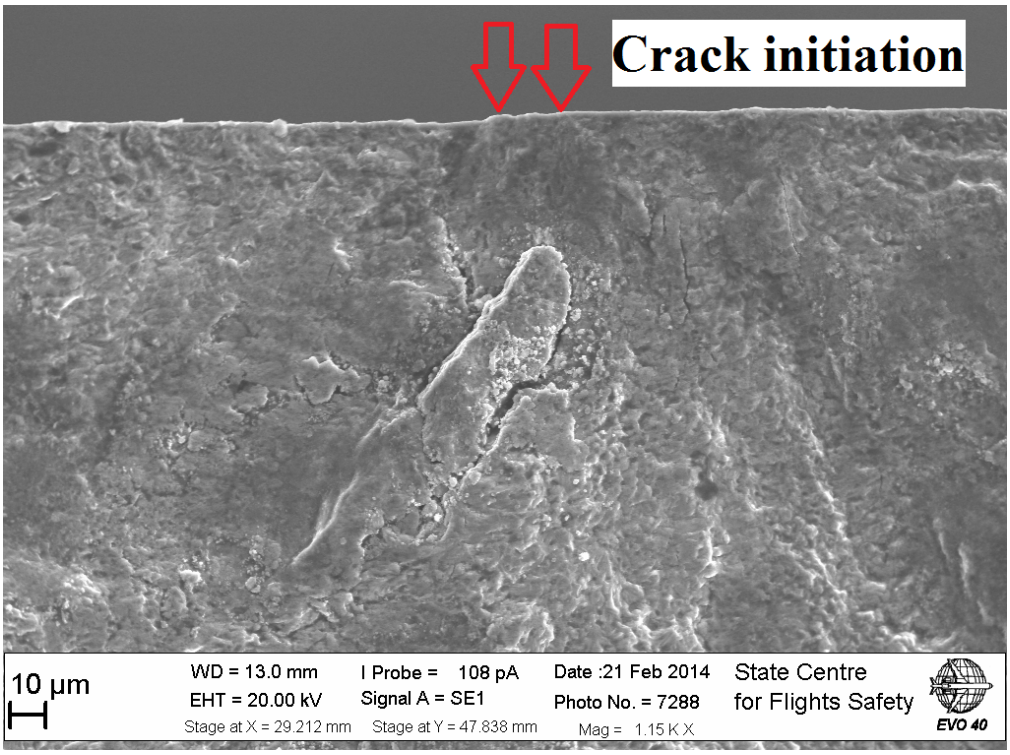

Figure 4.17: Details of crack initiation site in extruded VT3-1 under pure torsion

Far from the initiation site, the shear mechanisms of cracking turns to cracking under normal stress conditions and the fracture surface becomes clear. Starting from certain crack length the torsion crack starts to branch by forming typical wings or 'surfing waves' patterns, fig.4.18. These features of the fracture surface are formed by simultaneously crack growth in parallel planes. The crack moves from the crack initiation site into the bulk of material and turns to the plane parallel to the specimen's surface by forming 'pockets' at the fracture surface.

Forged VT3-1 titanium alloy

In the case of forged VT3-1 titanium alloy the crack initiation process seems to be more complex. The micro-structure with clear macro-zones and sharp borders between neighbouring clusters, significant disorientation between such zones makes the process of crack initiation and propagation less predictable. The fracture surface for forged titanium alloy (figure 4.19) is more perturbed compare to that formed in extruded VT3-1, figure 4.16 . The surface fatigue crack occurs in one of the two maximal shear stress planes (along or perpendicular to the specimen axis) and after turns to the plane of maximum normal stress.

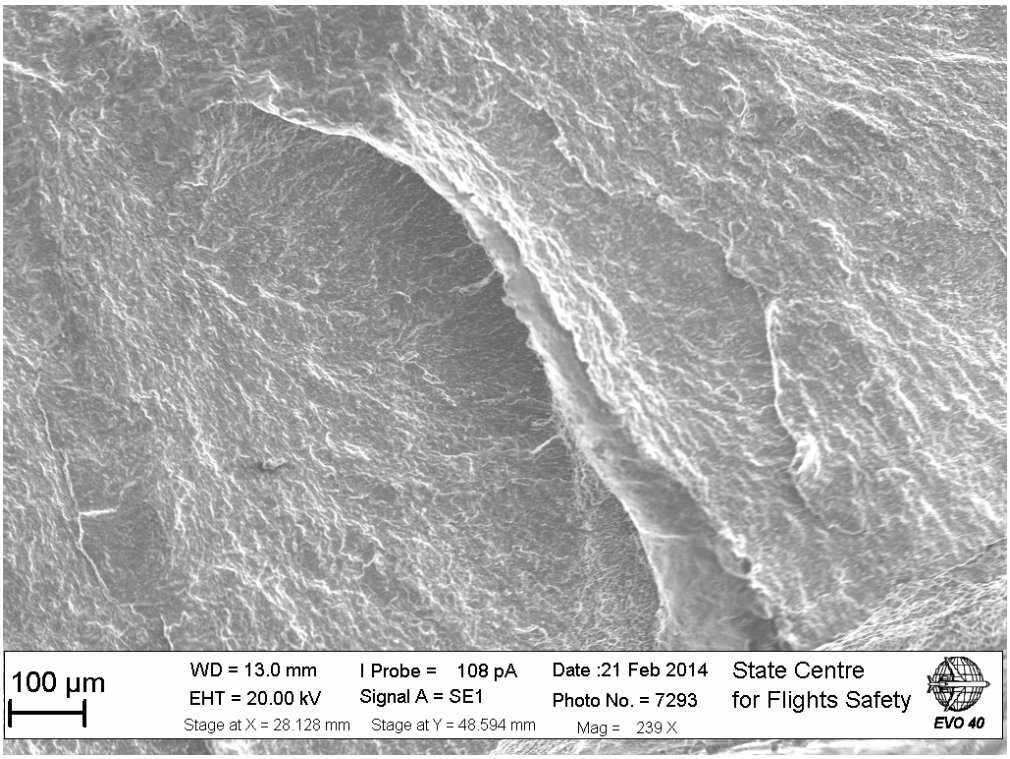

Figure 4.18: The 'surfing wave' fracture in extruded VT3-1 under pure torsion

The crack growing under the shear mode is longer for forged titanium alloy compared to extruded. But similarly to the extruded titanium, the fracture surface under shear mode is also often damaged by friction. Such morphology of fracture make difficult to establish the micro-mechanical mechanism of fatigue crack initiation in forged titanium alloy under pure torsion.

The torsion fatigue crack initiation is not always located at the surface of specimen. Sometimes, subsurface crack can be observed in forged VT3-1 titanium alloy, Fig. 4.20. In this case the crack initiated at location, where the macroscopic shear stress is not maximum. The example of internal crack initiation is shown on Fig. 4.21. The crack initiates from the border of structural element, marked in red on the picture. The secondary crack, which is present on the fracture surface shows, that considered initiation site is primary. This can be proved by the fact that fracture morphology around initiation site is already formed and the secondary crack interrupts the marks of crack propagation. The secondary crack propagated on the mutually perpendicular plane of maximal normal stresses. The fact of simultaneous crack growth in several planes make difficult the analysis of crack initiation sites and determination of the very first crack nucleation.

Frequently, several mutually perpendicular fatigue cracks nucleate almost from the same location but not all of them propagates longer than several tens of micrometers, figure 4.22.

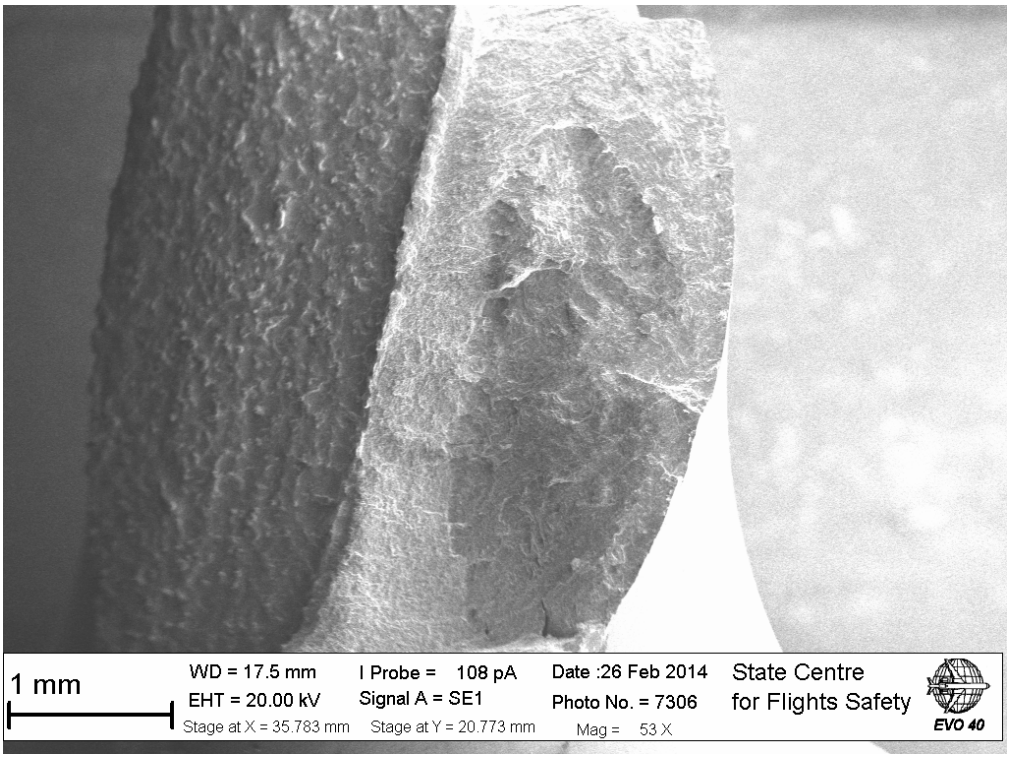

Figure 4.19: The fracture surface of forged VT3-1 under pure torsion

When the crack is long, the branching of crack path is very incentive in forged titanium alloy. Some almost equivalent torsion fatigue crack can growth in parallel planes up to the final crack length, figure 4.23.

4.7 Discussions and conclusion

As shown in Chapter IV, the new ultrasonic torsion machine working in continuous mode was successfully developed up to working prototype. The two different geometries for ultrasonic torsion horn were designed: as with shorter in-come part of 1/8 wavelength, as well with classical '1/4 wavelength part'. They are working well in the case of good finishing of horn lateral surface. However, keeping in mind the future development of torsion machine, namely an adaptation of ultrasonic torsion system for tests with superimposed positive static force, the classical design was chosen. The horn with '1/8' wavelength in-come part was designed to reduce the mass of ultrasonic horn, that allows to reduce the power consummation of the system, but as ultrasonic testing machine works in resonance regime, the power of piezoelectric transducer is enough to excite the vibrations in '1/4' wavelength horn. The successful sets of tests on forged and extruded titanium alloy has shown that ultrasonic torsion machine is capable to fail many structural materials such as two-phase titanium alloys,

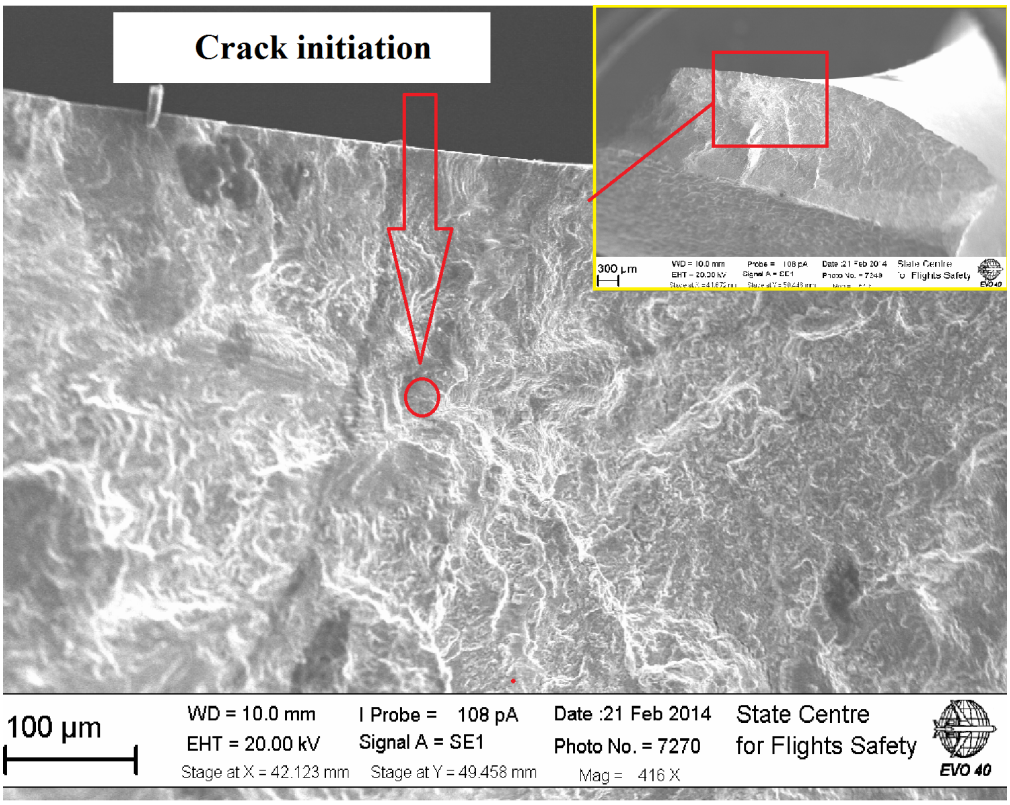

Figure 4.20: The fracture surface of forged VT3-1 under pure torsion

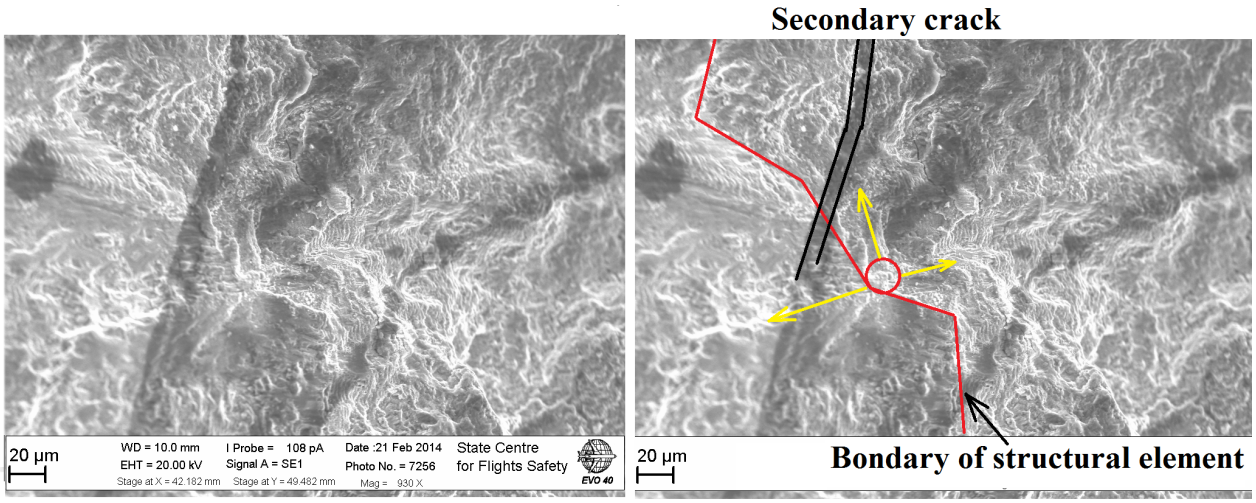

Figure 4.21: Internal crack initiation

used in aeronautic applications. Thus, regular fatigue tests under torsion can be carried out on material with high mechanical properties by using developed ultrasonic torsion testing

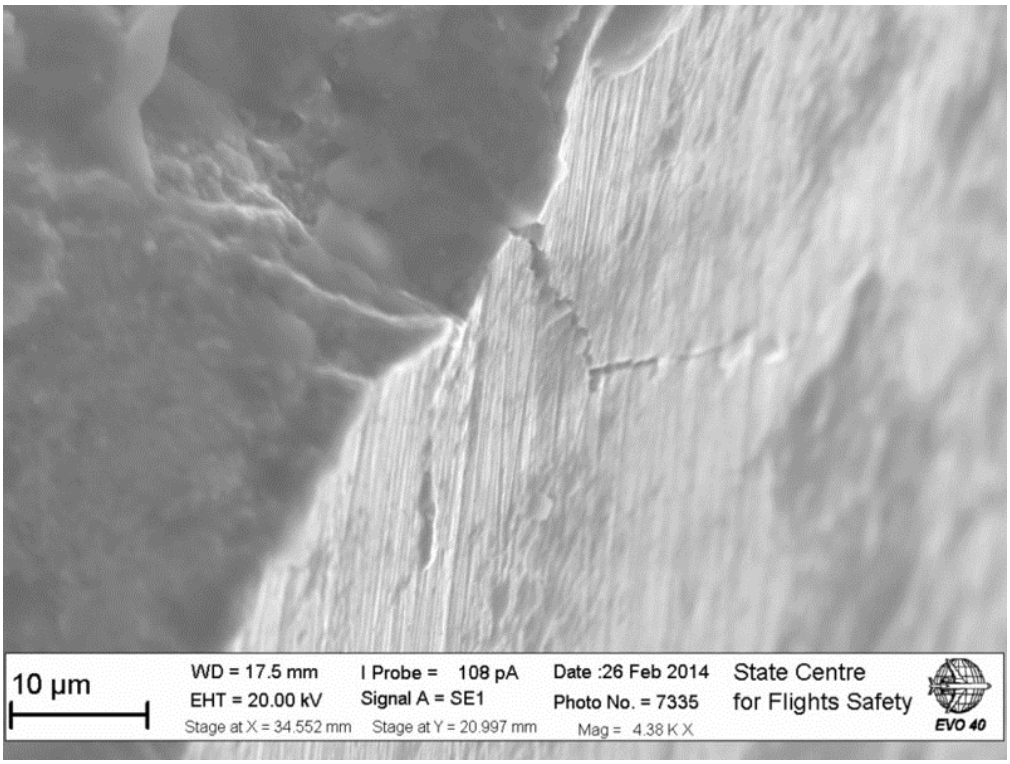

Figure 4.22: Non-propagated torsion crack on the surface of specimen

system.

The analysis of the specimen lateral surface have shown, that specimens were failed under pure shear mode. The crack path as in extruded, as well in forged titanium alloy is similar to the tests with low frequency performed in HCF range. Usually, the torsion fatigue crack under ultrasonic loading nucleate in the plane of maximal shear stress and after reaching a certain critical length turns to propagate on the plane of maximal nominal stress (45 degree respected to the specimen's axis). The results of investigations show, that several types of crack initiation can be realised: one single crack with initiation on maximum shear plane along or perpendicular to the specimen's axis; crack initiation on shear plane with following crack growth in two perpendicular cracks, which are orientated at 45 degree with respect to the specimen's axis. The ultrasonic torsion system has a control, which interrupts the test if the specimen natural frequency significantly drops. Thus, for all ductile material the problem of specimen's opening exists. A new method of specimen's 'opening' was developed for specimens with torsion crack. The new technique reduces the risk of fracture surface damage by high plastic deformation that may occurs during the 'opening'.

The very first result of ultrasonic fatigue torsion tests on the aeronautical VT3-1 two-phase titanium alloy were obtained. It has been found, that two types of crack initiation

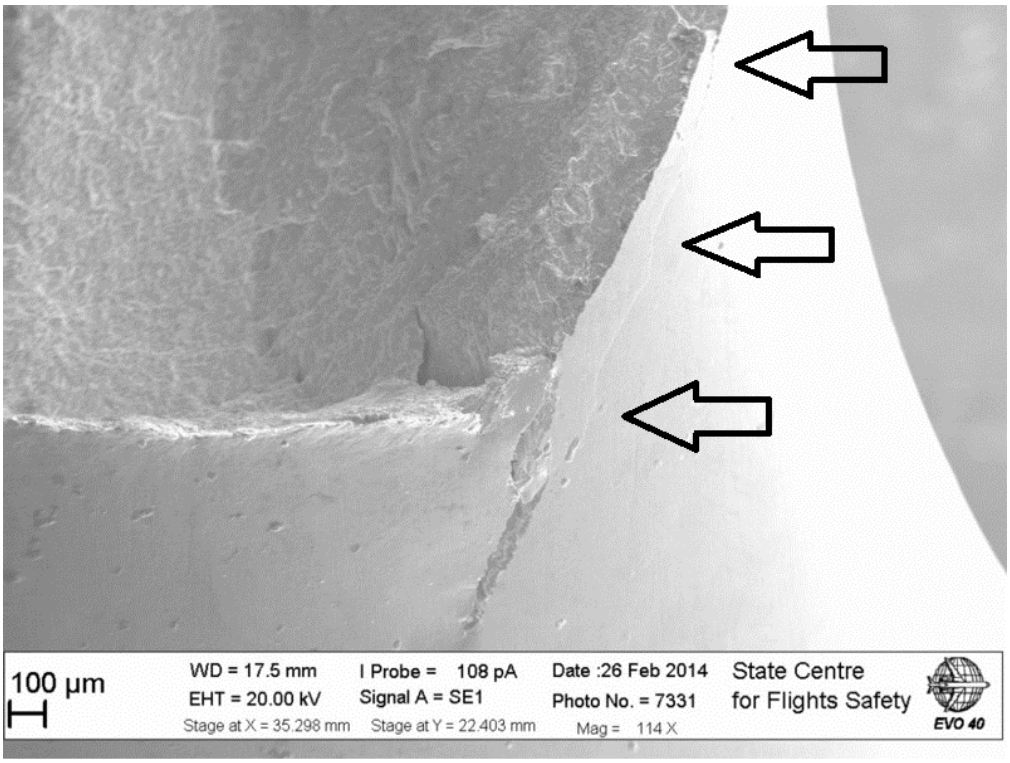

Figure 4.23: The twin of the main torsion crack as a result of crack branching

(surface and subsurface) can be observed as in forged, as well in extruded VT3-1 titanium alloy. In all cases the crack initiates on the plane of maximum shear stress and when the crack length reaches the size of several grains the crack bifurcates into the maximum normal stress plane. Sometimes, cracks growth up to a noticeable length in mutually perpendicular planes. Far from crack initiation site, the torsion crack starts to branch and sometimes the twin-cracks can growth in parallel to the main crack plane up to the last loading cycle.

The analysis of crack initiation site for forged titanium alloy have shown, that two types of crack initiation sites: surface and subsurface, can be found for VT3-1 alloy. In case of surface crack initiation, the nucleation site is often damaged by friction, which is typical for shear mode. In case of internal crack initiation, the crack nucleation site is more clear, that allows to assume, that components of normal stresses are also responsible for internal crack initiation even under the torsion loading. The internal crack under torsion loading occurs at the border of micro-structural elements, which are probably associated to the macro-zones, which were found for forged titanium alloy micro-structure. The fracture surface of forged titanium alloy is very perturbed, that highlights the complex micro-structure of forged VT3-1 titanium alloy. Far from the crack initiation site, the tendency to the crack growth in parallel planes (branching) is slightly noticeable. The developed crack has the tendency to turn in

direction to the specimen's surface, thus the torsion crack gets an elliptical form and does not reach even a half of specimen cross section.

In order to compare the mechanism of crack initiation and fatigue strength under the torsion loading for the same VT3-1 processed by extruded technology, the set of extruded specimens was investigated. The results have shown, that crack initiation in the case of extruded titanium alloy can be also located as at the specimen surface, as well in the bulk of material (subsurface initiation). The morphology of crack is less perturbed and a zone of branching can be determined. In the branching zone, the torsion crack growth in the parallel planes of maximum nominal stress. The developed crack has the similar tendency to turn in direction, parallel to the specimen surface. Such features of crack growth forms the 'surfing-wave' patterns on the fracture surface. The same patterns can be recognized on the fracture surfaces of forged material, but they are less expressed. Nonetheless, the branching process was not so expressed at the surface of specimens made of extruded VT3-1 titanium alloy.

Therefore, it seems that the existence of large zones, which can be called 'macro-zones' has an influence on the fatigue crack initiation and growth as under tension, as well under torsion loading. Such elements of micro-structure leads to significant branching of torsion crack and multi-crack origination. Moreover at the later stages of crack growth it can lead to twin cracks in the planes parallel to the main crack.

Chapter 5

Conclusion and perspectives

This PhD thesis has two main purposes: study the fatigue properties and crack initiation mechanisms in forged and extruded VT3-1 titanium alloy in VHCF range (10^6 - 10^{10} cycles); development of a new ultrasonic fatigue testing system for pure torsion tests in gigacycle regime and first experiments in torsion on the previous titanium alloys.

Forged VT3-1 titanium alloy.

Specimens made of forged VT3-1 titanium alloy were machined from aircraft Tu-154 compressor disk. The main part of specimens (3 sets between 6) were machined from the rim part of the disk, where a problem of additional stress field was assumed due to influence of blade vibrations. These sets of specimens were aimed to investigate the basic very high cycle fatigue properties and mechanisms of crack initiation under fully-reversed tension and torsion ultrasonic loadings. The other 3 sets of specimens were used to investigate a possible anisotropy in fatigue properties of the compressor disk due to forging. These specimens were machined from the plateau part of the disk in different directions (radial and circumferential) and all these specimens were designed for tensile fatigue tests. One set of specimens was used for fully-reversed fatigue tests in order to compare a fatigue properties between the rim and plateau parts. The last two sets were machined in two perpendicular directions in plane of the plateau. These two sets were used to investigate an anisotropy of fatigue properties within the plateau part of the disk. Moreover, these specimens were designed for pull-pull fatigue tests that make possible to derive a conclusion about the effect of mean normal stress on the VHCF properties and crack initiation mechanisms in forged VT3-1 titanium alloy.

Based on the results of fatigue tests on specimens machined from the rim part of the disk it can be stated that S-N curve for forged VT3-1 does not show a horizontal asymptote, i.e. fatigue strength is continuously decreasing with the number of cycles. The difference in median fatigue strengths at 10^6 and 10^9 reaches 15% that is significant. Experimental data

shows a significant scatter of fatigue life in VHCF regime. Under certain levels it reaches 3 orders of magnitude. Analysis of crack initiation mechanisms in forged VT3-1 shows a transition from surface crack to the subsurface origination with decreasing of stress amplitude. The transition from surface to subsurface initiation was found in the range of fatigue life from 10^6 to 10^7 cycles. In terms of stress amplitudes this transition is realized in the range from 415 to 430 MPa. Below $\sigma_a = 415MPa$ all the specimens are failed by subsurface crack. Based on precise analysis of crack initiation sites by Scanning Electron Microscopy (SEM) several subsurface crack initiation causes can be outlined. These mechanisms are (1) initiation from agglomeration (nodule) of coarse α-platelets; (2) borders of 'macro-zones' (large zones of similarity orientated α-platelets); (3) zones with significant segregation of chemical elements; (4) cracking with forming cleavage-like or smooth facets. The analysis of experimental data with taking into account the type of crack initiation mechanisms shows that these mechanisms are fatigue life controlling. Specimens with shorter fatigue life are typically exhibiting initiation from agglomeration of α-platelets or borders of macro-zones, while in case of longer fatigue life the crack initiation site is often a zone with chemical heterogeneities or smooth facets. All the observed mechanisms are in 'competition' between each other, but the sharp limits for each mechanism can not be determined.

The study on a possible anisotropy shows that there is no significant difference in fatigue properties between specimens machined from the rim and plateau parts of the disk. The same result was found for the specimens machined from the plateau part of the disk in different direction (radial, circumferential). The mechanisms of crack initiation are also independent from both the position and orientation of the specimen.

For the ultrasonic fatigue tests with positive stress ratio, the S-N curve also shows a permanent decrease in fatigue strength with increasing the number of cycles. The results are in well below the Goodman line in case of R=0.1. Likely there is a strong influence of mean normal stress on the VHCF crack initiation mechanism in forged VT3-1 titanium alloy. Under ultrasonic fatigue loading with superimposed static normal stress, the role of 'super-grain' boundaries becomes more important in fatigue damage accumulation compared to the fully reversed loading. The crack is typically initiated from such borders under R=0.1 loading. Moreover, the fracture surface shows large zones (several hundreds of micrometers) of quasi-brittle fracture. These zones are formed due to cracking by the border of macro-zones.

During this study several characteristic crack initiation mechanisms in forged VT3-1 titanium alloy were identified, but understanding the nature and building models of such mechanisms are still wanted. In order to do that, new investigations with more precise technique are required. In particular, the study of crystallographic orientation of smooth facets, zones with chemical heterogeneities and macro-zones is required. In case of macro-zones the

orientation of neighbouring zones is also should be studied. Probably there is a link between the crystallographic orientation of α-platelets within 'macro-zone', maximum disorientation between neighbouring 'macro-zones' and fatigue life. The knowledge about crystallographic orientation of object in crack initiation site will help to develop a model of fatigue crack initiation in VT3-1 based on models of plasticity in crystals.

During this work it was found that under positive stress ratio (R=0.1) the role of macro-zones borders becomes a dominating mechanism of crack initiation in forged VT3-1 titanium alloy. The further work in this direction should be an investigation on the same forged alloy under higher stress ratios (R=0.5, R=0.8 for example) in order to check the found tendency.

The absence of fatigue anisotropy between the rim and plateau parts of the disk should be explained. Probably it is due to the small size of α-platelets (several micrometers) and their random orientation, that makes macroscopic properties near isotropic. In order to prove this assumption additional numerous investigations on micro-structure forming during forging process should be carried out.

Extruded VT3-1 titanium alloy

For extruded VT3-1 titanium alloy, the S-N curve shows a permanent decrease of the fatigue strength with increasing number of cycles. The fatigue fractures were observed up to 10^9 cycles. The analysis of fracture surface shows that all the specimens have an internal fatigue crack with the same origination in all the cases of failure. It is related to the quasi-brittle fracture of agglomeration of very thin α-platelets. These platelets are formed within a primary β-grain. The crack initiation mechanism is the same for all the types of tensile fatigue tests whatever the stress ratios (R=-1, R=0.1, R=0.5).

The results of ultrasonic fatigue tests with positive stress ratios are lying between Goodman and Gerber lines for R=0.1 and on the Gerber line under higher stress ratio (R=0.5). In this case the fatigue behaviour of material is well described by existing empirical models (Goodman and Gerber). In contrary to the forged VT3-1 titanium alloy there is no 'macro-zones' in extruded alloy and the cracking mechanisms are practically the same. It was found that quasi-brittle fracture within primary beta phase have always an angle with the loading axis. All the investigated specimens show the same fatigue crack initiation mechanism, but different fatigue life. Thus, in case of extruded VT3-1 it could be interesting to analyse the size and orientation of such quasi-brittle facets and try to link it with the fatigue life.

Ultrasonic torsion tests

A new ultrasonic fatigue testing system for pure torsion tests was designed, built and installed during this PhD project. This axial machine is based on a piezoelectric converter creating a vibration in rotation and operating in continuous (no pulse pause repetitions). The

very first results on two-phase titanium alloy VT3-1 under torsion loading in VHCF regime were obtained. Like under tensile tests the VHCF strength under fully-revered torsion is continuously decreasing with increasing the number of cycles. The S-N curve has a larger slop compare with the tensile fatigue tests. It was shown, that as in case of forged, as well in case of extruded titanium two possible crack initiation mechanisms can be activated: surface and subsurface crack. The transition from one mechanism to another lead to shift to the remige of higher fatigue life (of about 10^9 cycles). As usual, the subsurface crack initiation needs a longer fatigue life compared to the surface initiation. The subsurface cracks are rare (1 specimen between 5 in case of forged titanium and 1 specimen between 9 in case of extruded titanium). The reason of subsurface crack initiation is still under discussion, because no strong defects of microstructure has been found in the site of torsion fatigue crack initiation. Typically, the macroscopic stress field under torsion tests consists of shear. The shear stress has its maximum at the surface of the specimen. Probably an internal crack initiation can be related to local normal stress components at the grain scale.

Thus, the further works on the torsion behaviour of titanium alloy should contains as experimental work (get more specimens with subsurface cracks initiations), as well microstructure sensitive calculations of stress-strain fields in titanium alloy under ultrasonic fatigue torsion loading.

Chapter 6

Abstract in English

Results

According to someresent investigations on unexpected fatigue failures in components of turbo-jet engines [1] made of titanium alloy, the main reason for that are high frequency vibrations. These vibration causes are air flow through the aircraft engine. The maximum frequency can reach of about 4500 Hz [2]. Such loading conditions lead to so-called Gigacycle or Very-High-Cycle Fatigue (VHCF) [3] of vibrating elements. Typically, the fatigue failure in the VHCF regime (10^7 - 10^{10} cycles) occurs under stress amplitudes being below the classical 'fatigue limit' defined according to ASTM standard between 10^6 and 10^7 cycles. Commonly, under such loading conditions, the crack initiation mechanism is changing from single surface crack (in high-cycle-fatigue) to subsurface single crack (in VHCF). In the case of subsurface cracking, the role of microstructure becomes very important. Fatigue crack initiates from different flaws or heterogeneities of microstructure, such as non-metallic inclusions in steels, porosities in cast materials, colonies of alpha-platelets in titanium alloys, grain boundaries and other defects and imperfections depending on the material. Moreover, for some types of microstructural flaws (inclusions) the fatigue properties depend from parameters of the flaw [55].

The objective of the present PhD research project is to investigate the possible mechanisms of fatigue crack initiations in the two-phase titanium alloy VT3-1 (close to Ta-6Al-4Mo under VHCF loading and associate them with inherent microstructural flaws of the microstructure. Different loading regimes and modes (tension-compression, tension-tension and torsion) were considered to study their influence on crack initiation mechanisms. Influence of technological process and material flow (anisotropy) on fatigue properties and crack initiation mechanisms are also investigated in this project. The engineering objective of the present PhD project was to develop a new ultrasonic fatigue testing system for torsion tests.

The material used in this study is the $\alpha + \beta$ titanium alloy VT3-1 processed in two differ-

ent technologies: forging and extruding. The source of forged Ti-alloy is an aircraft engine compressor disk. The disk was in-service for 6000 flights that is equal to the guaranteed safety lifetime. After non-destructive control, that is mandatory after in-service, the disk has been transferred for fatigue investigations as not damaged element. The source of extruded Ti-alloy is extruded bars produced by Russian Institution of Light Alloys.

The tensile fatigue tests on VT3-1 titanium alloy were performed by using ultrasonic fatigue testing system for push-pull fatigue tests [53] and the torsion fatigue tests were performed by using a new ultrasonic torsion fatigue testing machine studied and designed within this study [145]. Both types of test were aimed to study fatigue strength at 10^9 cycles and fatigue crack initiation mechanisms in VHCF range (10^6 - 10^{10} cycles). All the tests were carried out under constant amplitude loading in continuous regime (no pulse pause) in the laboratory air and at room temperature. The testing procedure was automatically stopped when presence of macroscopic crack was detected (by monitoring the resonance frequency drop).

The specimens were designed according to the gigacycle concept [3] and all of them have a natural frequency close to 20 kHz. The positions of specimen in the ingot were determined by the purpose of this PhD project, Fig. 6.1.

The three sets of tension-compression (R=-1) specimens were machined from the rim and plateau parts of compressor disk. These specimens were used to determine the fatigue strength at 10^9 cycles, crack initiation mechanisms, influence of material flow (anisotropy). The sets of tension-tension (R=0.1) specimens were machined from plateau part of the disk. These specimens were used to investigate the effect of mean normal stress on fatigue crack initiation mechanisms and VHCF properties. Moreover, these results can be used to investigate the effect of anisotropy of fatigue properties within the plateau part of the disk. Last, one set of specimens for ultrasonic torsion specimens was machined from the rim part of the disk in order to determine an effect of loading mode on the crack initiation mechanism.

Four sets of specimens were machined from the extruded bars to investigate the effect of technological manufacturing process on the fatigue properties and crack initiation mechanisms in VT3-1 titanium alloy. These sets are: (1) tension-compression with R=-1; (2) and (3) tension-tension with R=0.1 and R=0.5 respectively; (4) torsion tests.

The main tendency for all the results, is that there is no fatigue limit for VT3-1 titanium alloy and fatigue failures were observed beyond 10^8 cycles for all the types of loading regimes and modes: tension-compression, tension-tension, torsion. All the fracture surfaces were investigated by scanning electron microscopy (SEM) in order to determine the mechanism of fatigue crack initiation in VT3-1 titanium alloy under VHCF loading. It was found that the crack initiation mechanism is changing from single surface to the single subsurface crack in the case of forged VT3-1 beyond 10^6 - 10^7 cycles. In the case of extruded VT3-1 just a

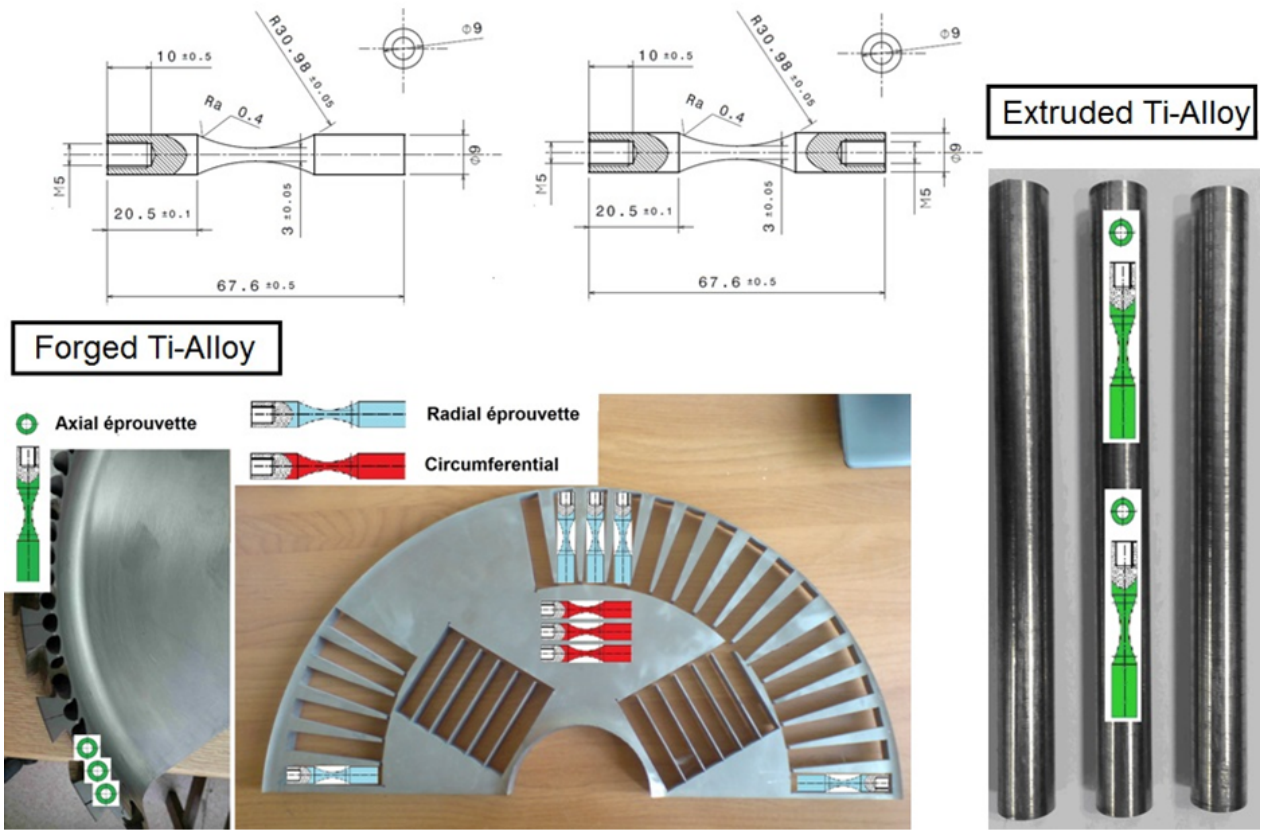

Figure 6.1: Position of specimens in the ingot: forged compressor disk and extruded bars

single subsurface crack initiation were observed, even at fatigue life of about 10^6 cycles. The detailed analysis on the crack initiation sites has shown that there are several mechanisms of subsurface fatigue crack initiation in forged VT3-1, while in the case of extruded Ti-alloy the mechanism is the same for all the specimens tested under tensile loading. In the case of torsion tests, the changing of crack initiation mechanisms was found for both materials. The fatigue life at which this transition was found is longer (about 10^9 cycles) compared to the tensile tests.

The main subsurface crack initiation mechanisms for forged VT3-1 are the following: (1) crack initiation from agglomeration (or cluster) of coarse alpha-platelets (defect of microstructure), (2) border of macro-zones (large clusters of alpha-platelets with similarl crystallographic orientation), (3) regions with chemical heterogeneities (segregation of stabilizing elements), (4) cracking with forming smooth facets. Under fatigue loading with positive normal mean stress, the mechanism of cracking from the borders of macro-zones turns to be the dominating initiation mechanism. In the case of torsion loading there is no other new micro-structural flaw responsible for subsurface crack initiation.

The main subsurface crack initiation mechanism for the extruded VT3-1 titanium alloy is quasi-cleavage of primary beta grains filled by very thin alpha-platelets. This mechanism was observed under all the loading ratios (R=-1, R=0.1 and R=0.5).

From the engineering point of view these crack initiation mechanisms lead to the following conclusions: (1) the macro-zones significantly reduce the fatigue properties of forged Ti-alloy under fatigue loading with positive stress ratios, while under fully-reversed loading this effect is less expressed; (2) primary beta-grains filled by thin alpha-platelets significantly reduce the fatigue properties of forged Ti-alloy under tensile loading, while under tensile mean loading there is no particular effect. The results of tensile-tensile tests are lying between Gerber and Goodman lines.

The PhD report

The PhD report consigns of 4 chapters. The Chapter 1 introduces the historical review on the problem of fatigue in metals and focused on the progress in knowledge about VHCF. It is shown a critical role of microstructure in the case of VHCF loading. The typical microstructures of two-phase alpha-beta titanium alloys are discussed and their influence on fatigue properties of such alloys. The ultrasonic fatigue test results available in the literature on typical two-phase titanium alloys are discussed too.

The Chapter 2 introduces the two materials or more exactly the unique VT3-1 alloy produced by two process (chemical composition, microstructure and mechanical properties), specimens (types, geometries and manufacturing locations in component or bars), experimental methods, conditions (tension-compression and tension-tension machines) and testing machine calibrations.

The Chapter 3 presents the results of tension-compression and tension-tension tests on all the types of tensile specimens. The analysis of the more representative fatigue crack initiation mechanisms is presented. SEM observations, a few EBSD and results of EDX analysis are discussing here.

Chapter 4 introduces the process of designing and installation of the new ultrasonic torsion testing machine. The details of experimental equipment and calibration methods are discussed in this chapter. The first results of ultrasonic torsion tests and analysis of fracture surfaces are also presented in this Chapter 4 on VT3-1 alloys.

The results of this study were presented on the following European and International conferences: 1. ECF-19 (Kazan, Russia, 2012); 2. Crack Path 2012 (Gaeta, Italy, 2012); 3. MSMF-7 (Brno, Czech Republic, 2013); 4. FDMD-2 (Paris, France, 2014); 5. VHCF-6 (Chengdu, China, 2014). Moreover, the results were also presented on several international workshops and regional conferencies. An international paper for Fat. Fract. Engng. Mater. Struct. International journal is under preparation for submission before end of 2014.

Chapter 7

Resumé étendu en français

Introduction

L'étude présentée dans ce manuscrit s'est déroulée aux Laboratoire Energetique, Mécanique et Electromagnetisme (LEME, Ville-d'Avray), Laboratoire Matériaux Endommagement Fiabilité et Ingénierie des Procédés (LAMEFIP, Talence) et Laboratoire au Centre de Sécurité des Vols en Transport Aérien (Cheremetievo-1, Moscou) . La thèse été dirigé par Emeritus Prof. Claude Bathias (LEME), Prof. Thierry Palin-Luc (LAMEFIP) et Prof. Andrey Shanyavskiy (Cheremetievo-1). L'étude été realisé en cooperation entre Paris Université 10 OUEST Nanterre La Defense et Moscou Université d'Aviation Technologique. Le financement a été accordée par l'entreprise LASUR dans le cadre de un bourse CIFRE.

L'objectif de ce travail été la problème de la fatigue dans un alliage de titane utilisé par l'industrie aéronautique. Le titane et ses alliages est largement utilisé dans le construction des avions et c'est pour ça il y a beaucoup des variations dans les types de chargement. Les alliages de titane sont utilisé pour fabrication les elements de la fuselage (resistance contre haut témperatures), train d'atterrissage (resistance contre la charge élevée et repetative), elements de turbine (la chargement avec haute frequence) [146]. En cas de les chargements répétitive élevée (la fatigue oligocyclique) et moyenne (la fatigue megacyclique), la problem de la fatigue est bien etablié et étudié. La multitude des résultats expérimentaux sont disponible dans le literature pour le titane. Cependant, en cas de chargement avec haute fréquence, typiquement l'amplitude de contrainte est suffisent plus bas par rapport de la fatigue oligocyclique et megacyclique, mais le number de répétitions est très grand. Ce régime de chargement est s'appelle la fatigue Gigacyclique [3]. Ce domain de la fatigue est nouveau et n'est pas encore bien étudié. Donc, il n'a y pas l'expérience suffisante pour déterminer les recommendations sur le conception contre la fatigue gigacyclique. Cette problème est devenu très grave dans l'industrie aeronautique. Dans le livre [3] c'était remarqué que la durée de

la vie typique pour certain elements de motor de un avion est approché le 10^{10} cycles et plus. La propriétés mécanique des matériaux sont pas bien étudié en raison des limites du technique expérimentale classiques. Les techniques expérimentales classiques pour l'essai de fatigue sont supposé la fréquence de chargement maxi et 100 Hz. Donc, un essai de fatigue jusqu'à 10^{10} cycles exiger plus que 3 ans. C'est pourquoi le design des éléments pour un motor etait basé sur les concepts de la fatigue oligocyclique et megacyclique. Cependant, cette approche ne permet pas de réaliser le fonctionnement de moteur sans fissuration de fatigue en service. En fin de 1990e, c'était rapporté une serié de fissuration inattendu dans un disque de compresseur des avions [1]. Analyse de ces fissurations était montré que la fatigue était provoqué par les vibration en frequence haute (pas moins de 1 kHz) [2]. Pour retrouver les raisons de fissuration dans un alliage de titane sous le chargement vibratoire et étudier les méchanisms d'amorçage de fissure à trés grand number de cycles un alliage de titane aéronautique était examine dans la régime de fatigue gigaciclique.

7.1 Matériaux

Selon l'objectif de ce travaille l'alliage de titane pour l'essai en fatigue était obtenu de l'industrie aeronautique. C'est le alliage de titane VT3-1 (Ti-6Al-4 Mo) traité en deux process thermomécanique different: forgage à chaud et extrusion . En cas de forgage le matériaux etait formé dans un disque de compresseur de l'avion, Fig.7.1a. Le disque était utilisé sur un avion Tu-154 pendant 6000 vols à peu près. Aprés l'exploitation il était demonté de la moteur et remplacé par un autre en service régulier. Le disque était bien vérifié par le contrôle non destructif et transféré à l'université pour l'essai de fatigue comme le disque non endommagé. Ce type de matériaux est rare et il est cher pour l'étude systematique. Le deuxième type de traitements thermomécanique (extrusion) est moins cher et permet realisé l'étude systematique. Cependant, il n'est pas clair est ce que c'est possible à extrapoler les results obtenu pour le titane extrudé sur le titane forgé. Ce étudé était realisé dans ce projet là. Le titane extrudé était obtenu du les barres de l'alliage de titane VT3-1, Fig.7.1b. Les barres sont fabriqué par l'institut des alliages léger de la Russie (VILS) laquelle produit les alliage pour l'industries aeronautique.

La composition chimique de l'alliage de titane VT3-1 est la même pour le disque et les barres. La composition est presenté dans le table 7.1. Des éléments d'alliage principale pour le VT 3-1 sont aluminium, molybdène et chrome.

L'aluminium est renforcé la phase alpha de le titane, tandis que le molybdène et le chrome sont renforce la phase beta. Donc, l'alliage de titane VT3-1 est deux-phases alliage avec le microstructure sensible à un traitement thermique. La microstructure a l'influence très grave

(a) (b)

Figure 7.1: Le matériaux pour l'essai en fatigue gigacyclique (a) le disque de compresseur de la moteur pour l'avion Tu-154, (b) les barres éxtrudé fabrique par l'institut des alliages legér.

Table 7.1: La composition chimique de l'alliage de titane VT3-1

Fe	C	Si	Cr	Mo	N	Al	Zr	O	H	Ti
0.2-0.7	< 0.1	0.15-0.4	0.8-2	2-3	< 0.05	5.5-7	< 0.5	< 0.15	< 0.015	Bal.

sur la propriété mécanique de le deux phases alliage de titane. L'alliage avec la même composition chimique peut étre traité pour obtenir la globular or lamellar microstructures. Dans un étude sur l'influence de la microstructure sur les propriétés mécanique de Ti-6Al-2Sn-4Zr-6Mo est montré la gros difference entre résistance de fatigue de la microstructure globular et lamellar. Cette différence est atteindré 300 MPa. Dont, l'étude sur la microstructure est nécessaire pour l'alliage de titane avant l'essai de fatigue.

7.2 Microstructure

Pour l'analyse de la microstructure plusieurs échantillons était prepare à partir du le disque de la turbine et les barres extrudé. Typiquement le processus de la forgeage favorise le développement de la fibrage dans l'object forgé. La fibrage peut être provoqué l'anisotropie dans les propriétés mécanique et changement de la morphologie du microstructure dans le

directions et positions différent. En cas de l'extrusion, la microstructure de l'alliage a la symétrie axial et plus régular dans les sections different de la barre. C'est l'assomption général, laquelle était vérifié par l'analyse de la microstructure.

La complexité de la microstructure forgé exiger le 3D analyse de la microstructure dans la chaque position étudié. Pour ce faire les échantillons cylindrique était fabriqué à partir du position different dans le disque de compresseur. En suit, ces échantillons cylindrique était coupé en trois parties par des plans perpendiculaires, Fig.7.2. La même technique a été employé pour l'analyse de la microstructure de l'alliage extrudé.

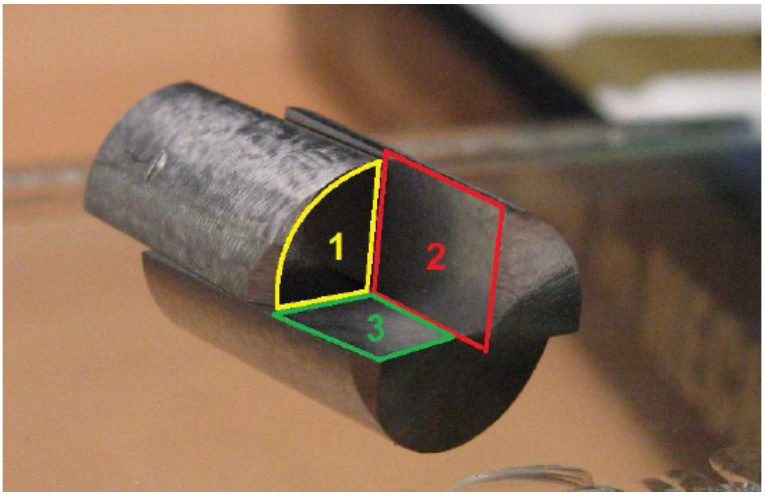

Figure 7.2: L'échantillon pour l'analyse de la microstructure en 3D (forgé et extrudé).

Chaque échantillon a été enrobé ou résine et a été polie mécaniquement. La surface poli a été attaqué par le KROLL (l'eau distillée 92 ml, HNO3 6 ml et HF 2 ml) pendant 40 sec pour l'observation de la microstructure. La microstructure typique de la titane forgé est represente par la alpha-platelets élongé laquelle sont séparé par le couche mince de la phase beta, Fig. 7.3.

Les tailles caractéristique de la lamelles sont 1-2 μm par 10 - 15 μm dans la direction de l'allongement. La phase alpha (la système réticulaire hexagonal) est blanc sur la Fig. 7.3, tandis que la phase beta (la système réticulaire cubique) est marqué comme noir. La même morphologie a été trouvé dans chaque facette de 3D analyse. L'analyse a été fait dans plusieurs position dans la jante et le plateau de le disque de compresseur.

En case de la microstructure d'un alliage de titane extrudé la morphologie de la phase alpha est beaucoup plus fine et moins élongé. Sur la facette à travers de la direction de l'extrusion, les tailles characteristique sont varié en cours de rayon. Au centre de la barre les tailles de la phase alpha sont plus ou moins 2 x 2 μm. Au bord de la barre les tailles de la alpha phase sont moins de 1 μm par 1 μm et la géométrie de la phase est présque round. En

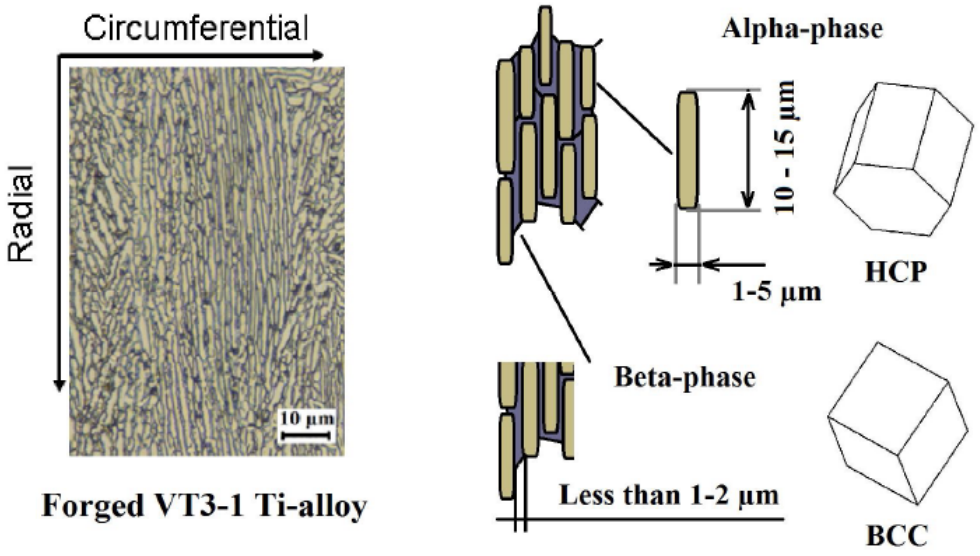

Figure 7.3: La microstructure typique de l'alliage de titane forgé

plus la microstructure au centre de la barre est bien perturbé par les defects produi par le process de le traitement thermomécanique. L'analyse de la microstructure sur la facette le long de l'axe d'extrusion a été montré la même variation de la taille de alpha phase en cours de rayon. La morphologie de la phase alpha est allongé le long de la direction de l'extrusion. Les 3D cartographies de la microstructure de l'alliage de titane forgé et extrudé sont présenté sur la Fig.7.4.

Le caractéristique particularité de la microstructure de le titane forgé est l'organisation des alpha lamelles dans les grand domaines de la similitude orientée plaquettes. Ce domaine a été s'appellé le 'macro-zones' [100] et c'était rémarqué l'influence du ces structures sur la résistance de fatigue en cas de la fatigue megacyclique. La taille de le 'macro-zone' est suffisant grand à partir de plusieurs centaines du micromètres au quelques millimètres, Fig.7.5. Typiquement les plaquettes de alpha phase laquelle se organisé dans un macro-zone sont plus fine par rapport de la taille caractéristique, Fig.7.3. Cependant, parfois il à y d'autre type de agglomération des plaquettes de la phase alpha dans laquelle la taille caractéristique est plus large par rapport de la taille normale. L'exemple de la zone avec les plaquettes rugueux est presenté au borde de la macro-zone sur la Fig.7.5 (sur la macrozone au milieu). C'est d'autre type de la defect grave de la microstructure de un alliage de tiane forgé.

Dans un alliage de titane extrudé la defect plus grave est la zone dans le centre de la barre. La morphologie de la microstructure ici est très sensible à la taille et geometrie de le grain de la phase beta. Très mince plaquettes de la phase alpha avec la même orientation

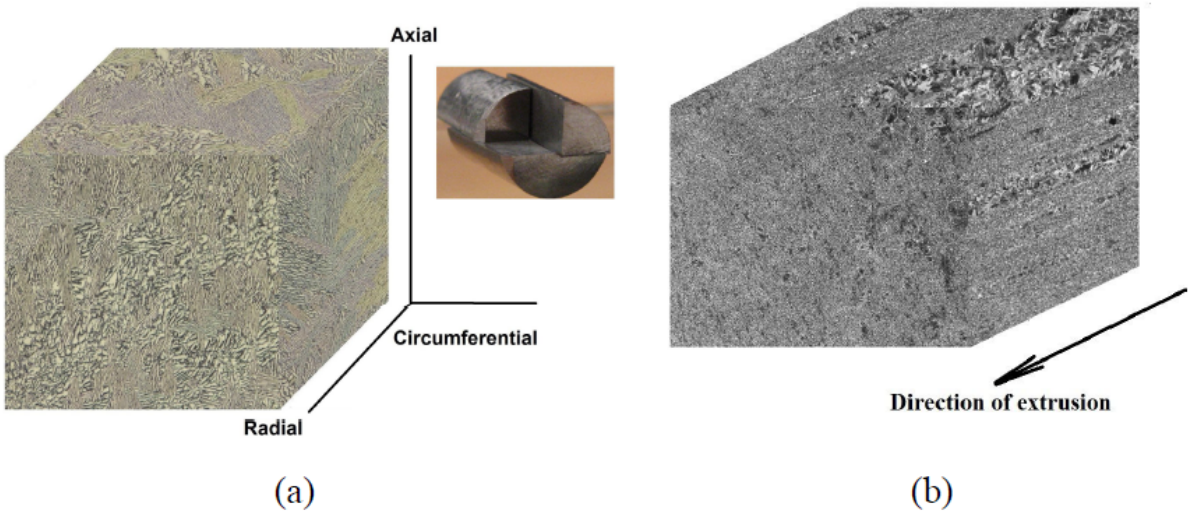

Figure 7.4: Les 3D cartographies de la microstructure (a) l'alliage de titane forgé, (b) l'alliage de titane extrudé

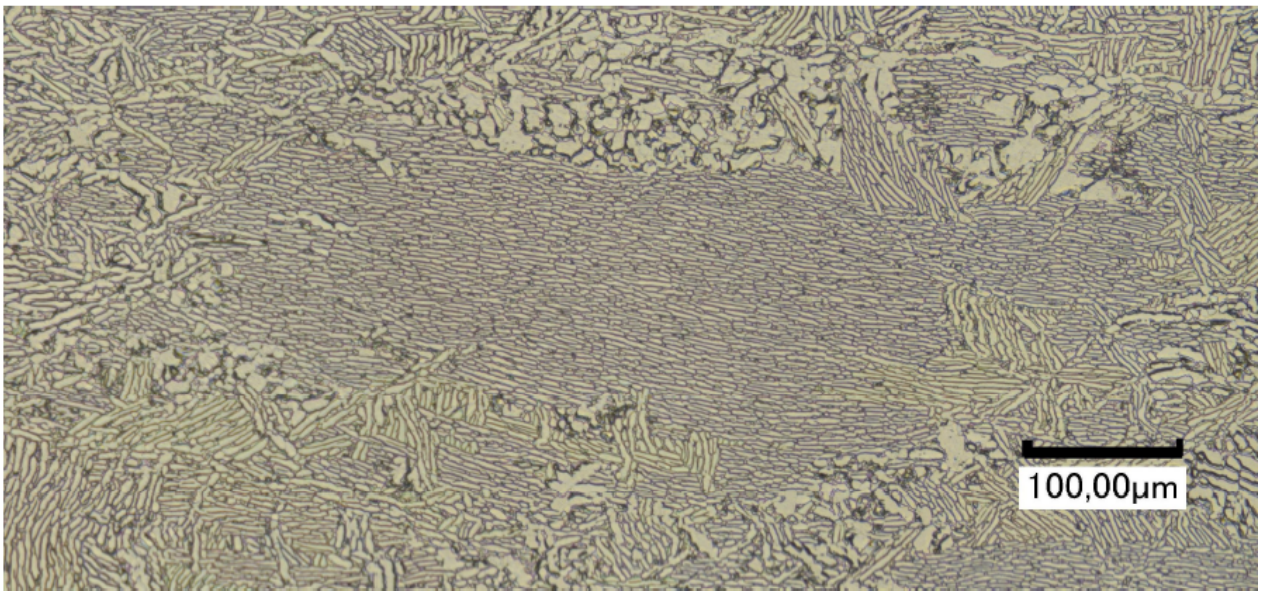

Figure 7.5: Le 'macro-zone' dans un alliage de titane VT3-1 forgé

remplir tout l'espace de grain bêta primaire, Fig.7.6.

Finalement, les microstructures des alliages de titane forgé et extrudé sont consiste les defects grave. Chaque fois c'est l'agglomération des plaquettes de la phase alpha. En case de le titane forgé la variation dans la morphologie est plus important par rapport de le titane extrudé. En case de l'alliage forgé l'agglomération de la plaquettes fin et rugueux, 'macro-zones' et quelques autres défauts a été trouvé. Il est nécessaire de souligner, comment il n'y

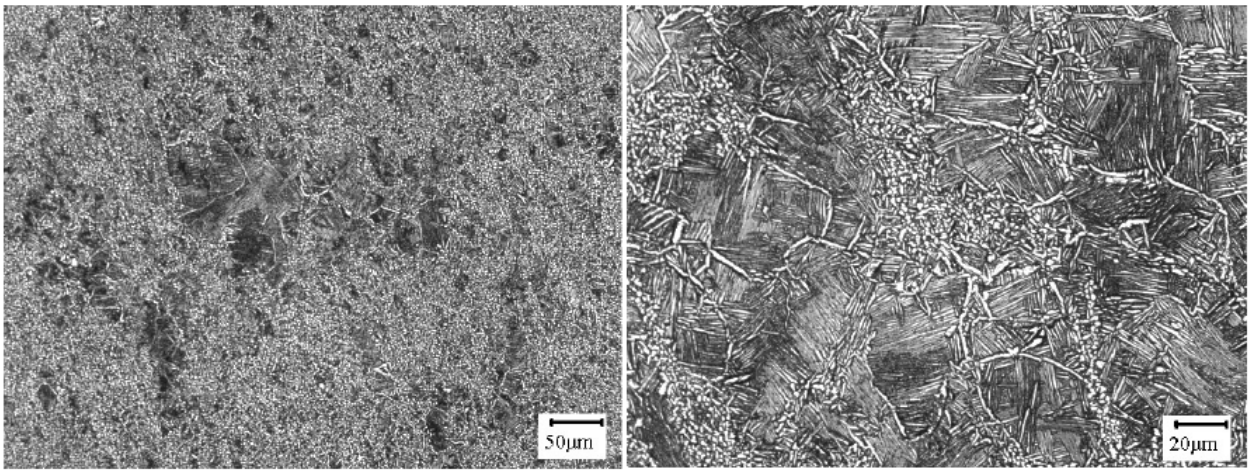

Figure 7.6: La defect de la microstructure de un alliage de titane VT3-1 extrudé (a) l'apparition de la microstructure dans le centre de la barre et (b) les grains de la phase beta primaire sont rampli par les plaquettes de la phase alpha

a pas aucune inclusion non métallique dans les deux alliage de titane. En cas d'un alliage de titane extrudé il à y juste une seul type de la defect grave c'est les plaquettes très fines de la phase alpha dans le grain beta primaire.

7.3 Microdureté

La microdureté a été étudié sur les échantillons coupé dans le trois planes perpendiculaire. La méthode d'essai était la mesure de dureté Vickers. Le poids utilisés est 500gr.; le temps de la penetration est 10 sec. Pour l'alliage de titane forgé toute les valeurs de microdureté trouvé sont presque la même pour chaque plan. La valeur moyenne de la dureté pour un alliage de titane forgé est 364 HV500. La dureté dans la macro-zone est normalement en peu plus bas par rapport de la valeur moyenne. Dans l'agglomérations de les plaquettes rugueux de la phase alpha, la microdureté est élevé.

En cas de l'alliage de titane extrudé la microdureté est en peu plus haute par rapport de le titane forgé. La valeur moyenne est 374 VH500. La microdureté à la centre de la barre est plus bas, Fig.7.7.

Si la point de mesure de la microdureté est dans un grain de la phase beta primaire, la valeur est suffisant plus bas par rapport de la valeur moyen, Fig.7.8.

C'est remarquable comment la microdureté dans une zone avec les plaquettes fin de la

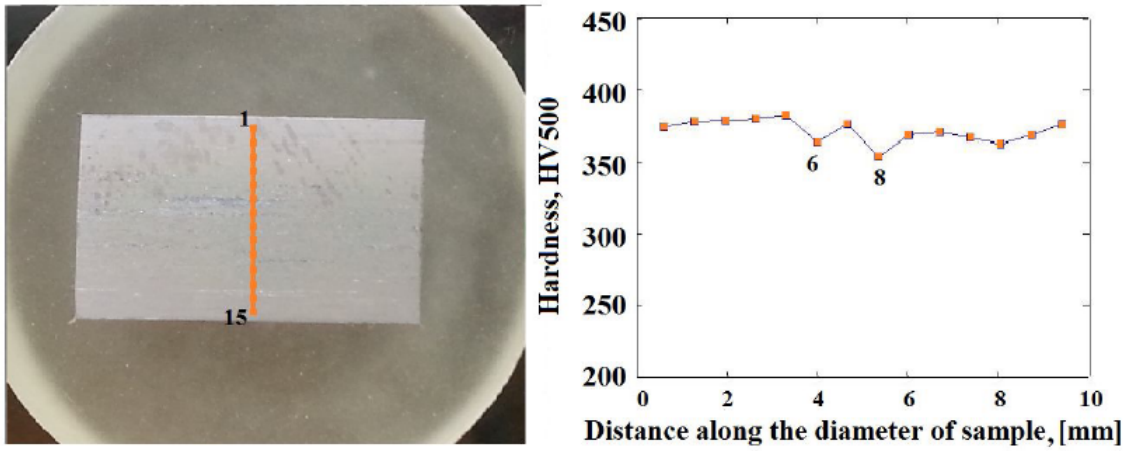

Figure 7.7: La microdureté d'un alliage de titane extrudé

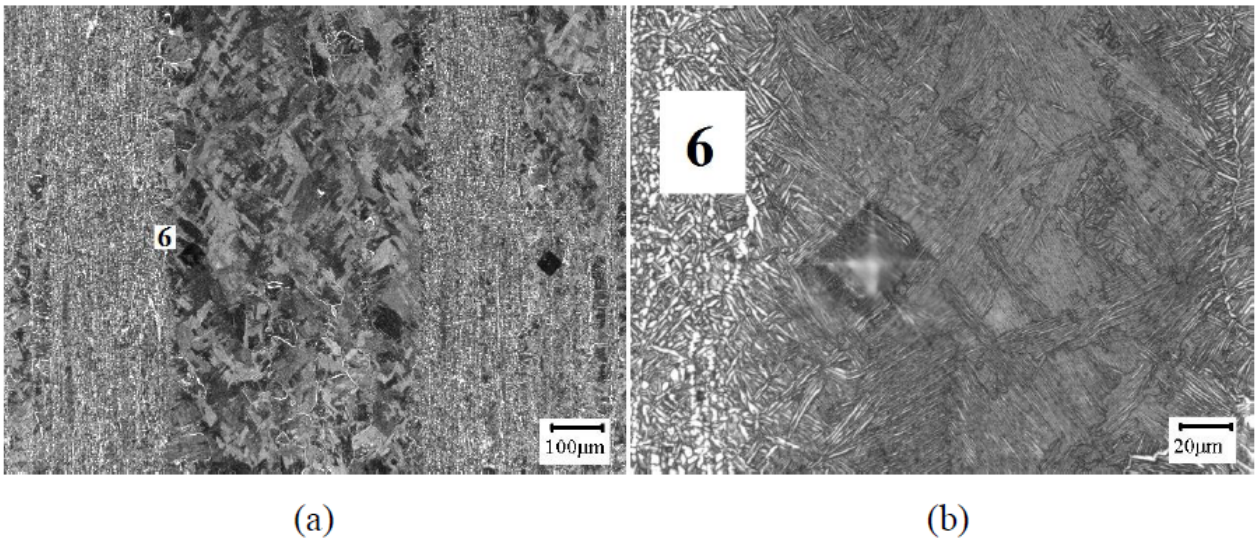

Figure 7.8: Le point N 6 de la mesure de la microdureté presenté sur la figure 7.7.

phase alpha toujours montre la microdureté plus bas par rapport de la valeur moyen. La valeur moyen est plus haute pour le titane éxtrudé.

La propriété mécanique

La propriété mécanique a été etudie pour le deux alliages de titane sur la même mini-échantillon de traction quasistatique, Fig.7.9. l'essai a été effectué sur une machine de traction INSTRON avec electromecanique activateur.

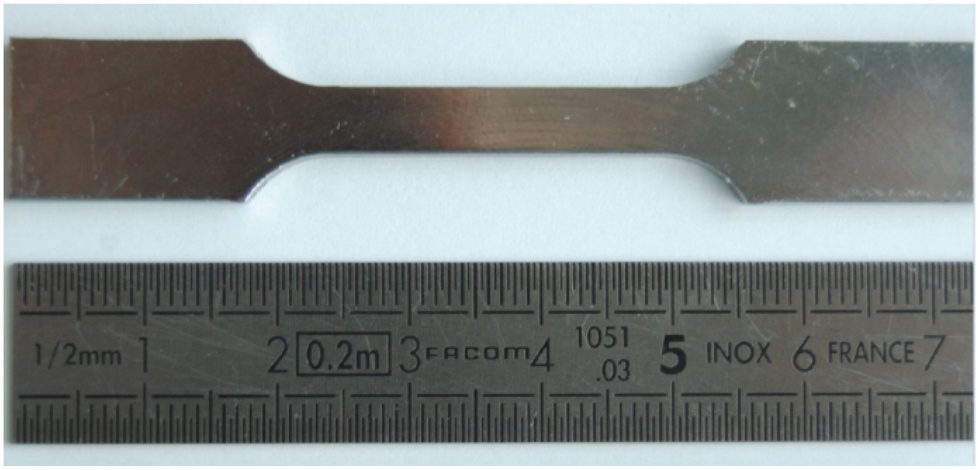

Figure 7.9: Le mini-échantillon pour l'essai de traction quasi-statique

Table 7.2: Les proprietés mécanique des alliages VT3-1 forgé et extrudé

Parameter	E (GPa)	E_{Dyn} (GPa)	$Rp_{0.2}$ (MPa)	Rm (MPa)	ϵ_R (%)
Forgé	114	116	950	989	6
Extrudé	106	110	1050	1107	13

La déformation prevu pour un alliage de titane VT3-1 est normalement limité par la valeur de 10 % pour le titane extrudé et 6 pour le titane forgé. Pour mesurer cette déformation une extensomètre avec la base outille de 25 mm a été engagé. Le chargement a été controlé en une mode de contrôle des déplacements. Le vitesse de chargement était 0.075 mm/min pour le chaque échantillon. Les résultats de l'étude sur la propriété mécanique sont presenté sur la Fig.7.10 et résumé dans le table 7.2.

Le deux alliages de titane sont montre bonne propriété mécanique avec clear plateau de la plasticité. La valeur de 6 % est typique pour un alliage de titane VT3- 1 forgé. La ductilité et toute les propriétés mécaniques d'un alliage éxtrudé sont plus haute par rapport de l'alliage forgé. Cependant la différence dans les limites d'elasticite est moins de 100 MPa.

7.4 Les échantillons et les équipements expérimentaux

L'objectif de ce thèse est la fatigue dans un alliage de titane à très grand number des cycles (jusquà 10^{10} cycles). Depuis le fin des années 1980 de la machines ultrasons sont éngagé pour l'essai de fatigue à très grand numbers des cycles [3]. Le principe de toutes machines ultrason

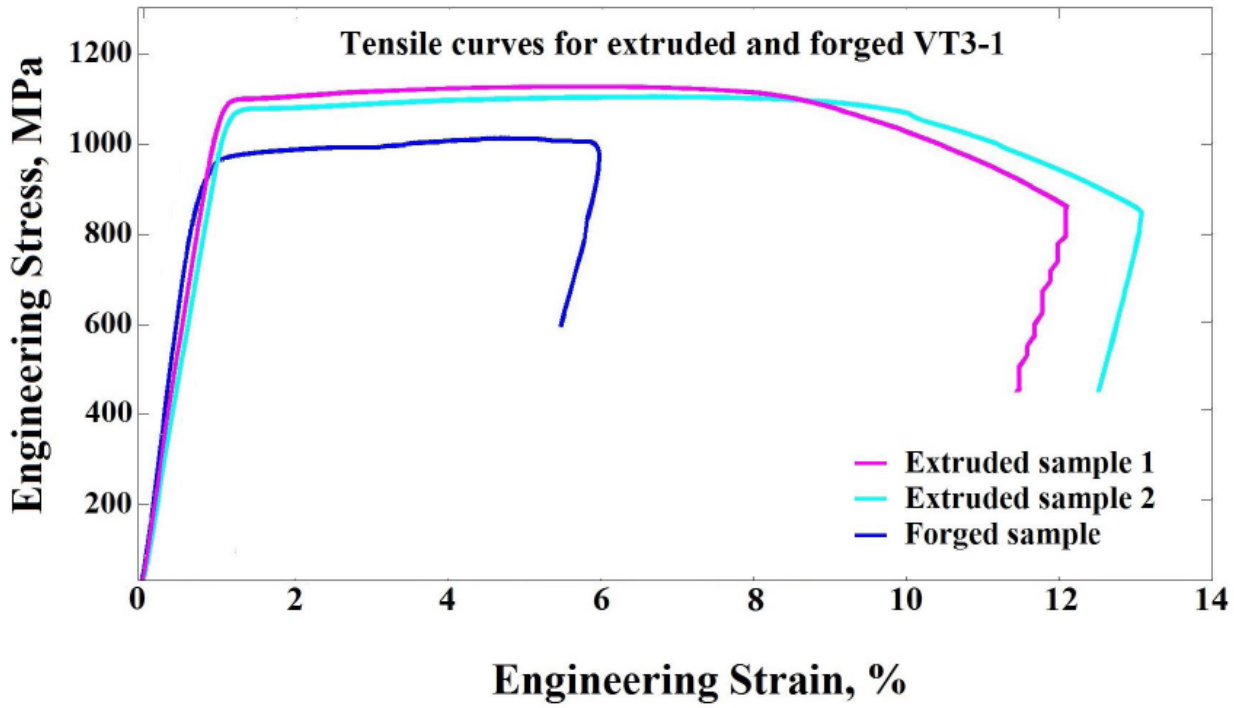

Figure 7.10: Les courbes de traction pour les alliages de titane forgé et extrudé

est basé sur un concept de la machine du Mason. Le concept et la première machine a été construit à l'année 1950, mais la diffusion de ce machine dans les laboratoires du le Monde était limité à cause de mauvais controles des parameters d'essai. Donc, la première machine ultrason pour l'essai de fatigue avec les contrôles par l'ordinateur était la machine construit dans la laboratoire de Prof. C.Bathias. Le schéma principale de ce machine est représenté sur la Fig.7.11.

La principe de fonctionnement de ce machine a été dessiné par Prof. C.Bathias et elle a été s'appelle 'Le concept gigacyclique' [3]. L'excitation de l'échantillon est realisé par les ondes élastiques à la frequence de les vibrations naturel de l'échantillon. En ce condition l'onde stationnaire est formé dans l'échantillon. L'échantillon est dessiné de la manière à le sablier et une node de déplacements est trouvé au milieu de l'échantillon, Fig.7.11. Pour garder ce conditions de vibration toutes élements de la machine sont dessiné à la manière d'avoir la même frequence de les vibration naturel. La machine est piloté par l'ordinateur avec la réaction i.e. en cas de les deviations des paramétérs de vibrations le logiciel va corriger ces paramétérs automatiquement.

Une machine ultrason dessiné dans la laboratoire de Prof.C.Bathias a été utilisé pour l'essai de fatigue gigacyclique sur l'alliage VT3-1. Ce machine était adopté pour l'essai avec un rapport de contrainte positive. Pour ce faire un soutien a été utilisé pour monter la

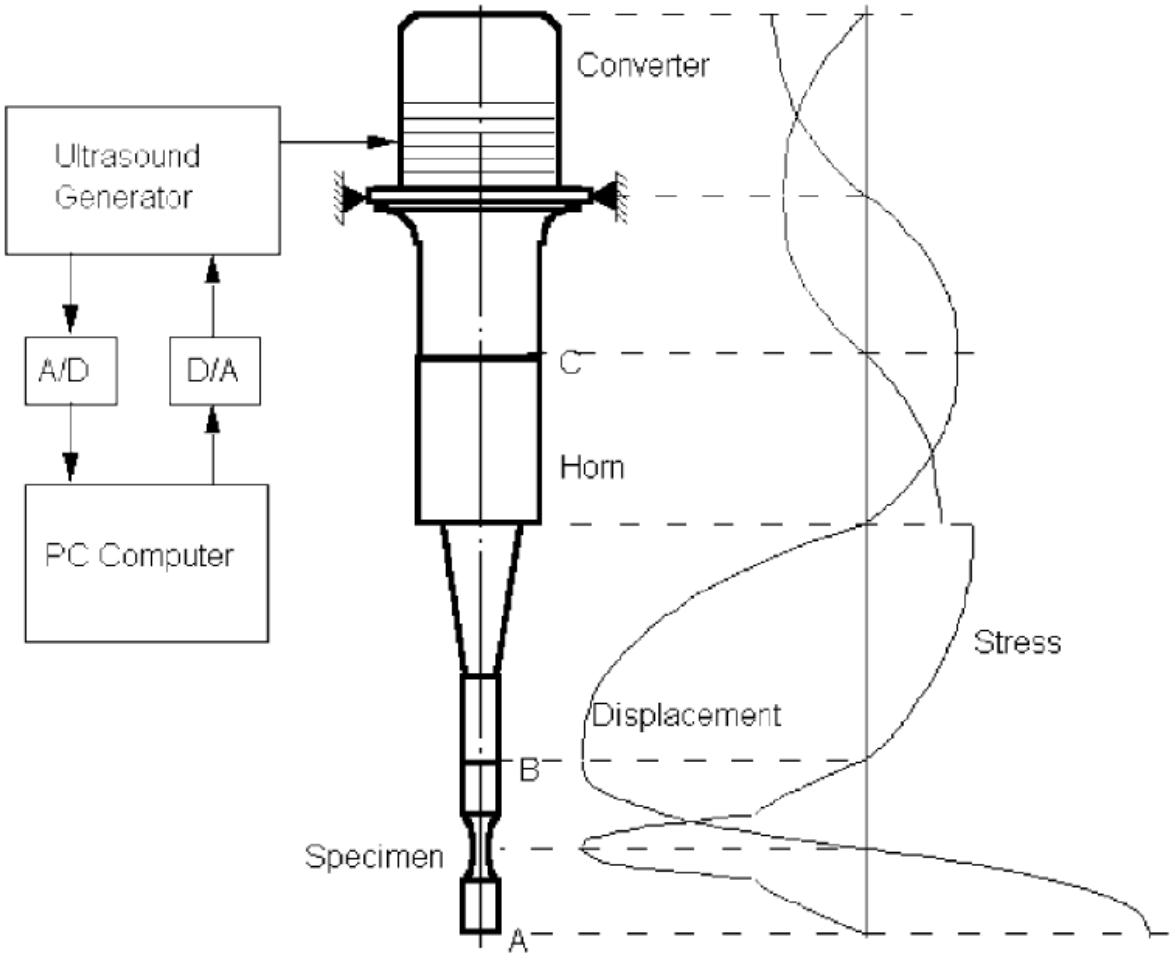

Figure 7.11: Le schéma principale du machine ultrason pour l'essai de fatigue

machine ultrason sur une machine de traction INSTRON. Le charge statique était appliqué sur les nodes des vibrations de la machine. Pour protéger de les modes de vibration un couche de la résine a été introduit dans la zone du contact. Les échantillons. Le deux types des échantillons a été utilisé pour l'essai de fatigue gigacyclique en chargement longitudinal: l'éprouvette avec une filetage pour l'essai en traction-compression, Fig.7.12a et avec les deux filetages pour l'essai en tractiontraction, Fig.7.12b. La géométrie des échantillon était dessiné pour chaque materiaux (forgé et extrudé) pour avoire une vibration naturel à la frequence d'operation de la machine.

Pour étudier l'anisotropie de la résistance de fatigue de l'alliage de titane VT3-1 forgé plusieurs jeux des échantillons a été fabriqué du le disque de compresseur. Ils sont étaient nommé: 0AXX (22 éprouvettes), 1AXX (10), 2RXX (8), 3RXX (7) et 4CXX (7). La total number des échantillons est 54. La nom est consiste de le numéro de jeux (0, 1, 2 et i.e.), la réference d'orientation de l'échantillon (A - axial, R - radial et C - circumferential), Fig.

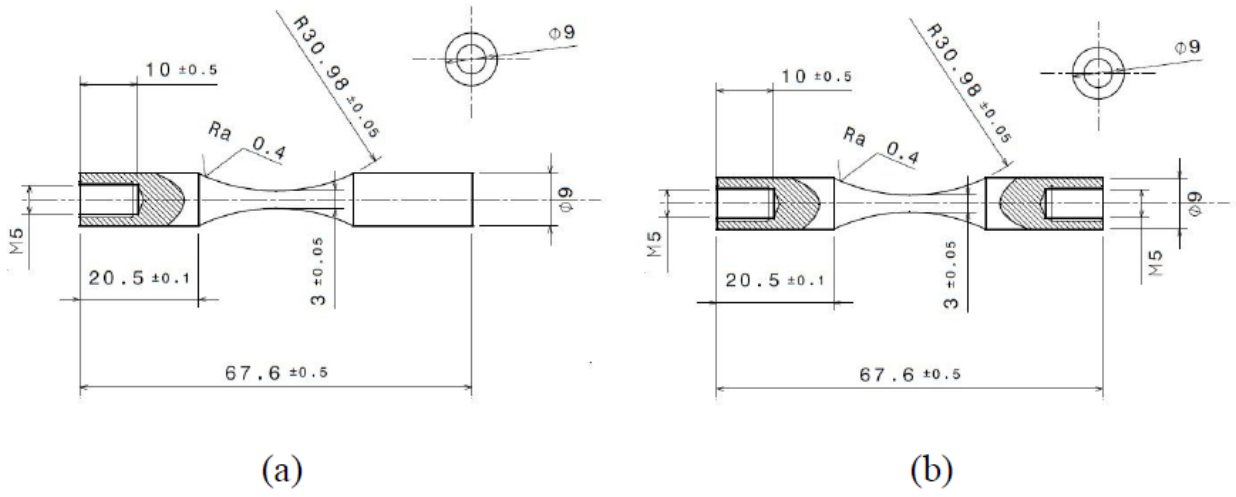

Figure 7.12: Les schemes des éprouvettes pour l'essai de la fatigue ultrason

7.13 et le numéro de l'éprouvette (01, 02, ... XX).

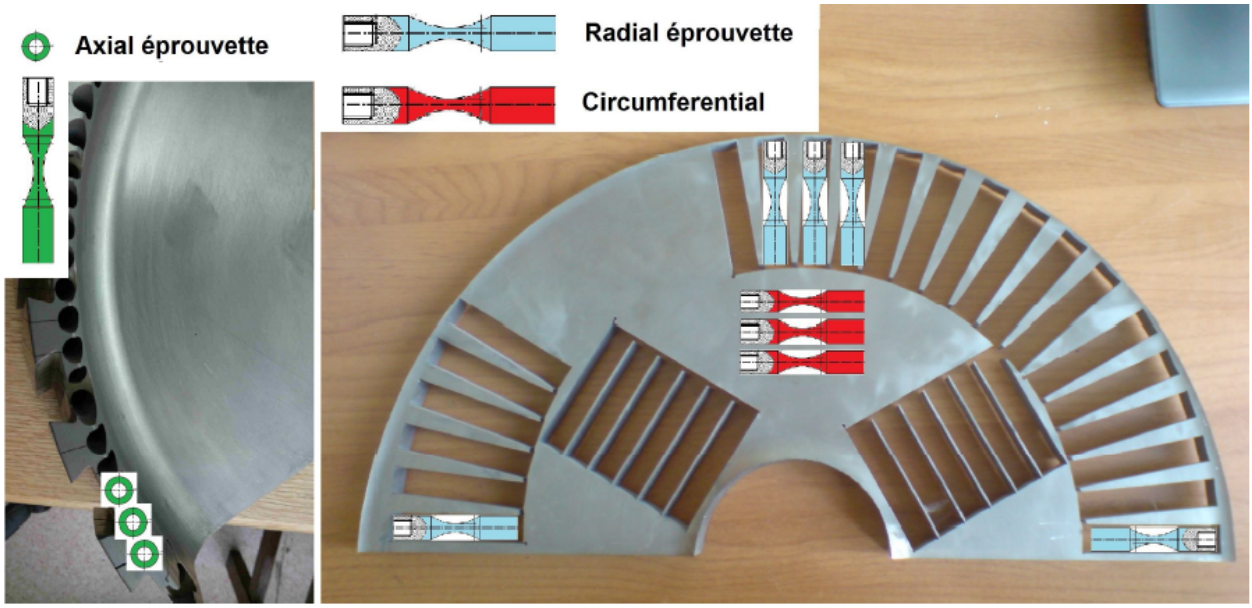

Figure 7.13: La position des échantillons dans un disque de le compresseur

Le plus grand jeux des échantillons (0AXX) a été dessiné pour l'étudier la résistance de fatigue générale de l'alliage de titane VT3-1 et la mécanisme d'amorçage d'une fissure en traction-compression (R=-1), Fig.7.12a. En suit, les jeux des échantillons 1AXX et 2RXX sont dessiné pour l'étudier un effect d'anisotropie. La géométrie (Fig.7.12a) et la régime de chargement sont la même pour le deux jeux des échantillons, la position dans le disque est

différent, Fig.7.13. Pour étudier l'effet de la charge statique (la contrainte moyen) sur la propriété mécanique et la mécanisme d'amorçage d'une fissure de fatigue, les deux jeux des échantillons (2RXX, Fig.7.12a et 3RXX, Fig.7.12b) était utilisé. La position et l'orientation des éprouvettes sont la même (la plateau de le disque et l'orientation radial) mais les régimes de chargement sont different: R=-1 pour 2RXX et R=0.1 pour 3RXX. Au fin pour l'étudier l'anisotropie dans la plateau de le disque de compresseur les deux dernier jeux des échantillon était dessiné: 3RXX et 4CXX. La géométrie pour ces échantillons est la même (Fig.7.12b), la régime de chargement est aussi la même (R=0.1), la position est la même (la plateau de le disque), mais l'orientations sont different: radial pour 3RXX et circumferential pour 4CXX.

Donc, basé sur ces études la conclusion pour l'effet de la charge statique et l'anisotropie sur la propriété mécanique et le type de la méchanisme d'amorçage d'une fissure de fatigue peut étre apportées.

Pour comparer les propriété mécanique de l'alliage de titane VT3-1 procédé en technique forgé et extrudé les trois jeux des échantillons était fabriqué à partir de la barres de titane extrude. La premiére jeu (R-1-Ext-XX) des éprouvettes est dessiné pour l'essai en régime traction-compression (R=-1), la géometrie est présenté sur la Fig.7.12a. Les deux jeux des échantillons supplémentaire (R01-Ext- XX et R05-Ext-XX) sont déssiné pour l'essai avec le chargement statique, Fig.7.12b, (R=0.1 et R=0.5 respectivement). La comparaison des propriété mécanique et les mécanismes d'amorçage est peut etre effectué basé sur les resultats des essai en régimes de R=-1 et R=0.1. Les résultats d'essai avec R=0.5 sont utilisés pour tracer la tendence résistance de fatigue de l'alliage de titane VT3-1 sous la rapport de contrainte élevé.

7.5 Les résultats des essais

L'essai sur l'alliage de titane forgé a été effectué à la temperature et sous le niveau de contrainte autour de 'la limite de fatigue' classique. Le premier résultats sont obtenu sur la jeux des échantillon 0AXX en traction-compression. Les résultats d'essai sont présenté sur la Fig.7.14. La caractéristique particularité des résultats sur l'alliage de titane VT3-1 est la dispersion grave de la durée de la vie. Sous le certain niveau de contrainte ce dispersion atteindre le trois ordres de grandeur. Pour Pour étudier la dispersion les surfaces de fissure sont observé par microscopie électronique à balayage (MEB).

L'analyse de la surface de fissure était montré la changement dans la méchanisme d'amorçage d'une fissure. Sous le niveau de contrainte élevé l'amorçage se produit par la surface d'échantillon, Fig.7.14 et 7.15. Typiquement, la durée de la vie est plus courte pour l'initiation surfacique par rapport d'autres échantillons.

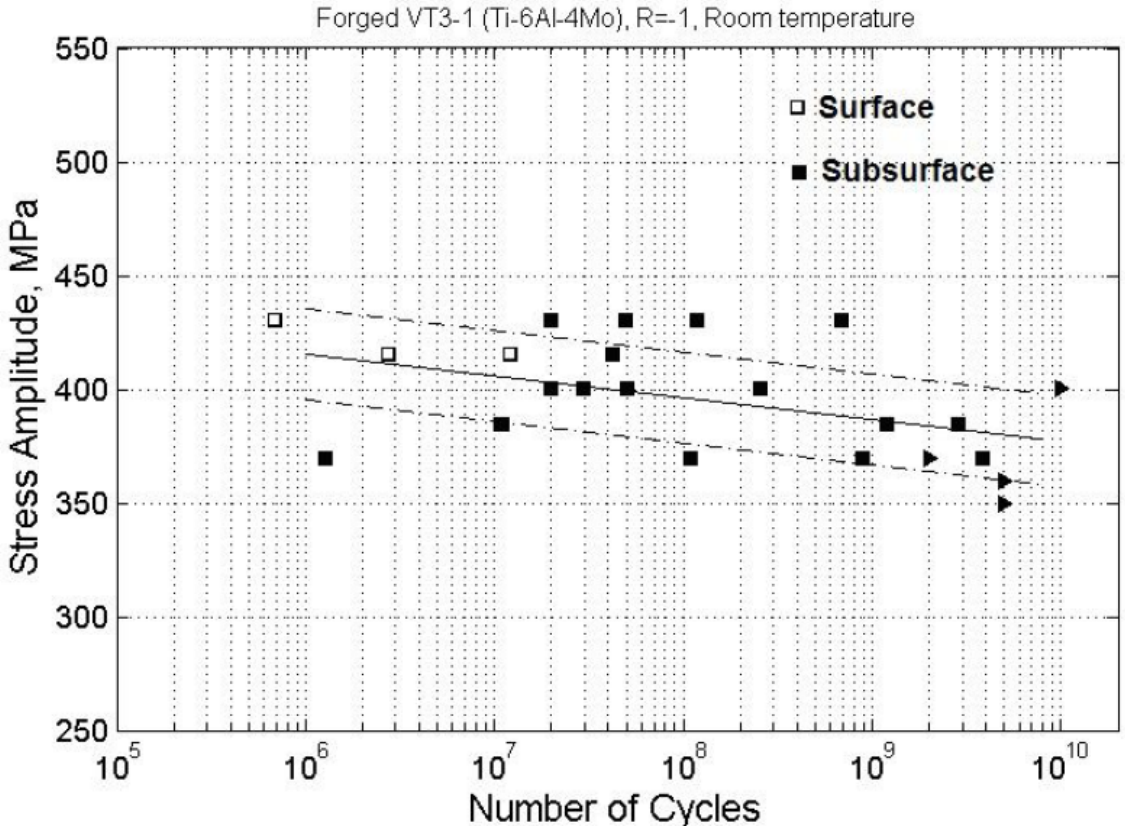

Figure 7.14: Les résultats d'essai de fatigue sur l'alliage de titane VT3-1 forgé, R=-1

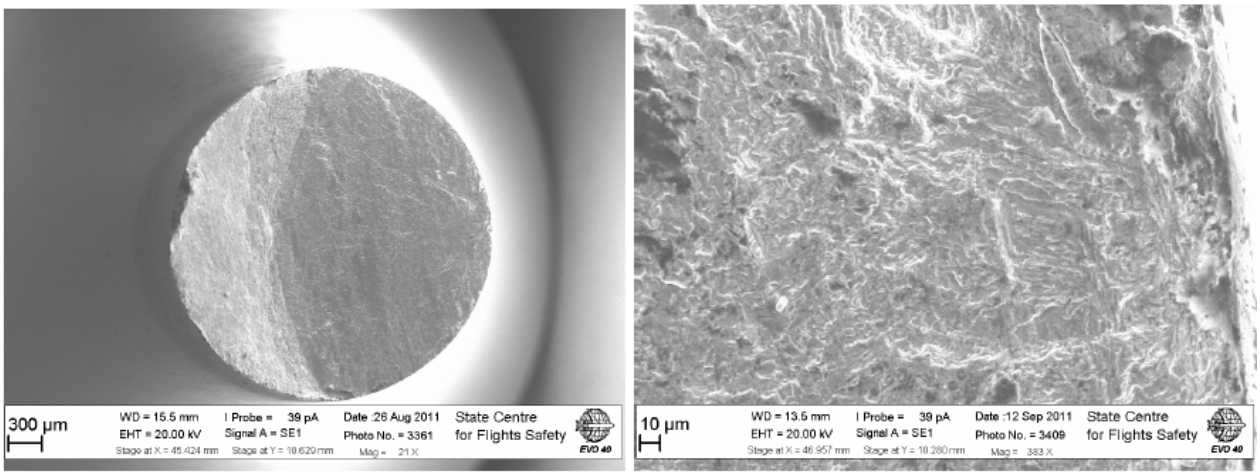

(a) (b)

Figure 7.15: L'amorçage de la fissure surfacique dans l'alliage de titane VT3-1, $\sigma_a = 415$ MPa,$N_f = 1.2 \times 10^7$ Cycles

Sous le niveau de contrainte plus bas, l'amorçage de fissure se produit à interieur de l'échantillon et associé à le defect de la microstructure. C'était trouvé comment sous la même niveau de contrainte la durée de la vie était plus courte pour l'échantillon dans laquelle l'amorçage se produit à cause de l'agglomeration des plaquettes de la phase alpha rugueux, Fig.7.16.

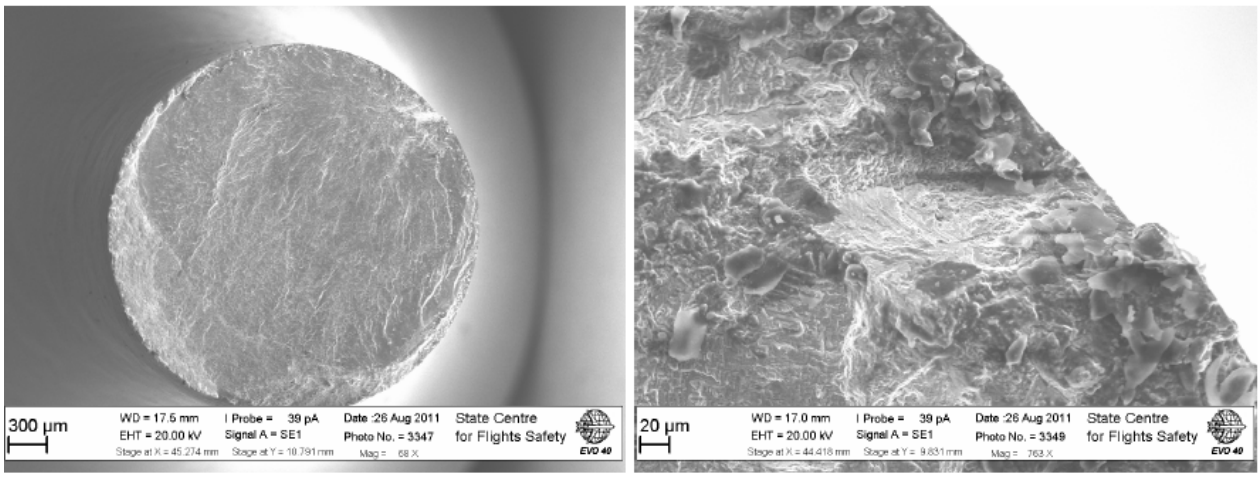

(a) (b)

Figure 7.16: L'amorçage de la fissure se produit à cause de l'agglomération des plaquettes de la phase alpha rugueux, $\sigma_a = 400$ MPa,$N_f = 2.98 \times 10^7$ Cycles

En ce cas l'amorçage de fissure est associé avec le clivage de l'agglomeration. Un autre type de défects laquelle est aussi la cause d'amorçage de fissure tôt sont les macro-zones, Fig.7.17.

En cas de l'amorçage de la fissure par la macro-zone la méchanisme est associé à l'accumulation d'endommagement par la fatigue sur la bord de la macro-zone. Probablement l'accumulation est plus intense entre les deux macro-zones avec le misorientation grave. L'analyse l'EBSD sur l'alliage de titane VT3-1, Fig.7.18 a été montré l'existance du macro-zones dans l'alliage avec misorientation jusqu'à 80 degré.

L'amorçage de la fissure dans un alliage de titane par les bords de la hétérogénéité de la microstructure est typique pour la chargement repetative sous l'amplitude bas. En cas de le titane forgé la taille et la misorientation des macro-zones sont très varié que produit la disper-tion grave de la durée de la vie comme même entre les resultats avec la même type d'initiation de fissure. La plus courte durée de la vie pour l'échantillon amorçé par le macro-zone est 10^7 cycles, tandis que plus long est 10^9 cycles. Le moyen durée de la vie avec l'amorçage de fissure par la macro-zone est 3 - 4 fois 10^7 cycles.

Quand la durée de la vie est plus long que 10^8 cycles, l'amorçage de la fissure est typ-

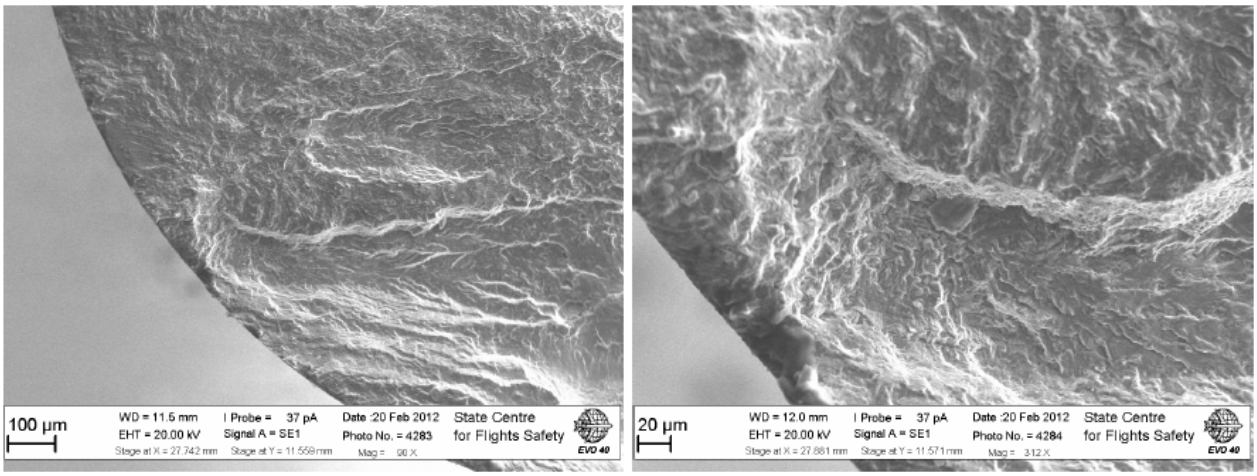

(a) (b)

Figure 7.17: L'amorçage de la fissure à cause de la macro-zone, $\sigma_a = 385$ MPa,$N_f = 1.08 \times 10^7$ Cycles

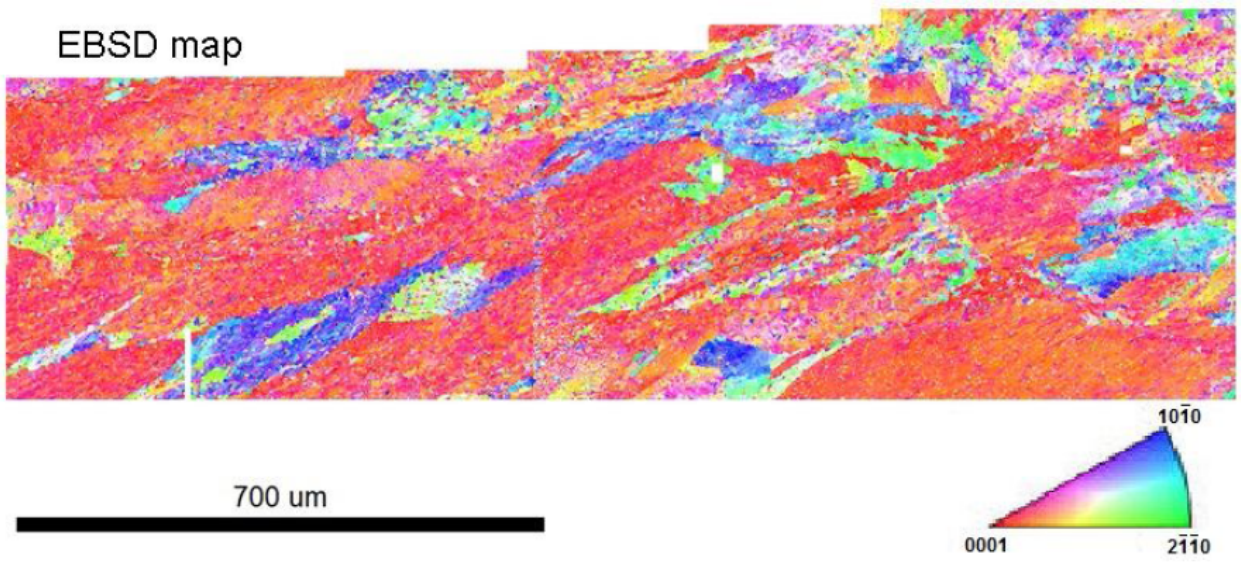

Figure 7.18: L'analuse l'EBDS sur l'alliage de titane VT3-1 forgé

iquement produit par la particularité de la microstructure avec la taille caractéristique est beaucoup plus petit par rapport de la taille de la macrozone, Fig. 7.19. En ce cas la facettes fragile sont se trouve dans le site d'initiation de une fissure de fatigue. La taille caractéristique de ces facettes est varié entre 1-2 et 5-10 micromètres. La morphologie n'est pas la même pour ces facets: les plus petite facets sont plus platn, Fig. 7.19; les plus grande (5-10 micromètres) facets sont plus rayée, Fig.7.20.

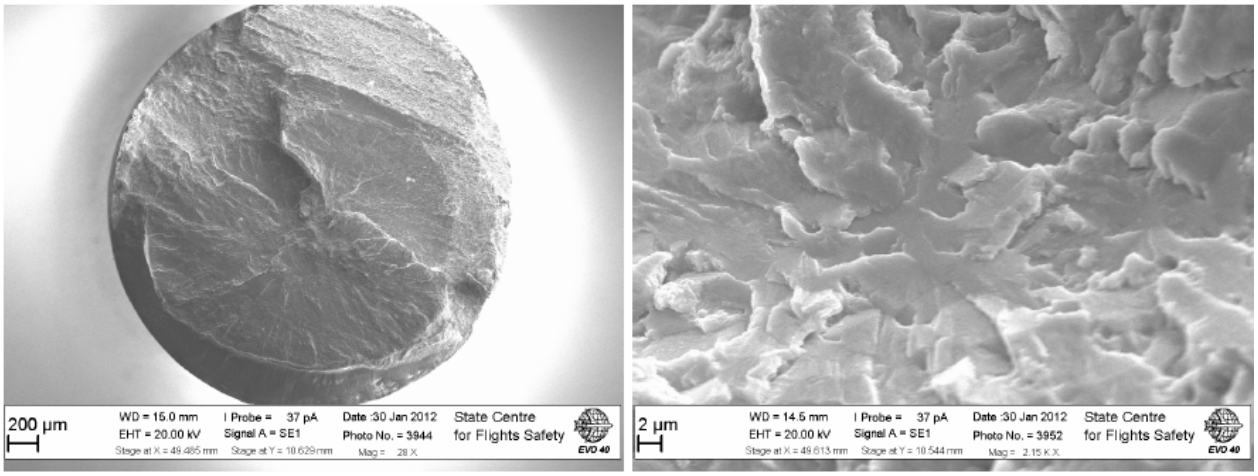

(a) (b)

Figure 7.19: L'amorçage de la fissure de fatigue avec formation de la facette fragile, $\sigma_a = 430$ MPa,$N_f = 1.18 \times 10^8$ Cycles

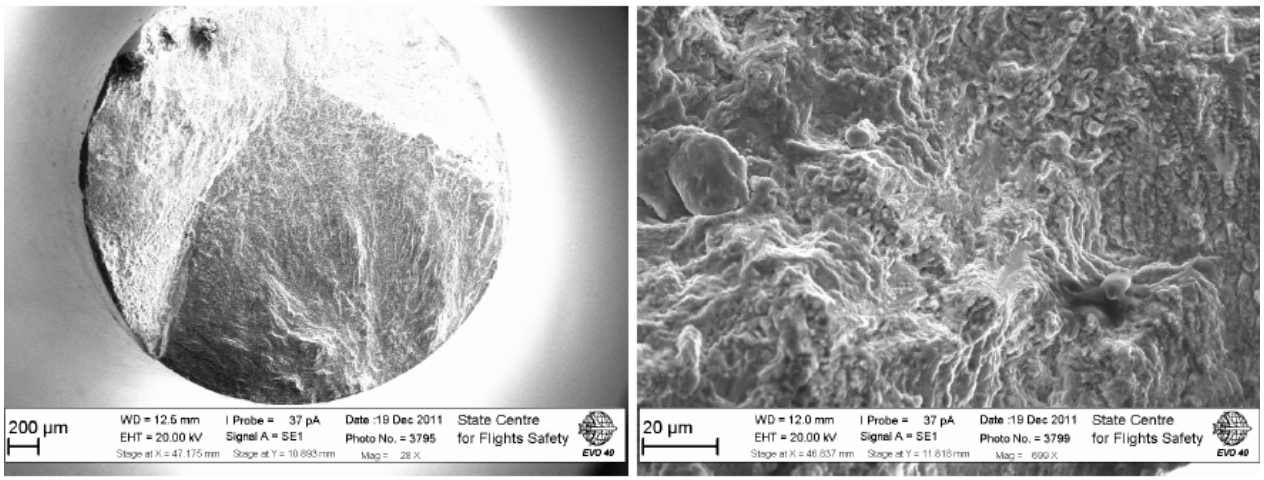

(a) (b)

Figure 7.20: L'amorçage de la fissure de fatigue avec formation de la facette, $\sigma_a = 385$ MPa,$N_f = 2.85 \times 10^9$ Cycles

L'amorçage avec la formation de la facette fragile, Fig.7.19, est bien connu dans le literature comme l'amorçage de la fissure de fatigue à la très grand numero des cycles. Ce type d'initiation a été explique par le clivage de la phase alpha par un plan de base de hcp. La facette présentée sur la Fig.7.19 est un grain de la phase alpha. Les même facettes étaient trouvé dans l'échantillons fissuré entre 10^8 et 10^{10} cycles. D'autre type de facettes

a été trouvé à la durée de la vie bien après de 10^9 cycles. Pour l'étudier la nature de ces facettes l'EDX analyse a été utilisé pour determiner la composition chimique de ce object. Le résultats sont montré perturbation grave dans la composition chimique par rapport de le composition normale, Fig.7.21.

Il montre que la concentration de l'aluminium est élevée à l'intérieur de la facette, tandis que la concentration de molybdène est très faible (non détectables). La concentration de molybdène est normale autour de ce facette. Ainsi, cet objet est une (ou plusieurs) plaquette de la phase alpha fissuré en la face de la direction d'allongement. Cette déclaration est confirmé par l'analyse de la microstructure et l'EDX analyse, Fig.7.22.

L'étude sur la composition chimique dans la phase alpha et beta a été montré la même tendance dans la distribution des elements. La concentration de molybdenum est très bas dans la plaquette de la phase alpha.

Résumant l'étudé sur la résistance de la fatigue de l'alliage de titane VT3-1 en régime Gigacyclique les résultats suivants peuvent être notés: (1) La course de la curve de fatigue montrer une ligne incliné aprés 10^6 cycles. La différence entre la résistance de fatigue à 10^6 est 10^9 cycles atteindre 60 MPa; (2) Il y à la changement de la mécanisme d'amorçage de la fissure de fatigue dans l'alliage de titane VT3-1 forgé. Sous l'amplitude de contrainte élevé il y à l'initiation surfacique, par contre sous l'amplitude bas, il y à l'amorçage à interieur de l'échantillon; (3) La dispersion de la durée de la vie est grave dans le régime gigacyclique pour l'alliage de titane VT3-1. Sous certain niveau de contrainte la dispersion atteindre trois ordres de grandeur; (4) Plusieurs mécanismes d'amorçage d'une fissure de fatigue a été trouvé dans l'alliage de titane VT3-1 sur la chargement gigacyclique. Il semble que ces mécanismes sont résponsable pour la difference dans la durée de la vie. Les résultat de l'essai de fatigue peut etre présenté dans le graph où chaque mécanisme est remarque, Fig.7.23.

La durée de la vie est depend de le type de la defect laquelle va placé dans une zone avec la chargement critique. L'agglomeration de les plaquettes de la phase alpha et macro-zones sont réduit la durée de la vie.

7.6 L'Anisotropie de la propriété mécanique

Pour étudier l'anisotropie d'un alliage de titane VT3-1 forgé les deux types de chargements a été utilisé. La première est la régime de traction-compression, R=-1 (jeux 1AXX et 2RXX). Le deuxième est la régime de traction-traction, R=0.1 (jeux 3RXX et 4CXX). Les résultats sont présenté sur la Fig.7.24 et 7.25 pour R=-1 tests et R=0.1 respectivement.

Les résultats d'essai sous la chargement de la traction-compression sont très proche et l'effect de l'orientation n'était pas trouvé. Probablement à cause très fin microstructure et

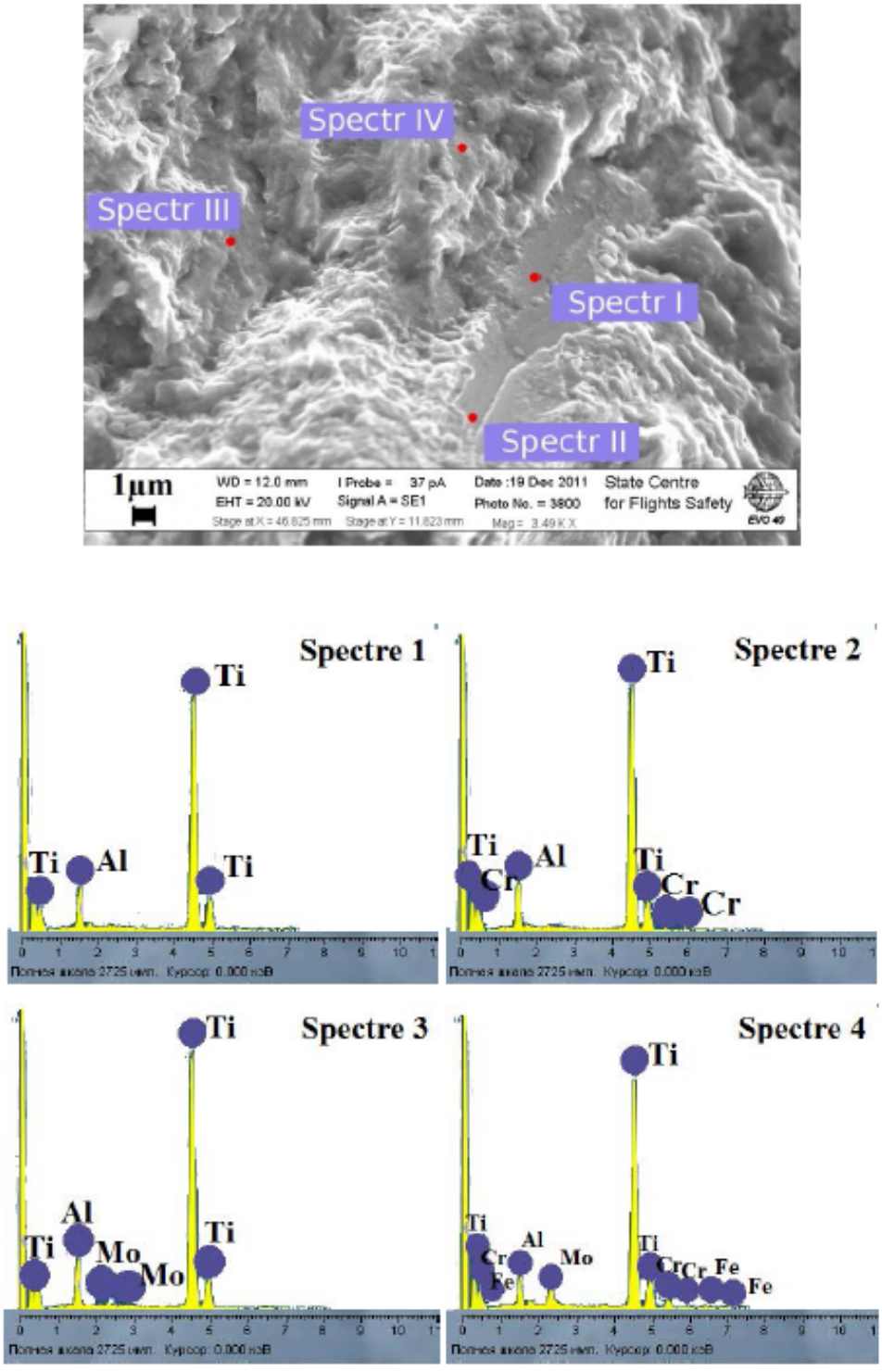

Figure 7.21: L'analyse de la composition chimique sur une facette fissure

plusieurs orientation de la macro-zones l'effect d'anisotropie est disparu comment dans le cas de polycristallin. En cas de les résultats de l'essai en traction-traction, le léger effet

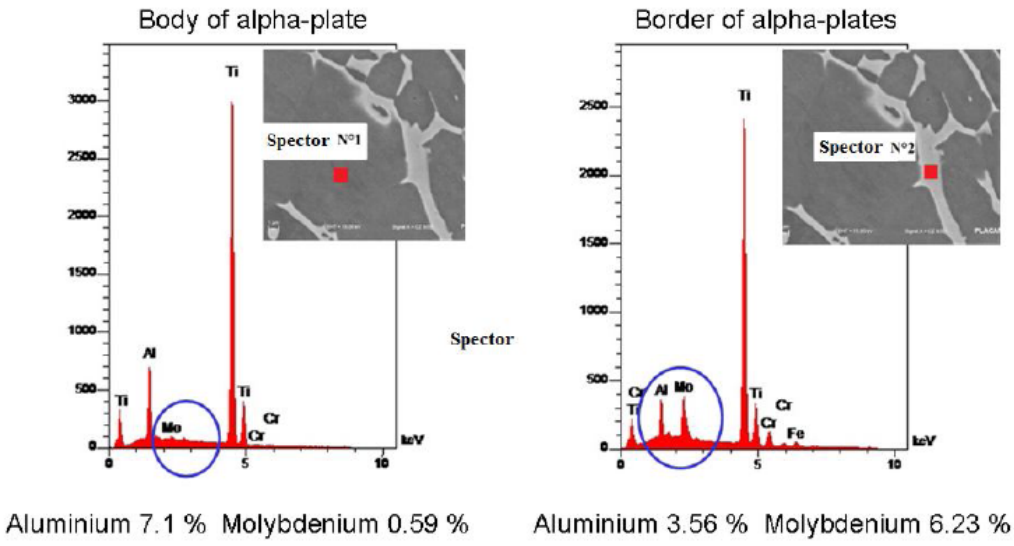

Figure 7.22: L'analyse EDX sur l'échantillon poli de l'alliage de titane forgé

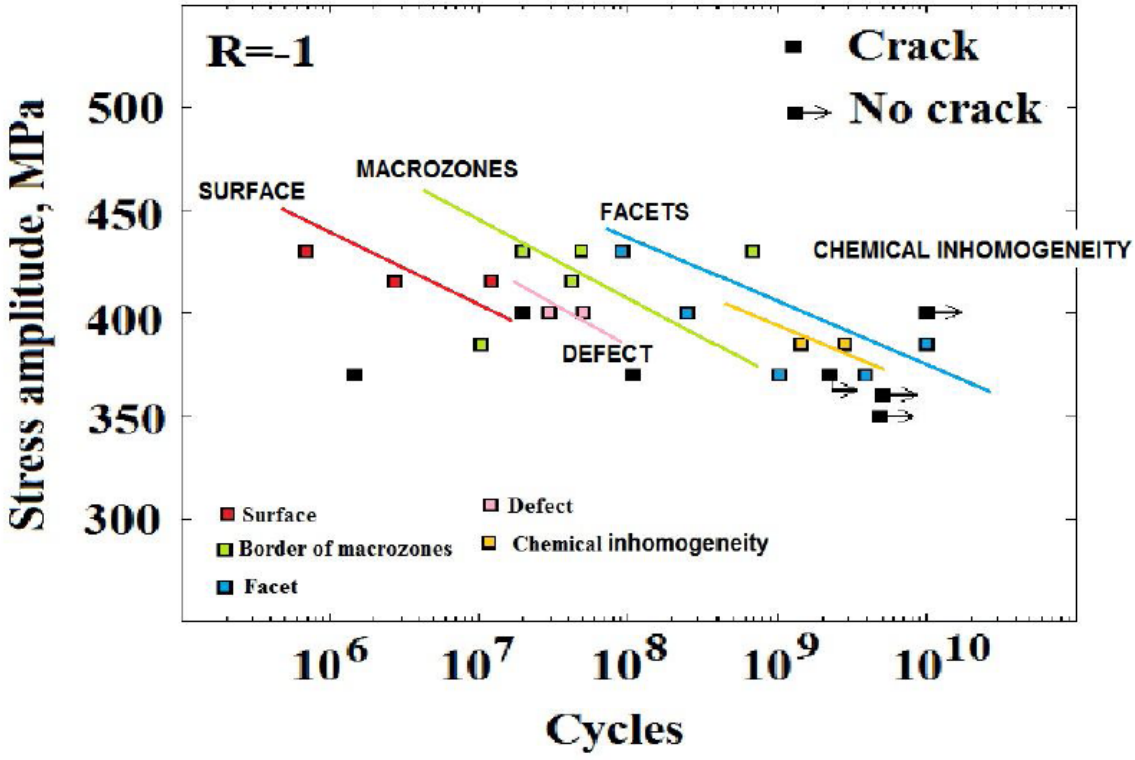

Figure 7.23: L'analyse EDX sur l'échantillon poli de l'alliage de titane forgé

d'orientation peuvent être distinguer. La propriété mécanique est en peu plus bas pour les échantillons coupé dans la direction circumferential. Mais comme même les résultats sont

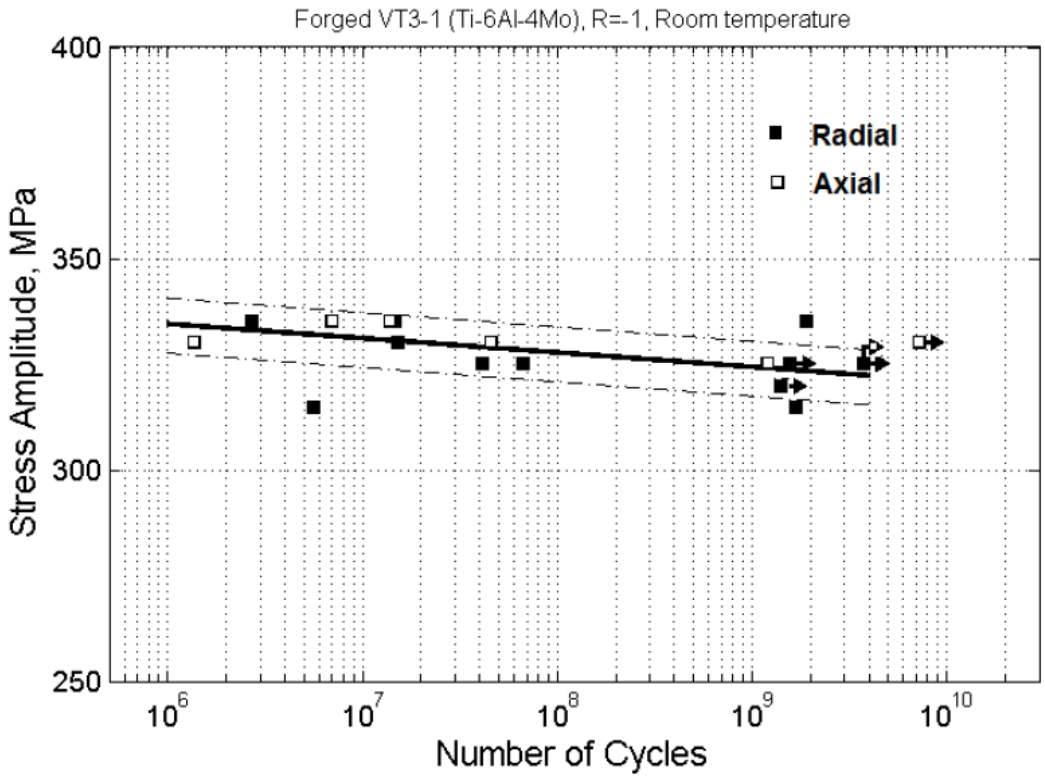

Figure 7.24: Les résultats d'essai de fatigue sous le chargement en traction-compression

très proche et la difference ne vont pas au-delà de l'erreur.

L'anisotropie dans la résistance de fatigue n'était pas trouvé ni entre les échantillons coupé à partir du la jante et plateau de le dusque, ni entre les échantillons coupé à partir du la plateau en deux directions different.

7.7 L'effet de la contrainte moyenne

Pour étudier l'effet de la contrainte moyenne sur la mécanisme de l'amorçage de la fissure les deux jeux des échantillons a été utilisé (2RXX et 3RXX). L'échantillons était coupé dans la même direction (Radial) à partir de la plateau de le disque de compresseur. Le résults sont présenté sur la Fig. 7.24 et 7.25 respectivement. Les mécanismes d'amorçage de la fissure était étudié avec MEB. Les résultats montrent le plus important role de la macro-zone dans l'accomadation de l'endommagement de fatigue, fig.7.26.

En case de la chargement en cours inversée (R1) la surface de fissure est typiquement présenté une mécanisme déjà trouvé pour cet alliage (voire Les mécanismes d'amorçage de la fissure dans VT3-1 forgé). En cas de la chargement en régime de traction-traction, la surface

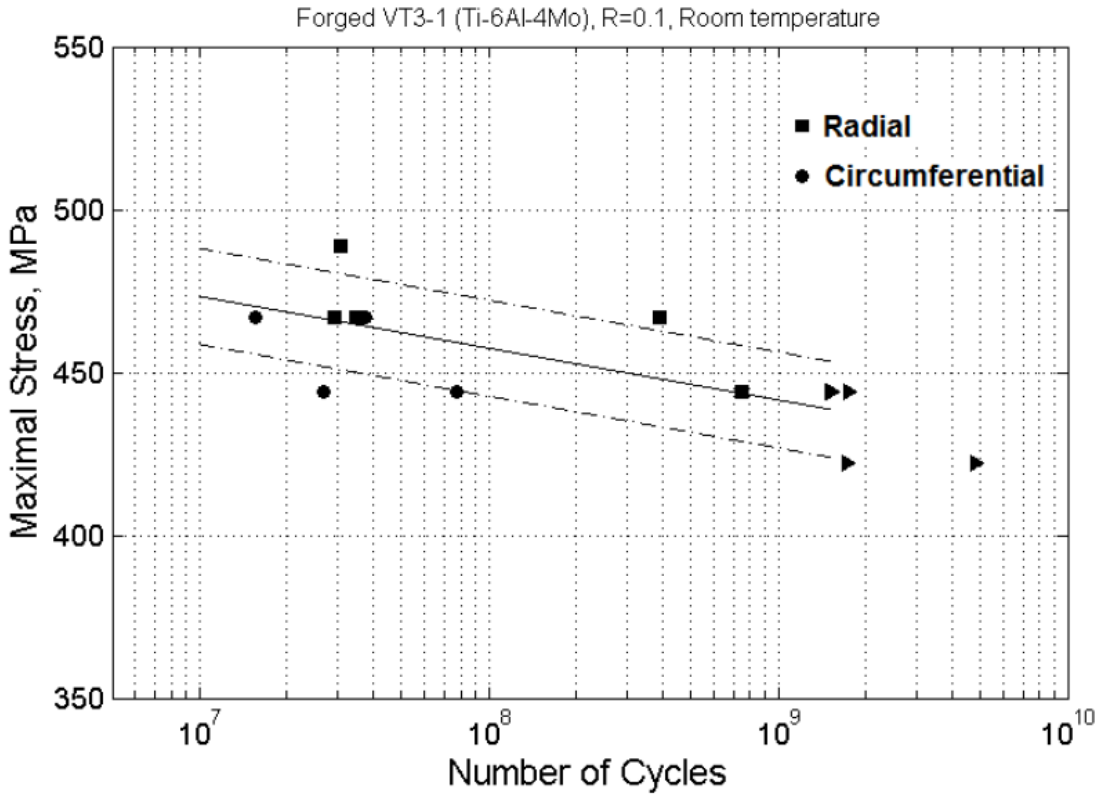

Figure 7.25: Les résultats d'essai de fatigue sous le chargement en traction-traction

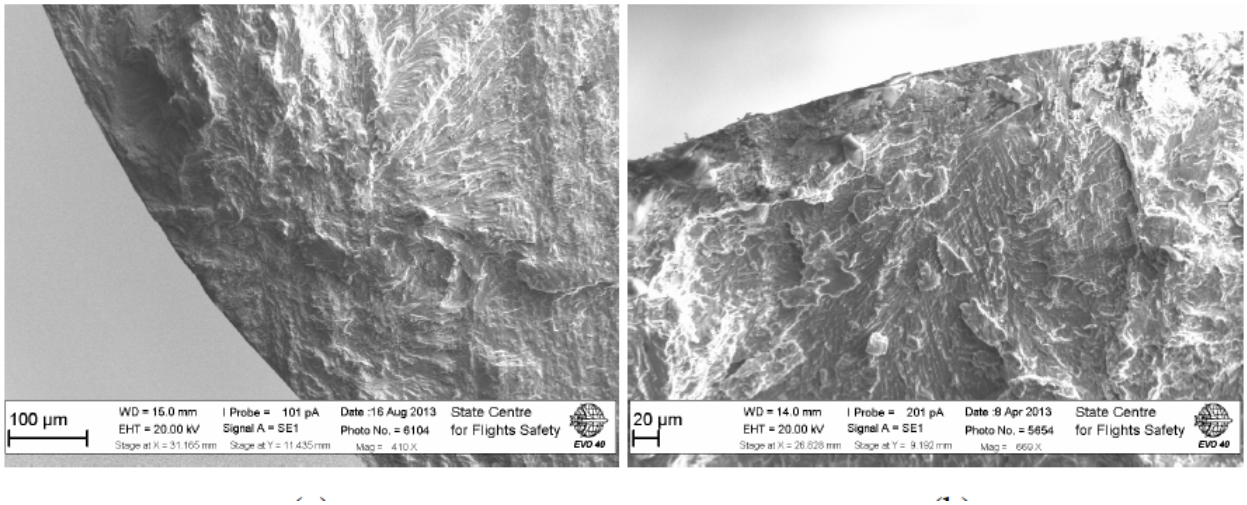

Figure 7.26: Les typique sites de l'amorçage de fissure (a) chargement R=-1, (b) R=0.1

de fissure montrer les grande zones de la fissure fragile, Fig. 7.26b. Chaque fois l'amorçage était produit par le bord de macrozone. L'analyse de la morphologie de la zone de la propagation de fissure était montré, que la fissure souvent passé par le bord de macro-zone.

Le mécanisme de l'initiation et propagation d'une fissure de fatigue dans l'alliage VT3-1 forgé sont determiné par la morphologie, orientation et taille de la macro-zone en présence de la contrainte statique positive.

7.8 La fatigue gigacyclique dans l'alliage de titane VT3-1 extrudé

Les trois type d'essai a été realisé sur l'alliage de titane extrudé: (1) tractioncompression R=-1; (2) traction-traction R=0.1 et (3) traction-traction R=0.5. Les résultats sorésultats sont présenté sur les Fig.7.27 - 7.29.

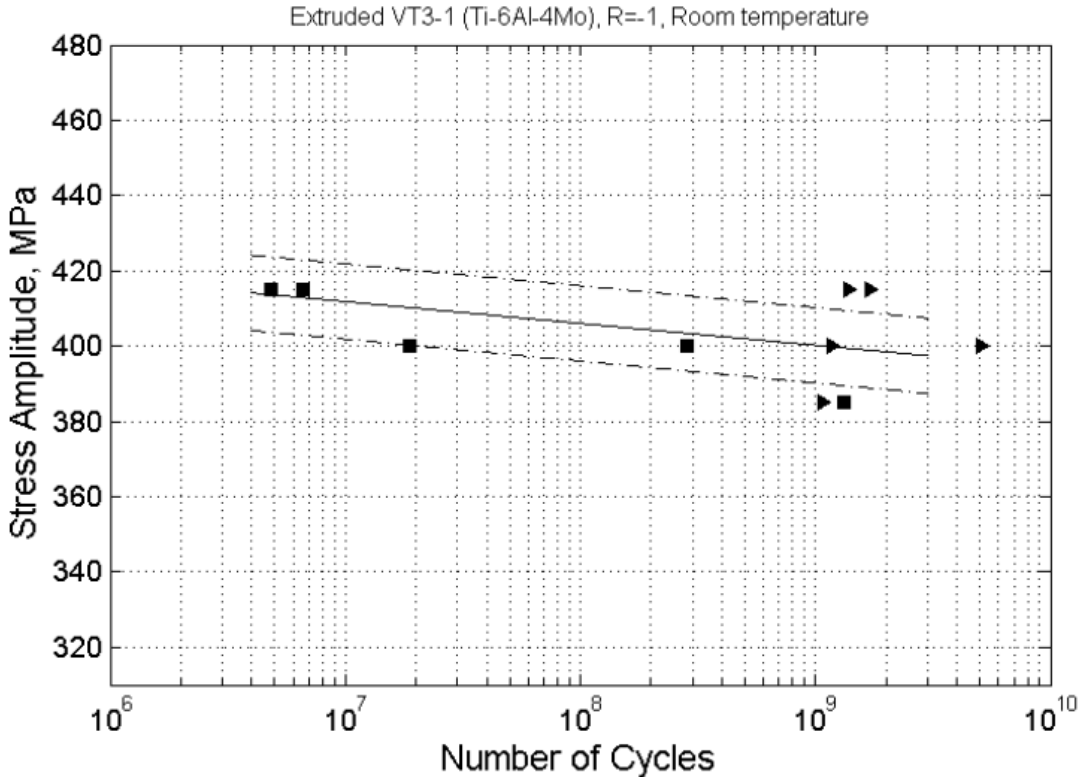

Figure 7.27: Les résultats d'essai de fatigue sur l"alliage VT3-1 extrudé, R=-1

L'analyse sur la surface de fissure était montré la même type d'amorçage de fissure pour chaque régime de chargement et pour toute les durée de la vie. L'initiation de la fissure de fatigue est associé avec le defect de la microstructure présente sur la Fig. 7.6. C'est l'agglomeration des plaquettes de la phase alpha dans un grain beta primaire. La l'initiation de fissure se produit la facettes quasi-fragile dans le site d'amorçage. Les exemples des sites

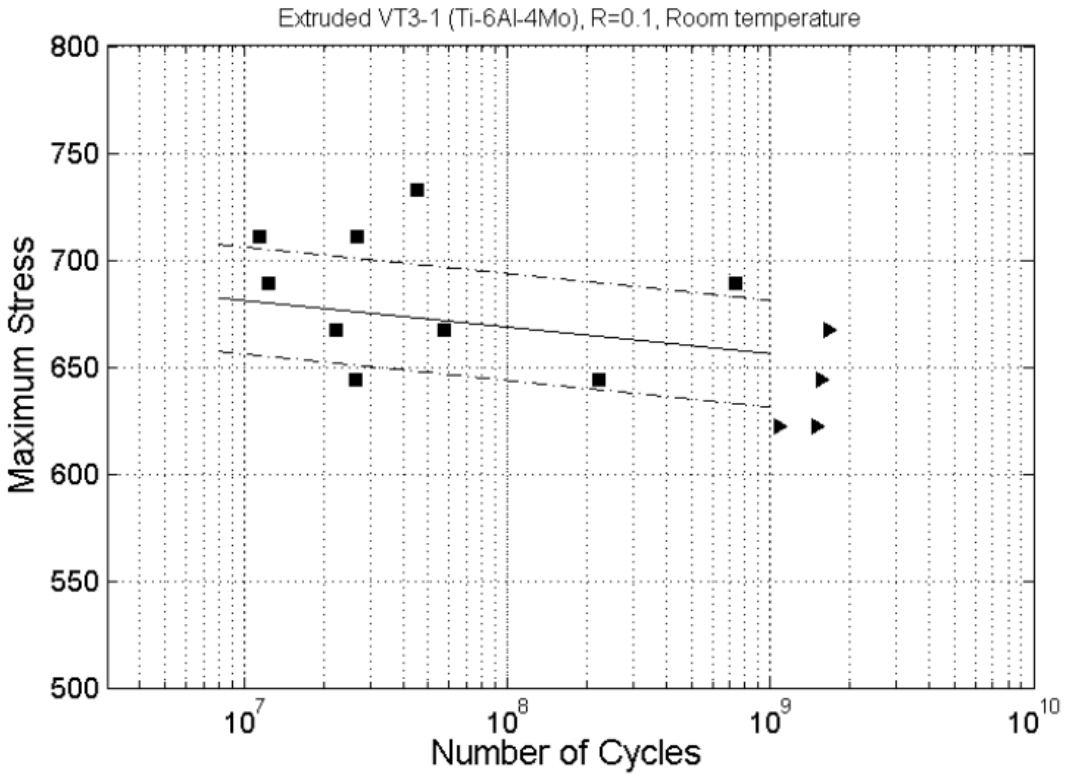

Figure 7.28: Les résultats d'essai de fatigue sur l"alliage VT3-1 extrudé, R=0.1

d'initiation dans les régimes de chargement different sont présenté sur la Fig.7.30.

Toute les échantillons investigué sont montré l'amorçage de fissure à l'interieur de l'échantillon. Donc, le defect de la microstructure est la paramètre de commande de vie pour le titane extrudé. La facette est toujours fissure à la face laquelle a l'angle par rapport de l'axe de chargement. C'est pour ça la surface de fissure de le titane extrudé souvent montrer les ailes de papillon, Fig.7.31. Ce type de la surface de fissure est ressemble la fissuration dans l'aciers. Mais en cas de le titane ce phénomène a la nature mécanique et ne associé par à la métallurgie.

La propriété mécanique de le titane extrudé est plus haut par rapport de le titane forge. Le titane extrude ne content pas les macro-zones et ses résistance de fatigue sous la charge statique est beaucoup mieux par rapport à le titane forge. L'amorçage est toujours la même et associé à le clivage de l'agglomeration des plaquettes de la phase alpha.

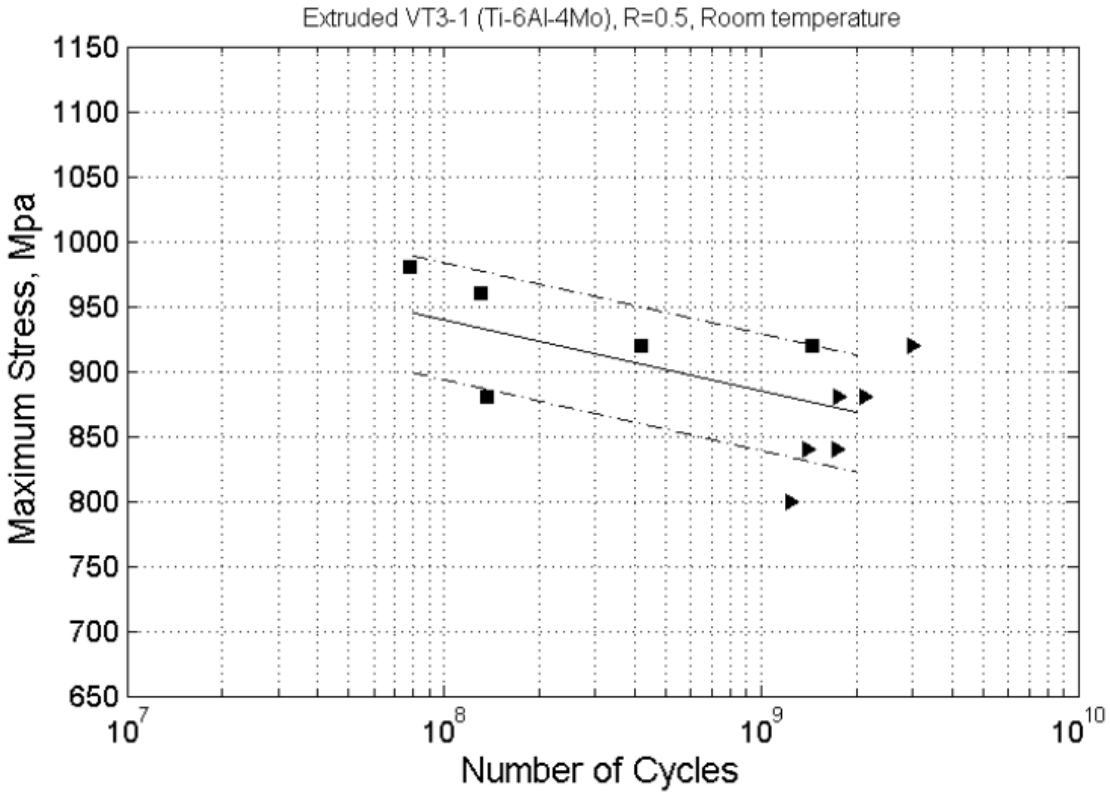

Figure 7.29: Les résultats d'essai de fatigue sur l"alliage VT3-1 extrudé, R=0.5

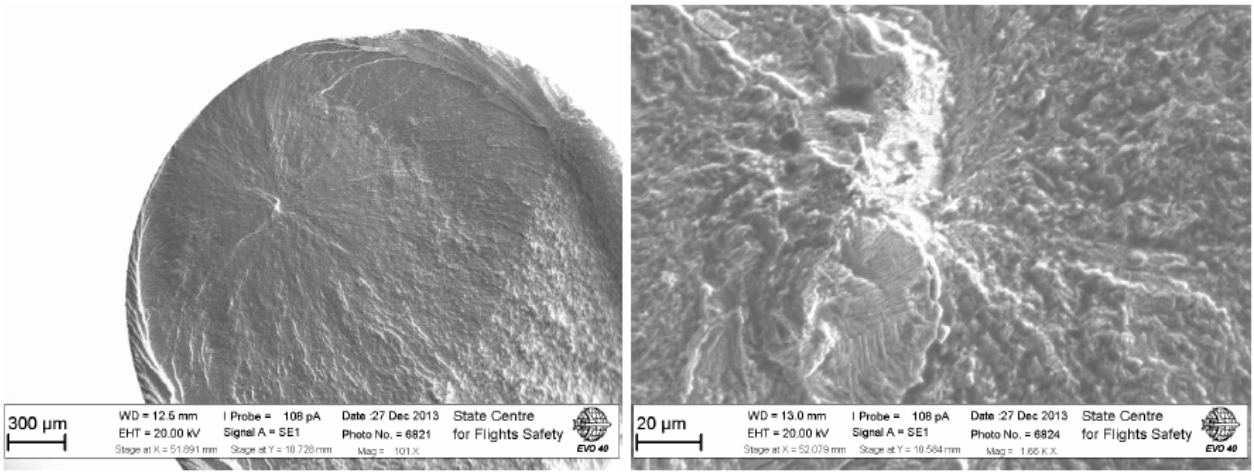

L'essai de traction-compression, R=-1

7.9 La Torsion

Le dernier projet réalisé dans ce thése est la création de une machine nouveau pour l'essai gigacuclique en torsion pure. La machine dessiné a été basé sur une transducer de torsion que

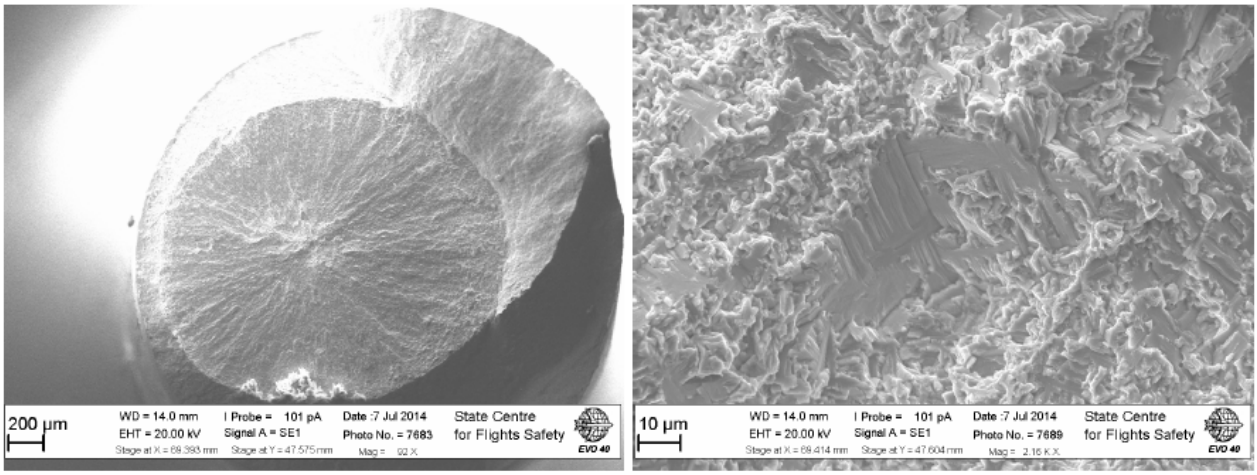

L'essai de traction-traction, R=0.1

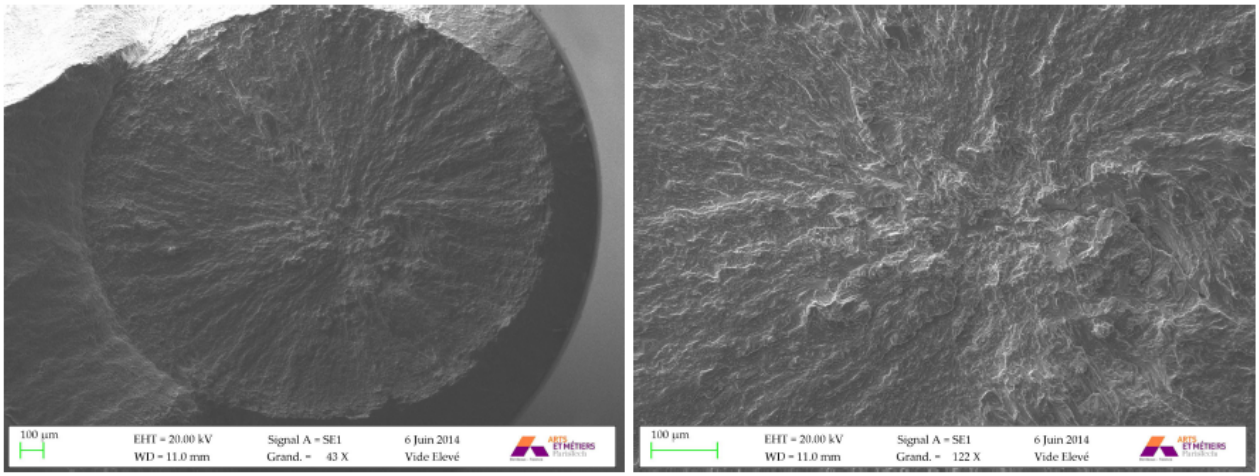

L'essai de traction-traction, R=0.5

Figure 7.30: Les sites d'amorçage de la fissure de fatigue dans l'alliage de titane VT3-1 extrudé sous le régimes de chargements different

est activé par signal sinusoidal electrique a la frequence de 20 kHz. Ce projet est confidentielle et just les concept général va discuté dans ce resumé. L'aperçu de la machine est représenté sur la Fig.7.32.

La machine se composent de transducteur piézoélectrique, sonotrode et l'échantillon. La transducteur est activé par le signal que vient de la generateur ultrasonor. Ce générateur est piloté par l'ordinateur et la logicielle speciaux. Toute la système est fonctionné à la frequence naturel de 20 kHz. La régime de fonctionnement est continu (sans pauses). Le refroidissement de l'échantillon pendant l'essai de fatigue est réalisé par l'air comprimé. La

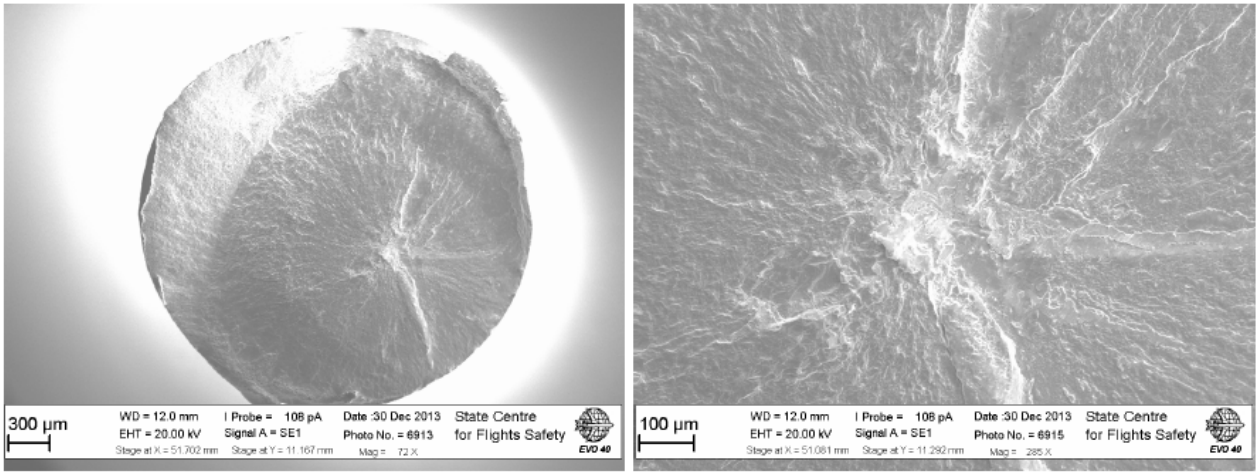

(a) (b)

Figure 7.31: Les ailes de papillon dans l'alliage de titane VT3-1 éxtrudé

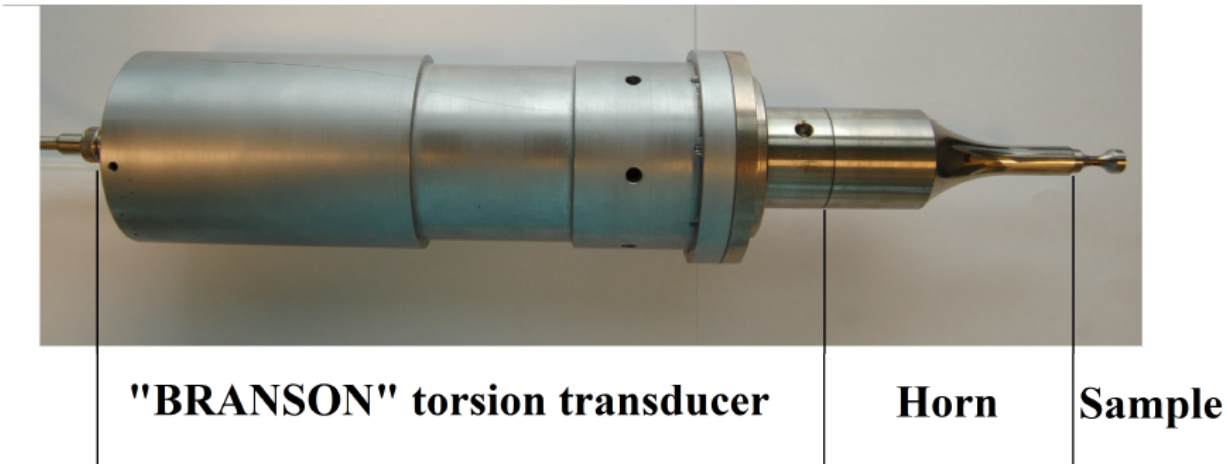

Figure 7.32: L'aperçu de la machine gigacyclique pour la torsion

machine est déssiné pour s'arrêter automatiquement en cas de la sauter de la frequence.

La premier l'essai de la machine de torsion a été effectué sur l'alliage de titane forgé. La géometrie de l'échantillon est présenté sur la Fig.7.33. Le deuxième l'essai a été réalisé sur l'alliage de titane extrudé. Tous les deux essai a été bien fait et les résultats sont présenté sur la Fig.7.34. Toute les échantillons a été cassé par une fissure de fatigue orienté à 45° par rapport à l'axe de chargement. L'analysis de la surface de fissure est montre le deux type d'amorçage pour l'alliage de titane VT3-1. Les fissures surfacique et subsurfacique a été trouvé dans l'alliage VT3-1 forgé et extrude après très grand number des cycles, Fig.7.35 - 7.38.

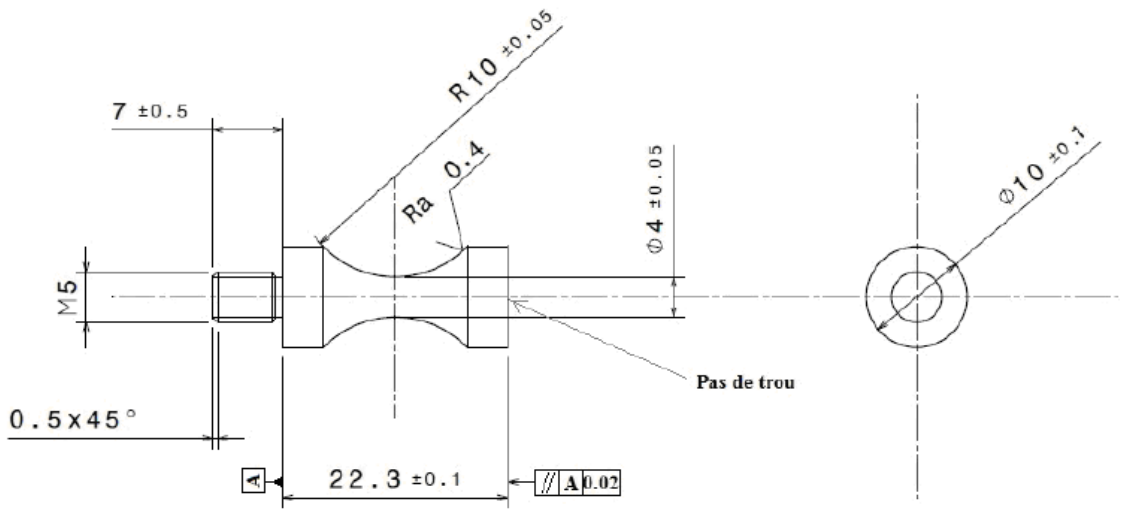

Figure 7.33: La géometrie de l'échantillon pour l'essai de torsion

L'initiation de la fissure de fatigue en torsion à l'intérieur de l'échantillon n'est pas typique et pour le titane VT3-1 a été montré pour la premier fois. Probablement ***c'est la premier résultat de l'essai ultrason en torsion sur l'alliage de titane***. Sur la base des premiers résultats, il est clair que la nouvelle machine est bien installé et fonctionne bien. Donc, le but de ce partie de la thèse est atteint avec succès.

7.10 Conclusion

Dans ce thèse plusieurs buts a été prévu: (1) étudier la résistance de fatigue à très grand number des cycles de l'alliage de titane VT3-1 forgé laqueele est utilisé pour production des disques de compresseur ; (2) établir les mécanismes typique d'amorçage d'une fissure de fatigue à très grand number des cycles ; (3) étudier l'anisotropie de la propriété mécanique d'un disque de compresseur forgé ; (4) étudier l'effet de la charge statique sur la mécanismes d'initiation d'une fissure de fatigue ; (5) comparer les propriétés mécaniques fatigue à très grand number des cycles des deux alliages de titane: forgé et extrudé; (6) construire une machine nouveau pour l'essai de fatigue gigacyclique en torsion pure ; (7) comparer les mécanismes d'amorçage d'une fissure de fatigue en chargement longitudinal et torsion à très grand number des cycles.
Tous les objectifs sont atteints avec succès dans ce thèse.

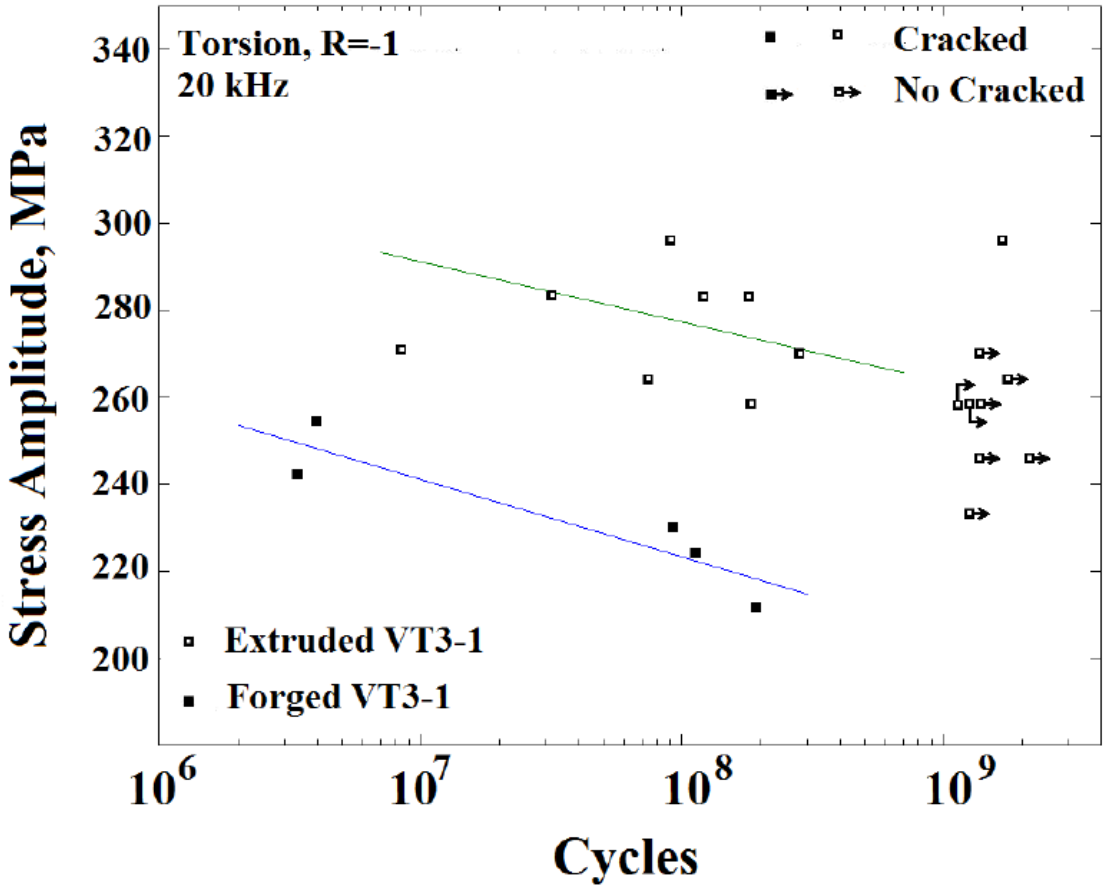

Figure 7.34: Les résults de l'essai sous le chargement de torsion ultrason (l'alliage de titane VT3-1)

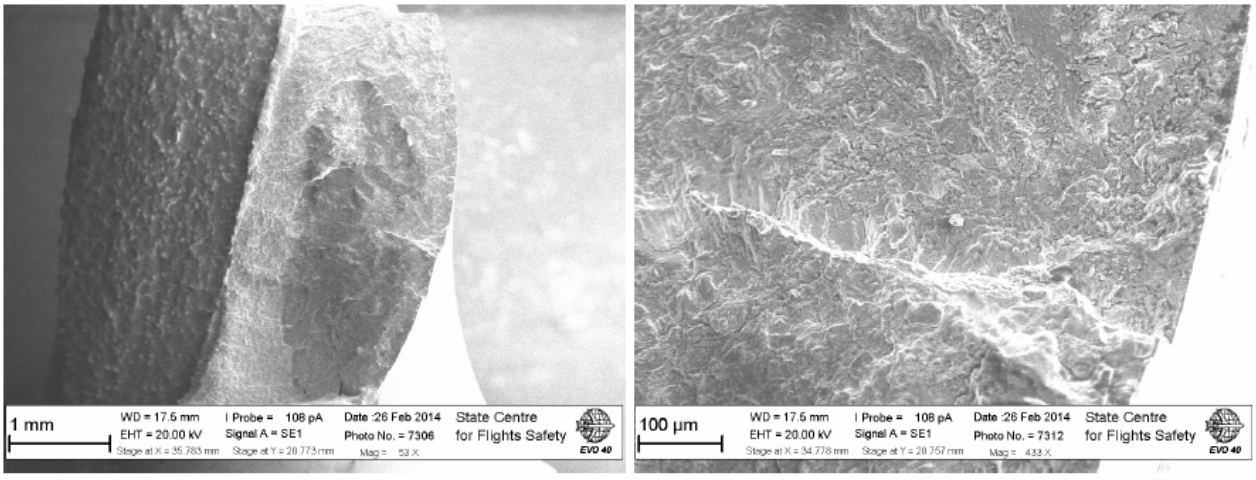

Figure 7.35: La fissure surfacique dans l'alliage VT3-1 forgé en torsion

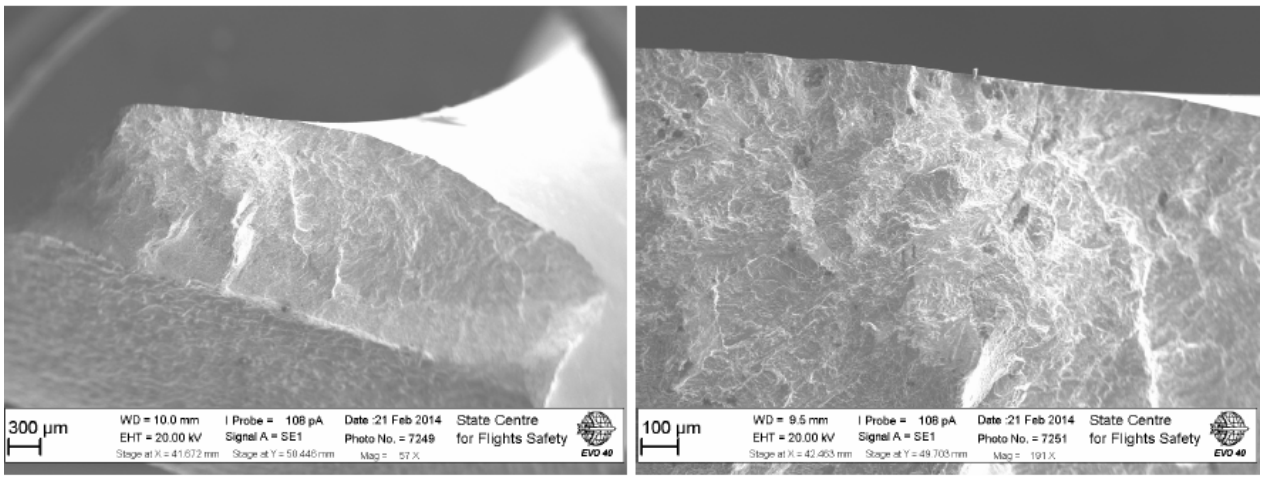

Figure 7.36: La fissure subsurfacique dans l'alliage VT3-1 forgé en torsion

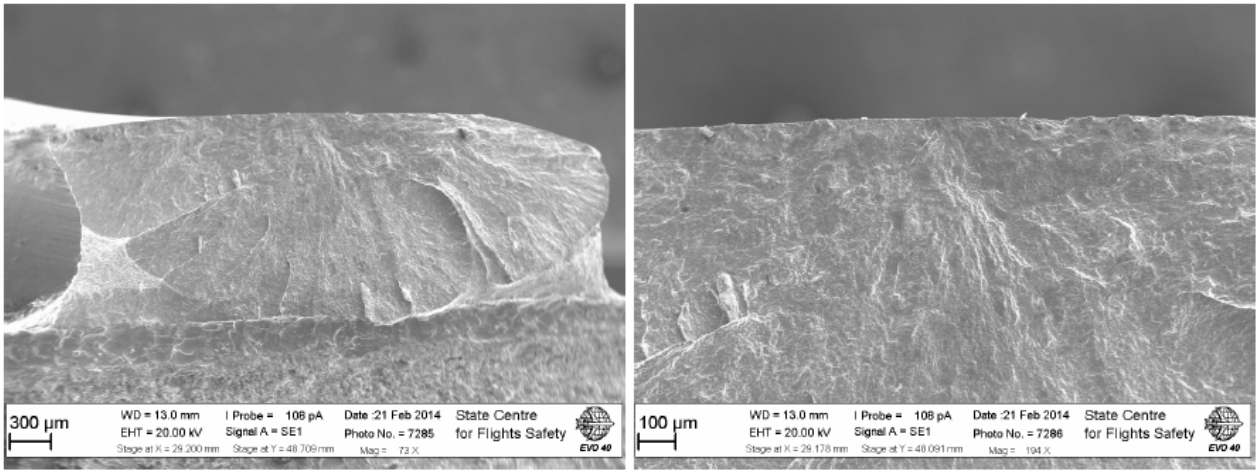

Figure 7.37: La fissure surfacique dans l'alliage VT3-1 éxtrudé en torsion

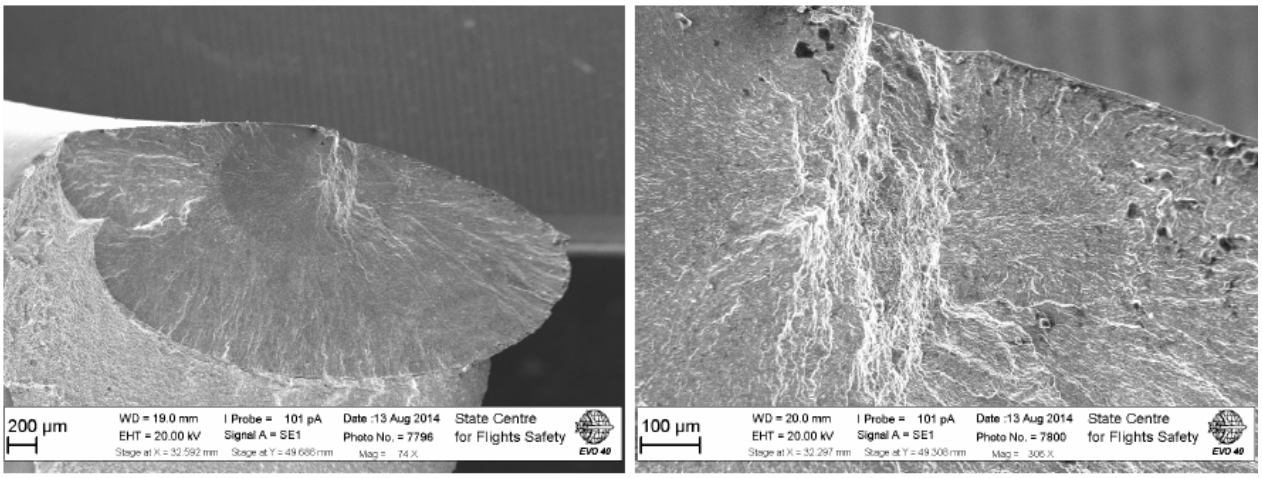

Figure 7.38: La fissure subsurfacique dans l'alliage VT3-1 extrudé en torsion

Bibliography

[1] Theodor Nicholas. Critical issues in high cycle fatigue. *International Journal of Fatigue*, 21:S221–S231, 1999.

[2] Shanyavskiy A.A. *Modeling of metals fatigue cracking. Synergetics in aviation.* Monograph, Ufa, Russia, 2007. in Russian.

[3] C.Bathias and P.C.Paris. *Gigacycle fatigue in mechanical practice.* Marcel Dekker, New York, 2005.

[4] Albert W.A.J. Uber treibseile am harz. *Archiv fur Mineralogie, Georgnosie*, 10:215 – 234, 1837. (*in german*).

[5] Schutz W. A history of fatigue. *Engineering Fracture Mechanics*, 54(2):263 – 300, 1996.

[6] Poncelet J.V. *Mechanique Industrielle.* Meline, Cans et Compagnie, Bruxelles, 1839. (*in french*).

[7] Timoshenko S.P. *History of The Strength of Materials.* McGraw-Hill Book Company, New York, 1953.

[8] Braithwaite F. On the fatigue and consequent fracture of metals. *Institution of Civil Engineers, Minutes of Proceedings*, XIII:463–474, 1854. London.

[9] Armand L. *Histoire des chemins de fer en France.* Les presse modern, Paris, 1966. (*in french*).

[10] Smith R.A. The versailles railway accident of 1842 and the first research into metal fatigue. *Fatigue'90*, 4(EMAS), 1990. Birmengham.

[11] York J.O. An account of a series of experiments on the comparative strength of solid and hollow axles. *Institution of Civil Engineers, Minutes of Proceedings*, 2:105–108, 1842. London.

[12] Rankine W.J.M. On the causes of the unexpected breakage of the journals of railway axles, and on the means of preventing such accidents by observing the law of continuity in their construction. *Institution of Civil Engineers, Minutes of Proceedings*, 2:105–108, 1842.

[13] McConnel J.E. On railway axles. *Proc.Ins.Mech.Engrs*, 13-27 October 1849. London.

[14] *Proceedings of Institution of Mechanical Engineers*, Jan. 1850. p.6.

[15] *Proceedings of Institution of Mechanical Engineers*, Apr. 1850. p.6.

[16] Morin A. *Resistance des matereaux*. 1853.

[17] Fairbairn W. Experiments to determine the effect of impact, vibratory action and long-continued changes of load on wrought-iron girders. *Philosophical Transactions*, 154, 1864.

[18] Wohler A. Bericht uber die versuche, welche auf der konigl. niederschlesisch-markischen eisenbahn mit apparaten zum messen der biegung und verdehung von eisenbahnwagenachsen wahrend der fahrt angestellt wurden. *Zeitschrift fur Bauwesen*, VIII:641 – 652, 1858. *in German*.

[19] Wohler A. Versuch zur ermittlung der auf die eisenbahnwagenachsen einwirkenden krafte und die widerstandsfahigkeit der wagen-achsen. *Zeitschrift fur Bauwasen*, X:583 – 616, 1860. *in German*.

[20] Moore H.F. and Kommers J.B. *The fatigue of metals*. McGraw-Hill Book, New York, 1927.

[21] Wohler A. Uber die festigkeits-versuche mit eisen und stahl. *Zeitschrift fur Bauwesen*, XX:73 – 106, 1870. *in German*.

[22] Spangenberg L. Uber das verhalten der metalle bei wiederholten anstrengungen. *Z. Bauw*, 24:473 – 495, 1874. and 25, 78 - 98.

[23] Schijvi J. Fatigue of structures and materials in the 20th century and the state of the art. *International Journal of Fatigue*, 25:679 – 702, 2003.

[24] Mann J.Y. *Bibliography on the fatigue of materials, components and structures, covering 1838 - 1969; 1970 - 1990*, volume 1-4. Pergamon Press.

[25] Humfrey J.C.W. Ewing J.A. The fracture of metals under repeated alternations of stress. *Phil Trans Roy Soc*, A200:241–50, 1903.

[26] Rosenhain W. Ewing J.A. The crystalline stritcfmre of metals. *Phil.Trans.*, 193:353, 1899.

[27] Gough H.J. and Hanson D. •. *Proc. Roy. Soc.*, 104:538, 1923.

[28] Polanyi M. Uber eine art gitterstorung, die einen kristall plastisch machen konnte. *Z. Phys*, 89:660 – 664, 1934.

[29] Taylor G.I. The mechanism of plastic deformation of crystals. part i. theoretical. *Proceedings of the Royal Society of London*, A 145(855):362 – 387, 1934.

[30] Orowan E. Theory of teh fatigue of metals. *Proc.Royal Society*, 171:79 – 105, 1939.

[31] Mott N.F. A theory of the origin of fatigue cracks. *Acta Metall*, 6:195–7, 1958.

[32] Hull D. Cottrell A.H. Extrusion and intrusion by cyclic slip in copper. *Proc Roy Soc*, A242:211–3, 1957.

[33] Head A.K. The growth of fatigue cracks. *Phil Mag*, 44:925–38., 1953.

[34] Basquin O.H. The experimental law of endurance tests. *Proc.Annual Meeting, American Society for Testing Materials*, 10:625 – 630, 1910.

[35] Kikuchi M. Naito T., Ueda H. •. *Mrtall Trans*, 15A::1431–6, 1984.

[36] Murakami Y. Effects of defects, inclusions and inhomogeneities on fatigue strength. *Fatigue*, 16:163 – 182, 1994.

[37] Bathias C. There is no infinite life in metallic materials. *FFEMS*, 22:559 – 565, 1999.

[38] Le Francois P. Drouillac C., Bathias C. How and why the fatigue sn curve does not approach an horizontal asymptote. *Int.J.Fatigue*, 23:143 – 151, 2001.

[39] Madayag A.F., editor. *Metal Fatigue: Theory and Design*. John Wiley, New York, 1969.

[40] Coffin Jr. L.F. Low cycle fatigue—a review. *Appl Mater Res*, 1:129, 1962.

[41] Hirschberg M.H. Mason S.S. Fatigue behavior in strain cycling in the low- and intermediate-cycle range. *Fatigue an Inter- disciplinary Approach. Syracuse University Press*, page 133–78, 1964.

[42] Langer B.F. Fatigue failure from stress cycles of varing amplitude. *Trans. ASME J. appl. Mech.*, 59:A160 – A162, 1937.

[43] Ryder D.A. Some quantitative information obtained from the examination of fatigue fracture surfaces. *Roy Aircraft Est, Tech Note Met*, 288, 1958.

[44] Schijve J. The significance of fractography for investigations of fatigue crack growth under variable- amplitude loading. *Fatigue Fract Engng Mater Struct*, 22:87 – 99, 1999.

[45] Irwin G.R. Analysis of stresses and strains near the end of a crack traversing a plate. *Trans ASME J Appl Mech*, 24:361–4, 1957.

[46] Anderson W.E. Paris P.C., Gomez M.P. A rational analytical theory of fatigue. *The Trend of Engineering*, 13:9 – 14, 1961.

[47] Elber W. *Fatigue crack propagation: some effects of crack closure on the mechanisms of fatigue crack propagation and cyclic tensile loading*. PhD thesis, University of New South Wales, 1968.

[48] W.Elber. Fatigue crack closure under cyclic tension. *Engineering Fracture Mechanics*, 2:37 – 44, 1970.

[49] Ritchie R.O. Mechanisms of fatigue-crack propagation in ductile and brittle solides. *International Journal of Fatigue*, 100:55 – 83, 1999.

[50] Wanhill R.J.H. Durability analysis using short and long fatigue crack growth data. In *National Conference Publication*, number 91/17, pages 100 – 104, Barton, Australia, 1991. Institution of Engineers.

[51] Pearson S. Initiation of fatigue cracks in commercial aluminium alloys and the subsequent propagation of very short cracks. *Engng Fract Mech*, 7:235–47, 1975.

[52] Miller K.J. The short crack problem. *Fatigue and Fracture of Engineering Materials and Structures*, 5(3):223 – 232, 1982.

[53] C.Bathias. Piezoelectric fatigue testing machines and devices. *International Journal of Fatigue*, 28:1438–1445, May 2006.

[54] Bathias C. Paris P.C. Huang Z., Wagner D. Subsurface crack initiation and propagation mechanisms in gigacycle fatigue. *Acta Materialia*, 58:6046 – 6054, 2010.

[55] Murakami Y. *Metal Fatigue: effect of small defects and nonmetallic inclusions*. Elsevier, 2002.

[56] Bathias C. Marines I., Bin X. An understanding of very high cycle fatigue of metals. *International Journal of Fatigue*, 25:1101 – 1107, 2003.

[57] Wheeler R. Larsen J.M. Szczepanski C.J., Jha S.K. Shade P.A. Demonstration of an in situ microscale fatigue testing technique on a titanium alloy. *International Journal of Fatigue*, 57:131 – 139, 2013.

[58] Murakami T. Nosho H. Shiozawa D., Nakai Y. Observation of 3d shape and propagation mode transition of fatigue crack in ti-6al-4v under cyclic torsion using ct imaging with ultra-bright synchrotron radiation. *International Journal of Fatigue*, 58:158 – 165, 2014.

[59] Goodman J. *Mechanics applied to engineering*. Longmans, Green and Co., London, 1899.

[60] Sendeckyj G.P. Constant life diagrams - a historical review. *International Journal of Fatigue*, 23:347 – 353, 2001.

[61] Nicholas T. Bellows R.S., Muli S. Validation of the step test method for generating haigh diagrams for ti-6al-4v. *International Journal of Fatigue*, 21:687 – 697, 1999.

[62] Miller J.L Howell F.M. •. In *ASTM Proceedings*, 1955.

[63] Gilormini P. Sauzay M. Surface and cyclic microplasticity. *Fatigue and Fracture of Engineering MAterials and Structures*, 23(7):573 – 579, 2000.

[64] Mughrabi H. Damage mechanisms and fatigue life: From the low to the very high cycle regime. *Procedia Engineering*, 55:636 – 644, 2013.

[65] Mughrabi H. In *Dislocations and Properties of Real Materials*, number 323, page 244. The institute of Metals, 1984. London.

[66] Ueda T. Murakami Y. Murakami Y., Nomoto T. On the mechanism of fatigue failure in the superlong life regime ($n > 10^7$ cycles) part i and part ii. *Fatigue and Fracture of Engineering Materials and Structures*, 23:893–902 and 903 – 910, 2000.

[67] Shiozawa K. Ochi Y. Nakajima T. Ogyma N. Sakai T., Takeda M. Experimental evidence of duplex s-n characteristics in wide life region for high strength steels. In *Proc. of FATIGUE 1999*, volume 1, pages 573 – 579, Beijing, 1999. Higher Education Press and West Midlands EMAS Ltd.

[68] Nishijima S. and Kanazawa K. Stepwise s-n curve and fish-eye failure in gigacycle fatigue. *Fatigue and Fracture of Engineering Materials and Structures*, 22:601 – 607, 1999.

[69] Hael Mughrabi. Fatigue an everlasting materials problem still en vogue. *Procedia Engineering*, 2:3–26, 2010.

[70] Claude Bathias. *Fatigue Limit in Metals*. Wiley, 2014.

[71] Szczepanski C.J. Larsen J.M., Jha S.K. et al. Reducing uncertainty in fatigue life limits of turbine engine alloy. *International Journal of Fatigue*, 57:103 – 112, 2013.

[72] Mughrabi H. Specific features and mechanisms of fatigue in the ultrahigh-cycle regime. *International Journal of Fatigue*, 28:1501 – 1508, 2006.

[73] Terentiev F.T. Ivanova V.S. *The nature of fatigue of metals*. Metallurgy, 1975. *in Russian*.

[74] Ravi Chandran K.S. Jha S.K. An unusual fatigue phenomenon: duality of s-n fatigue curve in the β-titanium alloy ti-10v-2fe-3al. *Scripta Materialia*, 48:1207 – 1212, 2003.

[75] Shiozawa K. Ochi Y. Nakajima M. Nakamura T. Oguma N. Sakai T., Takeda M. Experimntal reconfiguration of characteristic s-n property for high carbon chromium bearing steel in wide life region in rotating bending. *Journal of the Society of Material Science*, 49:779 – 785, 2000. In Japanese.

[76] Shanyavskiy A. Bifurcation diagram for in-service fatigued metals. *Procedia Engineering*, 2:241 – 250, 2010.

[77] French H. Fatigue and the hardening of steels. *Trans Am Soc Steel Treat*, 21:899 – 946, 1933.

[78] Klesnil M. The degree of damage at the french curve and at the fatigue limit during oscillating bend loading. *Metal Treat Drop Forging*, 55:55 – 63, 1965.

[79] Jones J.W. Pollock T. Kumar A., Torbet C.J. Nonlinear ultrasonics for in situ damage detection during high frequency fatigue. *Journal Appl Phys*, 58:2143–54, 2009.

[80] Bauschinger J. *Mitt Mech Tech Lab Munchen*, 13:1 – 115, •.

[81] Armstrong R.W. Antolovich S.D. Plastic strain localization in metals: origins and consequences. *Progress in Materials Science*, 59:1–160, 2014.

[82] F.P.E.Dunne D.L.McDowell. Microstructure-sensitive computation modeling of fatigue crack formation. *International Journal of Fatigue*, 32:1521 – 1542, 2010.

[83] P.C.Paris C.Bathias. Gigacycle fatigue of metallic aircraft components. *International Journal of Fatigue*, 32:894 – 897, 2010.

[84] H.Mughrabi. On the life-controlling microstructural fatigue mechanisms in ductile metals and alloys in the gigacycle regime. *Fatigue and Fracture of Engineering MAterials and Structures*, 22:633 – 641, 1999.

[85] C.Wang. *Microplasticity and Dissipation in Fatigue of ferum iron and steel after very high number of cycles*. PhD thesis, University Paris OUEST Nanterre La Defense, 2013.

[86] F.Pyczak B.Schonbauer S.Stanzl-Tschegg H.Mughrabi A.Weidner, D.Amberger. Fatigue damage in copper polycrystals subjected to ultrahigh-cycle fatigue below the psb threshold. *International Journal of Fatigue*, 32:872 – 878, 2010.

[87] L.Kunz P.Lukas. Specific features of high-cycle and ultra-high-cycle fatigue. *Fatigue and Fracture of Engineering MAterials and Structures*, 25:747 – 753, 2002.

[88] H.Tada C.Bathias I.Marines-Garcia, P.C.Paris. Fatigue crack growth from small to long cracks in vhcf with surface initiations. *International Journal of Fatigue*, 29:2072 – 2078, 2007.

[89] T.Sakai. Review and prospects for current studies on very high cycle fatigue of metallic materials for machine structural use. *Journal of Solid Mechanics and Materials Engineering*, 3(3):425 – 436, 2009.

[90] S.Ishihara K.Shiozawa, L.Lu. S-n curve characteristics and subsurface crack initiation behaviour in ultra-long life fatigue of a high carbon-chromium bearing steel. *Fatigue and Fracture of Engineering Materials and Structures*, 24:781 – 790, 2001.

[91] L.Lu K.Shiozawa. Very high-cycle fatigue behaviour of shot-peened high-carbon-chromium bearing steel. *Fatigue and Fracture of Engineering Materials and Structures*, 25:813–822, 2002.

[92] C.Leyens and M.Peters. *Titanium and Titanium alloys. Fundamentals and Aplications*. WILEY-VCH, 2003.

[93] Jones I.P. and Hutchinson W. B. Stress-state dependence of slip in ti – 6al – 4v and other h.c.p. metals. *Acta Metallurgica*, 29:951 – 968, 1981.

[94] Neeraj T. Hou D. Suri S., Viswanathan G.B. and Mills M.J. Room temperature deformation and mechanisms of slip transmission in oriented single-colony crystals of an alpha / beta titanium alloy. *Acta Materialia*, 47:1019–1034, 1999.

[95] Zupan M. Hemker K.J. Savage M.F., Tatalovich J. and Mills M.J. Deformation mechanisms and microtensile behavior of single colony ti-6242si. *Materials Sci- ence and Engineering*, A, 319-321:398 – 403, 2001.

[96] Suri S. Mills M.J., Hou D.H. and Viswanathan G.B. *Orientation relationship and structure of alpha/beta interfaces in conventional titanium alloys.* Boundaries and Interfaces in Materials, Warrendale, 1988.

[97] Lutjering G. Influence of processing on microstructure and mechanical properties of $\alpha + \beta$ titanium alloys. *Material Science and Engineering*, A243:32 – 45, 1998.

[98] Evans W.J. Bache M.R. Tension and torsion fatigue testing of a near-alpha titanium alloy. *International Journal of Fatigue*, 14(5):331 – 337, 1992.

[99] Chan K.S. Roles of microstructure in fatigue crack initiation. *International Journal of Fatigue*, 32:1428 – 1447, 2010.

[100] K. LeBiavant-Guerrier. *Etude d'amorcage de fissures de fatigue dans le Ti-6Al-4V.* PhD thesis, Ecole Centrale, 2000.

[101] Humbert M. Bocher P Jahazi M. Germain L, Gey N. Analyasis of sharp microstructure heterogeneinities a bimodal imi 834 bilet. *Acta Materialia*, 53(13):3535 – 3543, 2005.

[102] N. E. Paton J. C.Williams, R. G. Baggerly. Deformation behavior of hcp ti- al alloy single crystals. *Metallurgical and Materials Transactions A*, 33A:837–850, 2002.

[103] C.J.Szczepanski. *The Role of Microstructural Variability on the Very High Cycle Fatigue Lifetime Variability of the $\alpha + \beta$ Titanium Alloy, Ti-6Al-2Sn-4Zr-6Mo.* PhD thesis, The University of Michigan, 2008.

[104] Grosskreutz J.C. Benson D.K. and Shaw G.G. Mechanisms of fatigue in mill-annealed ti-6al-4v at room temperature and 600. *Metallurgical Transactions*, 3A:1239, 1972.

[105] Hall J.A. Fatigue crack initiation in alpha-beta titanium alloys. *International Journal of Fatigue*, 19(1):S23 – S37, 1997.

[106] Finnerty D.L. Walcher J.C. Sae paper 821437. In *Proceedings Aerospace Congress and Expositions*, October 1982.

[107] Lutjering G. Peters M., Gysler A. •. *Metal Transaction*, 15A:1597, 1984.

[108] Zaeffere S. A study of active deformation systems in titanium alloys: dependence on alloy composition and correlation with deformation texture. *Materials Science and Engineering A*, 344:20 – 30, 2003.

[109] Halford G. Cumulative fatigue damage modeling-crack nucleation and early growth. *International Journal of Fatigue*, 19:s253 – s260, 1997.

[110] Chesnutt J. C. Margolin H., Williams J. C. and Luetjering G. A review of the fracture and fatigue behavior of titanium alloys. *Titanium '80, page Science and Technology*, 1:169–216, 1980. Kyoto; Japan; 19-22 May.

[111] Mendez J.. Bridier F., Villechaise P. Analysis of slip and crack initiation pro- cesses activated by fatigue in a alpha/beta titanium alloy in relation with local crys- tallographic orientation. *Fatigue 2006 (electronic proceedings)*, 2006.

[112] Pommier S. LeBiavant K. and Prioul C. Local texture and fatigue crack initiation in a ti-6al-4v titanium alloy. *Fatigue and Fracture of Engineering Materials and Structures*, 25:527 – 545, 2002.

[113] Denkenberger R. Furrer D. Bhattacharyya D., Viswanathan G.B. and Fraser H.L.. The role of crystallographic and geometrical relationships between alpha and beta phases in an alpha/beta titanium alloy. *Acta Materialia*, 51:4679 – 4691, 2003.

[114] Beevers J. Ward-Close C.M. The influence of grain orientation on the mode and rate of fatigue crack trowth in α-titanium. *Metalurgical Transaction A*, 11A:1007 – 1017, 1980.

[115] Yuebo X. Suhua A., Zhongguang W. The fatigue deformation and fracture charachteristics of coarse grained policrystalline α-titanium. *Scripta Metallurgica*, 19:1089 – 1093, 1985.

[116] •. Low cycle fatigue behaviour of ti-6al-2sn-4. *Metallurgical Transaction*, 13A:257 – 268, 1982.

[117] Nian Zhou Sandvik Guocai Chai. Study of crack initiation or damage in very high cycle fatigue using ultrasonic fatigue test and microstructure analysis. *Ultrasonics*, 53:1406 – 1411, 2013.

[118] Blenkinsop P.A. Neal D.F. Internal fatigue origins in α - β titanium alloy. *Acta metallurgica*, 24, 1976.

[119] Endo M. McEvily A.J. On a mechanism for vhcf. In DVM, editor, *Fifth International Conference on Very High Cycle Fatigue*, ISBN 978-3-9814516-0-3, page 572, 2011.

[120] Larsen M.J. Jones J.W. Szczepanski C.J., Jha S.K. The role of microstructure on sequential stages of the very high cycle fatigue behavior of an $\alpha + \beta$ titanium alloy ti-6al-2sn-4zr-6mo. In Christ H.J. Berger C., editor, *Proceedings of Fifth International Conference on Very High Cycle Fatigue*, Berlin, Germany, 2011.

[121] Koss D.A. Chan K.S., Wojcil C.C. •. *Metallurgical Transaction A*, 1981.

[122] Randle V. Wilson R.J. Bache M.R., Evans W.J. Characterization of mechanical anisotropy in titanium alloys. *Material Science and Engineering*, A257:139 – 144, 1998.

[123] Bache M.R. Processing titanium alloys for optimum fatigue performance. *International Journal of Fatigue*, 21:S105 – S111, 1999.

[124] Oguma H. *Very High Cycle Fatigue properties of Ti-6Al-4V Alloy.* PhD thesis, Hokkaido University, 2006.

[125] Fukunaga K. Akahori T., Niinomi M. and Inagaki I. Effects of microstructure on the short fatigue crack initiation and propagation characteristics of biomedical al- pha/beta titanium alloys. *Metallurgical and Materials Transactions A*, 31A(8):1949 – 1958, 2000.

[126] Stubbington C.A. and Bowen A.W. Improvements in the fatigue strength of ti- 6al-4v through microstructure control. *Journal of Materials Science*, 9:941 – 947, 1974.

[127] Corderman R.R. Sutliff J.A. Woodfield A.P., Gorman M.D. and Yamrom B. Effect of microstructure on dwell fatigue behavior of ti-6242. *Titanium '95.*, 2:1116 – 1123, 1996. Birmingham; UK.

[128] Oja M. Matthews R. Davidson D.L., Tryon R.G. and Ravi Chandran K. S. Fatigue crack initiation in waspaloy at 20 deg c. *Metallurgical and Materials Trans- actions A*, 38:2214–2225, 2007.

[129] Wu T. Jago G. Bathias C., Bechet J. Une machine de fatigue vibratoire fonctionnant a temperature cryogenique et a 20 khz. *Application a l'etude du TA6VPQ a 20 kHz et 77 K*, 1994. Rapport - SEP, ITMA/CNAM.

[130] Banov M. Shanyavskiy A. The twining mechanism of subsurface fatigue cracking in ti-6al-2sn-4zr-2mo-0.1si alloy. *Engineering Fracture Mechanics*, 77:1896 – 1906, 2010.

[131] Russian State Standard GOST-19807-91. Titanium and wrought titanium alloys. Technical report, 2009.

[132] Shanyavskiy Andrey. Fatigue cracking simulation based on crack closure effect in al-based sheet materials subjected to biaxial cyclic loads. *Engineering Fracture Mechanics*, 78:1516 – 1528, 2011.

[133] A.Shanyavskiy C.Bathias C.Wang, A.Nikitin. An understanding of crack growth in vhcf from an internal inclusion in high strength steel. In *Proceedings of Crack Path 2012*, pages 267 – 278, 2012.

[134] Snegireva L.A. Fainbron A.S., Polkin I.S. The featuries of crack initiation and growth in granulated vt25u alloy under the low cycle fatigue loading. *Technology of light alloys*, 3:49 – 54, 2008.

[135] S.Stanzl-Tschegg. Very high cycle fatigue measuring techniques. *International Journal of Fatigue*, 60:2–17, 2013.

[136] E.K.Tschegg S.E.Stanzl-Tschegg, H.R.Mayer. High frequency method for torsion fatigue testing. *Ultrasonics*, 31(4):275–280, 1993.

[137] E.K.Tschegg. Sliding mode crack closure and mode iii fatigue crack growth in mild steel. *Acta metall*, 31(9):1323–1330, 1983.

[138] Xue H.Q. *Explanation on gigacycle fatigue of materials in tension, bending and torsion loading*. PhD thesis, CNAM, 2005.

[139] I.Marines-Garcia C.Bathias H.Q.Xue, E.Bayraktar. Torsional fatigue behaviour in gigacycle regime and damage mechanism of the perlitic steel. *Journal of Achievements in Materials and Manufacturing Engineering*, 31(2):391–397, 2008.

[140] C.Bathias H.Q.Xue. Crack path in torsion loading in very high cycle fatigue regime. *Engineering Fracture Mechanics*, 77:1866–1879, 2010.

[141] C.Bathias H.Xue, W.Tieying. Gigacycle behavior of cast aluminum in tension and torsion loading. *Transactions of Nanjin University of Aeronauties and Astronautics*, 28(1):32–37, 2011.

[142] H.Mayer M.Wakita K.Tanaka Y.Akiniwa, S.Stanzl-Tschegg. Fatigue strength of spring steel under axial and torsional loading in the very high cycle regime. *International Journal of Fatigue*, 30:2057–2063, 2008.

[143] H.Ishii K.Tohgo T.Fujii T.Yagasaki M.Harada Y.Shimamura, K.Narita. Fatigue properties of carburised alloy steel in very high cycle regime under torsion loading. *International Journal of Fatigue*, 60:57–62, 2014.

[144] G.Wagner D.Eifler S.Heinz, F.Balle. Analysis of fatigue properties and failure mechanisms of ti6al4v in the very high cycle fatigue regime using ultrasonic technology and 3d laser scanning vibrometry. *Ultrasonics*, 53:1433–1440, 2013.

[145] Palin-Luc T. Bathias C., Nikitin A. A new piezoelectric fatigue testing machine in pure torsion for gigacycle regime. In *Proceeding of VHCF6 conference*, 2014. Chengdu, China.

[146] Cowles B.A. High cycle fatigue in aircraft gas turbines - an industry perspective. *International Journal of Fatigue*, 80:147 – 163, 1996.

ANNEXES

ANNEX A

Gigacycle fatigue testing concept

The gigacycle fatigue testing concept is differ from conventional fatigue tests and it is not just a question of ultra high loading frequency. The conventional fatigue testing is always performed under the force vibration condition, while the ultrasonic loading deals with free vibrations of specimen at one of its natural frequency. The second important difference of ultrasonic testing is absolutely symmetric loading mode: the ends of specimens are assumed as a free, while the conventional tests needs to clump one of the end of specimen and the given force (or deformation) is applied to the another end. Therefore, the strain-stress field is not absolutely symmetrical even for specimens with geometric symmetry.

The ultrasonic testing concept is based on the theory of elastic waves propagation in elastic body. In order to better understand the details of gigacycle concept, some basic ideas of this theory will be introduced below. The differential equation for a general three-dimensional isotropic elastic body in a Cartesian coordinate are following

$$\rho\frac{\partial^2 u}{\partial t^2} = \frac{E}{1+\nu}\left(\frac{1}{1-2\nu}\cdot\frac{\partial e}{\partial x} + \nabla^2 u\right) \tag{7.1}$$

$$\rho\frac{\partial^2 v}{\partial t^2} = \frac{E}{1+\nu}\left(\frac{1}{1-2\nu}\cdot\frac{\partial e}{\partial y} + \nabla^2 v\right) \tag{7.2}$$

$$\rho\frac{\partial^2 w}{\partial t^2} = \frac{E}{1+\nu}\left(\frac{1}{1-2\nu}\cdot\frac{\partial e}{\partial z} + \nabla^2 w\right) \tag{7.3}$$

where u, v and w are displacement along x, y and z respectively. E and ν the Young's modulus and Poisson's ratio, ρ the mass density and ∇^2 the Laplacian. The e is volume dilatation which can be expressed in the next form

$$e = \frac{\partial u}{\partial x} + \frac{\partial v}{\partial y} + \frac{\partial w}{\partial z} \tag{7.4}$$

According to the elastic wave theory the following two types of wave may exist in an infinite isotropic elastic body: longitudinal and transverse waves. The velocities of these waves are not the same and can be expressed in terms of material constants

$$c_{long} = \sqrt{\frac{E(1-\nu)}{(1+\nu)(1-2\nu)\rho}} \tag{7.5}$$

$$c_{trans} = \sqrt{\frac{E}{2(1+\nu)\rho}} \tag{7.6}$$

Besides these two types of waves the surface wave may also be produced if there is a boundary of elastic body. The amplitude of vibrations is rapidly decreases with the distance from the surface and the wave velocity is less than the velocity inside the body. Without loss of generality, the one-dimension case of elastic wave propagation can be discussed for straight cylinder specimen to simplify the calculations, Fig. 7.39.

Let's assume the longitudinal wave to illustrate the basic ideas. The elastic wave comes from one end of the bar and travels through the length l, than it reflected from one the other end and returns to the initial place of entrance. In case of one-dimension problem, the equation for longitudinal wave velocity is the next

$$c = \sqrt{\frac{E}{\rho}} \tag{7.7}$$

and the system of differential equations reduced to the next form

$$\frac{\partial^2 u}{\partial t^2} = \frac{E}{\rho}\frac{\partial^2 u}{\partial x^2} \tag{7.8}$$

The solution of equation 7.8 is given by

$$u = \sum_{n=1}^{\infty} u_n(x,t) \tag{7.9}$$

where

$$u_n(x,t) = (A_{n-1} cos\frac{n\pi ct}{l} + B_{n-1} sin\frac{n\pi ct}{l}) cos\frac{n\pi x}{l} \tag{7.10}$$

The boundary conditions of ultrasonic fatigue testing require the displacement to be maximum at the both ends of the bar, whereas the strain vanishes at the same place. That is

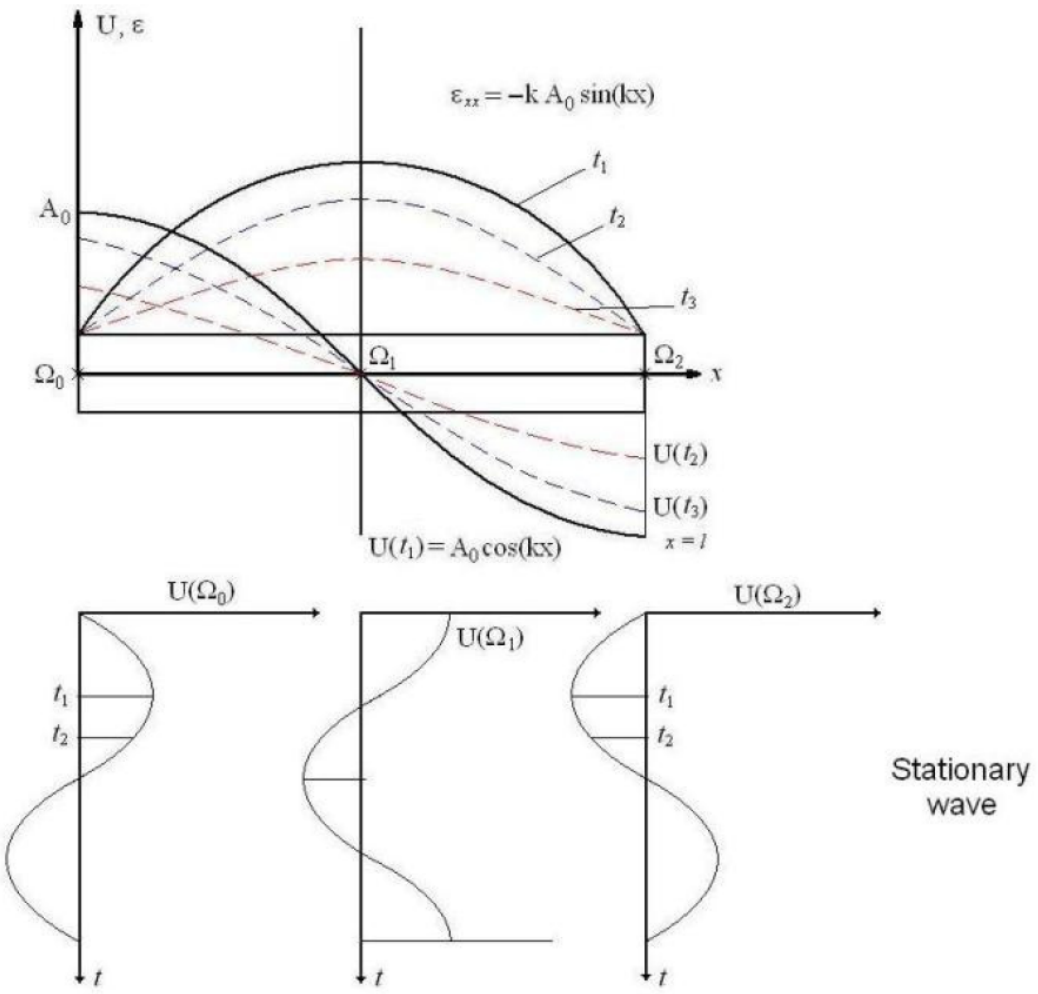

Figure 7.39: Displacement and strain variation in a cylindrical bar

$$(\frac{\partial u}{\partial x})|_{x=0,l} = 0 \tag{7.11}$$

For the first mode of vibrations, the equation (7.10) becomes

$$u(x,t) = A_0 cos(kx) sin(\omega t) \tag{7.12}$$

where

$$k = \frac{\pi}{l}, \qquad \omega = \frac{\pi c}{l} \tag{7.13}$$

The amplitude of vibration at each point along the bar is

$$U(x) = A_0 cos(kx) \tag{7.14}$$

where A_0 is the displacement amplitude at the end of the bar. The strain ϵ of each point is given by

$$\epsilon(x,t) = -kA_0 sin(kx) sin(\omega t) \tag{7.15}$$

with its maximum

$$\epsilon(x) = -kA_0 sin(kx) \tag{7.16}$$

the strain rate is

$$\dot{\epsilon} = -k\omega A_0 sin(kx) cos(\omega t) \tag{7.17}$$

with its maximum

$$\dot{\epsilon} = -k\omega A_0 sin(kx) \tag{7.18}$$

Thus, the analytical solution fro displacement, strain and therefore stress field within straight cylindrical bar can be obtained analytically. From equations (7.7) and (7.13) the resonance length of cylindrical bar can be derived as a function of frequency and elastic modulus of material

$$l = \frac{1}{2f}\sqrt{\frac{E_d}{\rho}} \tag{7.19}$$

for the first mode of vibration, where $f = \omega/2\pi$ is the frequency and E_d is the dynamic elastic modulus for consideration of dynamic effect. The node of displacement where the displacement vanishes and therefore the strain is maximum is located in the middle of cylindrical bar of length l. At the both ends the displacement is maximum and strain, stress and strain rate are vanished. Thus, at the $l = \frac{l}{2}$ we will have

$$u = 0, \qquad \epsilon = -kA_0, \qquad \sigma = -E_d kA_0, \qquad \dot{\epsilon} = -k\omega A_0 \tag{7.20}$$

at the ends of cylindrical bar $x = 0, l$

$$u = A_0, \qquad \epsilon = 0, \qquad \sigma = 0, \qquad \dot{\epsilon} = 0 \tag{7.21}$$

Thus, the length of specimens for ultrasonic testing is inversely proportional to the frequency. It's mean, that the very high frequencies of investigation (92 kHz or 199 kHz) are not practically use, because the size of specimen should be too small for working under the resonance conditions. The simple calculations for cylindrical bar made from steel shows, that at 199 kHz, the length of specimen should be around 13 mm. Thus, the more frequency of 20 kHz is optimal solution for accelerated tests. It provides to carry out a long life tests within relativity short time and at the same time provide to use big enough specimens to be able measure the displacements, strain and energy dissipation.

The principles of gigacycle testing can be applied to the specimens with reduced cross section in the similar way to the cylindrical bar. The main idea fro calculation is to separate the problem into two parts: analytical solution for reduced section and the analytical solution for cylindrical part of specimen. These two solution should be 'glued' at the transition plane. Thus, the full solution for specimen can be found. The details of analysis on analytical solution for specimens with hyperbolic profile in the gage section is given in the work of Claude Bathias [3]. The same principle is applied for designing the elements of ultrasonic torsion machine, such as ultrasonic horns. The description of piezoelectric testing machine is given in the next section.

ANNEX B

Gigacycle fatigue testing machines

The gigacycle fatigue testing machine is usually based on magneto-strictive or piezoelectric transducer, which is capable to transform the sinusoidal electric signal into mechanical vibration of the same frequency. The first machine using this principle was built by Warren Mason in 1950th USA. The first used in France of the machine working at high frequency was in 1967 year by Claude Bathias. The further use of high frequency machines was restrictive due to the lack of commercially available test equipment, forcing the individual investigators to work with improvised facilities not readily amenable to standardized experimental conditions [53]. With developing the high performance systems of controlling, the interest to the accelerated fatigue testing techniques has arise. At the time, there have no standards for testing procedure and testing machines for ultrasonic fatigue, that's why several laboratories over the all World had started to develop its own ultrasonic testing machines. Between others, the next laboratories should be outlined as leading laboratories in the fields of gigacycle fatigue: Claude Bathias in France, Willertz in United States, Stanzl in Austria, Ni in China Ishii in Japan and Puskar in Slovakia [3].Although ultrasonic fatigue test machines in these laboratories are not the same, some components are common to all machines. The three

most important are: (1) a high frequency generator that generates 20 kHz sinusoidal electrical signal, (2) a transducer that transforms the electrical signal into mechanical vibration, and (3) a control unit.

Early ultrasonic testing machines were capable to carry out just a longitudinal tension-compression tests, which further were modified to do a longitudinal tension-tension tests also. But the progress has been made to extend the ultrasonic fatigue technique to variable amplitude loading conditions, low or high temperature environments, torsional, bending or multi-axial tests, and so on. Despite on the different loading modes and regimes, the principle of ultrasonic piezoelectric fatigue testing is the same and can be schematically represented in the following form, Fig. 7.40.

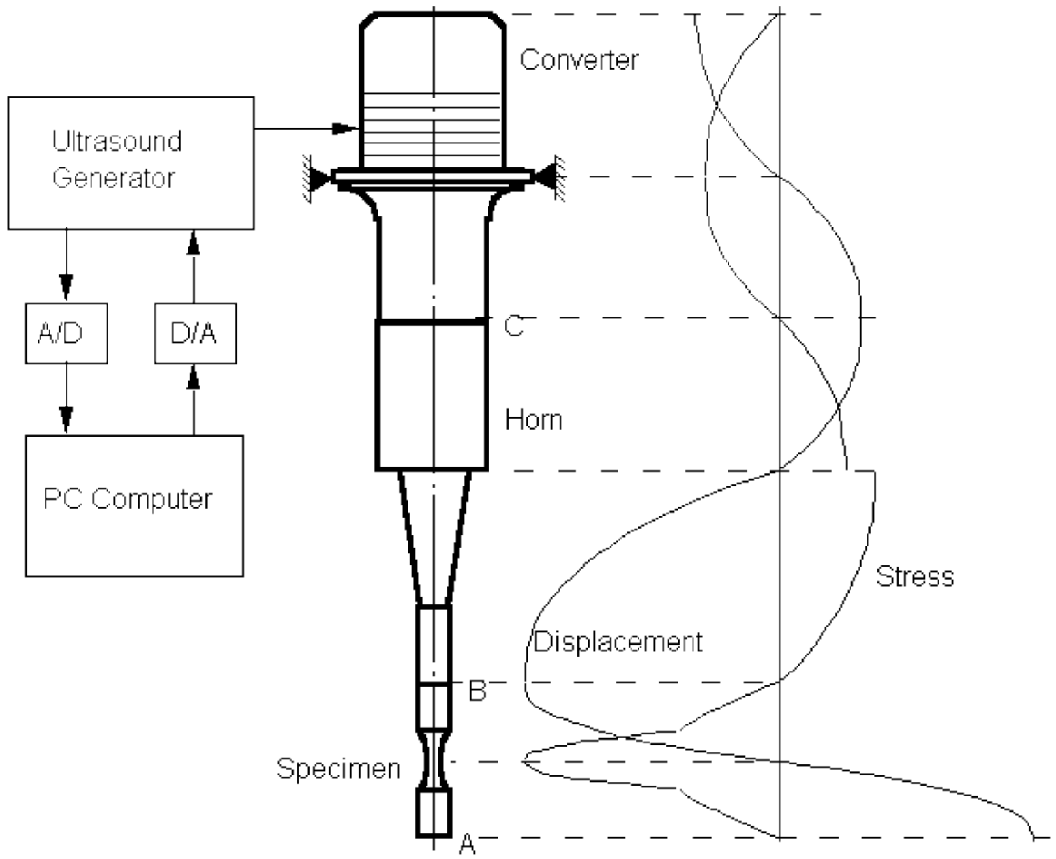

Figure 7.40: Schema of typical ultrasonic piezoelectric fatigue testing machine

As was mentioned above, the amplitude of vibration, generated by piezoelectric transducer is governed by tension of sinusoidal electric signal. Therefore, in order to control the ultrasonic fatigue testing machine, the high-performance personal computer with integrated milty-function board is used. The special software allows to command the amplitude of electrical signal and further permanently compare it with response of mechanically vibrated

system and if necessary to adjust the value. The generated by this software the control signal goes to the ultrasonic generator through the control box which is analog/digital - digital/analog converter. The control box is used to perform the communication between personal computer and ultrasonic generator. Further, the generator build the high frequency electrical signal based on low frequency control signal coming from software. The generated high-frequency signal goes to the piezoelectric transducer, there it transforms into mechanical vibration of the same frequency. The fatigue testing machine performs the scan of natural frequency of mechanically vibrated part of testing system. The range of working frequency for the testing machine is limited by 19500 Hz from the below and 20500 Hz from above. The natural frequency is determinate by ultrasonic generator automatically as changing of phase. The feedback of fatigue testing system allows to adjust the loading frequency to the natural frequency of vibrating part and also to control permanently the amplitude of vibration. Thus, the ultrasonic torsion machine turns into the correct working conditions.
The amplitude of vibration, which can be obtained by using piezoelectric converter is relativity small and often does not exceeds the value of several one - two tenths of microns. Therefore, the mechanically vibrating elements are used as for transverse of vibrations from piezoelectric transducer to the specimen, as well to amplify the amplitude of ultrasonic vibrations. All these elements, which called ultrasonic horns, are designed to be in resonance at the natural frequency of piezoelectric transducer and the mode of vibration should be the same. The distribution of displacement and stress (strain) field within the correctly designed mechanical part is shown on Fig. 7.40. The small amplitude vibrations comes to the ultrasonic horn at point 'C' and induces the longitudinal stationary waves. The geometry of ultrasonic horn is designed so, that to amplify the amplitude of mechanical vibrations.

Such fatigue testing technique can be adapted for different loading regimes, such as tension-tension by adding the static load, fretting fatigue by designing the special specimens, the bending tests by designing an additional support and specimens for bending, torsion by using the complex two-horns mechanical part. Also, the piezoelectric fatigue testing machine can be adapted to the tests in different environments, such as low temperature by using liquid gazes, elevated temperatures by using as a heating non contact element, as well high temperature oven. Moreover, the tests in aggressive environment, such as salt water can be performed by using ultrasonic fatigue testing system. Within the present research project, the tension-compression, tension-tension and torsion machine at ambiance temperatures will be used. Some more information about installation of these tests will be introduces in the Chapter II. The development of accelerated fatigue testing methods allows to investigate the behaviour of materials in the range of very long life. The results obtained over the all Word by using different testing machines has shown, that crack initiation under VHCF loading is occurs in the bulk of material even below the classical fatigue limit and the process of crack

initiation takes more than 90 % of total fatigue life. Thus, the ultrasonic fatigue machines allows to obtain the fracture surfaces and investigate the more interesting stage of fatigue damage accumulation in case of VHCF. The following section will summarize the progress in study of crack initiation stage for different materials and discuss the existing models of initiation in case of VHCF loading.

ANNEX C-1

Results of fatigue tests on S-, M- and L-XX series

Material: VT3-1 (Ti-6Al-4Mo)			**Forged Titanium Alloy**			
Name of test	Constant Amplitude Fatigue Tests with R=-1 on air					
Configuration:	TC and TGD ultrasonic horns				R=	-1
Lifetime aim	10^9 cycles				Frequency	19.9 kHz
Temperature	Room	Environment: Air			Machine	Ultasonic

•

Specimen Geometry:	Smooth		Method of examination	***	
Calibration:	Optical laser captor			Total	(Failed)
Useful diameter d(mm)	3		Number of tested samples	20	(20)
Equation:	$\sigma_a = 14.85 \times Displ(PC) + 0.237$			Dislp.Mode:	Ti-Nik
Units of Stress	MPa			Units of Displacement	μm

•

Test	Specimen	σ_a	σ_m	σ_{max}	N_f	Crack
1	S1	370	0	370	1.1×10^8	Crack
2	S2	385	0	385	2.85×10^9	Crack
3	S3	430	0	430	1.99×10^7	Crack
4	S4	400	0	400	2.53×10^8	Crack
5	S5	370	0	370	8.86×10^8	Crack
6	S6	430	0	430	6.79×10^8	Crack
7	S7	430	0	430	1.18×10^8	Crack
8	M1	370	0	370	2×10^9	No
9	M1	400	0	400	1.0×10^{10}	No
10	M2	415	0	415	1.2×10^7	Crack
11	M3	370	0	370	3.84×10^9	Crack
12	M4	385	0	385	1.1×10^7	Crack
13	M5	400	0	400	5.04×10^7	Crack
14	M6	400	0	400	2.98×10^7	Crack
15	M7	400	0	400	1.98×10^7	Crack
16	L1	350	0	350	5.0×10^9	Crack
17	L1	360	0	360	5.0×10^9	Crack
18	L2	385	0	385	1.08×10^7	Crack
19	L3	430	0	430	6.84×10^5	Crack
20	L4	415	0	415	4.22×10^7	Crack
21	L5	430	0	430	4.93×10^7	Crack

Material: VT3-1 (Ti-6Al-4Mo)				**Forged Titanium Alloy**		
Test	Specimen	σ_a	σ_m	σ_{max}	.....N_f.....	Crack
22	L6	385	0	385	1.19×10^9	Crack
23	L7	415	0	415	2.75×10^6	Crack
24	L8	370	0	370	1.26×10^6	Crack

ANNEX C-2

The fracture surfaces of tension-compression (R-1) fatigue specimens from forged VT3-1 titanium alloy (S-, M-, L-series)

S1,
$\sigma_a = 370$ MPa,
$N_f = 1.1 \times 10^8$

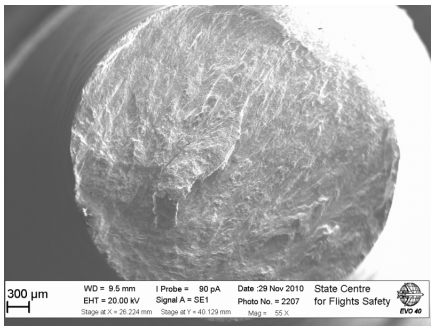

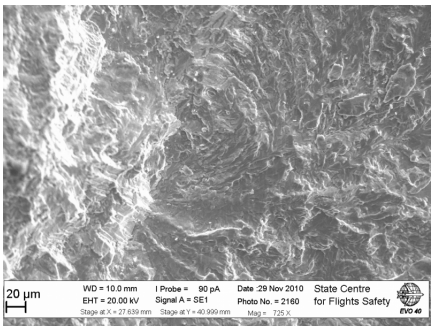

S2,
$\sigma_a = 385$ MPa,
$N_f = 2.85 \times 10^9$

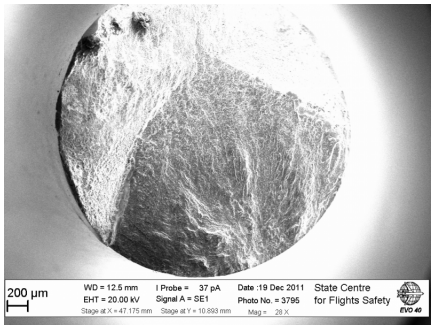

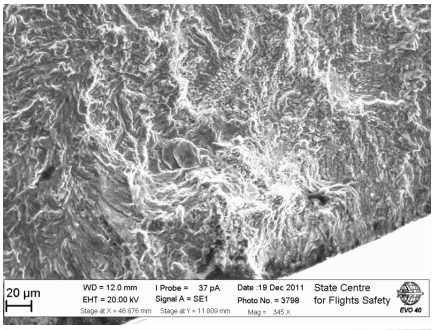

S3,
$\sigma_a = 430$ MPa,
$N_f = 1.99 \times 10^7$

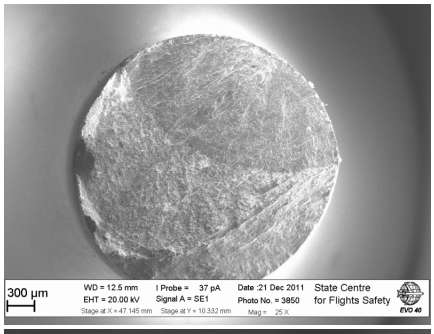

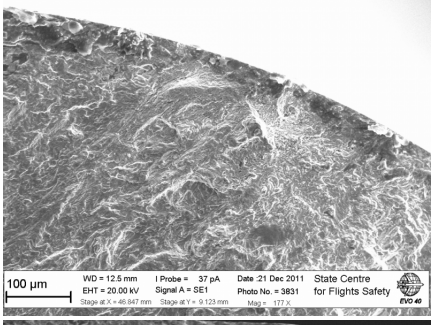

S4,
$\sigma_a = 400$ MPa,
$N_f = 2.53 \times 10^8$

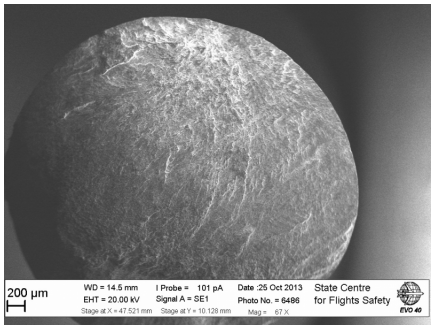

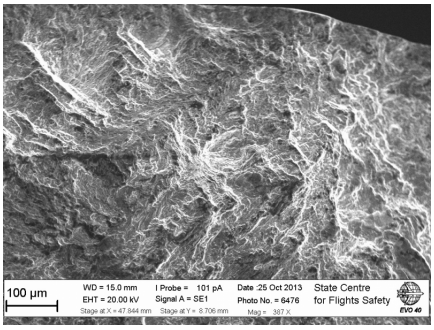

S5,
$\sigma_a = 370$ MPa,
$N_f = 8.86 \times 10^8$

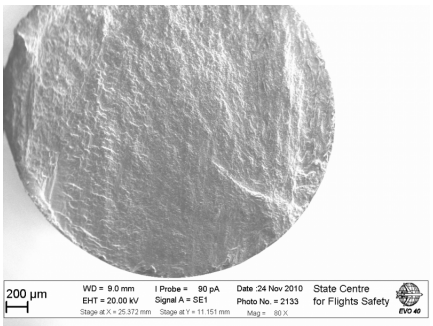

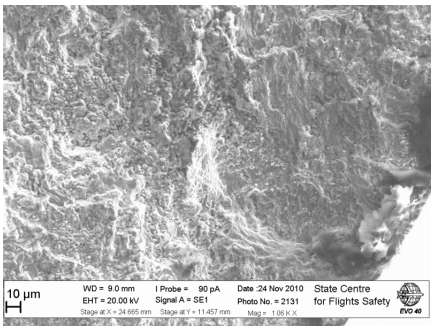

S6,
$\sigma_a = 430$ MPa,
$N_f = 6.79 \times 10^8$

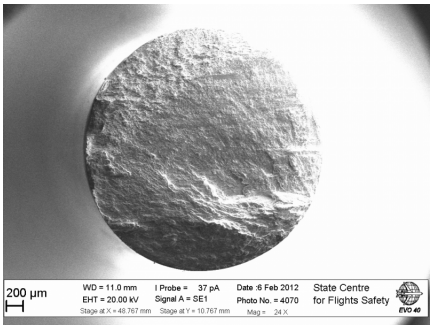

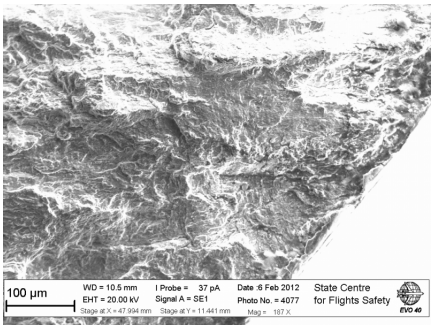

S7,
$\sigma_a = 430$ MPa,
$N_f = 1.18 \times 10^8$

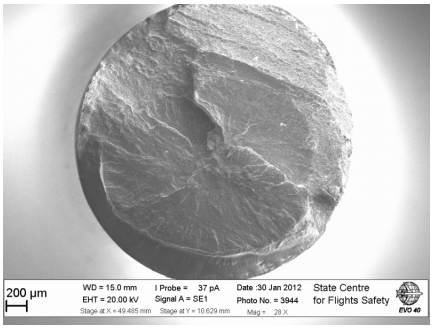

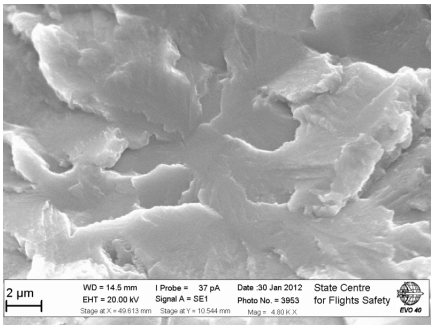

M2,
$\sigma_a = 415$ MPa,
$N_f = 1.2 \times 10^7$

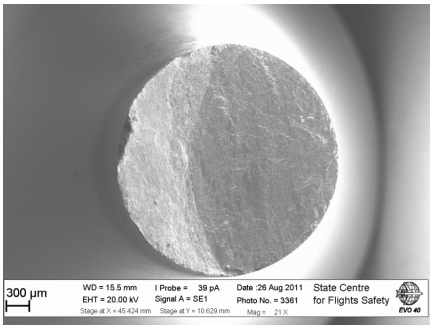

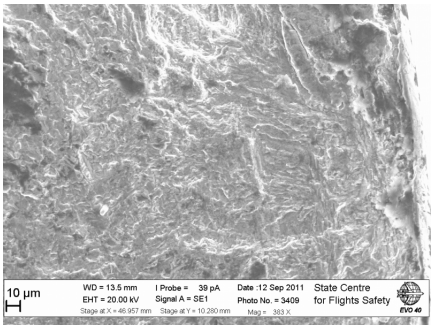

M3,
$\sigma_a = 370$ MPa,
$N_f = 3.84 \times 10^9$

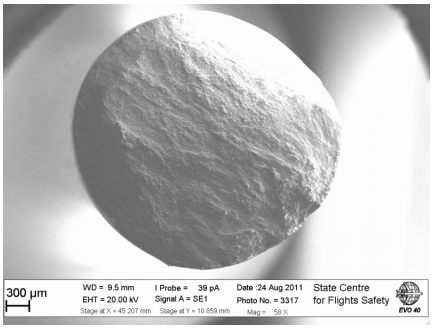

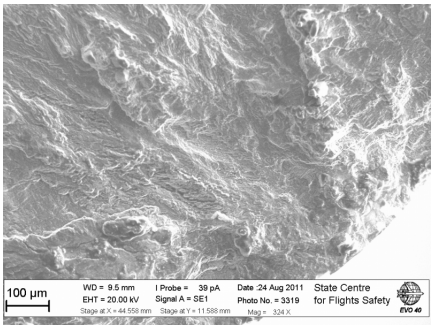

M4,
$\sigma_a = 385$ MPa,
$N_f = 1.1 \times 10^7$

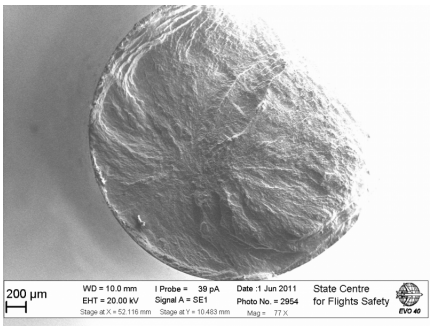

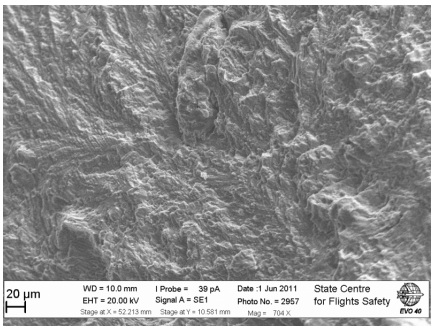

M5,
$\sigma_a = 400$ MPa,
$N_f = 5.04 \times 10^7$

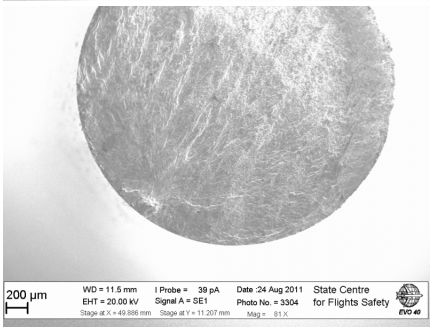

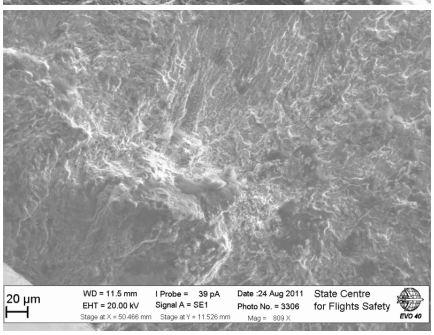

M6,
$\sigma_a = 400$ MPa,
$N_f = 2.98 \times 10^7$

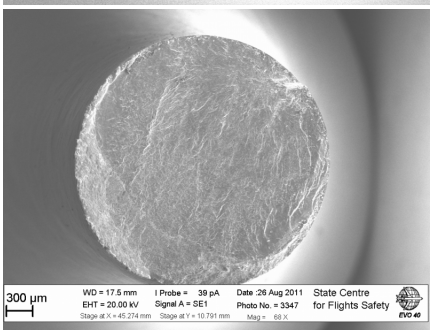

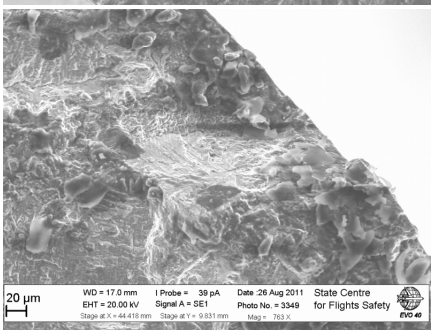

M7,
$\sigma_a = 400$ MPa,
$N_f = 1.98 \times 10^7$

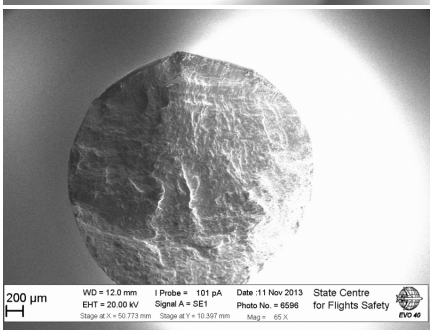

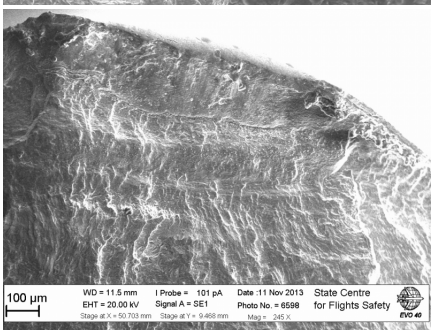

L2,
$\sigma_a = 385$ MPa,
$N_f = 1.08 \times 10^7$

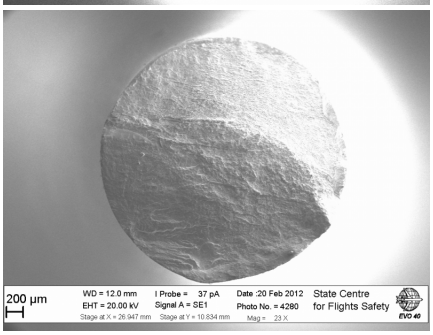

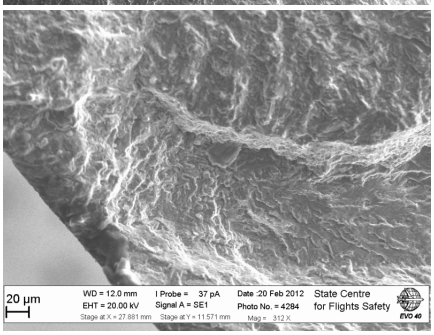

L3,
$\sigma_a = 430$ MPa,
$N_f = 6.84 \times 10^5$

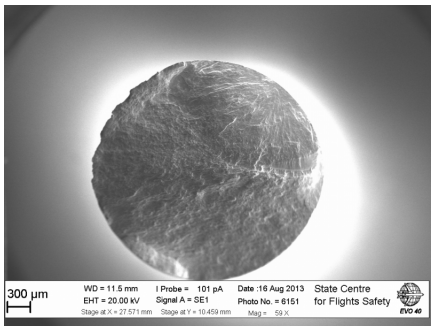

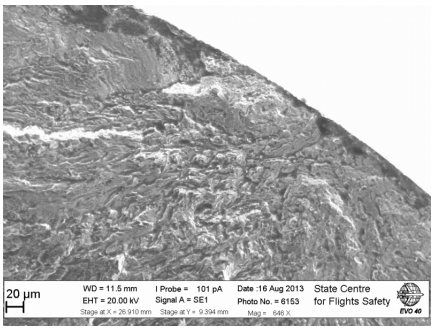

L4,
$\sigma_a = 415$ MPa,
$N_f = 4.22 \times 10^7$

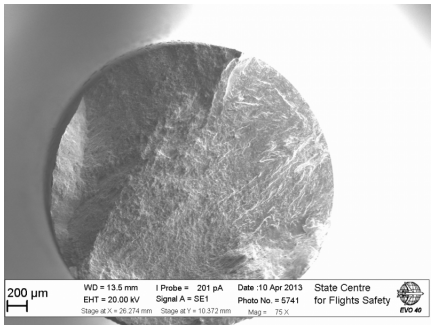

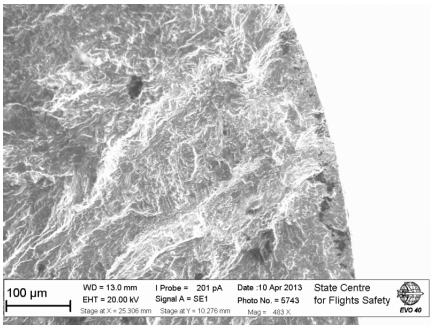

L5,
$\sigma_a = 430$ MPa,
$N_f = 4.93 \times 10^7$

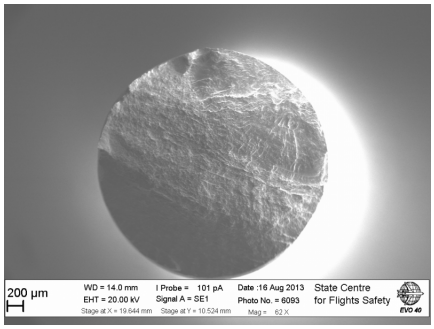

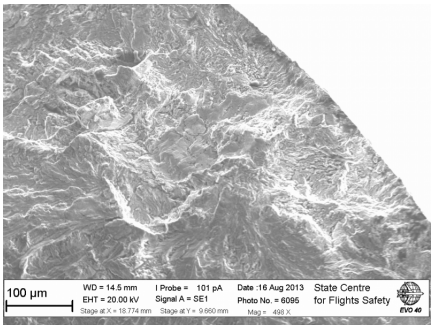

L6,
$\sigma_a = 385$ MPa,
$N_f = 1.19 \times 10^9$

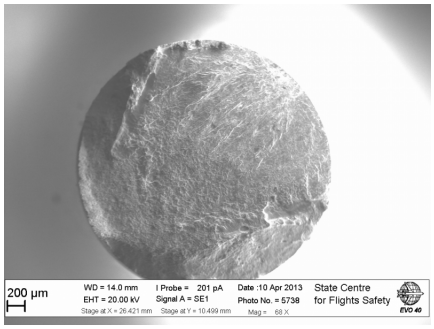

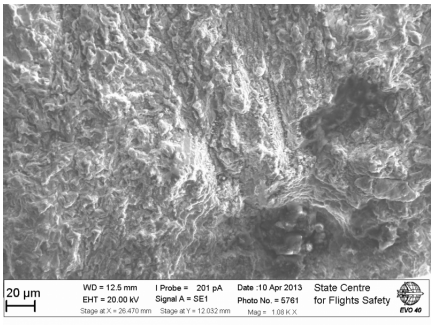

L7,
$\sigma_a = 415$ MPa,
$N_f = 2.75 \times 10^6$

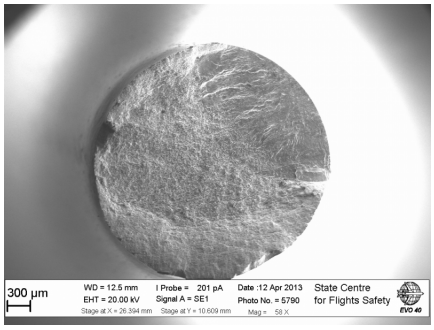

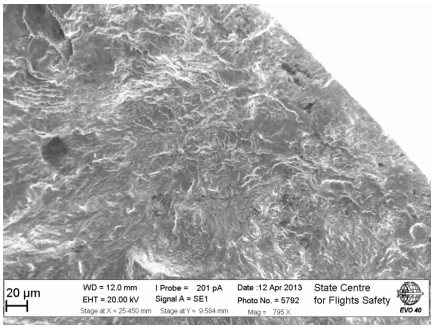

L8,
$\sigma_a = 370$ MPa,
$N_f = 1.26 \times 10^6$

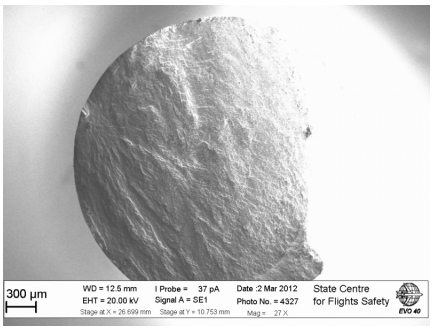

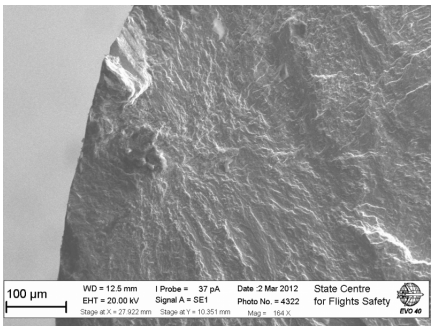

ANNEX D-1

Results of fatigue tests on 1AXX series

Material: VT3-1 (Ti-6Al-4Mo)			**Forged Titanium Alloy**			
Name of test	Constant Amplitude Fatigue Tests with R=-1 on air					
Configuration:	TC ultrasonic horns				R=	-1
Lifetime aim	10^9 cycles				Frequency	20.2 kHz
Temperature	Room	Environment: Air			Machine	Ultasonic

•

Specimen Geometry:	Smooth		Method of examination	Staircase	
Calibration:	Optical laser captor			Total	(Failed)
Useful diameter d(mm)	3		Number of tested samples	11	(8)
Equation:	$\tau_a = 14.91 \times Displ(PC) + 0.26$			Dislp.Mode:	Ti-Nik
Units of Stress	MPa			Units of Displacement	μm

•

Test	Specimen	σ_a	σ_m	σ_{max}	N_f	Crack
1	1A1	325	0	325	6.64×10^7	Crack
2	1A2	315	0	315	1.68×10^9	Crack
3	1A3	320	0	320	1.76×10^9	No Crack
4	1A4	325	0	325	4.56×10^9	No Crack
5	1A5	335	0	335	1.91×10^9	Crack
6	1A6	345	0	345	4.7×10^5	Crack
7	1A7	335	0	335	2.71×10^6	Crack
8	1A8	325	0	325	4.64×10^9	No Crack
9	1A9	315	0	315	5.61×10^6	Crack
10	1A10	335	0	335	1.46×10^7	Crack
11	1A11	325	0	325	4.1×10^7	Crack

ANNEX D-2

The fracture surfaces of tension-compression (R=-1) fatigue specimens from forged VT3-1 titanium alloy (axial, 1AXX series)

1A1,
$\sigma_a = 325$ MPa,
$N_f = 6.64 \times 10^7$

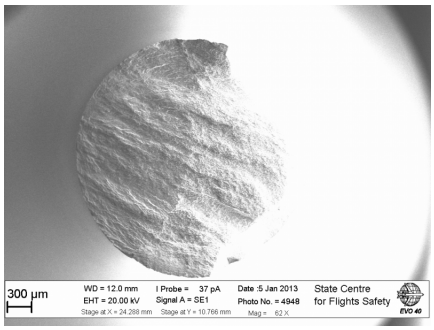

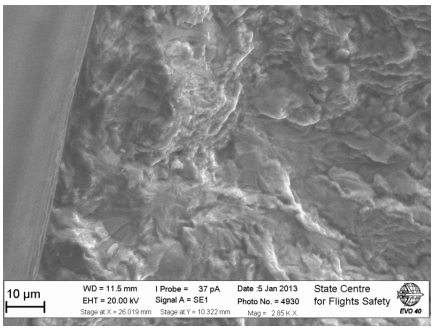

1A2,
$\sigma_a = 320$ MPa,
$N_f = 1.76 \times 10^9$

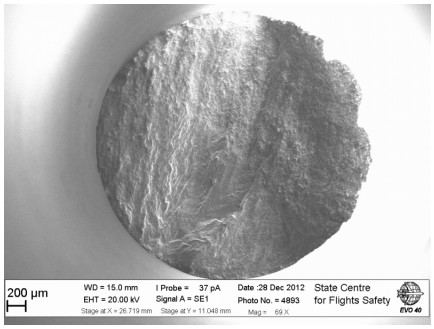

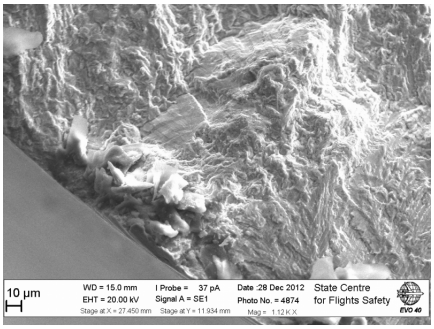

1A5,
$\sigma_a = 335$ MPa,
$N_f = 1.91 \times 10^9$

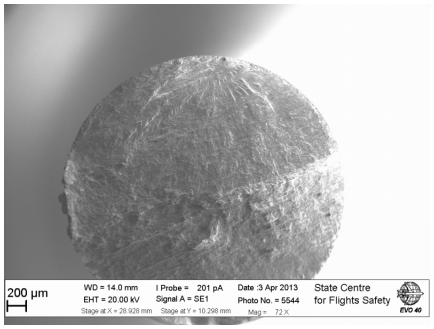

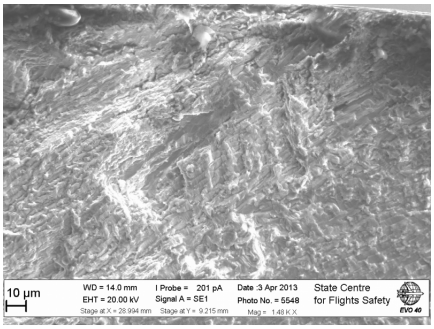

1A6,
$\sigma_a = 345$ MPa,
$N_f = 4.7 \times 10^5$

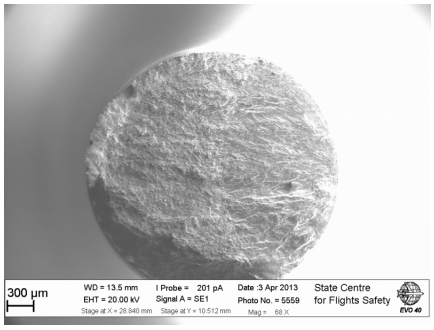

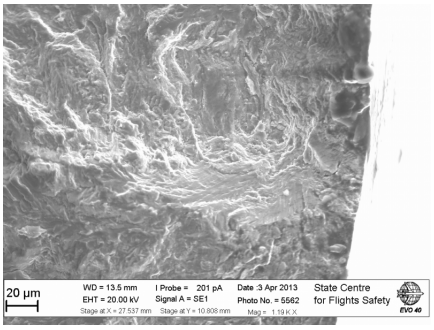

1A7,
$\sigma_a = 335$ MPa,
$N_f = 2.7 \times 10^6$

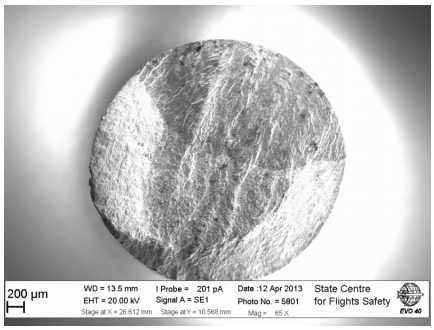

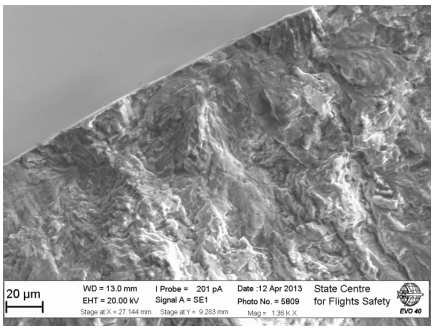

1A9,
$\sigma_a = 315$ MPa,
$N_f = 5.6 \times 10^6$

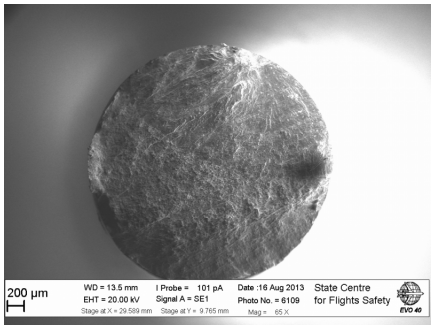

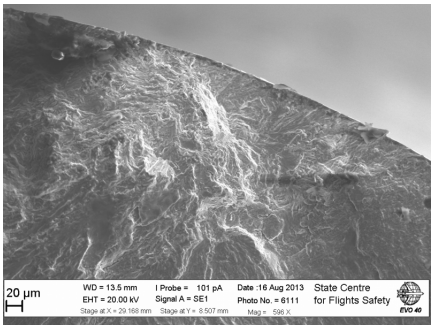

1A10,
$\sigma_a = 335$ MPa,
$N_f = 1.46 \times 10^7$

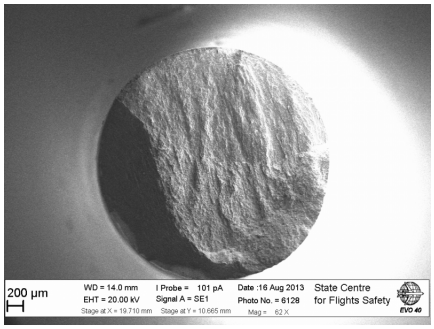

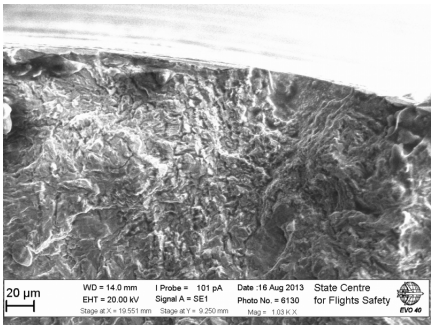

1A11,
$\sigma_a = 325$ MPa,
$N_f = 4.1 \times 10^7$

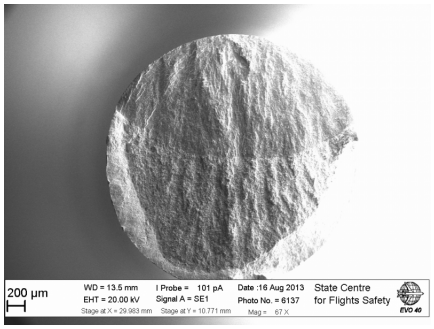

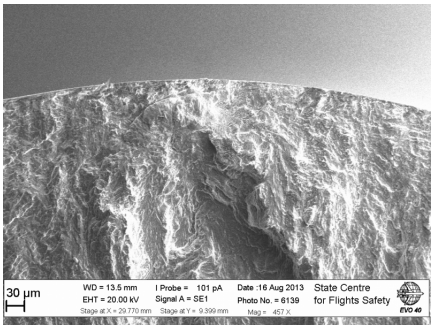

ANNEX E-1

Results of fatigue tests on 2RXX series

Material: VT3-1 (Ti-6Al-4Mo)			**Forged Titanium Alloy**		
Name of test	Constant Amplitude Fatigue Tests with R=-1 on air				
Configuration:	TC ultrasonic horns			R=	-1
Lifetime aim	10^9 cycles			Frequency	20.2 kHz
Temperature	Room	Environment: Air		Machine	Ultasonic

•

Specimen Geometry:	Smooth		Method of examination	Staircase	
Calibration:	Optical laser captor			Total	(Failed)
Useful diameter d(mm)	3		Number of tested samples	8	(6)
Equation:	$\tau_a = 14.91 \times Displ(PC) + 0.26$			Dislp.Mode:	Ti-Nik
Units of Stress	MPa			Units of Displacement	μm

•

Test	Specimen	σ_a	σ_m	σ_{max}	N_f	Crack
1	2R2	325	0	325	1.2×10^9	Crack
2	2R3	335	0	335	6.92×10^6	Crack
3	2R4	330	0	330	1.37×10^6	Crack
4	2R5	325	0	325	1.96×10^9	No Crack
5	2R6	330	0	330	1.52×10^7	Crack
6	2R7	330	0	330	8.9×10^9	No Crack
7	2R8	335	0	335	1.4×10^7	Crack
8	2R9	330	0	330	4.62×10^7	Crack

ANNEX E-2

The fracture surfaces of tension-compression (R=-1) fatigue specimens from forged VT3-1 titanium alloy (radial, 2RXX series)

2R2,
$\sigma_a = 325$ MPa,
$N_f = 1.2 \times 10^9$

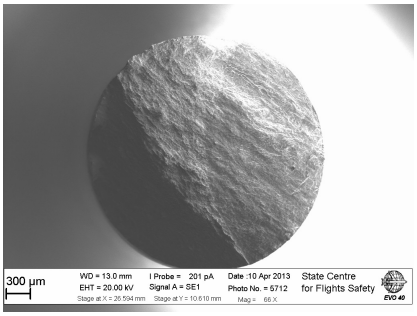

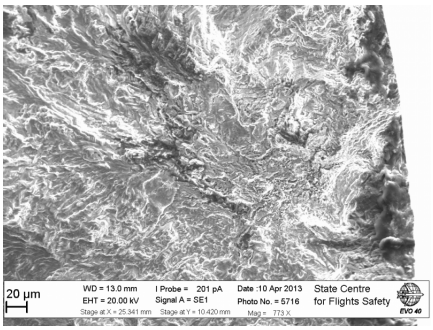

2R3,
$\sigma_a = 335$ MPa,
$N_f = 6.92 \times 10^6$

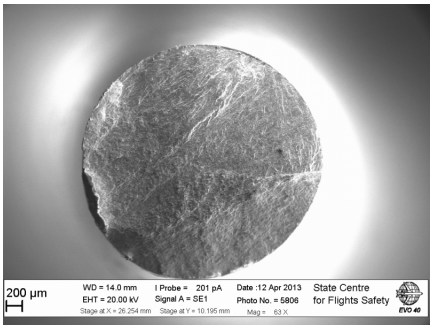

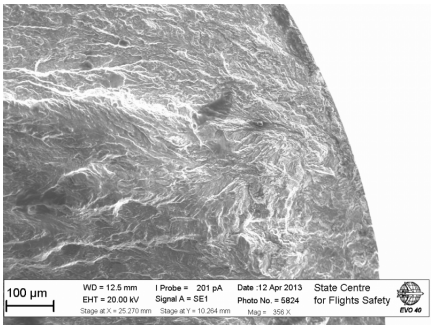

2R4,
$\sigma_a = 330$ MPa,
$N_f = 1.37 \times 10^6$

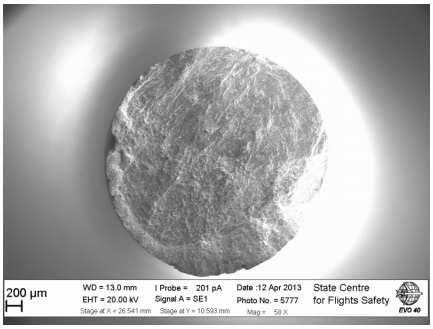

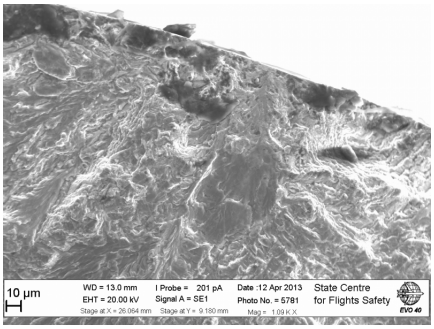

2R6,
$\sigma_a = 330$ MPa,
$N_f = 1.52 \times 10^7$

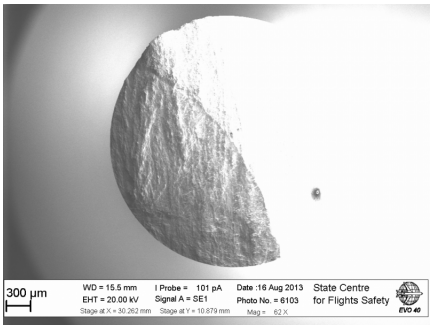

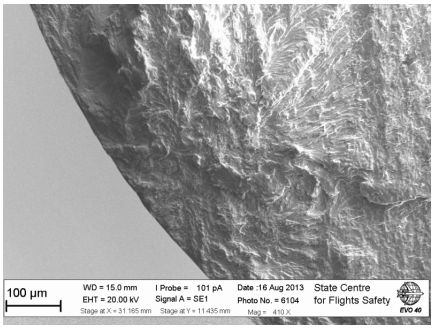

2R8,
$\sigma_a = 335$ MPa,
$N_f = 1.4 \times 10^7$

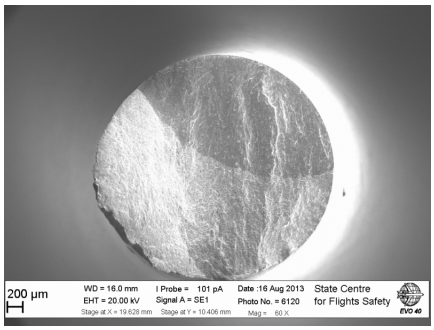

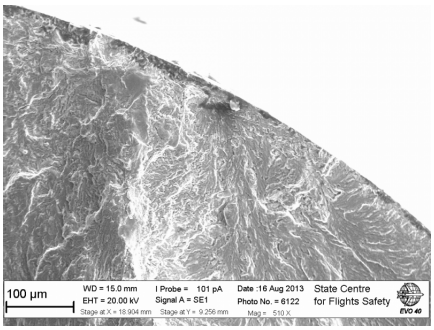

2R9,
$\sigma_a = 330$ MPa,
$N_f = 4.62 \times 10^7$

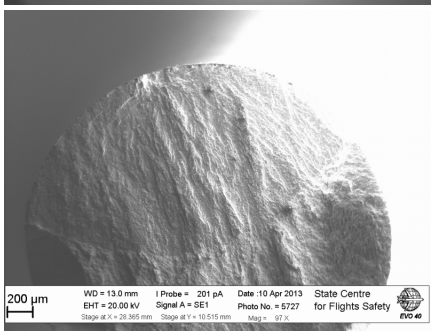

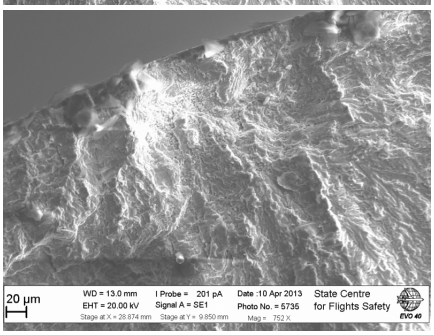

ANNEX F-1

Results of fatigue tests on 3RXX series

Material: VT3-1 (Ti-6Al-4Mo)			**Forged Titanium Alloy**			
Name of test	Constant Amplitude Fatigue Tests with R=0.1 on air					
Configuration:	TC ultrasonic horns				R=	0.1
Lifetime aim	10^9 cycles				Frequency	20.2 kHz
Temperature	Room	Environment: Air			Machine	Ultasonic

•

Specimen Geometry:	Smooth		Method of examination	Staircase	
Calibration:	Optical laser captor			Total	(Failed)
Useful diameter d(mm)	3		Number of tested samples	7	(2)
Equation:	$\tau_a = 14.91 \times Displ(PC) + 0.26$			Dislp.Mode:	Ti-Nik
Units of Stress	MPa			Units of Displacement	μm

•

Test	Specimen	σ_a	σ_m	σ_{max}	N_f	Crack
1	3R4	220	269	489	3.06×10^7	Crack
2	3R5	200	244	444	1.52×10^9	No Crack
3	3R6	210	257	467	3.9×10^8	Crack
4	3R7	210	257	467	3.49×10^7	Crack
5	3R8	210	257	467	2.93×10^7	Crack
6	3R9	200	244	444	1.51×10^9	No Crack
7	3R10	200	244	444	7.46×10^8	Crack

ANNEX F-2

The fracture surfaces of tension-tension (R=0.1) fatigue specimens from forged VT3-1 titanium alloy (radial, 3RXX series)

3R4,
$\sigma_a = 220$ MPa,
$\sigma_m = 269$ MPa,
$N_f = 3.06 \times 10^7$

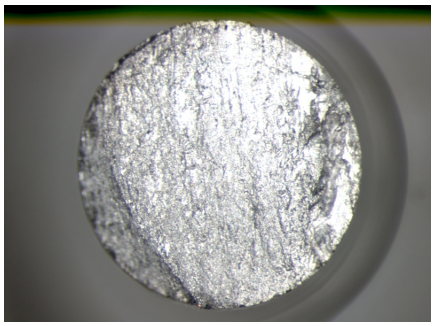

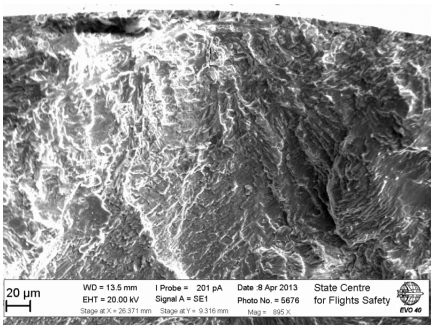

3R6,
$\sigma_a = 210$ MPa,
$\sigma_m = 257$ MPa,
$N_f = 3.9 \times 10^8$

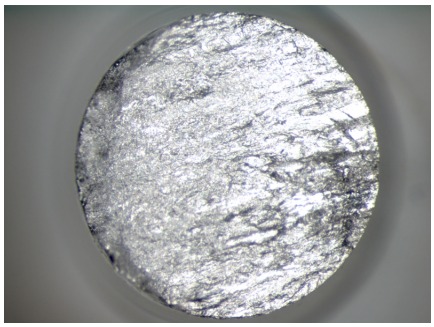

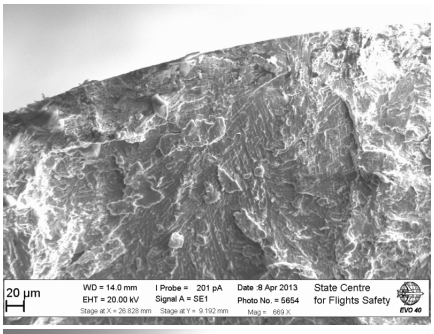

3R7,
$\sigma_a = 210$ MPa,
$\sigma_m = 257$ MPa,
$N_f = 3.49 \times 10^7$

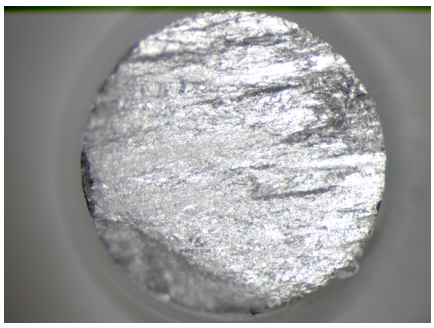

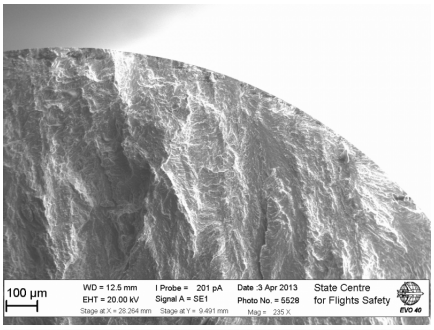

3R8,
$\sigma_a = 210$ MPa,
$\sigma_m = 257$ MPa,
$N_f = 2.93 \times 10^7$

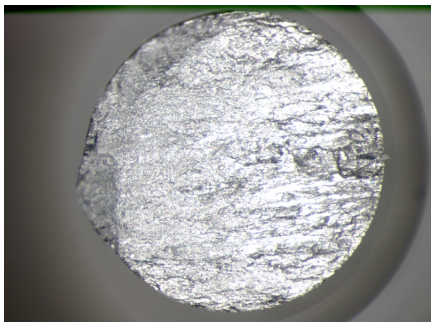

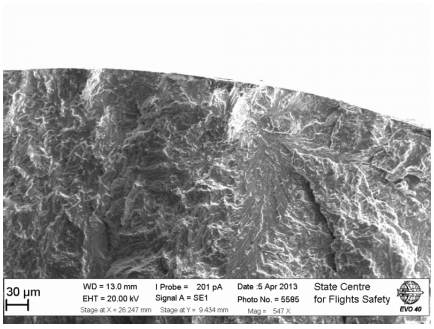

3R10,
$\sigma_a = 200$ MPa,
$\sigma_m = 244$ MPa,
$N_f = 7.46 \times 10^8$

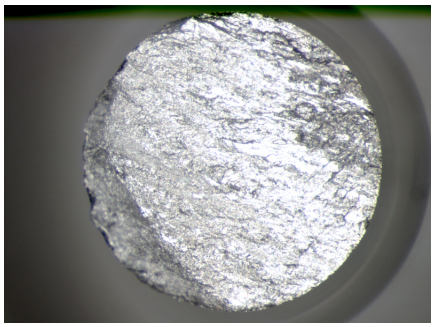

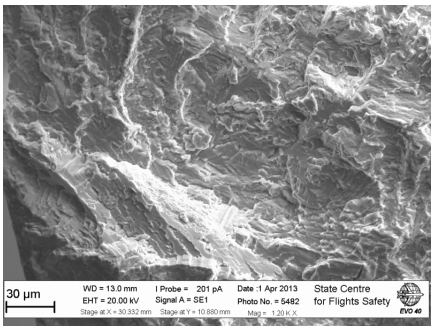

ANNEX G-1

Results of fatigue tests on 4CXX series

Material: VT3-1 (Ti-6Al-4Mo)			**Forged Titanium Alloy**			
Name of test	Constant Amplitude Fatigue Tests with R=0.1 on air					
Configuration:	TC ultrasonic horns				R=	0.1
Lifetime aim	10^9 cycles				Frequency	20.2 kHz
Temperature	Room	Environment: Air			Machine	Ultasonic

•

Specimen Geometry:	Smooth		Method of examination	Staircase	
Calibration:	Optical laser captor			Total	(Failed)
Useful diameter d(mm)	3		Number of tested samples	7	(4)
Equation:	$\tau_a = 14.91 \times Displ(PC) + 0.26$			Dislp.Mode:	Ti-Nik
Units of Stress	MPa			Units of Displacement	μm

•

Test	Specimen	σ_a	σ_m	σ_{max}	N_f	Crack
1	4C3	210	257	467	1.56×10^7	Crack
2	4C4	200	244	444	7.78×10^7	Crack
3	4C5	190	232	422	4.81×10^9	No Crack
4	4C7	200	244	444	2.7×10^7	Crack
5	4C8	190	232	422	1.72×10^9	No Crack
6	4C9	200	244	444	1.75×10^9	No Crack
7	4C10	210	257	467	3.77×10^7	Crack

ANNEX G-2

The fracture surfaces of tension-tension (R=0.1) fatigue specimens from forged VT3-1 titanium alloy (radial, 4CXX series)

4C3,
$\sigma_a = 210$ MPa,
$\sigma_m = 257$ MPa,
$N_f = 1.56 \times 10^7$

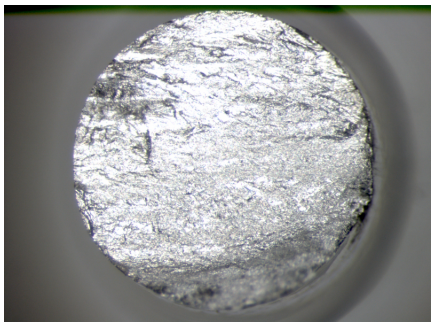

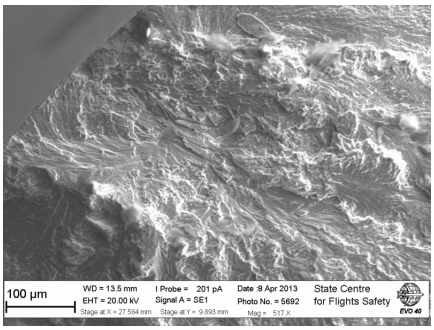

4C4,
$\sigma_a = 200$ MPa,
$\sigma_m = 244$ MPa,
$N_f = 7.78 \times 10^7$

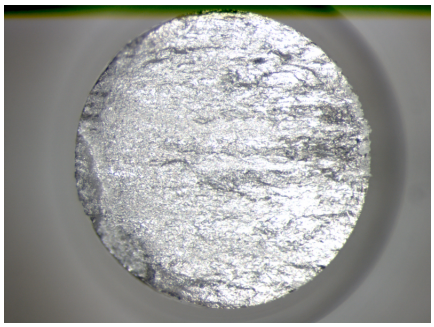

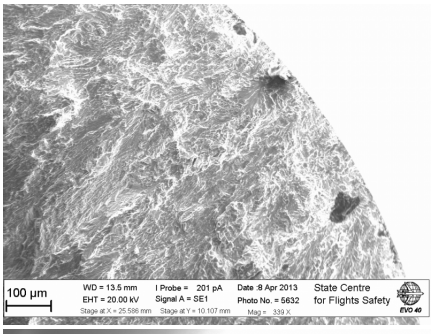

4C7,
$\sigma_a = 200$ MPa,
$\sigma_m = 244$ MPa,
$N_f = 2.7 \times 10^7$

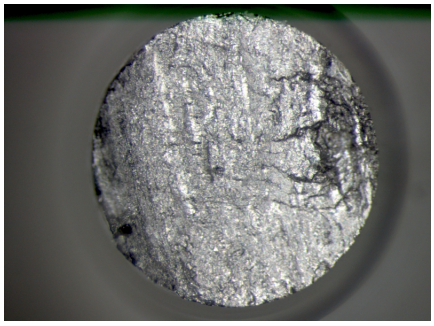

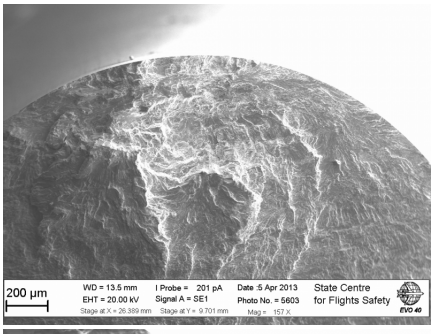

4C10,
$\sigma_a = 210$ MPa,
$\sigma_m = 257$ MPa,
$N_f = 3.77 \times 10^7$

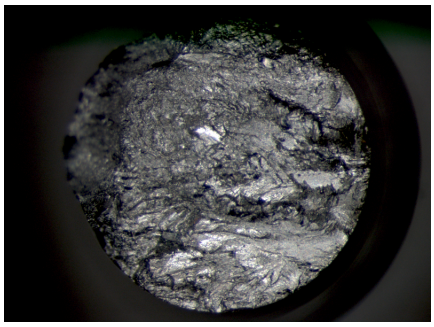

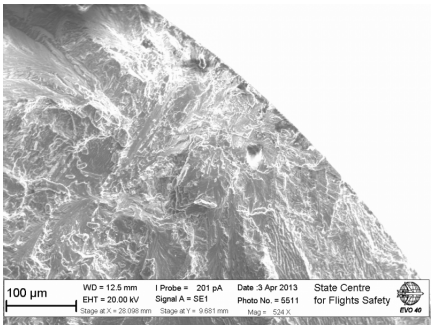

ANNEX H-1

Results of fatigue tests on R-1-Ext-XX series

Material: VT3-1 (Ti-6Al-4Mo)			**Extruded Titanium Alloy**		
Name of test	Constant Amplitude Fatigue Tests with R=0.1 on air				
Configuration:	Booster and TC ultrasonic horn			R=	0.1
Lifetime aim	10^9 cycles			Frequency	19.9 kHz
Temperature	Room	Environment: Air		Machine	Ultasonic

•

Specimen Geometry:	Smooth		Method of examination	Staircase method	
Calibration:	Strain-gauge 1-LY13-0.6/120 HBM			Total	(Failed)
Useful diameter d(mm)	3		Number of tested samples	11	(5)
Equation:	$\sigma_a = 16.314 \times Displ(PC) + 0.237$			Dislp.Mode:	TC-PSA
Units of Stress	MPa			Units of Displacement	μm

•

Test	Specimen	σ_a	σ_m	σ_{max}	N_f	Crack
1	Sp-3-B1	0	400	400	1.88×10^7	Crack
2	Sp-1-B4	0	385	385	1.08×10^9	No Crack
3	Sp-1-B1	0	415	415	6.63×10^6	Crack
4	Sp-2-B4	0	400	400	1.18×10^9	No Crack
5	Sp-3-B4	0	415	415	1.39×10^9	No Crack
6	Sp-1-B5	0	430	430	3.93×10^4	Crack
7	Sp-2-B5	0	415	415	4.81×10^6	Crack
8	Sp-1-B6	0	400	400	2.84×10^8	Crack
9	Sp-2-B3	0	385	385	1.33×10^9	Crack
10	Sp-3-Ls	0	400	644	5.07×10^9	No Crack
11	Sp-4-Ls	0	415	415	1.71×10^9	No Crack

ANNEX H-2

The fracture surfaces of tension-compression (R=-1) fatigue specimens from extruded VT3-1 titanium alloy

Test Information	Overview on fracture surface	Fatigue crack initiation site
Sp-1-B1, $\sigma_a = 415$ MPa, $N_f = 6.63 \times 10^6$	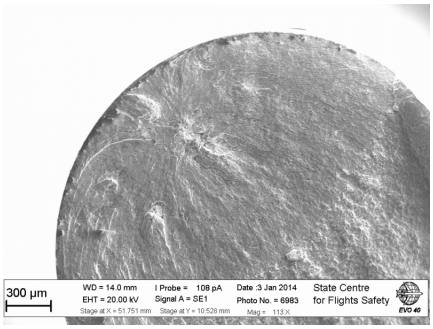	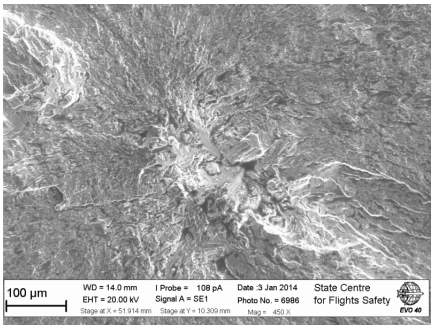
Sp-1-B6, $\sigma_a = 400$ MPa, $N_f = 2.84 \times 10^8$	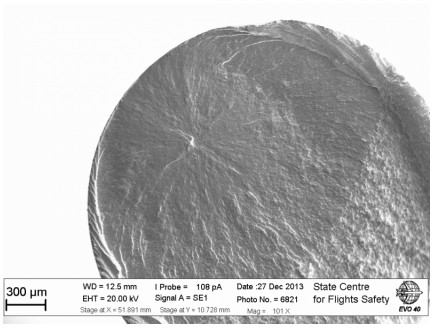	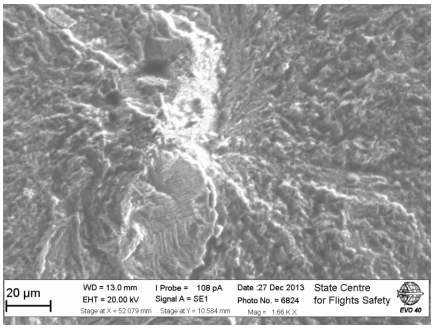
Sp-2-B3, $\sigma_a = 385$ MPa, $N_f = 1.33 \times 10^9$	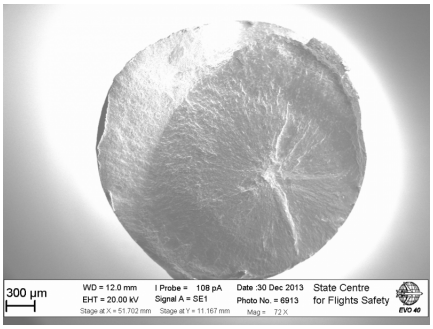	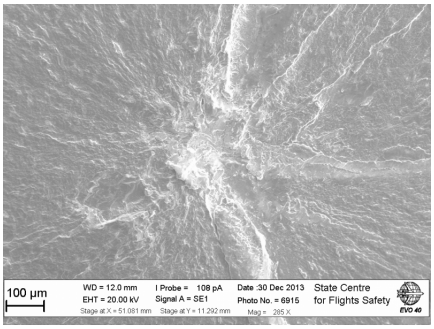
Sp-2-B5, $\sigma_a = 415$ MPa, $N_f = 4.81 \times 10^6$	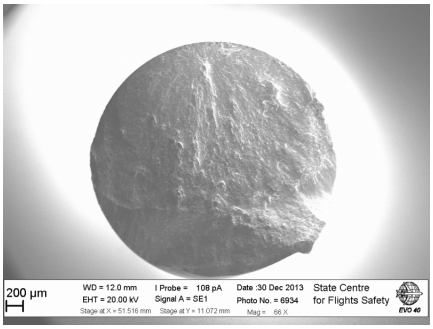	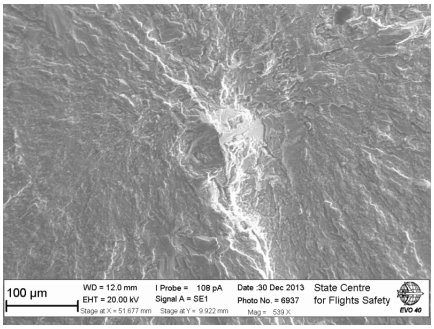

Sp-3-B1, $\sigma_a = 400$ MPa, $N_f = 1.88 \times 10^7$

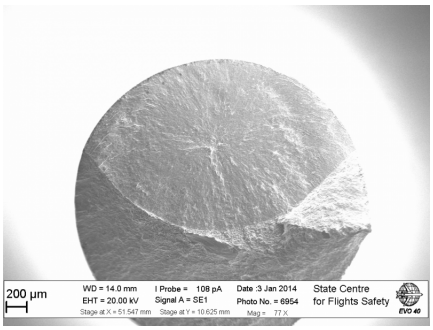

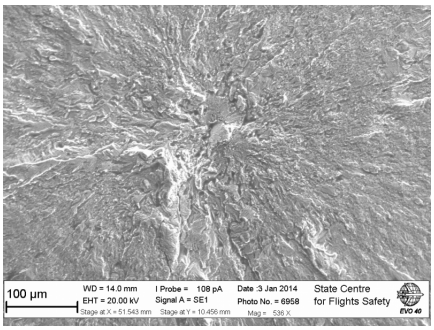

ANNEX J-1

Results of fatigue tests on R01-Ext-XX series

Material: VT3-1 (Ti-6Al-4Mo)			**Extruded Titanium Alloy**		
Name of test	Constant Amplitude Fatigue Tests with R=0.1 on air				
Configuration:	Booster and TC ultrasonic horn			R=	0.1
Lifetime aim	10^9 cycles			Frequency	20.2 kHz
Temperature	Room	Environment: Air		Machine	Ultasonic

•

Specimen Geometry:	Smooth		Method of examination	Staircase method	
Calibration:	Strain-gauge 1-LY13-0.6/120 HBM			Total	(Failed)
Useful diameter d(mm)	3		Number of tested samples	10	(6)
Equation:	$\sigma_a = 16.314 \times Displ(PC) + 0.237$			Dislp.Mode:	TC-PSA
Units of Stress	MPa			Units of Displacement	μm

•

Test	Specimen	σ_a	σ_m	σ_{max}	N_f	Crack
1	R01Ext02	403	330	733	4.55×10^7	Crack
2	R01Ext03	391	320	711	1.14×10^7	Crack
3	R01Ext04	367	300	667	1.66×10^9	No
4	R01Ext05	379	310	689	7.39×10^8	Crack
5	R01Ext06	367	300	667	5.75×10^7	Crack
6	R01Ext07	354	290	644	2.64×10^7	Crack
7	R01Ext08	342	280	622	1.08×10^9	No
8	R01Ext09	354	290	644	2.23×10^8	Crack
9	R01Ext10	342	280	622	1.49×10^9	No
10	R01Ext11	354	290	644	1.56×10^9	No
11	R01Ext13	354	290	644	1.56×10^9	No
12	R01Ext14	310	379	689	1.23×10^7	Crack
13	R01Ext15	300	367	667	2.243×10^7	Crack
14	R01Ext16	320	391	711	2.687×10^7	Crack

ANNEX J-2

The fracture surfaces of tension-tension (R=0.1) fatigue specimens from extruded VT3-1 titanium alloy

Test Information	Fracture surface on optical microscopy	Fracture surface on SEM microscopy
R01-Ext-02, $\sigma_a = 330$ MPa, $\sigma_m = 403$ MPa, $N_f = 4.55 \times 10^7$	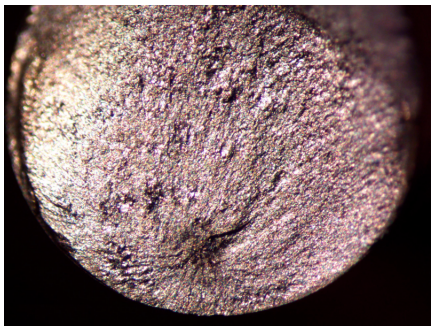	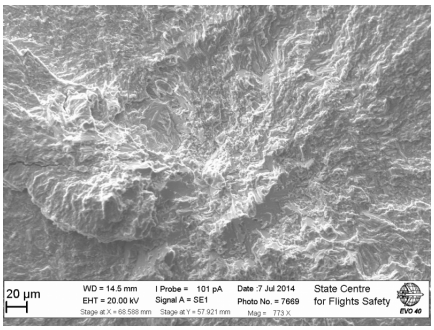
R01-Ext-03, $\sigma_a = 320$ MPa, $\sigma_m = 4391$ MPa $N_f = 1.14 \times 10^7$		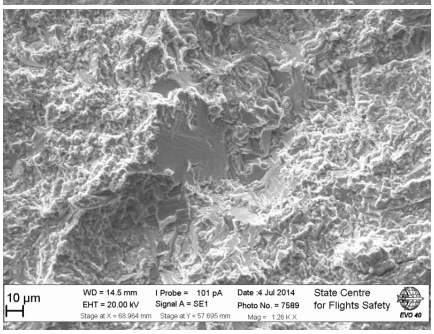
R01-Ext-05, $\sigma_a = 310$ MPa, $\sigma_m = 379$ MPa, $N_f = 7.39 \times 10^8$	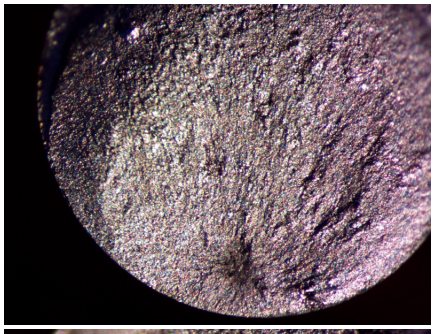	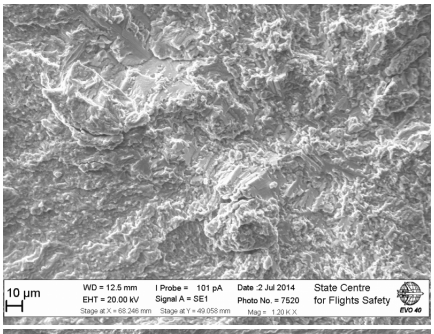
R01-Ext-06, $\sigma_a = 300$ MPa, $\sigma_m = 367$ MPa, $N_f = 5.75 \times 10^7$	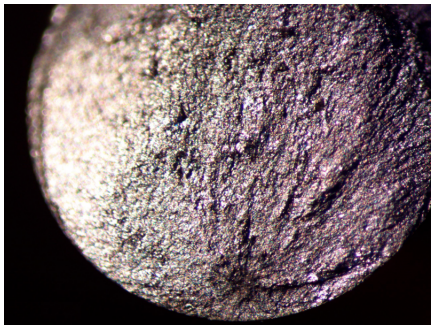	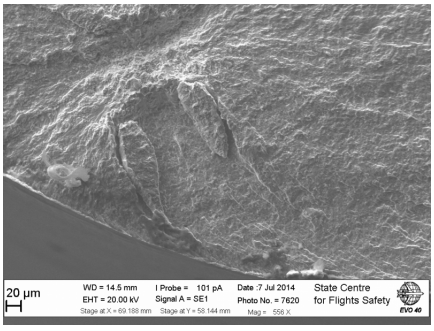

R01-Ext-07,
$\sigma_a = 290$ MPa,
$\sigma_m = 354$ MPa,
$N_f = 2.64 \times 10^7$

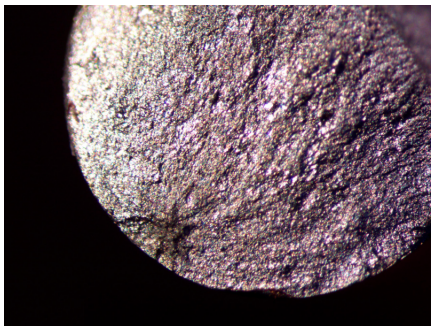

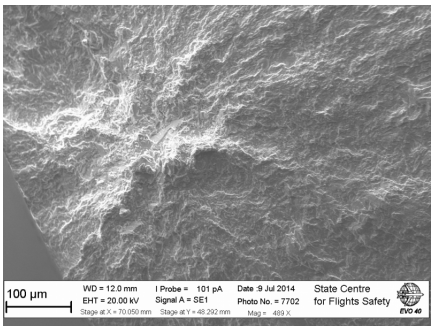

R01-Ext-09,
$\sigma_a = 290$ MPa,
$\sigma_m = 354$ MPa,
$N_f = 2.23 \times 10^8$

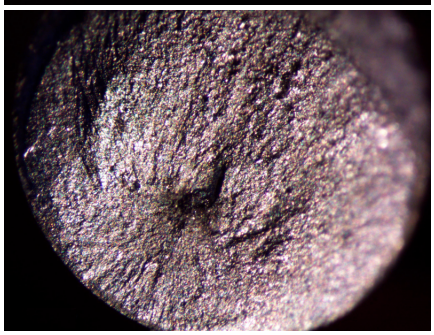

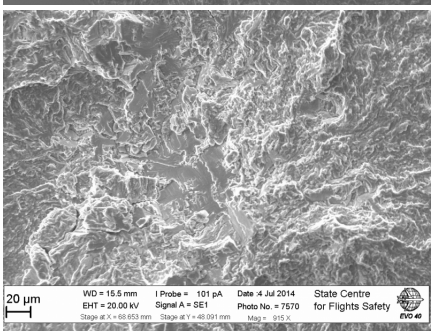

R01-Ext-14,
$\sigma_a = 310$ MPa,
$\sigma_m = 379$ MPa,
$N_f = 1.23 \times 10^7$

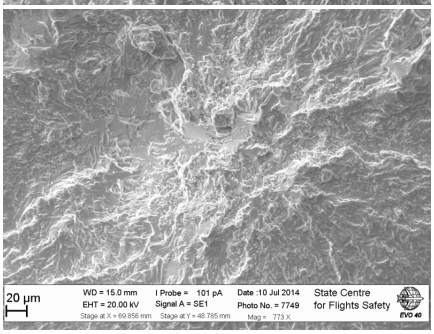

R01-Ext-15,
$\sigma_a = 300$ MPa,
$\sigma_m = 367$ MPa,
$N_f = 2.243 \times 10^7$

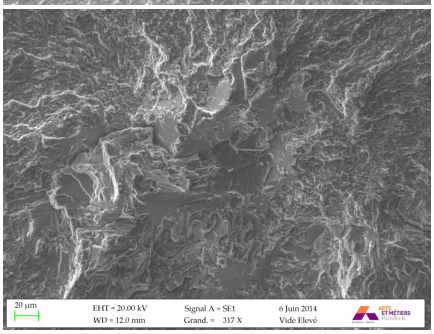

R01-Ext-16,
$\sigma_a = 320$ MPa,
$\sigma_m = 391$ MPa,
$N_f = 2.687 \times 10^7$

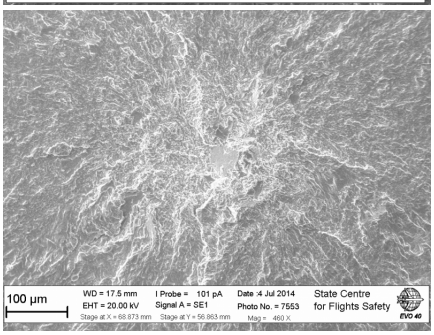

ANNEX K-1

Results of fatigue tests on R05-Ext-XX series

Material: VT3-1 (Ti-6Al-4Mo)			**Extruded Titanium Alloy**		
Name of test	Constant Amplitude Fatigue Tests with R=0.5 on air				
Configuration:	Booster and TC ultrasonic horn			R=	0.5
Lifetime aim	10^9 cycles			Frequency	20.2 kHz
Temperature	Room	Environment: Air		Machine	Ultasonic

•

Specimen Geometry:	Smooth		Method of examination	Staircase method	
Calibration:	Strain-gauge 1-LY13-0.6/120 HBM			Total	(Failed)
Useful diameter d(mm)	3		Number of tested samples	10	(6)
Equation:	$\sigma_a = 16.314 \times Displ(PC) + 0.237$			Dislp.Mode:	TC-PSA
Units of Stress	MPa			Units of Displacement	μm

•

Test	Specimen	σ_a	σ_m	σ_{max}	N_f	Crack
1	R05Ext01	200	600	800	1.24×10^9	No Crack
2	R05Ext02	210	630	840	1.74×10^9	No Crack
3	R05Ext03	220	660	880	1.36×10^8	Crack
4	R05Ext04	210	630	840	1.4×10^9	No Crack
5	R05Ext05	220	660	880	2.13×10^9	No Crack
6	R05Ext06	230	690	920	3.0×10^9	No Crack
7	R05Ext07	240	720	960	1.31×10^8	Crack
8	R05Ext08	230	690	920	4.17×10^8	Crack
9	R05Ext09	220	660	880	1.75×10^9	No Crack
10	R05Ext10	230	690	920	1.45×10^9	Crack
11	R05Ext11	240	720	960	7.82×10^7	Crack

ANNEX K-2

The fracture surfaces of tension-tension (R=0.5) fatigue specimens from extruded VT3-1 titanium alloy

Test Information	Fracture surface on optical microscopy	Fracture surface on SEM microscopy
R05-Ext-03, $\sigma_a = 220$ MPa, $\sigma_m = 660$ MPa, $N_f = 1.36 \times 10^8$	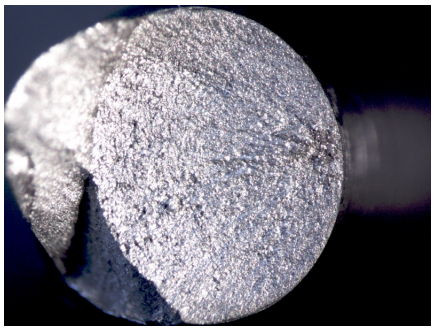	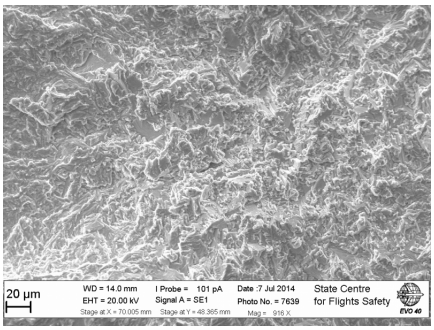
R05-Ext-07, $\sigma_a = 240$ MPa, $\sigma_m = 720$ MPa $N_f = 1.31 \times 10^8$		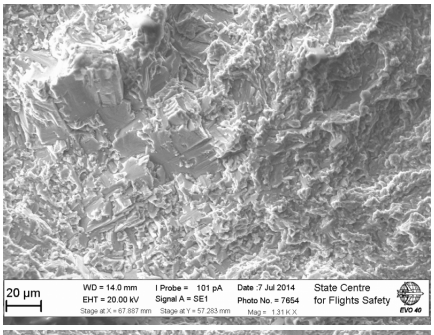
R05-Ext-08, $\sigma_a = 230$ MPa, $\sigma_m = 690$ MPa, $N_f = 4.17 \times 10^8$		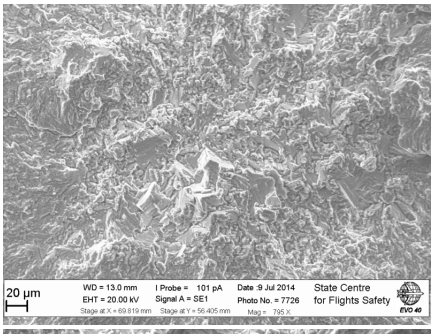
R05-Ext-10, $\sigma_a = 230$ MPa, $\sigma_m = 690$ MPa, $N_f = 1.45 \times 10^9$		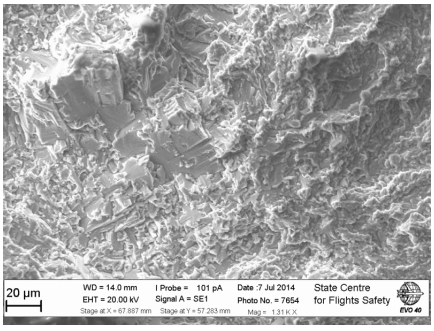

R05-Ext-11,
$\sigma_a = 240$ MPa,
$\sigma_m = 720$ MPa,
$N_f = 7.816 \times 10^7$

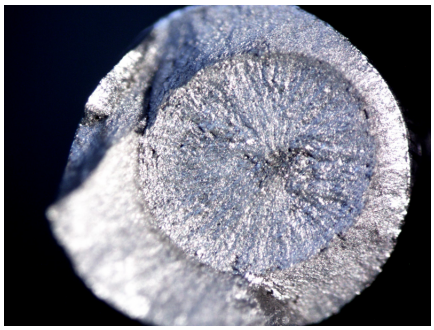

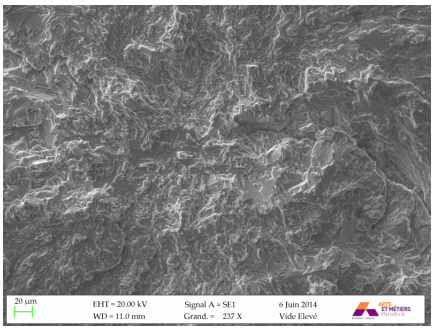

ANNEX L-1

Results of fatigue tests on Torsion Specimens FTXX series

Material: VT3-1 (Ti-6Al-4Mo)			**Forged Titanium Alloy**		
Name of test	Constant Amplitude Fatigue Torsion Tests with R=-1 on air				
Configuration:	Direct torsion ultrasonic horns			R=	-1
Lifetime aim	10^9 cycles			Frequency	20.3 kHz
Temperature	Room	Environment: Air		Machine	Ultasonic

•

Specimen Geometry:	Smooth		Method of examination	***	
Calibration:	Optical laser captor			Total	(Failed)
Useful diameter d(mm)	4		Number of tested samples	5	(5)
Equation:	$\tau_a = 61.2 \times Displ(PC) + 18.2$			Dislp.Mode:	2903
Units of Stress	MPa			Units of Displacement	μm

•

Test	Specimen	τ_a	τ_m	σ_{max}	N_f	Crack
1	FT1	254	0	254	3.96×10^6	Crack
2	FT2	242	0	242	3.37×10^6	Crack
3	FT3	230	0	230	9.22×10^7	Crack
4	FT4	224	0	224	1.13×10^8	Crack
5	FT5	212	0	212	1.92×10^8	Crack

ANNEX L-2

The fracture surfaces of Torsion (R=-1) fatigue specimens from forged VT3-1 titanium alloy (axial, FT-XX series)

FT1,
$\tau_a = 254$ MPa,
$N_f = 3.96 \times 10^6$

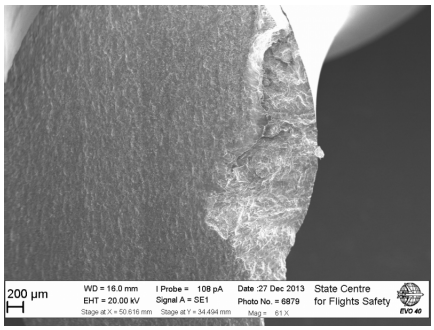

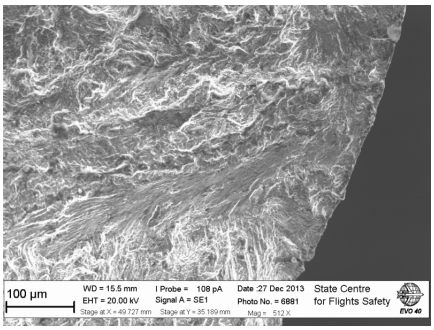

FT2,
$\tau_a = 242$ MPa,
$N_f = 3.37 \times 10^6$

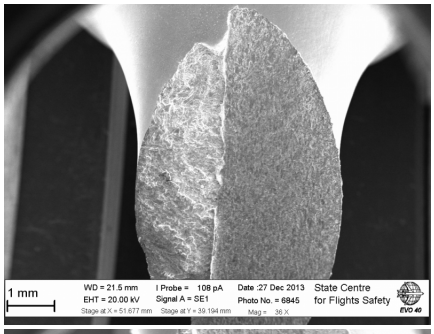

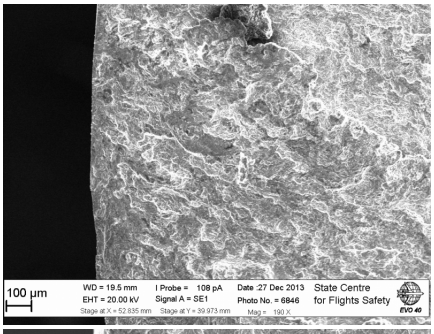

FT3,
$\tau_a = 230$ MPa,
$N_f = 9.22 \times 10^7$

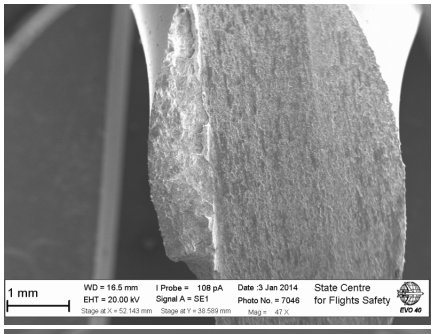

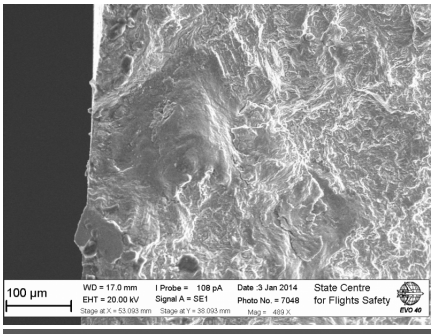

FT4,
$\tau_a = 224$ MPa,
$N_f = 1.13 \times 10^8$

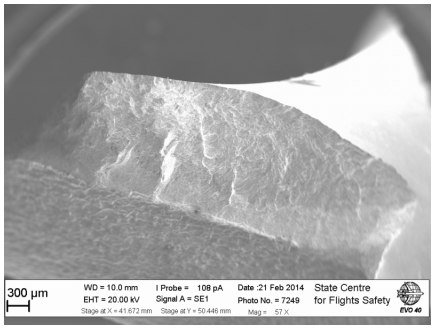

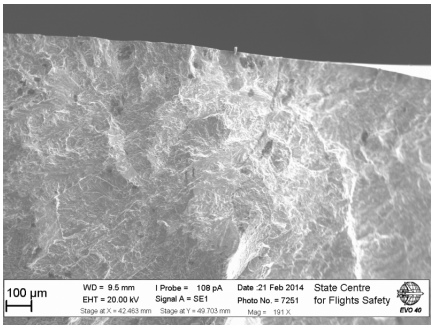

FT5,
$\tau_a = 212$ MPa,
$N_f = 1.92 \times 10^8$

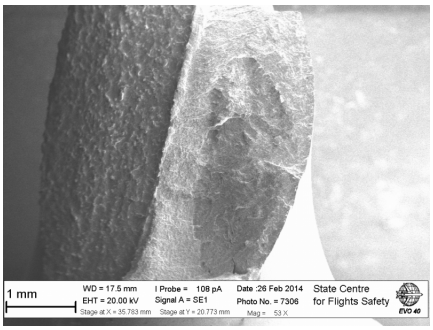

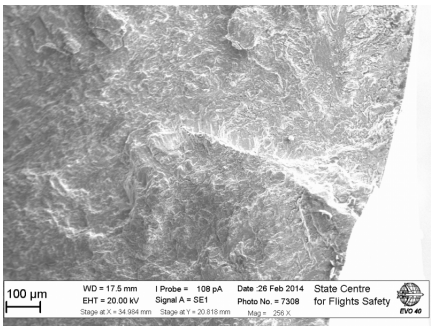

ANNEX M-1

Results of fatigue tests on T-Ext-XX series

Material: VT3-1 (Ti-6Al-4Mo)			**Extruded Titanium Alloy**		
Name of test	Constant Amplitude Fatigue Torsion Tests on air				
Configuration:	Direct ultrasonic torsion horns			R=	-1
Lifetime aim	10^9 cycles			Frequency	20.3 kHz
Temperature	Room	Environment: Air		Machine	Ultasonic

•

Specimen Geometry:	Smooth		Method of examination	Staircase	
Calibration:	Strain-gauge 1-XY41-0.6/120 HBM			Total	(Failed)
Useful diameter d(mm)	4		Number of tested samples	17	(8)
Equation:	$\tau_a = 62.74 \times Displ(PC) + 9.87$			Dislp.Mode:	Ti-Nik
Units of Stress	MPa			Units of Displacement	μm

•

Test	Specimen	τ_a	τ_m	τ_{max}	N_f	Crack
1	T-Ext-1	258	0	258	1.837×10^8	Crack
2	T-Ext-2	233	0	233	1.257×10^9	No
3	T-Ext-3	258	0	258	1.255×10^9	No
4	T-Ext-4	296	0	296	9.05×10^7	Crack
5	T-Ext-5	283	0	283	1.211×10^8	Crack
6	T-Ext-6	271	0	271	1.367×10^9	No
7	T-Ext-7	283	0	283	1.786×10^8	Crack
8	T-Ext-8	271	0	271	2.819×10^8	Crack
9	T-Ext-9	283	0	283	3.17×10^7	Crack
10	T-Ext10	246	0	246	2.114×10^9	No
11	T-Ext11	258	0	258	1.378×10^9	No
12	T-Ext12	271	0	271	8.365×10^6	Crack
13	T-Ext13	271	0	271	4.732×10^9	No
14	T-Ext14	246	0	246	1.364×10^9	No
15	T-Ext15	265	0	265	7.357×10^7	Crack
16	T-Ext16	258	0	258	1.135×10^9	No
17	T-Ext17	258	0	258	1.758×10^9	No

ANNEX M-2

The fracture surfaces of Torsion (R=-1) fatigue specimens from extruded VT3-1 titanium alloy (T-Ext-XX series)

T-Ext-1,
$\tau_a = 258$ MPa,
$N_f = 1.84 \times 10^8$

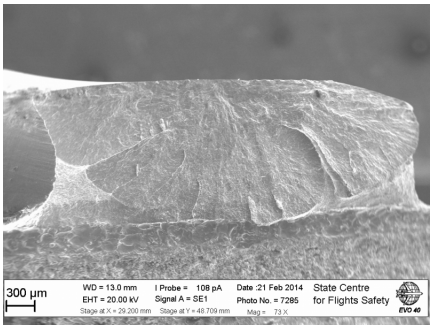

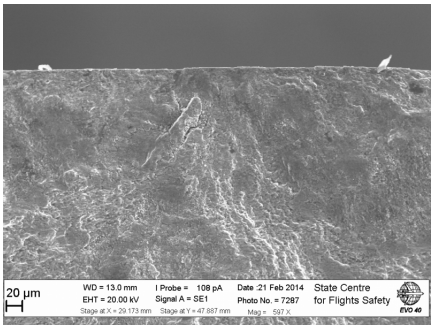

T-Ext-2,
$\tau_a = 296$ MPa,
$N_f = 1.67 \times 10^9$

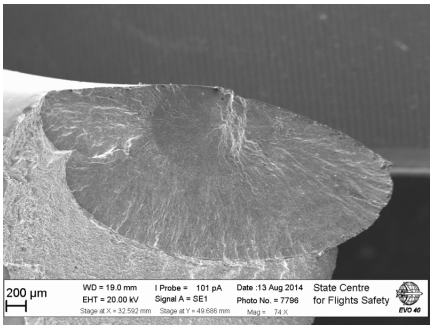

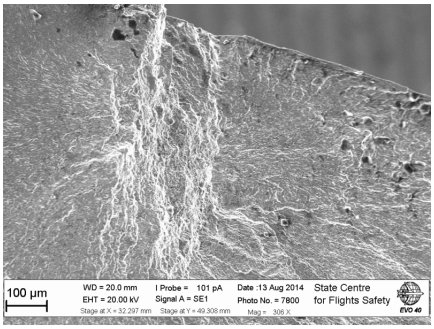

T-Ext-9,
$\tau_a = 283$ MPa,
$N_f = 3.17 \times 10^7$

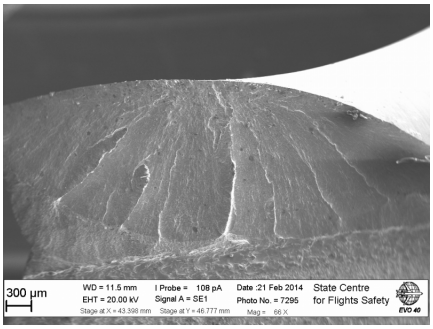

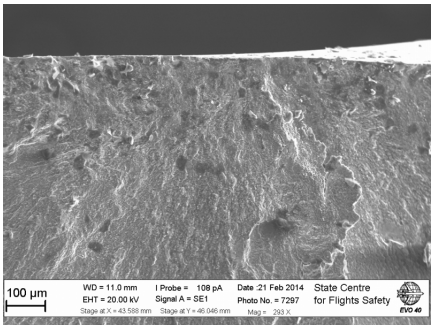

T-Ext-12,
$\tau_a = 270$ MPa,
$N_f = 8.37 \times 10^6$

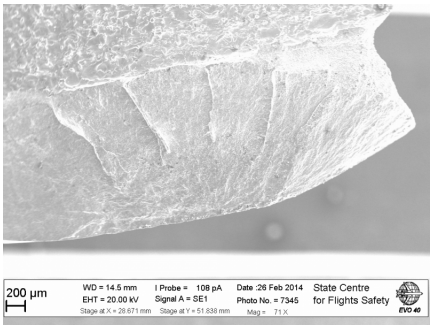

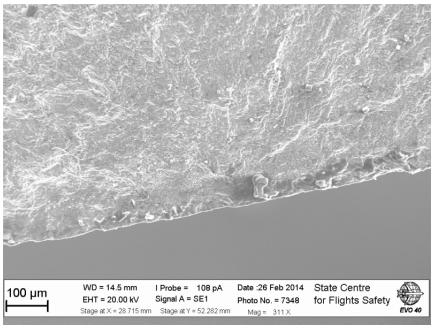

ANNEX N-1

Specimen for tension-compression fatigue tests, diameter = 10 mm

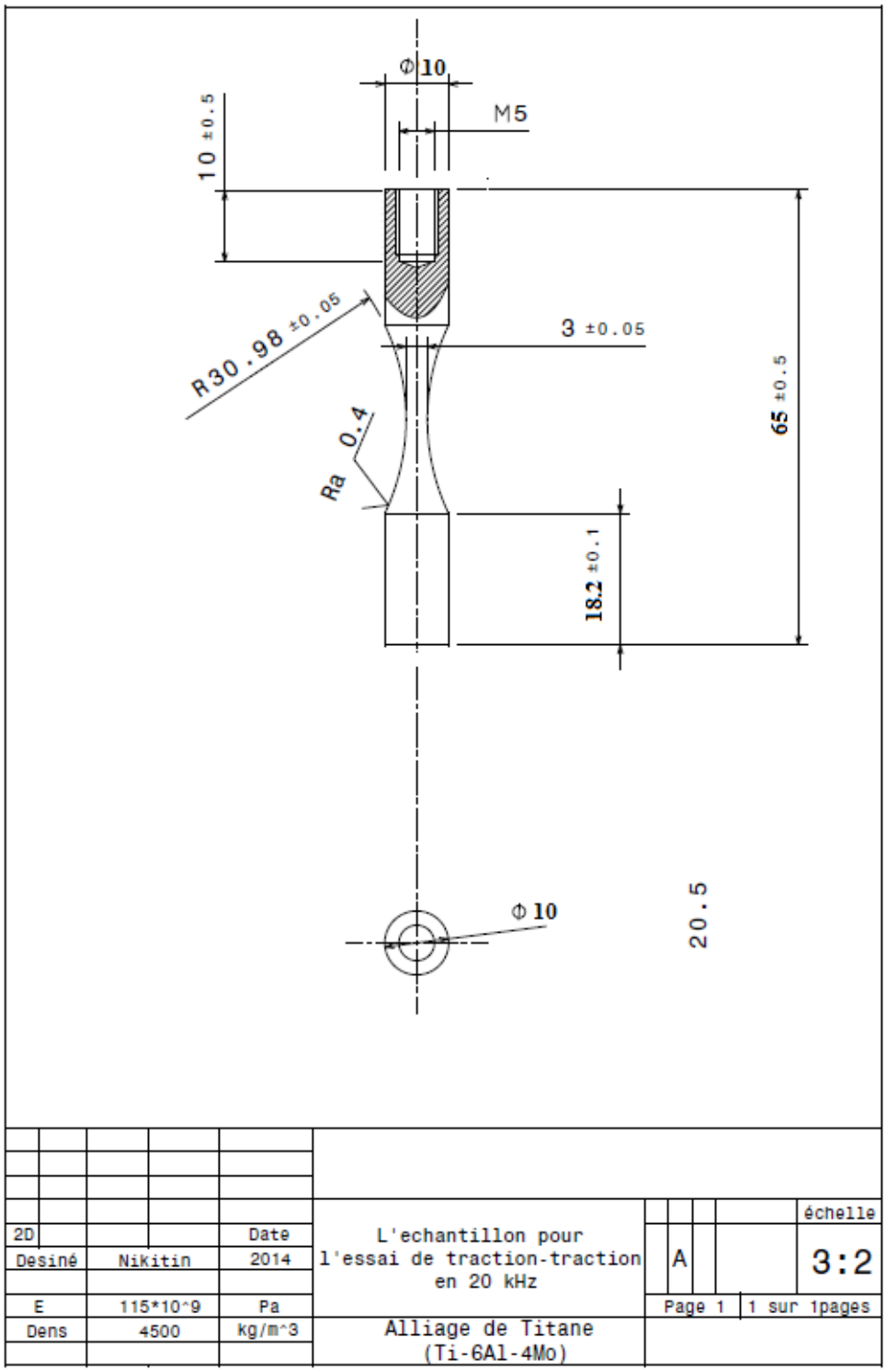

2D		Date	L'echantillon pour l'essai de traction-traction en 20 kHz		échelle
Desiné	Nikitin	2014		A	3:2
E	115*10^9	Pa		Page 1	1 sur 1pages
Dens	4500	kg/m^3	Alliage de Titane (Ti-6Al-4Mo)		

ANNEX N-2

Specimen for tension-tension fatigue tests, diameter = 10 mm

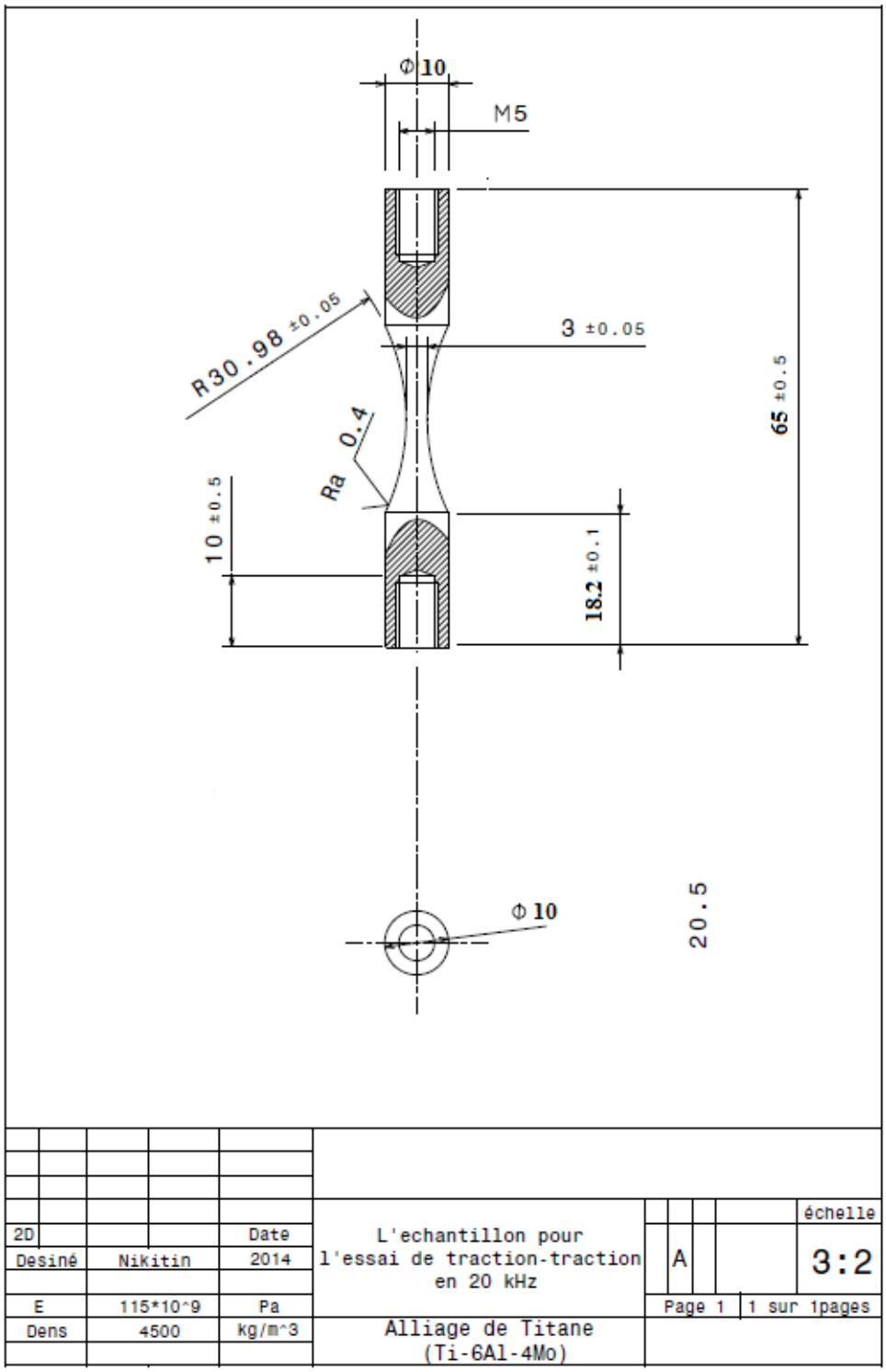

2D		Date	L'echantillon pour l'essai de traction-traction en 20 kHz		échelle
Desiné	Nikitin	2014		A	3:2
E	115*10^9	Pa		Page 1	1 sur 1pages
Dens	4500	kg/m^3	Alliage de Titane (Ti-6Al-4Mo)		

ANNEX N-3

Specimen for tension-compression fatigue tests, diameter = 9 mm

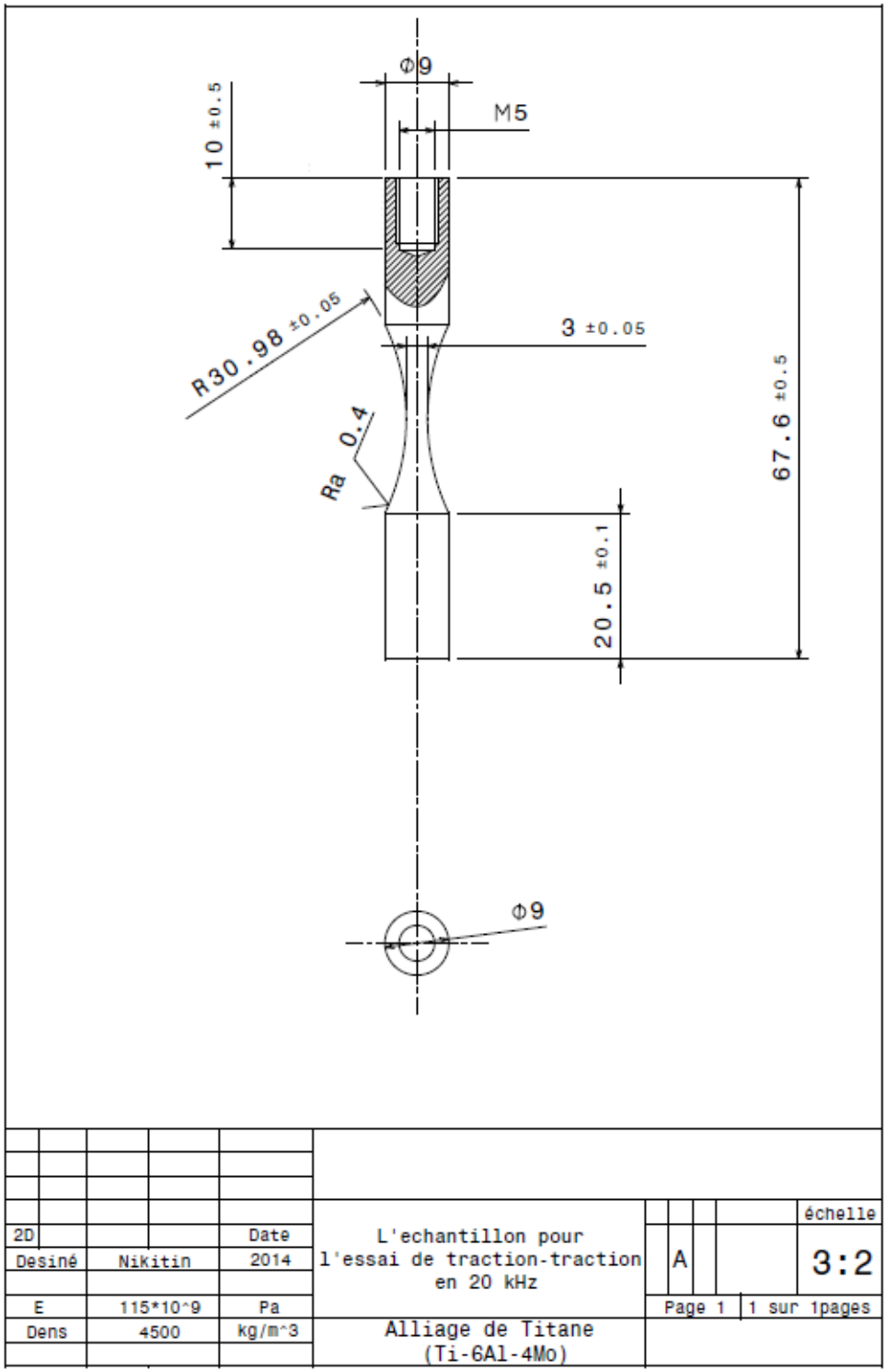

					échelle
2D			Date	L'echantillon pour l'essai de traction-traction en 20 kHz	A	3:2
Desiné	NiKitin		2014		
E	115*10^9		Pa		Page 1 | 1 sur 1pages
Dens	4500		kg/m^3	Alliage de Titane (Ti-6Al-4Mo)	

ANNEX N-4

Specimen for tension-tension fatigue tests, diameter = 9 mm

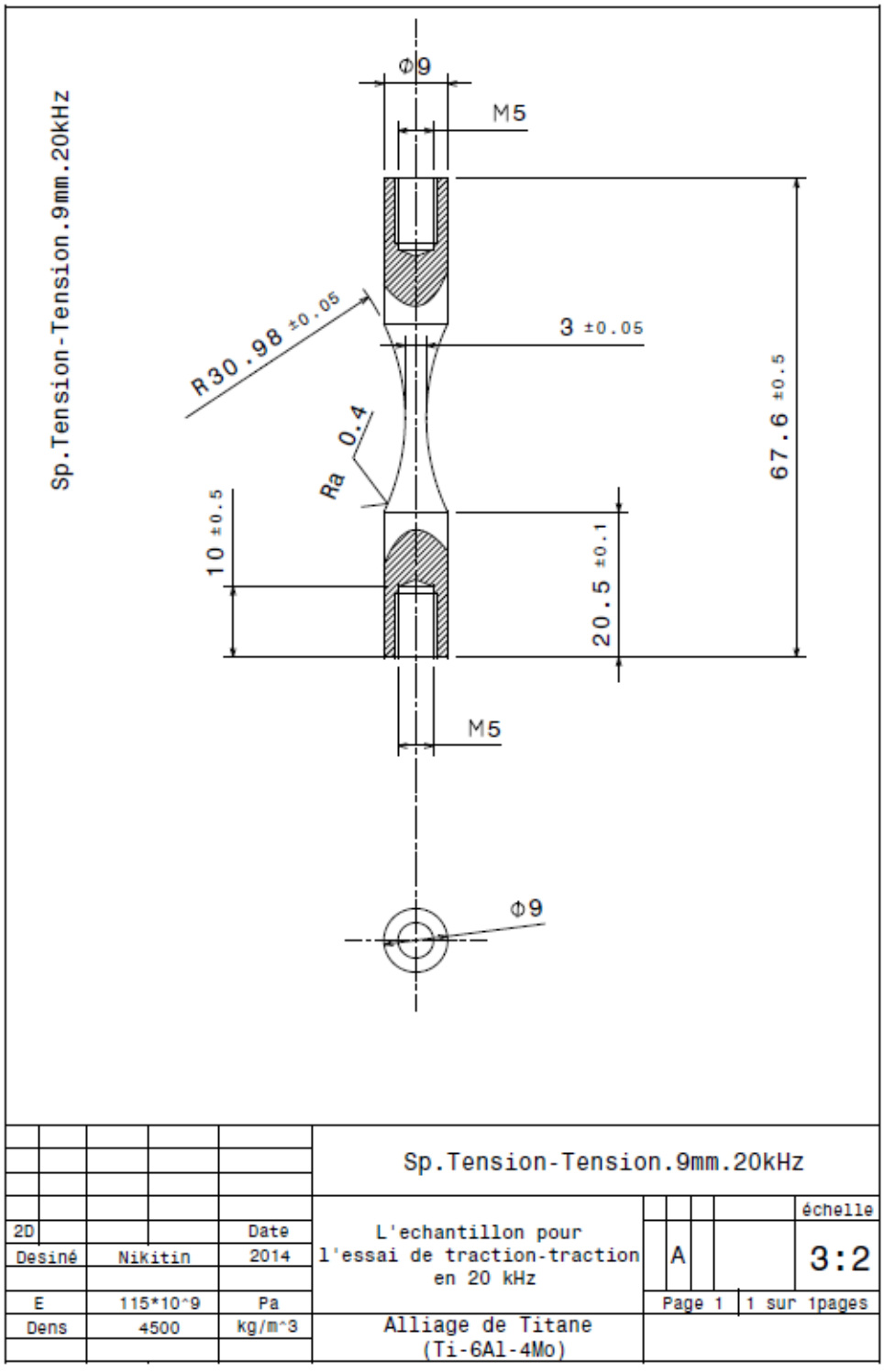

ANNEX N-5
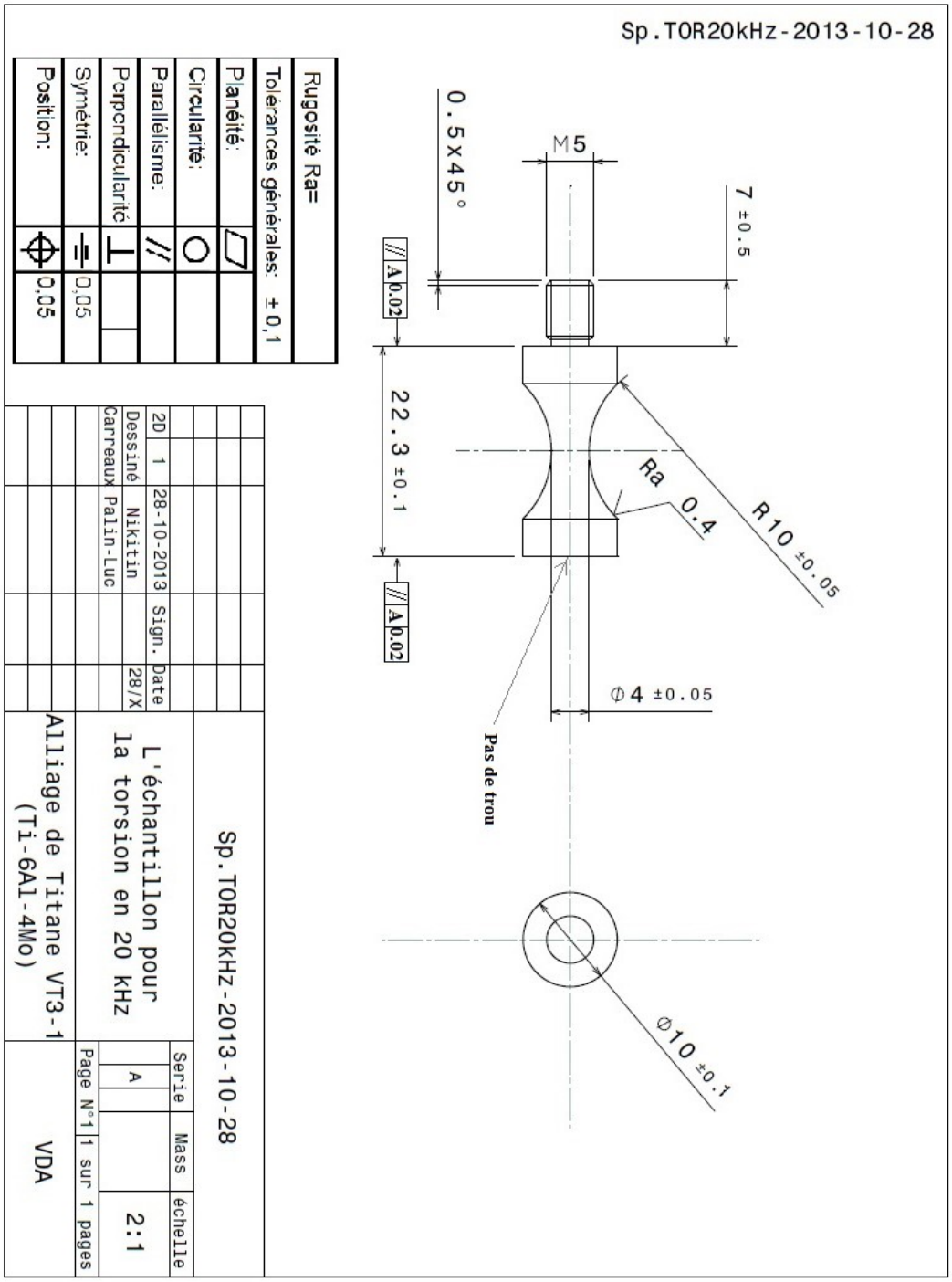
Torsion specimen for ultrasonic fatigue tests